The Role of BCA2 in Receptor Tyrosine Kinase Endocytosis and Breast Cancer

A thesis submitted for the degree of Philosophiae Doctor in Cardiff University

by

Jennifer Mary Wymant

September 2014

Cardiff School of Pharmacy and Pharmaceutical Sciences
Cardiff University

Abstract

Breast Cancer Associated gene 2 (BCA2), is a little-studied E3 ligase that is overexpressed in 56% of all primary breast cancers and has been linked with increased cell proliferation and invasion *in vitro*. BCA2 has been implicated in EGFR degradation however there is conflicting evidence surrounding its function and effect on receptor biology. This project aimed to elucidate the role of BCA2 in EGFR endocytosis and downregulation and to determine its link with breast cancer survival.

Data generated with online mRNA analysis tools indicated that high BCA2 levels were often associated with improved breast cancer prognosis. *In silico* studies also demonstrated that many genes coexpressed with BCA2 were regulators of membrane trafficking and suggested that BCA2 expression was repressed by HER2/EGFR/Ras signalling.

Experimentally, it was shown that siRNA depletion of BCA2 led to increased EGFR protein levels while transient BCA2 overexpression reduced levels of the receptor. It was found that BCA2 overexpressing, EGF stimulated cells demonstrated reduced lysosomal degradation of both receptor and ligand. Associated with this, downstream EGFR signalling in BCA2 overexpressing cells was reduced in magnitude but prolonged in duration and ultimately cell viability was impaired.

These findings support a role for BCA2 in the endolysosomal system. In agreement with this it was shown that BCA2 overexpression inhibited the vesicle membrane association of Rab7, a regulator of late endocytosis and reported BCA2 interactor.

Transferrin receptor levels and transferrin uptake were unaffected by BCA2 overexpression suggesting trafficking effects may be restricted to EGFR, a distinct class of receptor and/or to later (degradation) stages of endocytosis.

This thesis provides a detailed exploration of BCA2 biology and presents evidence of a functional role for the protein in the endocytic regulation of EGFR. The mechanism/s underlying the complex relationship between BCA2 and breast cancer outcome have yet to be fully determined.

For my family, inherited and acquired.

In memory of Gillian Mary Dainty

Acknowledgements

I would first and foremost like to thank my principal supervisor Prof. Arwyn Jones for his invaluable teaching, guidance and inspiration. Most importantly I would like to thank Prof. Jones for his unwavering support and patience. *Diolch yn fawr.*

I am also hugely grateful to my co-supervisors Dr. Andrew Westwell and Dr. Stephen Hiscox whose support and input have helped to enrich the project.

I would like to express my gratitude to my wonderful fellow lab members and friends: Dr. Edd Sayers, Helen Wiggins, Lin He, Noura Elissa, Hope Roberts-Dalton and Dr. Paul Moody. My warmest thanks also to others from the School of Pharmacy whose friendship, support, advice and technical assistance has been immeasurably helpful both personally and academically: Rebecca Bellerby, Harsha Siani, Rob Gutteridge, Valentina Ferarri, and Sophie Emery thank you so much for everything. I couldn't have done it without you all.

I would like to thank our collaborators Prof. Mike Clague and Prof. Sylvie Urbe at Liverpool University whose generosity with resources and expertise have greatly enhanced the project. Also from Liverpool University I would like to thank Alice Howarth for her role in providing the stable cells and for her friendship and support.

Thanks also to Dr. Pete Watson and Kez Cleal whose input in lab meetings has been extremely useful for troubleshooting and guiding the project.

Many thanks to Dr. Keith Hart and Barrie Francis in Cardiff CBS for sharing their time and expertise and for kindly allowing me to use their sequencing facilities.

Thank you to Dr. Aled Clayton and Dr. Jason Webber for allowing me to collaborate on an interesting and fruitful research project.

Thank you also to Dr. Alexa Bishop, Dr. Karen Reed and Dr. Fiona Wylie for providing me with support and opportunities to pursue my passion for science engagement.

For their past guidance, advice and support I would like to thank my rotation project supervisor Dr. Zaruhi Poghosyan, my undergraduate personal tutor Gavin Knight and project supervisor Prof. Geoff Pilkington.

I am extremely grateful to Cancer Research UK for their generous funding and for the freedom to pursue my chosen PhD project. Thanks also to Prof. Trevor Dale and all those involved in coordinating the Cancer Studies programme for the wonderful academic opportunity.

Thank you so much to all my lovely friends who have supported and encouraged me, especially Ashley Gaius Willis.

Last but not least I would like to express my deepest thanks to my amazing family, in particular to Glen Smith, Paul Wymant and Chris Wymant. Everything I have achieved I owe to you all, AMLA.

Table of Contents

List of Figures and Tables

List of publications

Wymant, J.M, Hiscox, S. Westwell, A., Urbé, S., Clague, M. and Jones, A.T. 2014. 479: **The role of Breast Cancer Associated gene 2 in EGFR endocytosis, downregulation and breast cancer survival**. *European Journal of Cancer.* 50(supplement 5).

Webber, J.P., Spary, L.K., Sanders, A.J., Chowdhury, R., Jiang, W.G., Steadman, R., Wymant, J., Jones, A.T., Kynaston, H., Mason, M.D., Tabi, Z. and Clayton, A. 2015. **Differentiation of tumour-promoting stromal myofibroblasts by cancer exosomes.** *Oncogene* 34: 290-302.

Wiggins, H.L., Wymant, J.M., Solfa, F., Hiscox, S.E., Taylor, K.M., Westwell, A.D. and Jones, A.T. 2015. **Disulfiram-induced cytotoxicity and endo-lysosomal sequestration of zinc in breast cancer cells**. *Biochemical Pharmacology* 93(3), p. 332-42.

Pereira, P., Pedrosa, S.S, Wymant, J.M., Sayers, E., Correia, A., Vilanova, M., Jones, A.T. and Gama, F.M. 2015 (*accepted*). **siRNA inhibition of endocytic pathways to characterize the cellular uptake mechanisms of folic acid functionalized glycol chitosan nanogels**. *Molecular Pharmaceutics.*

Abbreviations

AF-1	Activating function 1
AF-2	Activating function 2
ALDH1	Aldehyde dehydrogenase 1
ANOVA	Analysis of variance
AP1	Activator protein 1
AREG	Amphiregulin
ATCC	American type culture collection
BCA	Bicinchoninic acid
BCA2	Breast cancer associated gene 2
BCMPG	Breast cancer molecular pharmacology group
BED	Blocking ErbB2 degradation
BHK	Baby hamster kidney
BLAST	Basic local allignment search tool
BRCA1	Breast cancer type 1 susceptibility protein
BRCA2	Breast cancer type 2 susceptibility protein
BTC	Betacellulin
CBS	Central biotechnology services
CDK2	Cyclin dependent kinase 2
ChIP	Chromosome immunoprecipitation
CME	Clathrin mediated endocytosis
Co-IP	Co-immunoprecipitation
CSC	Cancer stem cell
CvME	Caveolae-mediated endocytosis
DBD	DNA binding domain
DEC	Decorin
DIC	Differential interference contrast
DNA	Deoxyribonucleic acid
DSHB	Developmental studies hybridoma bank
DUB	Deubiquitinating enzyme
E2	Oestradiol
EACR	European Cancer Research Association
ECL	Enhanced chemiluminescence
EDTA	Ethylenediaminetetraacetic acid

EGF	Epidermal growth factor
EGFR	Epidermal growth factor receptor
EMBL	European Molecular Biology Laboratory
EMT	Epithelial to mesenchymal transition
EPG	Epigen
EPR	Epiregulin
ER	Oestrogen receptor
ERE	Oestrogen response element
ESCRT	Endosomal sorting complex for transport
FBS	Foetal bovine serum
FISH	Fluorescence in situ hybridisation
FRT	Flippase recognition target
FRET	Förster *resonance energy transfer*
GC-RMA	GeneChip robust multiarray averaging
GEO	Gene expression omnibus
GFP	Green fluorescent protein
GOBO	Gene expression based outcome
Grb2	Growth factor receptor-bound protein 2
HA	Haemagluatanin
HB-EGF	Heparin binding EGF
HER2	Human epidermal growth factor receptor 2
HRT	Hormone replacement therapy
HSP	Heat shock protein
IF	Immunofluorescence
IL-3	Interleukin 3
IP	Immunoprecipitation
NB	Northern blotting
NFκB	Nuclear factor kappa-light-chain-enhancer of activated B cells
NICE	National Institute for Health and Clinical Excellence
NMR	Nuclear magnetic resonance
NP40	Nonidet P40
NPI	Nottingham prognostic index
NRG	Neuregulin
M6PR	Mannose 6 phosphate receptor

MAPK	Mitogen activated protein kinase
MEM	Multi experiment matrix
MTOC	Microtubule organising centre
mTOR	Mammalian target of rapamycin
MVB	Multivesicular body
OCT1	Octamer transcription factor 1
PAGE	Polyacrylamide gel electrophoresis
PARP	poly ADP ribose polymerase
pBCA2	Phosphorylated/phospho-BCA2
PBS	Phosphate buffered saline
PCR	Polymerase chain reaction
PFA	Paraformaldehyde
PI	Prognostic index
PI3K	Phosphatidylinositol 3-kinase
PR	Progesterone receptor
PVDF	Polyvinylidene fluoride
RFS	Relapse free Survival
RGGT	Rab geranylgeranyl transferase
RNF115	Ring finger protein 115
RPM	Revolutions per minute
RSR	Relative survival rate
RTK	Receptor tyrosine kinase
SCID	Severe combined immunodeficiency
SDM	Site directed mutagenesis
SDS	Sodium dodecyl sulphate
SERD	Selective oestrogen receptor downregulator
SERM	Selective oestrogen receptor modulator
SNP	Single nucleotide polymorphism
SP1	Specificity protein 1
TCA	Trichloroacetic acid
TE	Tris EDTA
Tf	Transferrin
TfR	Transferrin receptor
TGFα	Transforming growth factor alpha
TGN	*Trans* Golgi network

TMR	Tetramethyl rhodamine
TNM	Tumour nodes metastases
UK	United Kingdom
VEGF	Vascular endothelial growth factor
WB	Western blotting
ZN364	Zinc finger protein 364

Chapter 1: Introduction

1.1 Cancer

Cancer is a hypernym that encompasses a number of diseases characterised by aberrant cell division, survival and motility (WHO 2011). Cancer develops from cells in which critical genomic mutations have given rise to altered gene expression and/or abnormal protein function. This process of malignant transformation generally involves multiple, sequential mutations that may be inherited or spontaneously acquired (Bertram 2000).

Cancer constitutes a substantial burden of disease and incidence continues to rise. GLOBOCAN figures show that, worldwide, around 14.1 million individuals were newly diagnosed with cancer in 2012. Cancer is also a major cause of global mortality: in 2012 over 8.2 million deaths were attributed to this group of diseases; a figure which is predicted to rise to 13 million by 2030 (WHO 2012; Ferlay *et al.* 2013).

The taxonomy of cancer is dependent on both the morphological and molecular features of the disease. Gross classification is typically based on the organ/tissue of origin and the type of cell from which the disease evolved. Cancers are often further sub-classified according to particular traits such as chromosome abnormalities, expression of prognostic proteins, drug resistance etc. (Berman 2004). The stage of a cancer is also an important disease descriptor and broadly speaking relates to the size of a tumour and the degree to which it has spread (Piccirillo and Feinstein 1996).

1.2 Breast Cancer

1.2.1 Epidemiology

Breast cancer is a significant cause of morbidity and mortality worldwide. In 2012 GLOBOCAN reported an annual, global incidence of around 1.67 million and mortality of over 520 thousand. Breast cancer is the second most common form of all cancers and is the most frequently diagnosed cancer in females (Ferlay *et al.* 2013).

There is a great deal of variation in breast cancer incidence and survival between global regions of differing socio-economic development. In the developed world, disease detection and treatment success rates are relatively high compared with those in less developed areas. As a result, the 5-year relative survival rate (RSR) for breast cancer is above 80% in North America, Japan and much of Western Europe while Slovakia and Brazil have rates below 60% and in Algeria the 5-year RSR is only 40% (Coleman *et al.* 2008). Despite significant advances in clinical intervention, breast cancer incidence is still rising, even in the Western world. The UK incidence per 100,000 women increased by over 30% between 1989 and 2009 and breast cancer is now the most common form of cancer in Britain (CRUK 2011). The reasons behind the rise in breast cancer rates are complex and multifactorial. The increase is partly due to positive changes: better disease detection as a result of improved testing methods, greater public awareness and the introduction of a national screening programme. Since age is a key risk factor for breast cancer, as life expectancy has increased so too has incidence (WHO 2014). There are a number of lifestyle factors, primarily those influencing life-time

oestrogen exposure, that are also thought to have contributed to the increased frequency of breast cancer. Such factors include: increased alcohol consumption, obesity and the use of hormone replacement therapy (HRT) by post-menopausal women (McPherson *et al.* 2000).

1.2.2 Pathophysiology

As with all malignancies, breast cancer arises when somatic or heritable aberrations in cellular DNA lead to the acquisition of oncogenic traits. The vast majority of breast cancers are adenocarcinomas, so called because they develop from the glandular epithelial cells that make up the lactiferous ducts and lobules of the breast (Fig. 1-1). 70-80% of breast cancers are ductal and 10-15% are lobular in origin (CRUK 2011).

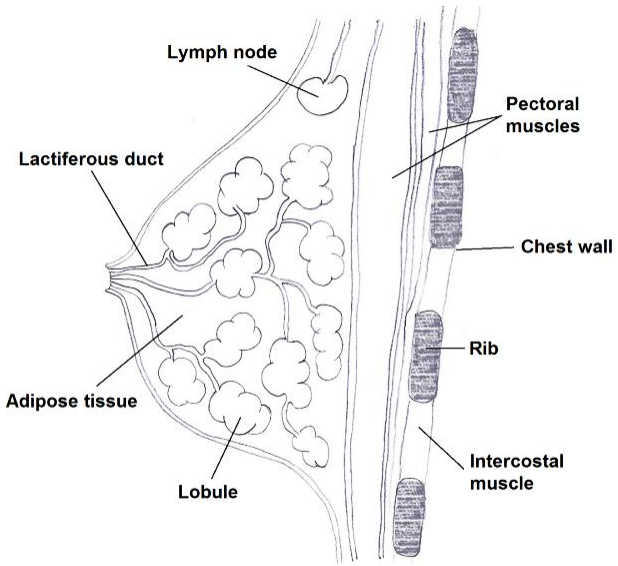

Figure 1-1: Gross anatomy of the breast (sagittal section). Most breast cancers originate from the lactiferous (milk) ducts or lobules. As the disease progresses tumours will spread through the breast tissue either outwards to the skin or inwards towards and/or through the chest wall. Highly invasive breast cancers will spread into the lymph nodes and/or blood vessels before metastasising to other organs.

Following transformation, breast cancer cells proliferate *in situ*, the malignant cells initially drawing nutrients from the surrounding tissues by passive diffusion. As a tumour expands angiogenic factors are

secreted by malignant cells to promote the formation of a new capillary network from the normal breast vasculature. The development of a nutritive blood supply supports the continued growth of expanding tumour masses. Invasive breast cancers will then spread from the duct or lobe of origin, through the basement membrane and into the surrounding breast tissues (local invasion). If tumour cells reach and enter the bloodstream, or if there is regional lymph node involvement, then there is a high risk that the cancer will metastasise to distant sites such as the bones, brain and liver (Fig. 1-2) (Fidler 2003; Steeg 2003). In non-invasive disease the basement membrane remains intact and malignant cells are limited to their original position. Non-invasive breast cancers, the most common of which are ductal and lobular carcinoma *in situ,* can eventually progress to invasive disease and have high risks of recurrence (Wiechmann and Kuerer 2008).

The growth and development of the majority of breast cancers is driven by the hormone oestrogen but more aggressive tumours rely on growth factors for oncogenic progression. The importance of the oestrogen receptor (ER) and growth factor receptors in breast carcinogenesis will be covered in later sections (1.2.6 and 1.2.7).

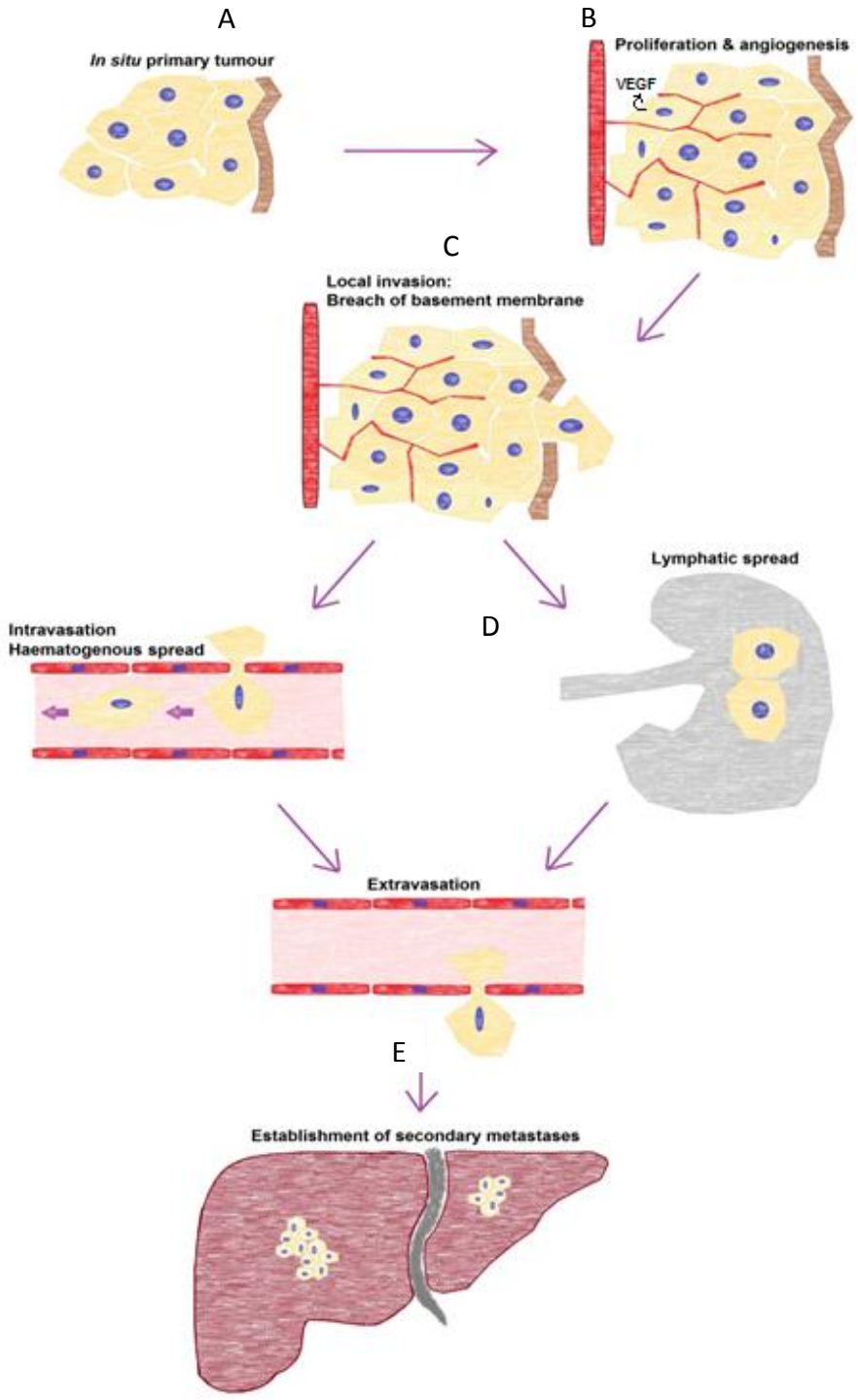

Figure 1-2: The development and progression of breast cancer. Primary breast tumours develop from aberrantly proliferative cells that have failed to undergo apoptosis following irreparable DNA damage. A) By taking up nutrients from surrounding tissue, tumours can grow to around 1-2mm diameter but in order to expand further a dedicated blood supply is needed. B) Malignant cells secrete angiogenic signalling proteins, such as Vascular Endothelial Growth Factor (VEGF), which stimulate the development of a tumour capillary network. C) Undetected and untreated, breast cancers spread through the breast and may reach the skin or grow through the chest wall. D) Ultimately invasive breast cancers reach and enter the bloodstream either directly or via the lymphatic system. E) Circulating breast cancer cells can then spread to other organs and tissues where micrometastases form and eventually develop into secondary/metastatic tumours.

1.2.3 Breast cancer classification

Breast cancers are classified according to the Tumour Nodes Metastases (TNM) staging system which categorizes disease based on measures of tumour size and spread.

In addition to staging, breast cancers are also "graded" from 1-3 or low-high (depending on the system used). Histological grade describes the potential aggressiveness of a tumour based on the degree of cellular differentiation. Differentiation is the process by which cells develop from progenitor stem cells into specialised cell types. In the context of staging: the degree of differentiation refers to how closely the tumour cells resemble the cell types from which the cancer developed.

Breast cancer grade depends on measures of malignant cell morphology, organization and proliferation. Grading is important for determining disease prognosis and usually influences the aggressiveness of the therapeutic approach (Elston and Ellis 1991; Rakha *et al*. 2010).

The Nottingham prognostic index (NPI) is a system for predicting patient outcome based on key histopathalogical indicators. In the NPI, breast cancers are classified according to the score produced by following calculation: (0.2 x S) x N x G. S is the tumour size in centimetres, N is the number of lymph nodes involved and G is the tumour grade. Tumour grade is determined by scoring from 1-3 in each of the following three categories: nuclear pleomorphism, mitotic rate and glandular formation. Nuclear pleomorphism/atypia relates to the degree of irregularity in the size, shape and staining intensity of malignant cell nuclei. Mitotic rate is

a measure of the number of cells in the tumour periphery that are in metaphase, anaphase or telophase. Glandular formation describes the degree of structural normality within the tumour *i.e.* the percentage of cells which are organized into the typical lobular/tubular structures of breast tissue. Histopathologists will microscopically examine a tumour and, based on quantitative and qualitative assessment, will assign a score between 3 and 9. A score of 3-5 indicates a low grade/grade I tumour which is well differentiated, 6-7 represents an intermediate/grade II tumour that is moderately differentiated. A grade score of 8-9 reflects high/grade III disease *i.e.* an highly aggressive, poorly differentiated tumour (Elston and Ellis 1991; Galea *et al*. 1992).

The molecular classification of breast cancer subdivides disease according to the expression of key genetic markers (Table 1-1). Stratification of breast cancer into the subtypes Luminal A, Luminal B, Basal-like and HER2 is important for patient prognosis and treatment.

Table 1-1: The main molecular subtypes of breast cancer. Figure compiled from: (Schnitt 2010; Zhang *et al.* 2014)

	Luminal A	Luminal B	Basal-like	HER2
Percentage of breast cancers	≈ 40%	≈ 30%	≈ 15%	≈ 15%
ER	Positive	Positive	Negative	Negative
HER2 expression	Negative	Positive **OR** high Ki-67 (proliferation)	Negative	Positive
Cytokeratins	Luminal markers: CK8$^+$ and CK18$^+$	Luminal markers: CK8$^+$ and CK18$^+$	Basal markers: CK5/6$^+$, 14$^+$, 17$^+$	
Other overexpressed genes	GATA$^-$3, XBP-1, FOXA1, and ADH1B	FGFR1, EGFR, Ki-67, cyclin D1, CCNB1 and MYBL2	EGFR, c-Kit, FOXC1, p63, P-cadherin, vimentin, laminin	GRB7
Targeted treatment response	Respond to endocrine therapy (tamoxifen/ aromatase inhibitors)	Endocrine therapy response more variable than in luminal A. Trastuzumab for HER2+ tumours.	Insensitive to endocrine therapy or trastuzumab. Some response to platinum-based chemotherapy, PARP inhibitors and anti-angiogenics	Trastuzumab. De novo or acquired trastuzumab resistant tumours treated with combined PI3K/mTOR inhibitor
5-year RSR	95%	50%	30%	30%

1.2.4 Treatment

There is no single treatment for breast cancer. Therapy involves a combination of different approaches designed to remove or reduce the tumour burden and to prevent its recurrence or further progression. Generally the more aggressive and advanced the disease, the more drastic the therapeutic approach will be. However, a patient's personal needs and wishes are also taken into consideration when planning their particular treatment regimen. Thus breast cancer treatment usually reflects a balance between effectiveness and tolerability of side-effects.

Surgery is the therapeutic mainstay of breast cancer treatment. Surgical options range from wide local excision (lumpectomy) to radical mastectomy and lymph node resection which involves removal of the breast, the muscles of the chest wall and the lymph nodes (CRUK 2011).

Typically surgical intervention will be followed by a course of radiotherapy. Radiotherapy involves the use of ionising particles or high energy electromagnetic waves to destroy cancer cells. Ionising radiation directly causes breaks and mutations in DNA as well as generating cytotoxic free-radicals and peroxides that damage both the DNA and cellular proteins. Cells can ordinarily repair DNA breaks but it is thought that radiation treatment, of a high enough dose and long enough duration, saturates the DNA repair pathways such that exposed cells are irreparably and fatally damaged. Radiotherapy is targeted to the tissues surrounding the excised tumour in order to remove any residual/locally spread disease. Although radiotherapy is targeted to the tumour site, the treatment is not specific for cancer cells: there is a great deal of collateral

damage to the irradiated healthy tissues surrounding the cancer (Dormand *et al.* 2005).

Chemotherapy is a common adjuvant to both surgery and radiotherapy. Chemotherapy regimens usually involve combinations of different drugs that are designed to exert the greatest possible damage to the tumour cells with minimal damage to healthy cells. The major difference between malignant and healthy cells that is exploited by most chemotherapeutic agents is the rate of cell division. Because cancer cells are much more proliferative than normal cells, drugs designed to inhibit cell division have a greater effect on cancerous tissue. Unfortunately therapeutic specificity is limited because highly proliferative tissues such as the colonic epithelium are also damaged by these agents. Chemotherapy is particularly important in the treatment of ER^- breast cancers and high-risk ER^+ disease. Some of the common chemotherapeutic agents are described in Table 1-2; a typical treatment regimen will involve combinations of these drugs.

Table 1-2: Common chemotheraputic agents for the treatment of breast cancer and their mechanisms of action. Figure compiled from: (Cerqueira *et al.* 2007; CRUK 2011; Brenner and Stevens 2013)

Drug	Type of drug	Mechanism of action
Fluorouracil (5FU)	Anti-metabolite	Inhibits thymidylate synthase, preventing synthesis of thymidine and therefore inhibiting DNA replication.
Epirubicin	Intercalating agent	Causes intercalation of DNA strands, inhibiting DNA replication and RNA synthesis.
Cyclophosphamide	Alkylating agent	Metabolised to phosphoramide mustard which causes cross-links within and between DNA strands. Inhibits DNA and RNA synthesis.
Methotrexate	Anti-metabolite	Inhibits Dihydrofolate reductase which is required for synthesis of thymidine and therefore DNA. Methotrexate also inhibits RNA synthesis since folate is necessary for cells to make adenine and guanine.
Doxorubicin	Intercalating agent	Causes intercalation of DNA strands, inhibiting DNA replication and RNA synthesis.
Docetaxel	Anti-mitotic	Binds to and prevents depolymerisation of microtubules, thereby inhibiting cell division and the accumulation of tubulin promotes apoptosis.
Mitoxanthone	Intercalating agent	Inhibits topoisomerase II causing intercalation of DNA strands, inhibiting DNA replication and RNA synthesis.
Mitomycin C	Alkylating agent	Causes cross-links within and between DNA strands. Inhibits DNA and RNA synthesis.
Gemcitabine	Anti-metabolite	Incorporated into DNA and prevents further addition of bases. Inhibits ribonucleotide reductase preventing deocyribonucleotide synthesis. DNA synthesis inhibition.

In addition to relatively non-specific chemotherapy, targeted treatments have been developed which will be discussed in more detail in the sections on the oestrogen receptor (1.2.6) and receptor tyrosine kinases (1.2.7).

1.2.5 Aetiology

The root cause of breast cancer, as for all cancers, is genetic alteration in cells. Of the many risk factors that have been identified for cancer, the vast majority relate to variables that increase the likelihood of DNA mutations occurring.

In breast cancer, most risk factors for disease development are hormonal; more specifically they are oestrogen dependent. It has been shown that the longer an individual is exposed to oestrogen (i.e. the larger their oestrogen window) the greater their risk of developing breast cancer. Reproductive history therefore has an important aetiological influence on the disease: being female, early menarche, not having children, high body fat, having hormone replacement therapy (HRT) are all factors known to increase breast cancer risk (Henderson 2006). The role of oestrogen in breast cancer development will be covered more thoroughly in section 1.2.6.

Gender is the single biggest risk factor for breast cancer: females are over 100 times more likely to develop the disease than males (IARC 2008). Prognosis is often thought to be poorer in men as a result of reduced disease awareness and longer delays before medical advice is sought (Fentiman *et al.* 2006). When survival figures are standardised for age at diagnosis and cancer stage there appears to be no significant difference in prognosis between genders (Gómez-Raposo *et al.* 2010).

After gender, age is the next most important risk factor for developing breast cancer. The effect of age can in part be explained by cumulative

risk: the chance of DNA damage occurring, and therefore the likelihood of malignant transformation, accrues over time. Figures show that the lifetime risk of a UK female developing breast cancer is 1 in 8 but the majority (81%) of cases are diagnosed in those over 50 years old (CRUK 2011). A number of key genetic events are associated with mammary carcinogenesis including mutation of the critical tumour suppressor gene TP53 and upregulation of the HER2 oncoprotein.

Most breast cancers develop sporadically from acquired mutations but a small proportion of breast cancers are familial in origin. Between 5 and 10% of breast cancers are thought to arise from inherited breast cancer genes (Khadim *et al.* 2013). Breast cancer type 1 and 2 susceptibility proteins (BRCA1 and BRCA2) are tumour suppressor enzymes that are involved in double-stranded DNA break repair. Cells lacking functional BRCA1 or BRCA2 amass critical chromosomal aberrations such as breaks, centrosome amplification and aneuploidy (Welcsh and King 2001). Germline mutations in the BRCA1 and BRCA2 genes have been shown by meta-analysis to increase the carrier's risk of developing breast cancer. Before the age of 70, the risk of breast cancer is raised by 47-66% in BRCA1 mutation carriers and 40-57% of those with BRCA2 mutations (Chen and Parmigiani 2007).

1.2.6 Oestrogen Receptors and Breast Cancer

The oestrogen receptors (ERs), ER-α and ER-β, are nuclear hormone receptors and as such are ligand inducible transcription factors that regulate the expression of an array of genes. Both receptors have been

implicated in breast cancer though the role of ER-α is better understood and considered to be of greater importance in the disease. Where ER^+ breast cancer is discussed, ER-α is the receptor being referred to.

The genes, signalling proteins and cellular processes affected by ER-α and -β vary widely between and within tissues, though the two receptors often act antagonistically. Different interacting cofactors can also induce disparate downstream responses from the ERs so a single cell may respond differently to oestrogen stimulation depending on context (McDonnell and Norris 2002).

The normal physiological roles of oestrogens and the ERs in controlling breast and reproductive growth, development and function are well characterised. Interactions between oestrogens and the ERs are also known to affect other processes such as bone remodelling, blood pressure regulation and clotting factor synthesis (Oelkers 1996; Raisz 1999).

ER-α and ER-β share considerable homology but differences in the activating function (AF-1) domains of ER-α and ER-β are thought to confer the two receptors with differing abilities to stimulate gene expression (Singh and Kumar 2005). The AF-1 domain in ER-α renders strong transcriptional activity to the receptor that is not conferred by the equivalent domain in ER-β. Moreover, the AF-1 ER-β has been shown to contain a repressive motif that when removed enhances the transcriptional activity of the receptor (Hall and McDonnell 1999).

In the absence of steroid hormone ligand, ERs are bound to an inhibitory complex of heat shock proteins (HSPs; Fig. 1-3). The binding of an

oestrogen ligand to an ER stimulates dissociation of the HSPs and promotes receptor dimerization, nuclear translocation and DNA binding. In the classical genomic pathway of ER activity: ER dimers then bind to recognition sequences called oestrogen response elements (EREs), which are found in the promoter regions of target genes. Once ERs are bound to EREs, transcriptional cofactors and chromatin remodelling proteins are recruited by the AF-1 and AF-2 domains. The cofactors that are recruited can vary and may be transcriptional coactivators or corepressors. The complexes formed by the ERs, ligands and cofactors then alter the expression of downstream genes (Weinberg 2006).

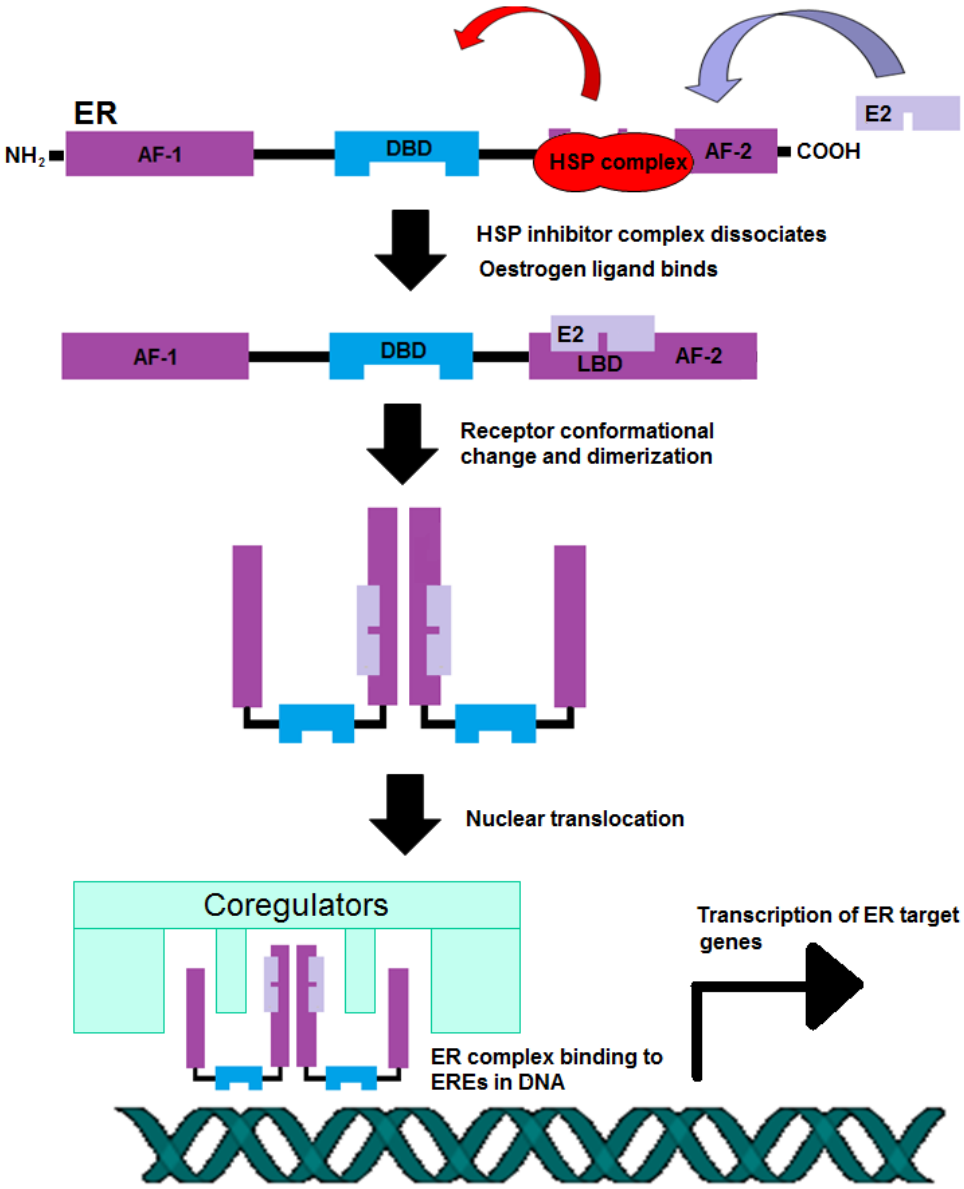

Figure 1-3 E2 induced transcription of ER target genes. Oestradiol (E2) binds to the ligand binding domain (LBD) of the ER, and the HSP inhibitory complex dissociates. The ER undergoes conformational change and then forms a dimer-ligand complex before being translocated to the nucleus. The ER dimer forms a transcriptional complex with coregulator proteins and binds via the DNA binding domain (DBD) to EREs in the promoter regions of target genes (Driggers and Segars 2002; Nilsson *et al.* 2011)

Ligand activated ERs can also indirectly affect gene expression by interacting with other transcription factors and modulating their function. This transcriptional cross-talk is known as the non-classical genomic ER pathway, an example of which is the relationship between ER-α and nuclear factor kappa-light-chain-enhancer of activated B cells (NFκB). Target genes of NFκB have been shown to be downregulated by ER-α,

and the two transcription factors appear to be mutually co-repressive (Gionet *et al.* 2009).

ER-α can also regulate gene transcription in a ligand-independent manner. It has been shown that the ER-α can be phosphorylated at serine 118 in the AF-1 domain by mitogen activated protein kinase (MAPK). Phosphorylation of ER-α by MAPK enhances the transcriptional activity of the hormone receptor (Kato *et al.* 1995). MAPK is a key protein in growth factor signalling by receptor tyrosine kinases (RTKs), a family of cell-surface receptors that are also important in breast cancer (see section 1.2.7). Through MAPK there is cross-talk between the RTK and ER-α signalling pathways and effector mechanisms. The phosphorylation and transcriptional activity of ER-α can be increased by pathways that enhance MAPK phosphorylation e.g. by cell stimulation with epidermal growth factor (EGF). Overexpression of wild-type or constitutively active MAPK, or of the upstream signalling protein Ras, also enhance ER-α transcriptional activity (Kato *et al.* 1995; Bunone *et al.* 1996). Ligand-independent activation of ER-α is also achieved via phosphorylation of other serines in the AF-1 domain e.g. ser167 which is phosphorylated by Akt (Martin *et al.* 2000). Akt is a serine/threonine kinase and an important pro-survival oncogene owing to its role in inhibiting apoptosis. Akt is activated by growth factor stimulation and as such represents another key overlap between hormone and growth factor receptor actions. In addition to interaction with downstream signalling proteins, ER-α has been shown to directly interact with RTKs such as EGFR. ER-α can associate with the endocytic scaffold protein caveolin-

1 (see section 1.2.8.2) at the cell membrane where it can induce transactivation of RTKs and promote downstream receptor signalling (Razandi *et al.* 2002; Razandi *et al.* 2003). Bi-directional cross-talk between ER-α and growth factor receptors and their downstream signalling kinases is increasingly thought to be important in breast cancer resistance to endocrine therapy (Shou *et al*. 2004; Gee *et al.* 2005; Wang *et al*. 2011b).

ER-α has been shown to be overexpressed in at least 70% of breast cancers and the links between oestrogen exposure and mammary carcinogenesis are well-established (Anderson *et al.* 2002). Downregulation of ER-β has been reported in invasive breast cancers but its role in breast cancer is less well understood than ER-α (Roger *et al.* 2001; Skliris *et al.* 2003)

Oestrogens have been shown to have direct mitogenic effects on ER-α positive breast cancers. Oestradiol (E2) increases the number of mitotic breast cancer cells in hormone treated cultures (Doisneau-Sixou *et al.* 2003). The proliferative effects are partly attributed to upregulation of the ER target proteins c-Myc and cyclin D whose expression rapidly increases in response to E2 (Butt *et al.* 2005). Cyclin D directly drives cell cycle progression by promoting G1/S phase transition. c-Myc is a transcription factor, and proto-oncogene, that promotes transcription of pro-proliferative cyclins and downregulates the cell cycle inhibitor p21. ER-α has also been shown to promote cell survival. For example, expression of the anti-apoptotic protein Bcl-2 has been shown to be

induced by E2 stimulation of ER^+ breast cancer cells (Teixeira *et al.* 1995).

Endocrine therapies that target oestrogen synthesis and ER signalling have displayed profound efficacy in the treatment of ER-positive breast cancers. Treatment with Tamoxifen reduces the rate of recurrence of these tumours by nearly 50% and mortality by 30%. Nonetheless, the issues of de novo and acquired therapeutic resistance pervade and are believed to affect around 25-50% of all cases (Musgrove and Sutherland 2009).

Tamoxifen binds to the ER, inducing dimersation and nuclear transport but inhibiting cofactor recruitment to, and therefore transcriptional activity of, the AF-2 domain (Shiau *et al.* 1998). Function of the AF-1 domain remains intact, in fact Tamoxifen has been shown to promote transcription of AF-1 responsive genes (Tzukerman *et al.* 1994). Different tissues have different patterns of AF-1 and AF-2 responsive genes: AF-2 genes are more prevalent in the breast while AF-1 genes are predominantly found in the uterus. Tamoxifen is consequently described as a selective oestrogen receptor modulator (SERM) as it can act as an agonist or an antagonist depending on the histological context (Ring and Dowsett 2004). The inability of Tamoxifen to completely abolish the transcriptional activity of ER-α is thought to be a contributing factor in therapeutic resistance.

Anastrazole (Arimidex®) is a third generation aromatase inhibitor that prevents oestrogen biosynthesis from androgen precursors. The strategy of aromatase inhibition was developed in order to overcome the problems

of Tamoxifen's ER agonist activity. In a large scale phase 3 clinical trial anastrozole demonstrated greater efficacy (increased disease free survival) and fewer side-effects than Tamoxifen for over 9000 post-menopausal women who had early stage breast cancer. Therapeutic resistance was however still reported for anastrazole and osteoporosis was a notable side-effect (Howell *et al.* 2005). Following surgery, anastrazole is now the recommended first-line hormone treatment for ER^+ breast cancer according to National Institute for Health and Clinical Excellence (NICE) guidelines (CRUK 2011).

The need for better ER-targeted therapies led to the development of selective oestrogen receptor downregulators (SERDs) such as fulvestrant (Faslodex®). Fulvestrant has a high affinity for the ER and competes with E2 for the LBD. Binding of fulvestrant to the ER inhibits receptor dimerization, nuclear transport and cofactor interaction (Fawell *et al.* 1990; Dauvois *et al.* 1993). Degradation of the ER is also accelerated when bound to fulvestrant leading to a significant reduction in receptor numbers, attenuation of signalling and ablation of all ER transcriptional function (Morris and Wakeling 2002).

Fulvestrant shows greater potency than Tamoxifen against ER^+ breast tumours in the laboratory and is associated with reduced development of resistant disease. Fulvestrant also shows activity against Tamoxifen-resistant disease models (Osborne *et al.* 1995). Fulvestrant has demonstrated efficacy slightly superior to anastrazole and equal tolerability in a double-blind randomized clinical trial in Tamoxifen resistant disease (Osborne *et al.* 2002). Fulvestrant is not currently

approved over anastrazole in the UK for use in locally advanced or metastatic breast cancer (NICE 2011).

Increased expression, activity and downstream signalling of growth factor receptors is also thought to contribute to resistance to endocrine therapies via enhanced ER agonist activity (Gee *et al.* 2005; Nicholson *et al.* 2007) as well as acting independently of ER in ER^- disease. Proteins with connections to both ER and RTK function may therefore represent important targets for predicting, preventing or reversing hormone refractory breast cancer. Such proteins may also be useful targets for the treatment of ER^- cancers that are critically dependent on growth factor receptor expression and downstream signalling.

1.2.7 Receptor Tyrosine Kinases and Breast Cancer

Receptor Tyrosine Kinases (RTKs) such as EGFR, HER2 and c-Met are transmembrane proteins that are essential for normal cell function but are often overexpressed/ineffectively downregulated in breast cancer. Estimates vary, but in one of the largest studies to date, EGFR overexpression was demonstrated in 18% of breast cancers and HER2 positivity in 18% of cases. High levels of EGFR and HER2 were associated with a more aggressive cancer phenotype and poorer prognosis in patients who had received adjuvant systemic therapy and/or had suffered relapse (Rimawi *et al.* 2010).

c-Met is another RTK that is expressed in normal epithelial cells but is upregulated in breast cancer. Around 20–30% of all breast tumours have

been shown to overexpress c-Met and high levels of the receptor are associated with poor clinical outcome (Lengyel *et al.* 2005).

EGFR and HER2 belong to the ErbB family of RTKs of which there are four, structurally homologous, members: EGFR (ErbB1, HER1), HER2 (ErbB2), HER3 (ErbB3) and HER4 (ErbB4).

All ErbB receptors have an ectodomain which can, in all family members but HER2, bind to compatible extracellular ligands. A summary of all documented ErbB ligands is shown in Figure 1-4.

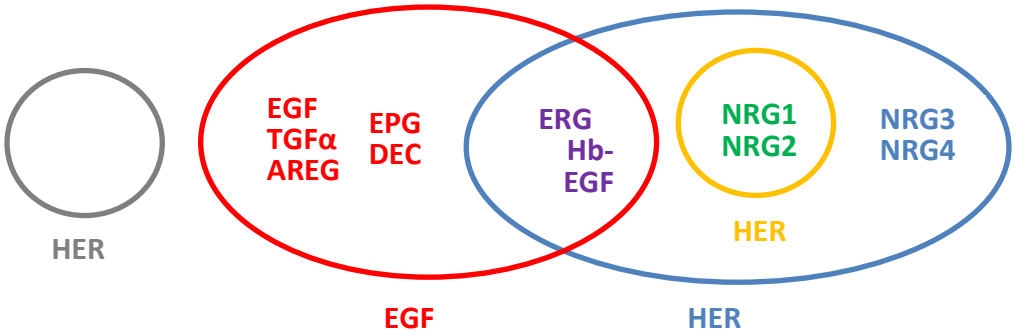

Figure 1-4: Unique and shared ligands of the ErbB receptors. Circles/ovals represent named receptors. Ligands are listed within limits of their activating receptor. Overlapping regions reflect & contain shared ligands. HER2 is an orphan receptor with no known ligands. EGF = epidermal growth factor, TGFα = transforming growth factor alpha, AREG = amphiregulin, EPG = epigen, DEC = decorin, ERG = epiregulin, HB-EGF = heparin binding EGF, BTC = betacellulin, NRG = neuregulin. Figure compiled from: (Harris *et al*. 2003; Lin and Winer 2004; Bouyain *et al*. 2005; Iozzo *et al.* 1999; Schneider and Yarden, 2014)

When activated by ligand binding, RTKs initiate signalling cascades that transduce mitogenic, angiogenic, pro-migratory and survival signals to the nucleus. The sequence of activation events in the ErbB family can be summarized as: homo- or heterodimerization of ligand-bound receptors followed by receptor activation through trans-autophosphorylation of intracellular tyrosine residues. All but one of the ErbB receptors has a

cytosolic domain with tyrosine kinase functionality (Fig. 1-5). The exception is HER3 which lacks crucial catalytic residues and as such is generally considered to be "kinase dead". There is however evidence that in certain conditions HER3 may possess some kinase activity, e.g. when in a heterodimer with HER2 (Shi *et al.* 2010).

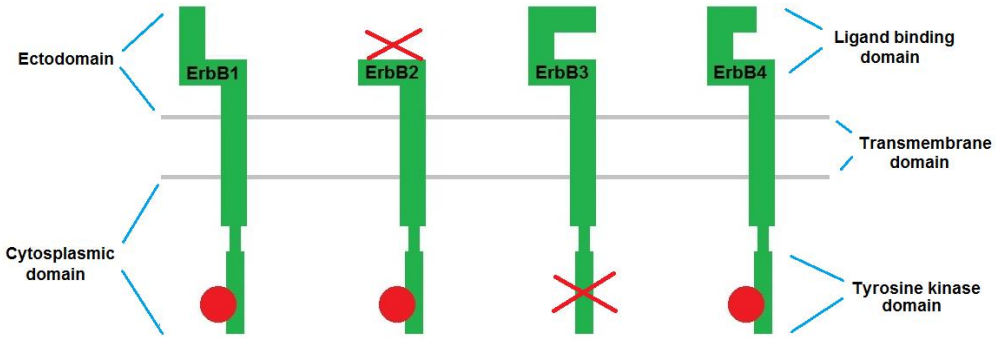

Figure 1-5: Domain structure of the ErbB family of RTKs. ErbB2 (HER2) is an orphan receptor with no known ligands. ErbB3 has no/minimally active tyrosine kinase domain.

Activation of RTKs initiates pro-oncogenic intracellular phosphorylation cascades. EGFR and HER2 predominantly signal via the MAPK and Phosphatidylinositol 3-Kinase (PI3K) pathways. Overexpression of EGFR/HER2 leads to increased MAPK and PIK3/Akt signalling and to aberrant transcription of genes associated with malignant transformation. Some examples of upregulated genes include: cell division cycle-associated protein 7 (CDCA7) (Trang *et al.* 2009), FOS-like antigen 1 (FOSL1) and osteopontin (OPN) (Janka *et al.* 2010). CDCA7 and FOSL1 stimulate proliferation and osteopontin is an anti-apoptotic protein, and all are associated with malignant overexpression. Due to changes in gene expression profile, RTK overexpressing cells are immortalised, highly proliferative and have an enhanced capacity to adhere, invade, metastasise and promote angiogenesis (Nicholson *et al.* 2007).

The activation and signalling of c-Met shares many similarities with the ErbB receptors: activation is primarily induced by ligand binding and downstream signalling is mainly via the pro-oncogenic MAPK and PI3K/Akt pathways. The role of dimerisation in c-Met activation and signalling is less well understood but dimerization is known to occur by ligand-dependant and independent mechanisms. Ligand-independent dimerisation of c-Met and mutations in the dimerisation domain of the receptor are thought to be important in cancer (Wickramasinghe and Kong-Beltran 2005).

Overexpression of RTKs in breast cancer enables therapeutic targeting. For example, the humanised monoclonal antibody trastuzumab (Herceptin®) and the small molecule inhibitor gefitinib (IRESSA®) have exhibited activity against $HER2^+$ and $EGFR^+$ breast cancers respectively (Normanno *et al.* 2009). Despite some successes with these therapies, present strategies are still far from perfect. For example, 15% of patients with early stage breast cancers relapse in spite of trastuzumab treatment and those with metastatic disease often develop resistance to the inhibitor (Nanda 2007).

Despite relatively wide usage in the treatment of $HER2^+$ breast cancer, trastuzumab's mechanism of action is not yet fully understood but is known to be complex. Trastuzumab binds HER2 with high affinity and this has been shown to inhibit cellular proliferation and promote apoptosis via a number of mechanisms, including: decreased cyclin dependent kinase 2 (CDK2) activity (Lane *et al.* 2001), reduced PI3K/Akt signalling (Nagata *et al.* 2004) and inhibited DNA repair and

synthesis following chemo- and radiotherapy (Pietras *et al.* 1994; Pietras *et al.* 1999). The induction of immune based cytotoxic responses (antibody and complement mediated) has also been described for trastuzumab (Stockmeyer *et al.* 2003), and the mAb has also demonstrated anti-angiogenic activity via reduced VEGF production (Izumi *et al.* 2002). Trastuzumab induced HER2 downregulation via increased receptor endocytosis (see section 1.2.8) has been reported and may contribute to the mAb's anti-cancer effects (Cuello *et al.* 2001). In 2009 (Ben-Kasus *et al.*) suggested that trastuzumab and HER2 may form lattices at the cell membrane which collapse into the cytoplasm and are subject to lysosomal degradation, a phenomenon the group had previously reported for anti-EGFR mAbs (Friedman *et al.* 2005). HER2 itself has been shown to be resistant to internalisation, a property attributed to a number of factors including, the receptor's association with membrane protrusions (Hommelgaard *et al.* 2004), inhibited clathrin pit formation (Cortese *et al.* 2013) and to a cystosolic region of HER2 termed the "blocking ErbB2 degradation" (BED) domain (Shen *et al.* 2008). Internalisation-resistance reduces receptor downregulation allowing prolonged activation and downstream signalling, potentially important factors in trastuzumab resistance. Other mechanisms believed to contribute to trastuzumab resistance include: constitutive activation of downstream HER2 signalling pathways, masking of the trastuzumab epitope by mucin-4 overexpression, increased compensatory signalling through other ErbB receptors and cross-talk between IGF-R1 and HER2 signalling pathways (Nahta and Esteva 2006).

Therapeutic resistance to EGFR inhibitors has been linked to alterations in receptor endocytosis (Hopper-Borge *et al.* 2009). Gefitinib's activity against EGFR overexpressing cancers is a result of the drug competitively inhibiting ATP-binding in the tyrosine kinase domain of EGFR. Gefitinib binding to this intracellular site ablates receptor phosphorylation and tyrosine-kinase activity which in turn suppresses pro-growth and survival signalling (Tiseo *et al.* 2010). In gefitinib sensitive non-small cell lung cancer (NSCLC) cells EGFR is rapidly internalised and degraded following ligand stimulation. However, gefitinib resistant NSCLC cell lines have shown impaired EGFR downregulation compared with sensitive cell counterparts (Ono *et al.* 2004). Aberrant accumulation of EGFR in early endosomes of resistant cells has also been described in both the presence and absence of gefitinib (Nishimura *et al.* 2007). Squamous cell carcinoma of the head and neck (SCCHN) cells that are resistant to the EGFR inhibitor mAb cetuximab show aberrant persistence of EGFR on the cell membrane following ligand stimulation (Wheeler *et al.* 2008). Together these findings suggest that impaired endocytic trafficking may be involved in conferring therapeutic resistance. There is a need to better understand the mechanisms governing RTK endocytosis and to identify potential mechanisms and targets for promoting receptor downregulation.

1.2.8 Downregulation of Receptor Tyrosine Kinases

Endocytosis is the process by which cells internalise ligand-bound receptors. There are a number of internalisation routes through which RTKs are trafficked and generally-speaking these routes may be divided

into two categories: clathrin-mediated endocytosis (CME) and clathrin independent endocytosis.

1.2.8.1 Clathrin-Mediated Endocytosis

Clathrin and various accessory proteins are recruited to the site of activated receptors where they assemble into a layered structure on the local membrane. (See Figure 1-6 for a schematic diagram of RTK endocytosis). The membrane surrounding the receptor then invaginates and pinches off, forming a clathrin-coated vesicle containing the receptor and ligand. The C-terminus of the receptor remains exposed to the cytosol and continues to activate signalling pathways during vesicle translocation (Wieffer *et al.* 2009). Vesicles are shuttled into the cell before being uncoated and associating with Rab5. Rab5 is a member of the Rab family of small GTPase proteins that are responsible for coordinating membrane trafficking. Rab5 mediates vesicle transport to, and fusion with, the early endosome and has also been implicated in clathrin pit formation (McLauchlan *et al.* 1998). The early endosome is a peripheral, membrane-bound organelle where many endocytic pathways intersect. Receptors are sorted in early endosome and subsequently trafficked along different routes (Jovic *et al.* 2010).

From the early endosome, a receptor may follow one of three pathways: fast or slow recycling (exocytosis) or degradation. Fast recycling is coordinated by Rab4 and is the process by which receptors are rapidly shuttled back to the cell membrane. Slow recycling is organized by Rabs

4 and 11. Degradation is coordinated by Rab7, a protein responsible for receptor sorting in late endosomes and transport to lysosomes.

The late endosome or multivesicular body (MVB) is a large sorting compartment that is densely packed with lumenal vesicles. MVB maturation and receptor internalisation into the MVB is controlled by the endosomal sorting complex for transport (ESCRT) machinery comprised of ESCRT-I, -II and -III. The ESCRT-I complex recognises receptors that have been targeted for degradation by ubiquitin tags on the receptor's cytoplasmic tail (for more detailed discussion about ubiquitination see Section 1.2.9). The binding of ubiquitinated receptor to the ESCRT-1 complex effectively tethers the receptor to the maturing endosome and prevents it from being recycled. ESCRT-II and –III are then recruited and mediate further receptor sorting and invagination of the endosomal membrane around the receptor. Eventually the vesicle-bound receptor buds off into the MVB lumen and the ESCRT machinery can be recycled (Katzmann *et al.* 2002; Raiborg and Stenmark 2009). Receptors in the late endosome no longer actively signal as they are fully enclosed within its multivesicular structure. Receptors (and ligands) are broken down in lysosomes by acid hydrolases, marking the end of the degradation pathway.

Rab7 controls receptor trafficking to the lysosome by mediating fusion of the MVB and the lysosome. The GTPase is also critically involved in lysosome biogenesis, acidification and localisation (Bucci *et al*. 2000; Vanlandingham and Ceresa 2009). Interestingly, Rab7 appears to have a dual, potentially antagonistic role in endocytosis through an interaction

with the E3 ligase, and subject of this thesis, BCA2. The consequence of the interaction has been shown separately to *inhibit* and *promote* RTK degradation (Mizuno *et al*. 2003; Sakane *et al*. 2007; Smith *et al*. 2013). For more detailed discussion of the interaction between BCA2 and Rab7 see section 1.5.2.

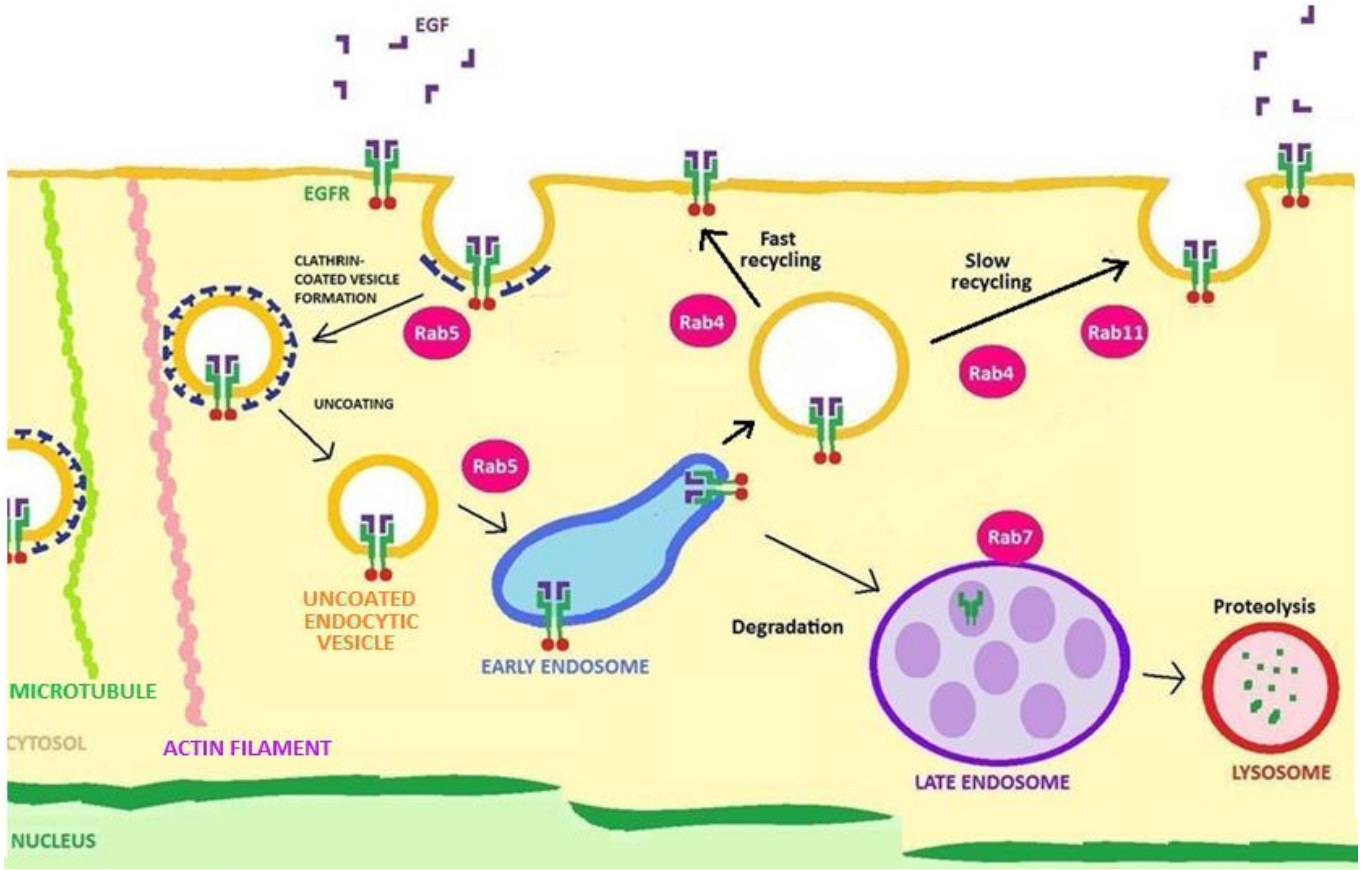

Figure 1-6: Receptor Tyrosine Kinase Endocytosis. Following internalisation and transport to early endosomal sorting compartments, activated receptor tyrosine kinases (RTKs) such as EGFR may be trafficked along one of three main endocytic pathways: A) Fast or slow recycling of RTKs maintains receptor numbers on the cell surface and facilitates repeated stimulation and prolonged oncogenic signalling. B) The degradation pathway leads to cessation of signalling as the RTKs become bound within the multivesicular structure of the late endosome. The receptors and their ligands are ultimately destroyed by acid hydrolase enzymes in the lysosomes.

The importance of endosomal signalling has been demonstrated by a number of *in vitro* studies. Recruitment and activation of downstream signalling proteins at early endosomes has been demonstrated in EGF stimulated cells following receptor internalisation (Wang *et al*. 2002). One study showed reduced activation of downstream EGFR signalling when receptor endocytosis was inhibited (Vieira *et al*. 1996) and another showed that the subcellular localisation of EGFR during endocytosis is important for modulating cellular effects such as viability (Hyatt and Ceresa 2008). *In vivo* research examining the role and significance of endosomal signalling is more limited. A study by Schenck *et al.* in 2008 showed that endosomal regulation of Akt signalling was important for vertebrate development. Depletion of the endosomal protein Appl1 (which interacts with Akt) was shown to specifically decrease downstream activation of glycogen synthase kinase 3 (GSK3)-β while phosphorylation of tuberous sclerosis protein-2 (TSC2) was not reduced. Studies in Drosophila mutants engineered to block cargo entry into specific endosomal compartments have demonstrated that Notch must enter early endosomes to undergo cleavage and instigate signalling (Vaccari *et al*. 2008). It was suggested that diseases such as cancer and developmental disorders involving aberrant Notch signalling, may arise from, or involve, endocytic defects that impair endosomal entry of Notch.

Various molecules involved in regulating RTK endocytosis have also been implicated in cancer. Rab5 has a role in the regulating downstream integrin signalling with functional consequences for cell survival and migration (Torres *et al.* 2010). Rab7 has been shown to affect cell

survival and adhesion via coordination of the later stages of EGFR and HER2 endocytosis (Wang *et al*. 2011a).

1.2.8.2 Clathrin Independent Endocytosis

Clathrin independent pathways are most often classified according to the key proteins governing the internalisation process: caveolae-mediated endocytosis (CvME), Arf6-dependent, flotillin-1-dependent, Cdc42-dependent and RhoA-dependent endocytosis. Macropinocytosis is also considered to be a NCME and is the process by which cells engulf more substantial volumes of extracellular fluid through membrane ruffling and the formation of large macropinosome vesicles (Doherty and McMahon 2009). Of these pathways, the most relevant to RTK internalisation are CvME and macropinocytosis.

CvME is a form of raft-dependent endocytosis: oligomerised caveolin proteins assemble in microdomains (rafts) in the plasma membrane. Cholesterol accumulation in the microdomains allows membrane invagination and the formation of caveolin associated vesicles (caveosomes). Caveosome budding from the cell surface is mediated by dynamin II (Nabi and Le 2003). Caveosomes can fuse with early endosomes, linking CvME and CME pathways (Parton and Simons 2007).

Sigismund *et al.* in 2005, 2008 and 2013 published data showing that low concentrations of EGF (< 3ng/mL) lead to EGFR internalisation solely by CME but high EGF concentrations (>20 ng/mL) stimulated EGFR internalisation by CvME. These works also demonstrated that CME was

required for prolonged EGFR signalling but was not essential for receptor degradation. Contrary to these findings, however, are data from Rappaport *et al.* (2009) which showed that EGFR does not localize to caveolae either prior to or following activation.

Macropinocytosis can be induced by EGF stimulation. In response to stimulation with this growth factor, cells have been shown to produce large waves / circular dorsal ruffles which proceed inwards from the cell surface, engulfing extracellular material. This membrane ruffling is associated with dramatic reorganization of filamentous actin. In the study by Orth *et al.* (2006) ligand-induced ruffles were responsible for the sequestration and internalization of approximately half of the EGF-bound EGFR from the cell surface.

1.2.9 E3 Ligases and Breast Cancer

E3 ligases are a family of enzymes that are involved in the post-translational modification of proteins through the addition of smaller regulatory protein tags: either ubiquitin or small ubiquitin like modifiers (SUMO). The addition of an Ub or SUMO tag can alter the stability, localisation and activity of cellular proteins. Ubiquitination and sumoylation are homologous modification processes that begin with the activation of the protein tags by E1 enzymes. E1-activases adenylate Ub/SUMO at the expense of one adenosine-5'-triphosphate (ATP) molecule. This is followed by the attachment of activated Ub/SUMO to E2-conjugase proteins. Finally the tags are transferred to target proteins by E3 ligases. E3 ligases mediate formation of isopeptide bonds between

the C-terminus of Ub/SUMO tags and the internal lysines of specific substrate proteins (Mani and Gelmann 2005). The process is summarised in Figure 1-7.

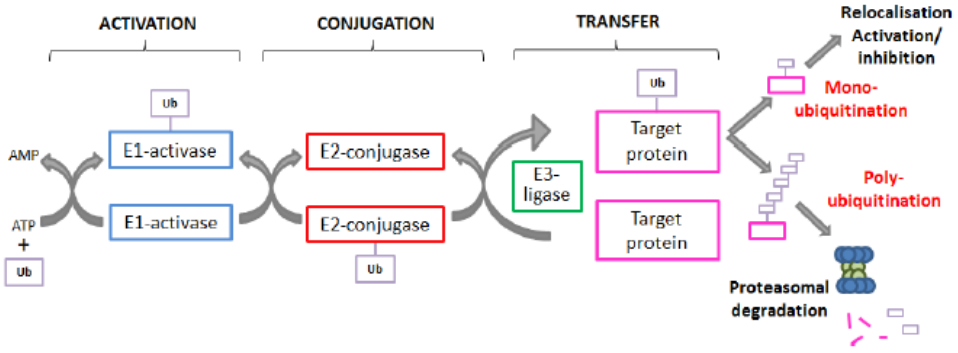

Figure 1-7: The process of ubiquitination. Ubiquitination begins with ACTIVATION of Ub by E1-activase enzymes. This is followed by CONJUGATION of Ub to E2 conjugase enzymes. E3-ligase enzymes then mediate the TRANSFER of Ub to substrate proteins. The addition of a single Ub tag (mono-ubiquitination) can influence the substrate's activity and trafficking. The addition of a chain of Ub moieties to a target protein is a signal for degradation by the 26S proteasome.

Two main classes of E3 ligase exist: the adaptor ligases and the homologous to the E6AP carboxyl terminus (HECT) type. Adaptor E3 ligases can be subdivided into those that contain: a really interesting new gene (RING) finger, a U-box, or a plant homeo domain (PHD). HECT-type E3 ligases, directly bind to E2-conjugated ubiquitin via a thioester bond before delivering the ubiquitin to a target protein. In contrast, adaptor-type E3 ligases mediate transfer of ubiquitin to the substrate protein from the E2 conjugase without actively binding to the tag (Mani and Gelmann 2005).

Dysregulation of E3 ligase expression and/or function has potentially critical consequences within the cell. Depending on the particular substrates of an E3 ligase, altered expression or functional activity could potentially result in accumulation of proto-oncoproteins and/or a reduction in tumour suppressors. A number of E3 ligases have been implicated in breast cancer including: BRCA1, RNF11, c-Cbl, Efp and breast cancer associated protein

2 (BCA2) (Burger *et al.* 2006). The importance of the latter protein in breast cancer will be discussed in more detail in section 1.3.

c-Cbl is an E3 ligase that is activated and recruited to EGFR upon ligand binding. C-Cbl has been shown to ubiquitinate activated EGFR at the plasma membrane and to remain associated with the receptor during endocytosis (de Melker *et al*. 2001). Others have shown that c-Cbl continues to ubiquitinate EGFR after internalisation (Umebayashi *et al.* 2008). Through its role in RTK ubiquitination and downregulation, loss or mutation of c-Cbl has been linked with oncogenesis (Peschard *et al*. 2001; Bao *et al.* 2003).

1.3 BCA2

Breast Cancer Associated gene 2 (BCA2) is named for the disease in which its overexpression was first identified. Differential display and subtractive hybridization screening in normal and malignant mammary cell lines revealed that BCA2 was significantly upregulated in breast cancer (Burger *et al.* 2005). Functional links between BCA2 expression and breast cancer pathology have since been suggested by *in vitro* experiments and clinical expression analyses (Brahemi *et al.* 2010; Burger *et al.* 2010).

1.3.1 The BCA2 gene

BCA2 is found on chromosome 1q21.1 (Fig. 1-8). The long arm of chromosome 1 is a region often associated with cytogenetic abnormalities in breast cancer (Bièche *et al.* 1995). An increase in 1q copy number has been reported in 55% of primary breast cancers and the

aberration is significantly correlated with positive ER status (Rennstam *et al.* 2003). It has been proposed that there may be an overlap between the breast cancers that are affected by chromosome 1 partial polysomy and those in which BCA2 is overexpressed (Burger *et al.* 2005). However, possible links between chromosome amplification and BCA2 have not been explored experimentally and so may not exist or be biologically significant. It has been reported that although gain of 1q is common in breast cancer, corresponding genetic overexpression is relatively rare. Indeed, BCA2 was not among those genes identified in a screen for overexpression correlating with 1q copy increase (Orsetti *et al.* 2006). This same study also showed that the long arm of chromosome 1 contained a number of candidate oncogenes thus if BCA2 overexpression were to be correlated with 1q gain in breast cancer, non-specific/bystander upregulation would need to be ruled out. Gene coexpression studies form part of the *in silico* research carried out as part of this project, see Chapter 3.

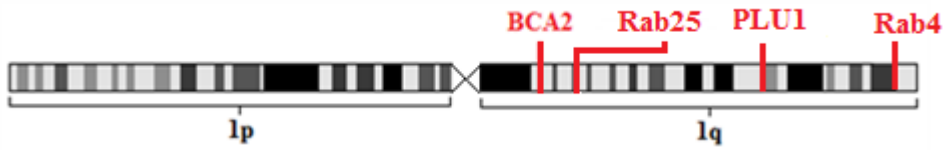

Figure 1-8: Ideogram showing the location of the BCA2 gene on chromosome 1q21.1. Also labelled are RAB25, PLU1 and Rab4, candidate oncogenes from chromosome 1 shown to be overexpressed in cancers associated with increased 1q copy number (Orsetti *et al.* 2006).

1.3.2 The BCA2 protein

The BCA2 gene codes for a 304 amino acid protein, the sequence of which is highly conserved in chordates. Key structural domains are also maintained in species from other phyla. Conserved BCA2 regions that

have been identified and explored in the literature include: a RING-H2 domain, a zinc finger, a site that is purported to be phosphorylated by Akt and residues that are autoubiquitinated (Fig. 1-9). These key domains are thought to allow BCA2 to interact with a range of other proteins and to be important for the protein's roles in cellular function and disease (Amemiya *et al.* 2008). BCA2 has a number of aliases and the majority of these relate to the protein's functional domains and interaction partners e.g. zinc finger protein 364 (ZNF364), RING finger protein 115 (RNF115) and *Rab7-interacting* RING finger *protein* (Rabring7).

No structural data has yet been obtained for BCA2 by experiment but a homology model of the RING-H2 domain has been created using the nuclear magnetic resonance (NMR) structure of an homologous protein as a template (Brahemi *et al*. 2010). The homology model was produced to enable screening for potential BCA2 inhibitors that would target the zinc co-ordinates in the RING-H2 domain. The schematic of BCA2 structural domains in Fig. 1-9 is based on this model. For further information on BCA2 as a therapeutic target see section 1.7.

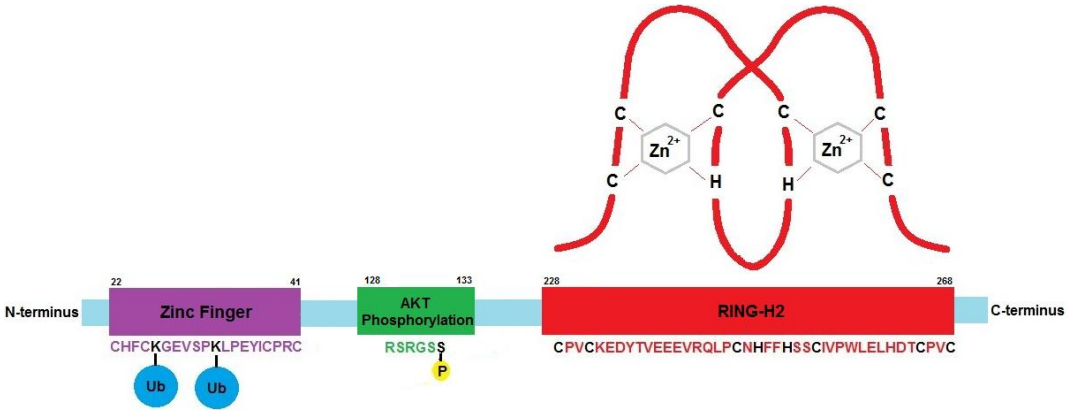

Figure 1-9: Key functional domains of the BCA2 protein. Figure complied from (Brahemi *et al.* 2010; Bacopulos *et al.* 2012).

The RING-H2 domain of BCA2 is structurally characteristic of an E3 ligase and has been shown to confer autoubiquitination functionality to the protein upon interaction with the E2-conjugase UbcH5b (Amemiya *et al.* 2008). Autoubiquitination is a typical attribute of E3 ligases and is believed to be an essential mechanism for regulating their stability in cells (Zhang and Xiong 2001; Wu *et al.* 2004) . Mutation of the critical zinc-coordinate cysteine residues in the RING-H2 domain (Fig. 1-9) abolishes BCA2's facility for autoubiquitination. As a result of reduced proteasomal targeting, RING-H2 mutant BCA2 accumulates in cells (Amemiya *et al.* 2008).

The interaction between BCA2 and Akt is potentially significant for the protein's role in apoptotic inhibition and cancer. Evidence for the existence of BCA2's Akt phosphorylation site is fairly limited. *In silico* analyses show that the internal region of BCA2 contains a consensus Akt phosphorylation site (RXRXXS) but only one experiment has shown that the phosphorylation actually occurs. The *in vitro* phosphorylation assay involved incubating recombinant BCA2 with recombinant Akt and radioisotope 32P-γATP at 37 or 4^{o}C. When the samples were separated by SDS-PAGE, radiolabelled bands signifying phospho-BCA2 (pBCA2) were only detected in the 37ºC reaction. The authors concluded that BCA2 was phosphorylated by Akt (Connor *et al.* 2005) but no further data have been published to conclusively show that the phosphorylation occurs in cells or *in vivo.* Akt activity has however been indirectly linked to BCA2 stability: cells co-transfected with GST-BCA2 and constitutively active Akt show higher levels of BCA2 protein (Bacopulos

et al. 2012). It has also been claimed that the Akt phosphorylation site (and by inference that phosphorylation of BCA2) is required for BCA2 to interact with the endocytic co-ordinator Rab7 (Burger *et al.* 2006). However, no data have been published to support this assertion.

1.4 Subcellular localisation of BCA2

Using antibodies recognising endogenous or overexpressed BCA2 reveals a high degree of variability with respect to subcellular localisation.

BCA2 localisation has variously been shown or described in the literature as:

- Nuclear (in MCF-7 cells) by Amemiya *et al.* (2008).
- Cytoplasmic and or late endosome/lysosome associated (in BHK cells) by Mizuno *et al.* (2003)
- Punctate cytoplasmic staining (MCF-7 cells) by Bacopulos *et al.* (2012)
- Faint cytoplasmic and intense nucleolar staining (in MCF-7 cells) by Kona *et al.* (2012)

The Human Protein Atlas (HPA) is an antibody-based proteomics project where antibodies are tested for determining expression and localisation of target proteins. An anti-BCA2 antibody has been screened by HPA researchers and different subcellular distributions were reported: the tested cell lines showed nucleolar and/or reticular-like staining.

From the available IF data it is very difficult to get a clear picture of the true subcellular localisation of endogenous BCA2. There appears to be a great deal of variability between and even within cell lines. The difference may reflect true biological heterogeneity or may be the result

of using different antibodies and different methods of fixing and processing the cells for IF. Since no antibodies have been suitably validated for IF, it is difficult to assess the reliability of the published localisation data. The true subcellular distribution of BCA2 therefore remains to be discovered.

1.5 BCA2 and Breast Cancer

The role of BCA2 in breast cancer was first explored in detail in a 2005 publication by Burger *et al*. A large scale tissue microarray analysis of archived samples showed that BCA2 was overexpressed in 56% of primary invasive breast cancers. Accompanying *in vitro* data indicated an oncogenic role of the protein: siRNA depletion of BCA2 significantly reduced cell growth and invasion of T47D (ER^+) breast cancer cells while overexpression of BCA2 in NIH3T3 (mouse) cells increased proliferation by 50%. Further analysis of the archived patient samples revealed that high levels of nuclear BCA2 were present in 74% of ER positive tumours and this was associated with improved disease-free survival for regional recurrence and reduced lymph node metastasis. The correlations with positive prognostic factors were thought to relate to the relationship between BCA2 and the ER rather than to reflect a tumour suppressive role of the E3 ligase. The archive studies additionally indicated that BCA2 did not affect overall survival. Survival was not examined by breast cancer subtype and this gap in our understanding still remains. More work is required to explore the relationship between BCA2 function and outcome in breast cancer.

1.5.1 BCA2 and the oestrogen receptors

BCA2 appears to have an important role in ER positive breast cancer. 74% of ER^+ breast cancers also overexpress BCA2 (Burger *et al.* 2005) but in addition to this correlative relationship, there is mounting evidence that the two proteins may be mutually regulatory. The BCA2 promoter contains multiple, ERE half-sites and the ERα has been shown by chromosome immunoprecipitation (ChIP) to bind to these elements (Kona *et al*. 2012). ChIP is a method of determining whether a protein (such as a transcription factor) binds to a particular region of the DNA. This is achieved by first cross-linking the genomic DNA and interacting proteins. The DNA is then sheared and antibody coated beads are used to extract the protein of interest. Crosslinked DNA is then eluted, purified and sequenced.

Dual luciferase reporter assays have also been used to show that protein expression downstream of the BCA2 promoter is ER-α responsive (Kona *et al*. 2012). These findings are supported by data which show that endogenous BCA2 expression is oestradiol (E2) inducible at the mRNA level by Northern blotting (NB) and at the protein level by Western blotting (WB) and immunofluorescence (IF) (Burger *et al*. 2010; Burger and Westwell 2011; Kona *et al*. 2012). Other potential transcriptional regulators of BCA2 have been found by *in silico* approaches but have not been explored experimentally. Binding sites for the following transcription factors have been predicted by bioinformatic analysis of the BCA2 promoter (Burger *et al*. 2010):

- Progesterone receptor (PR)
- NFκB
- Octamer transcription factor (OCT1)
- Activator protein 1 (AP1)
- YY1
- T3R
- Specificity protein 1 (SP1)

Further to the evidence for transcriptional regulation of BCA2 by ER-α there is also some, more speculative, data which suggest that BCA2 may have a role in the regulation of ER-α. ER-α and BCA2 have been described as co-localised in the nucleus (Burger *et al.* 2010) but interaction of the two proteins has not been demonstrated, e.g. by Förster *resonance energy transfer* (FRET) or co-immunoprecipitation (Co-IP).

The transcriptional activity of ERα is modulated by ubiquitination and by sumoylation. It has been postulated that BCA2 may sumoylate ERα as the two proteins share an interaction partner in the E2 SUMO conjugating protein Ubc9 (Burger *et al.* 2010). Ubc9 has been shown to promote activation of ER-α through sumoylation of the receptor's hinge region (Sentis S *et al.* 2005). GST pull-down experiments and dual IF have demonstrated that BCA2 and Ubc9 interact *in vitro*. The authors of the paper in which this was shown suggested that BCA2 may therefore be involved in a reciprocal regulatory loop with ER-α but this remains unproven (Burger *et al.* 2010).

1.5.2 BCA2 and Receptor Tyrosine Kinase Endocytosis

BCA2 has been shown in three publications to affect the endocytic degradation of EGFR. The first paper to explore the role of BCA2 in EGFR trafficking was published in 2003 by Mizuno *et al.* BCA2 was identified as a Rab7 binding partner by Cytotrap screening and

subsequent investigations demonstrated that Rab7 interacted with the N-terminus of BCA2. The data from the *in vitro* studies suggested that the BCA2 was recruited to the late endosomes and lysosomes by the GTP-bound (active) form of Rab7. The recruitment caused perinuclear aggregation of late endolysosomes and resulted in impaired EGF degradation. The effects were shown by co-transfection of His-BCA2 and EGFP-Rab7 (and Rab7 mutants) into baby hamster kidney (BHK) cells. IF-microscopy analysis was performed to visualise the co-localisation and re-localisation effects. EGF degradation was measured using a trichloroacetic acid (TCA) assay with ^{125}I-labelled EGF. Although the experiments were all performed in BCA2 and Rab7 overexpressing systems, the data suggested that BCA2 may be an important regulator of EGFR trafficking. A hypothesis to explain the effects may be that BCA2 competitively inhibits Rab7-mediated delivery of vacuolar ATPase to the lysosomes. This might then lead to the altered lysosomal pH and localization shown in the study (Mizuno *et al.* 2003).

Interestingly in 2007 the same research group published a second, seemingly contradictory, article in which BCA2 was suggested to have the opposite effect on EGFR degradation. In experiments with human embryonic kidney (HEK293) cells, Sakane *et al.* (2007) showed that BCA2 promoted ligand-induced EGFR degradation. Again a BCA2 overexpression system was used but this time EGFR was also exogenously introduced by transfection. Degradation was measured by immunoprecipitation (IP) and WB. The data showed that after one and three hours of EGF treatment, the levels of EGFR were reduced in BCA2

over-expressing HEK293 cells compared with mock-transfected controls, though the difference was slight. In cells cotransfected with BCA2, EGFR, c-Cbl and ubiquitin however BCA2 *inhibited* EGFR degradation.

A study published in 2013 by (Smith *et al.*) examined the relationship between BCA2 and EGFR trafficking by shRNA depletion of BCA2 in HeLa cervical cancer cells . Data were presented that showed BCA2 promoted EGFR and c-Met degradation. IP and WB data showed that level of EGFR and phosphorylated (pEGFR) in EGF-stimulated HeLa remained higher in BCA2 depleted cells at 30 min compared with controls. By 60 min however EGFR levels were comparable between the two groups. The study also incorporated Co-IP which demonstrated that BCA2 could directly interact with EGFR *in vitro* and that this interaction was dependent on c-Cbl. BCA2 was also shown to ubiquitinate EGFR, notable because this is the first documented substrate of BCA2's E3 ligase activity. Other key data from the paper include microscopy which shows that a) the number of multivesicular bodies (MVBs) was reduced in BCA2 depleted cells and b) that BCA2 depletion caused EGFR to accumulate in late endolysosomal compartments.

The relationship between BCA2 and EGFR endocytosis and downregulation is clearly complex. More work is needed to fully elucidate the effects of BCA2 on EGFR biology and the mechanism/s behind them.

1.6 Other interaction partners of BCA2

BCA2 has been shown to interact with a number of other proteins including: 14-3-3σ, hHR23a, MM-1 and tetherin (Miyakawa *et al.* 2009; Bacopulos *et al.* 2012; Narita *et al.* 2012)

14-3-3σ is a tumour suppressor and positive regulator of p53 that acts by antagonising ubiquitination of p53 by Mdm2. It has been shown to interact with BCA2 via a conserved binding site between amino acids 133 and 140 (SRPDRSPS). Transfection of increasing quantities of plasmid encoding BCA2 into cells with fixed amounts of a plasmid for 14-3-3σ indicated that BCA2 may negatively regulate the tumour suppressor. Levels of 14-3-3σ were progressively depleted in response to increasingly overexpressed BCA2 and authors suggested that 14-3-3σ may therefore be a substrate of BCA2's E3 ligase activity (Bacopulos *et al.* 2012)

hHR23a (the human homolog of rad23) is a DNA repair protein that can also abrogate proteasomal degradation of proteins by inhibiting the formation of polyubiquitin chains (Ortolan *et al.* 2000). hHR23a has been shown to prevent BCA2 autoubiquitination and to promote its cellular stability (Bacopulos *et al.* 2012)

Tetherin, also known as BST-2 is a lipid raft associated, transmembrane protein that is involved in the interferon dependent antiviral response pathway (Van Damme *et al.* 2008). Tetherin restricts the budding of virions from human immunodeficiency virus (HIV) infected cells. Overexpression of BCA2 in tetherin positive HeLa cells has been shown

to promote tetherin-mediated inhibition of HIV particle release. This was also supported by co-transfection of BCA2 and tetherin in negative HOS cells where the BCA2-tetherin interaction promoted HIV restriction. BCA2 was also shown to promote trafficking of the unreleased, intracellular HIV particles to the lysosomes for degradation (Miyakawa *et al.* 2009). More recently BCA2 has also demonstrated tetherin-independent anti-viral activity which it exerts by promoting ubiquitination and lysosomal degradation of HIV-1 gag, inhibiting virus particle assembly and release (Nityanandam, and Serra-Moreno 2014).

BCA2 has been shown to form a complex with, and to mono-ubiquitinate, a c-myc binding protein MM-1. Monoubiquitination of MM-1 by BCA2 appears to downregulate c-myc and reduce cellular proliferation. The proposed model states that when levels of c-myc are raised, BCA2 binds to MM-1 which is then monoubiquitinated. The Ub tag causes the complex to translocate to the nucleus where it binds to c-myc. c-myc is then poly-ubiquitinated by BCA2's E3 ligase activity and is degraded by the proteasome. The reduced cellular proliferation reported in BCA2 transfected cells was thought to relate to reduced expression of c-myc regulated genes that promote cell cycle progression such as cyclin D1 (Narita *et al.* 2012).

1.7 BCA2 as a zinc binding protein and therapeutic target

Disulfiram (DSF) is a zinc-ejecting agent that has been suggested to have selective activity against BCA2 overexpressing breast cancer cells (Brahemi *et al*. 2010). It has been proposed that DSF can inhibit BCA2

by modifying cysteine residues and expelling zinc from the RING-H2 domain (Fig. 1-9).

The therapeutic potential of targeting BCA2 has been demonstrated in siRNA depletion experiments which show decreased proliferation in cells with diminished BCA2 levels (Burger *et al*. 2005). DSF has shown micromolar activity against high BCA2 expressing MCF-7 breast cancer cells. Putative BCA2 negative/low MDA-MB-231 cells become sensitised to DSF when transfected with ER-α to induce BCA2 expression (Brahemi *et al.* 2010). Experiments conducted as part of this project and a co-running Cancer Research Wales project suggest the cytotoxic effect may pertain to altered intracellular zinc levels and endolysosomal function rather than BCA2 expression (Wiggins *et al.* 2014, 2015).

Overall there is fairly limited evidence to support the use of DSF as a specific inhibitor of BCA2 (Brahemi *et al*. 2010). Overexpression of ER-α in the "triple negative" cell line MDA-MB-231 may have conferred DSF sensitivity to the cells but this is not necessarily an effect mediated by BCA2. Expression of ER-α in MDA-MB-231 cells has been shown by others to induce upregulation of many genes associated with cell proliferation and survival e.g. hepatoma-derived growth factor, insulin-like growth factor binding proteins 1 and 3 and the cytokine interleukin 7R-α (Levenson *et al.* 2002). In the study by Brahemi *et al*. (2010) DSF sensitivity may have been conferred to the MDA-MB-231/ER-α cells by upregulation of one or a combination of many other ER regulated genes. The effect of ER-α induced DSF sensitivity cannot therefore conclusively

be attributed to BCA2. There may be greater therapeutic potential in targeting BCA2 with DSF analogues structurally tailored to specifically inhibit BCA2, indeed such drugs showed greater anti-breast cancer efficacy than DSF in the Brahemi *et al.* studies. Despite this, DSF is a more appealing potential cancer treatment since it is already available as an aldehyde dehydrogenase 1 (ALDH1) inhibitor for the treatment of alcohol dependence. DSF toxicity/side effects are extremely rare so should efficacy be supported by research, patients could begin receiving DSF much sooner than would be possible with a new drug. A caveat to this however is that the specificity of DSF is poor: DSF has been shown to affect a number of cellular proteins including vATPase and β-tubulin though the effects were seen at higher concentrations than used in our experiments (Potchoo *et al.* 1986; Johnson *et al.* 2010).

The well documented effect of DSF on ALDH1 may actually be a mechanism that could be exploited in breast cancer treatment. Mammary cancer stem cells have been shown to express significantly elevated levels of ALDH1 and therefore may be more sensitive to its inhibition (Charafe-Jauffret *et al.* 2010). ALDH1 inhibition has been shown to reduce the chemo- and radiotherapeutic resistance of a stem-like population of breast cancer cells (Croker and Allan 2012). DSF may present an effective, inexpensive and minimally toxic adjuvant to standard breast cancer therapies.

1.8 Hypothesis

There is a need for further research to explore BCA2's role in EGFR endocytosis, downregulation and signalling, particularly with consideration of cellular context in data analysis and interpretation. There is also a need to examine the effects of BCA2 on breast cancer survival in different disease subtypes, again to explore possible context-dependent effects that may help to explain some of the current conflict in the literature with regard to BCA2 function and pathology.

The hypothesis for this study is:

BCA2 plays an important role in breast cancer development and progression involving its effects on EGFR trafficking.

1.9 AIMS

The overall purpose of this project is to extend the body of existing BCA2 knowledge and to resolve some of the apparent conflict in the current literature. This will be achieved by meeting the following key aims:

- **Investigate the role of BCA2 in breast cancer development, progression, resistance and prognosis. This will include exploration of links with breast cancer subtypes, ErbB expression and signalling and additional analyses of co-expressed genes.**
- **Determine the subcellular localisation of BCA2**
- **Describe the role of BCA2 in EGFR endocytosis and signalling**

1.10 References

Amemiya, Y., Azmi, P. and Seth, A. 2008. Autoubiquitination of BCA2 RING E3 ligase regulates its own stability and affects cell migration. *Molecular Cancer Research* 6(9), p. 1385.

Anderson, W. F., Chatterjee, N., Ershler, W. B. and Brawley, O. W. 2002. Estrogen receptor breast cancer phenotypes in the Surveillance, Epidemiology, and End Results database. *Breast Cancer Research and Treatment* 76(1), p. 27-36.

Bacopulos, S., Amemiya, Y., Yang, W., Zubovits, J., Burger, A., Yaffe, M. and Seth, A. K. 2012. Effects of partner proteins on BCA2 RING ligase activity. *BMC Cancer* 12(1), p. 63.

Bao, J., Gur, G. and Yarden, Y. 2003. Src promotes destruction of c-Cbl: implications for oncogenic synergy between Src and growth factor receptors. *Proceedings of the National Academy of Sciences* 100(5), p. 2438-43.

Ben-Kasus, T., Schechter, B., Lavi, S., Yarden, Y. and Sela, M. 2009. Persistent elimination of ErbB-2/HER2-overexpressing tumors using combinations of monoclonal antibodies: relevance of receptor endocytosis. *Proceedings of the National Academy of Sciences* 106(9), p. 3294-9.

Berman, J. 2004. Tumor classification: molecular analysis meets Aristotle. *BMC Cancer* 4(1), p. 10.

Bertram, J. S. 2000. The molecular biology of cancer. *Molecular Aspects of Medicine* 21(6), p. 167-223.

Bièche, I., Champème, M. H. and Lidereau, R. 1995. Loss and gain of distinct regions of chromosome 1q in primary breast cancer. *Clinical Cancer Research* 1(1), p. 123-7.

Bouyain, S., Longo, P.A., Li, S., Ferguson, K.M. and Leahy, D.J. 2005. The extracellular region of ErbB4 adopts a tethered conformation in the absence of ligand. *Proceedings of the National Academy of Sciences* 102(42), p. 15024-9.

Brahemi, G., Kona, F. R., Fiasella, A., Buac, D., Soukupová, J., Brancale, A., Burger, A. M. and Westwell, A. D. 2010. Exploring the structural requirements for inhibition of the ubiquitin E3 ligase breast cancer associated protein 2 (BCA2) as a treatment for breast cancer. *Journal of Medicinal Chemistry* 53(7), p. 2757-65.

Brenner, G. M. and Stevens, C. W. 2013. *Pharmacology*. 4th edition ed. Philadelphia, PA (USA): Elsevier Saunders.

Bucci, C., Thomsen, P., Nicoziani, P., McCarthy, J. and van Deurs, B. 2000. Rab7: a key to lysosome biogenesis. *Molecular Biology of the Cell* 11(2), p. 467-80.

Bunone, G., Briand, P., Miksicek, R. and Picard, D. 1996. Activation of the unliganded estrogen receptor by EGF involves the MAP kinase pathway and direct phosphorylation. *The EMBO Journal* 15(9), p. 2174.

Burger, A., Amemiya, Y., Kitching, R. and Seth, A. K. 2006. Novel RING E3 ubiquitin ligases in breast cancer. *Neoplasia (New York, NY)* 8(8), p. 689.

Burger, A. and Westwell. 2011. Anti-cancer therapeutic agents. WO Patent WO/2011/097,218.

Burger, A. M., Gao, Y., Amemiya, Y., Kahn, H. J., Kitching, R. , Yang, Y., Sun, P., Narod, S. A., Hanna, W. M. and Seth, A. K. 2005. A novel RING-type ubiquitin ligase breast cancer-associated gene 2 correlates with outcome in invasive breast cancer. *Cancer Research* 65(22), p. 10401.

Burger, A. M., Kona, F., Amemiya, Y., Gao, Y., Bacopulos, S. and Seth, A. K. 2010. Role of the BCA2 ubiquitin E3 ligase in hormone responsive breast cancer. *The Open Cancer Journal* 3(1), p. 116.

Butt, A. J., McNeil, C. M., Musgrove, E. A. and Sutherland, R. L. 2005. Downstream targets of growth factor and oestrogen signalling and endocrine resistance: the potential roles of c-Myc, cyclin D1 and cyclin E. *Endocrine-Related Cancer* 12(Supplement 1), pp. S47-S59.

Cerqueira, N. M., Fernandes, P. A. and Ramos, M. J. 2007. Understanding ribonucleotide reductase inactivation by gemcitabine. *Chemistry-A European Journal* 13(30), p. 8507-15.

Charafe-Jauffret, E., Ginestier, C., Iovino, F.,Tarpin, C., Diebel, M., Esterni, B., Houvenaeghel, G., Extra, J. M., Bertucci, F. and Jacquemier, J. 2010. Aldehyde dehydrogenase 1–positive cancer stem cells mediate metastasis and poor clinical outcome in inflammatory breast cancer. *Clinical Cancer Research* 16(1), p. 45-55.

Chen, S. and Parmigiani, G. 2007. Meta-analysis of BRCA1 and BRCA2 penetrance. *Journal of Clinical Oncology* 25(11), p. 1329-33.

Coleman, M. P., Quaresma, M., Berrino, F., Lutz, J. M., De Angelis, R., Capocaccia, R., Baili, P., Rachet, B., Gatta, G. and Hakulinen, T. 2008. Cancer survival in five continents: a worldwide population-based study (CONCORD). *The Lancet Oncology* 9(8), p. 730-56.

Connor, M. K., Azmi, P. B., Subramaniam, V., Li, H. and Seth, A. 2005. Molecular characterization of ring finger protein 11. *Molecular Cancer Research* 3(8), p. 453.

Cortese, K., Howes, M.T., Lundmark, R., Tagliatti, E., Bagnato, P., Petrelli, A., Bono, M., McMahon, H.T., Parton, R.G. and Tacchetti, C. 2013. The HSP90 inhibitor geldanamycin perturbs endosomal structure and drives recycling ErbB2 and transferrin to modified MVBs/lysosomal compartments.*Molecular Biology of the Cell* 24, p. 129–44.

Croker, A. K. and Allan, A. L. 2012. Inhibition of aldehyde dehydrogenase (ALDH) activity reduces chemotherapy and radiation resistance of stem-like ALDHhiCD44+ human breast cancer cells. *Breast Cancer Research and Treatment* 133(1), p. 75-87.

CRUK. 2011. *Breast Cancer* [Online]. Available at: http://info.cancerresearchuk.org/cancerstats/types/breast/ [Accessed: 30th April 2012].

Cuello, M., Ettenberg, S. A., Clark, A. S., Keane, M. M., Posner, R. H., Nau, M. M., Dennis, P. A. and Lipkowitz, S. 2001. Down-regulation of the erbB-2 receptor by trastuzumab (herceptin) enhances tumor necrosis factor-related apoptosis-inducing ligand-

mediated apoptosis in breast and ovarian cancer cell lines that overexpress erbB-2. *Cancer Research* 61(12), p. 4892-4900.

Dauvois, S., White, R. and Parker, M. G. 1993. The antiestrogen ICI 182780 disrupts estrogen receptor nucleocytoplasmic shuttling. *Journal of Cell Science* 106(4), p. 1377-88.

de Melker, A. A., van der Horst, G., Calafat, J., Jansen, H. and Borst, J. 2001. c-Cbl ubiquitinates the EGF receptor at the plasma membrane and remains receptor associated throughout the endocytic route. *Journal of Cell Science* 114(11), p. 2167-78.

Doherty, G. J. and McMahon, H. T. 2009. Mechanisms of endocytosis. *Annual Review of Biochemistry* 78, p. 857-902.

Doisneau-Sixou, S., Sergio, C., Carroll, J., Hui, R., Musgrove, E. and Sutherland, R. 2003. Estrogen and antiestrogen regulation of cell cycle progression in breast cancer cells. *Endocrine-Related Cancer* 10(2), p. 179-86.

Dormand, E. L., Banwell, P. E. and Goodacre, T. E. E. 2005. Radiotherapy and wound healing. *International Wound Journal* 2(2), pp. 112-27.

Driggers, P. H. and Segars, J. H. 2002. Estrogen action and cytoplasmic signaling pathways. Part II: the role of growth factors and phosphorylation in estrogen signaling. *Trends in Endocrinology & Metabolism* 13(10), p. 422-7.

Elston, C. and Ellis, I. 1991. Pathological prognostic factors in breast cancer. I. The value of histological grade in breast cancer: experience from a large study with long-term follow-up. *Histopathology* 19(5), p. 403-10.

Fawell, S. E., White, R., Hoare, S., Sydenham, M., Page, M. and Parker, M. G. 1990. Inhibition of estrogen receptor-DNA binding by the" pure" antiestrogen ICI 164,384 appears to be mediated by impaired receptor dimerization. *Proceedings of the National Academy of Sciences* 87(17), p. 6883-7.

Fentiman, I. S., Fourquet, A. and Hortobagyi, G. N. 2006. Male breast cancer. *The Lancet* 367(9510), p. 595-604.

Ferlay, J., Soerjomataram, I., Ervik, M., Dikshit, R., Eser, S., Mathers, C., Rebelo, M., DM, P., Forman, D. and Bray, F. 2013. GLOBOCAN 2012 v1.0, Cancer Incidence and Mortality Worldwide: IARC CancerBase No. 11 [Internet]. Lyon, France: International Agency for Research on Cancer.

Fidler, I. J. 2003. The pathogenesis of cancer metastasis: the 'seed and soil'hypothesis revisited. *Nature Reviews Cancer* 3(6), p. 453-8.

Friedman, L. M., Rinon, A., Schechter, B., Lyass, L., Lavi, S., Bacus, S. S., Sela, M. and Yarden, Y. 2005. Synergistic down-regulation of receptor tyrosine kinases by combinations of mAbs: implications for cancer immunotherapy. *Proceedings of the National Academy of Sciences of the United States of America* 102(6), p. 1915-20.

Galea, M.H., Blamey, R.W., Elston, C.E. and Ellis, I. 1992. The Nottingham Prognostic Index in primary breast cancer. *Breast Cancer Research & Treatment* 22(3), p.207-19

Gee, J., Robertson, J., Gutteridge, E., Ellis, I., Pinder, S., Rubini, M., and Nicholson, R. 2005. Epidermal growth factor receptor/HER2/insulin-like growth factor receptor signalling and oestrogen receptor activity in clinical breast cancer. *Endocrine-Related Cancer* 12(Supplement 1), p. S99-S111.

Gionet, N., Jansson, D., Mader, S. and Pratt, M. 2009. NF-κB and estrogen receptor α interactions: Differential function in estrogen receptor-negative and-positive hormone-independent breast cancer cells. *Journal of Cellular Biochemistry* 107(3), p. 448-59.

Gómez-Raposo, C., Zambrana Tévar, F., Sereno Moyano, M., López Gómez, M. and Casado, E. 2010. Male breast cancer. *Cancer Treatment Reviews* 36(6), p. 451-7.

Hall, J. M. and McDonnell, D. P. 1999. The estrogen receptor beta-isoform (ERbeta) of the human estrogen receptor modulates ERalpha transcriptional activity and is a key regulator of the cellular response to estrogens and antiestrogens. *Endocrinology* 140(12), p. 5566-78.

Harris, R.C., Chung, E. and Coffey, R.J. 2003. EGF receptor ligands. *Experimental Cell Research* 284(1), p. 2-13.

Henderson, I. C. 2006. Risk factors for breast cancer development. *Cancer* 71(S6), p. 2127-40.

Hommelgaard, A. M., Lerdrup, M. and van Deurs, B. 2004. Association with membrane protrusions makes ErbB2 an internalization-resistant receptor. *Molecular Biology of the Cell* 15(4), p. 1557-67.

Hopper-Borge, E. A., Nasto, R. E., Ratushny, V., Weiner, L. M., Golemis, E. A. and Astsaturov, I. 2009. Mechanisms of tumor resistance to EGFR-targeted therapies. *Expert Opinion on Theraputic Targets* 13(3), p. 339-62.

Howell, A., Cuzick, J., Baum, M., Buzdar, A., Dowsett, M., Forbes, J. F., Hoctin-Boes, G., Houghton, J., Locker, G. and Tobias, J. 2005. Results of the ATAC (Arimidex, Tamoxifen, Alone or in Combination) trial after completion of 5 years' adjuvant treatment for breast cancer. *Lancet* 365(9453), p. 60-2.

Hyatt, D. C. and Ceresa, B. P. 2008. Cellular localization of the activated EGFR determines its effect on cell growth in MDA-MB-468 cells. *Experimental Cell Research* 314(18), p. 3415-25.

IARC. 2008. World Cancer Report. [Online]. Available at: http://www.iarc.fr/en/publications/pdfs-online/wcr/2008/ index.php [Accessed: 20th October 2011].

Iozzo, R.V., Moscatello, D.K., McQuillan, D.J. and Eichstetter, I.1999. Decorin is a biological ligand for the epidermal growth factor receptor. *Journal of Biological Chemistry* 274(8), p.4489-92.

Izumi, Y., Xu, L., di Tomaso, E., Fukumura, D. and Jain, R. K. 2002. Tumour biology: herceptin acts as an anti-angiogenic cocktail. *Nature* 416(6878), p. 279-80.

Janka, T., Johannes, H., Michael, K., Martin, E. and Svenja, M. 2010. Gene expression analysis after receptor tyrosine kinase activation reveals new potential melanoma proteins. *BMC Cancer* 10, p. 386.

Johnson, R. M., Allen, C., Melman, S. D., Waller, A., Young, S. M., Sklar, L. A. and Parra, K. J. 2010. Identification of inhibitors of

vacuolar proton-translocating ATPase pumps in yeast by high-throughput screening flow cytometry. *Analytical Biochemistry* 398(2), p. 203-11.

Jovic, M., Sharma, M., Rahajeng, J. and Caplan, S. 2010. The early endosome: a busy sorting station for proteins at the crossroads. *Histology and Histopathology* 25(1), p. 99.

Kato, S., Endoh, H., Masuhiro, Y., Kitamoto, T., Uchiyama, S., Sasaki, H., Masushige, S., Gotoh, Y., Nishida, E. and Kawashima, H. 1995. Activation of the estrogen receptor through phosphorylation by mitogen-activated protein kinase. *Science* 270(5241), p. 1491-4.

Katzmann, D. J., Odorizzi, G. and Emr, S. D. 2002. Receptor downregulation and multivesicular-body sorting. *Nature reviews Molecular Cell Biology* 3(12), p. 893-905.

Khadim, M., Eastwood, P., Price, J., Morrison, P. and Khan, K. 2013. Multidisciplinary one-stage risk-reducing gynaecological and breast surgery with immediate reconstruction in BRCA-gene carrier women. *European Journal of Surgical Oncology (EJSO)* 39(12), p. 1346-50.

Kona, F. R., Stark, K., Bisoski, L., Buac, D., Cui, Q. and Dou, Q. P. 2012. Transcriptional activation of breast cancer-associated gene 2 by estrogen receptor. *Breast Cancer Research and Treatment*, p. 1-9.

Lane, H., Motoyama, A., Beuvink, I. and Hynes, N. 2001. Modulation of p27/Cdk2 complex formation through 4D5-mediated inhibition of HER2 receptor signaling. *Annals of Oncology* 12(suppl 1), p. S21-S22.

Lengyel, E., Prechtel, D., Resau, J. H., Gauger, K., Welk, A., Lindemann, K., Salanti, G., Richter, T., Knudsen, B. and Vande Woude, G. F. 2005. C-Met overexpression in node-positive breast cancer identifies patients with poor clinical outcome independent of Her2/neu. *International Journal of Cancer* 113(4), p. 678-82.

Levenson, A. S., Svoboda, K. M., Pease, K. M., Kaiser, S. A., Chen, B., Simons, L. A., Jovanovic, B. D., Dyck, P. A. and Jordan, V. C. 2002. Gene expression profiles with activation of the estrogen receptor α-selective estrogen receptor modulator complex in breast cancer cells expressing wild-type estrogen receptor. *Cancer Research* 62(15), p. 4419-26.

Lin, N.U. and Winer, E.P. 2004. New targets for therapy in breast cancer: small molecule tyrosine kinase inhibitors. *Breast Cancer Research* 6(5), p. 204-10.

Mani, A. and Gelmann, E. P. 2005. The ubiquitin-proteasome pathway and its role in cancer. *Journal of Clinical Oncology* 23(21), p. 4776-89.

Martin, M. B., Franke, T. F., Stoica, G. E., Chambon, P., Katzenellenbogen, B. S., Stoica, B. A., McLemore, M. S., Olivo, S. E. and Stoica, A. 2000. A Role for Akt in mediating the estrogenic functions of Epidermal Growth Factor and Insulin-Like Growth Factor I 1. *Endocrinology* 141(12), p. 4503-11.

McDonnell, D. P. and Norris, J. D. 2002. Connections and regulation of the human estrogen receptor. *Science's STKE* 296(5573), p. 1642.

McLauchlan, H., Newell, J., Morrice, N., Osborne, A., West, M. and Smythe, E. 1998. A novel role for Rab5–GDI in ligand sequestration into clathrin-coated pits. *Current Biology* 8(1), p. 34-45.

McPherson, K., Steel, C. and Dixon, J. 2000. ABC of breast diseases: breast cancer—epidemiology, risk factors, and genetics. *British Medical Journal* 321(7261), p. 624.

Miyakawa, K., Ryo, A., Murakami, T., Ohba, K., Yamaoka, S., Fukuda, M., Guatelli, J. and Yamamoto, N. 2009. BCA2/Rabring7 promotes tetherin-dependent HIV-1 restriction. *PLoS Pathogens* 5(12), p. e1000700.

Mizuno, K., Kitamura, A. and Sasaki, T. 2003. Rabring7, a novel Rab7 target protein with a RING finger motif. *Molecular Biology of the Cell* 14(9), p. 3741-52.

Morris, C. and Wakeling, A. 2002. Fulvestrant ('Faslodex')--a new treatment option for patients progressing on prior endocrine therapy. *Endocrine-Related Cancer* 9(4), p. 267-76.

Musgrove, E. A. and Sutherland, R. L. 2009. Biological determinants of endocrine resistance in breast cancer. *Nature Reviews Cancer* 9(9), p. 631-43.

Nabi, I. R. and Le, P. U. 2003. Caveolae/raft-dependent endocytosis. *The Journal of Cell Biology* 161(4), p. 673-7.

Nagata, Y., Lan, K.-H., Zhou, X., Tan, M., Esteva, F. J., Sahin, A. A., Klos, K. S., Li, P., Monia, B. P. and Nguyen, N. T. 2004. PTEN activation contributes to tumor inhibition by trastuzumab, and loss of PTEN predicts trastuzumab resistance in patients. *Cancer Cell* 6(2), p. 117-27.

Nahta, R. and Esteva, F.J. 2006. HER2 therapy: Molecular mechanisms of trastuzumab resistance. Breast Cancer Research 8, p.215.

Nanda, R. 2007. Targeting the human epidermal growth factor receptor 2 (HER2) in the treatment of breast cancer: recent advances and future directions. *Reviews on Recent Clinical Trials* 2(2), p. 111-6.

Narita, R., Kitaura, H., Torii, A., Tashiro, E., Miyazawa, M., Ariga, H. and Iguchi-Ariga, S. M. M. 2012. Rabring7 degrades c-Myc through complex formation with MM-1. *PloS One* 7(7), p. e41891.

NICE. 2011. Fulvestrant for the treatment of locally advanced or metastatic breast cancer. NICE technology appraisals [TA239].

Nicholson, R., Hutcheson, I., Jones, H., Hiscox, S., Giles, M., Taylor, K. and Gee, J. M. W. 2007. Growth factor signalling in endocrine and anti-growth factor resistant breast cancer. *Reviews in Endocrine & Metabolic Disorders* 8(3), p. 241-53.

Nilsson, S., Koehler, K. F. and Gustafsson, J.-Å. 2011. Development of subtype-selective oestrogen receptor-based therapeutics. *Nature Reviews Drug Discovery* 10(10), p. 778-92.

Nishimura, Y., Bereczky, B. and Ono, M. 2007. The EGFR inhibitor gefitinib suppresses ligand-stimulated endocytosis of EGFR via the early/late endocytic pathway in non-small cell lung cancer cell lines. *Histochemistry and Cell Biology* 127(5), p. 541-53.

Nityanandam, R, and Serra-Moreno, R. 2014. BCA2/Rabring7 targets HIV-1 Gag for lysosomal degradation in a tetherin-independent manner. *PLoS Pathogens* 10(5), e1004151

Normanno, N., Morabito, A., De Luca, A., Piccirillo, M. C., Gallo, M., Maiello, M. R. and Perrone, F. 2009. Target-based therapies in breast cancer: current status and future perspectives. *Endocrine-Related Cancer* 16(3), p. 675-702.

Oelkers, W. K. H. 1996. Effects of estrogens and progestogens on the renin-aldosterone system and blood pressure. *Steroids* 61(4), p. 166-171.

Ono, M., Hirata, A., Kometani, T., Miyagawa, M., Ueda, S.-i., Kinoshita, H., Fujii, T. and Kuwano, M. 2004. Sensitivity to gefitinib (Iressa, ZD1839) in non-small cell lung cancer cell lines correlates with dependence on the epidermal growth factor (EGF) receptor/extracellular signal-regulated kinase 1/2 and EGF receptor/Akt pathway for proliferation. *Molecular Cancer Therapeutics* 3(4), p. 465-72.

Orsetti, B., Nugoli, M., Cervera, N., Lasorsa, L., Chuchana, P., Rougé, C., Ursule, L., Nguyen, C., Bibeau, F. and Rodriguez, C. 2006. Genetic profiling of chromosome 1 in breast cancer: mapping of regions of gains and losses and identification of candidate genes on 1q. *British Journal of Cancer* 95(10), p. 1439-47.

Orth, J. D., Krueger, E. W., Weller, S. G. and McNiven, M. A. 2006. A novel endocytic mechanism of epidermal growth factor receptor sequestration and internalization. *Cancer Research* 66(7), p. 3603.

Ortolan, T. G., Tongaonkar, P., Lambertson, D., Chen, L., Schauber, C. and Madura, K. 2000. The DNA repair protein Rad23 is a negative regulator of multi-ubiquitin chain assembly. *Nature Cell Biology* 2(9), p. 601-8.

Osborne, C., Pippen, J., Jones, S., Parker, L., Ellis, M., Come, S., Gertler, S., May, J., Burton, G. and Dimery, I. 2002. Double-blind, randomized trial comparing the efficacy and tolerability of fulvestrant versus anastrozole in postmenopausal women with advanced breast cancer progressing on prior endocrine therapy: results of a North American trial. *Journal of Clinical Oncology* 20(16), p. 3386-95.

Osborne, C. K., Coronado-Heinsohn, E. B., Hilsenbeck, S. G., McCue, B. L., Wakeling, A. E., McCleland, R. A., Manning, D. L. and Nicholson, R. I. 1995. Comparison of the effects of a pure steroidal antiestrogen with those of tamoxifen in a model of human

breast cancer. *Journal of the National Cancer Institute* 87(10), p. 746-50.

Parton, R. G. and Simons, K. 2007. The multiple faces of caveolae. *Nature reviews Molecular Cell Biology* 8(3), p. 185-94.

Peschard, P., Fournier, T. M., Lamorte, L., Naujokas, M. A., Band, H., Langdon, W. Y. and Park, M. 2001. Mutation of the c-Cbl TKB domain binding site on the Met receptor tyrosine kinase converts it into a transforming protein. *Molecular Cell* 8(5), p. 995-1004.

Piccirillo, J. F. and Feinstein, A. R. 1996. Clinical symptoms and comorbidity: significance for the prognostic classification of cancer. *Cancer* 77(5), p. 834-42.

Pietras, R., Fendly, B., Chazin, V., Pegram, M., Howell, S. and Slamon, D. 1994. Antibody to HER-2/neu receptor blocks DNA repair after cisplatin in human breast and ovarian cancer cells. *Oncogene* 9(7), p. 1829-38.

Pietras, R. J., Poen, J. C., Gallardo, D., Wongvipat, P. N., Lee, H. J. and Slamon, D. J. 1999. Monoclonal antibody to HER-2/neureceptor modulates repair of radiation-induced DNA damage and enhances radiosensitivity of human breast cancer cells overexpressing this oncogene. *Cancer Research* 59(6), p. 1347-55.

Potchoo, Y., Braguer, D., Peyrot, V., Chauvet-Monges, A., Sari, J. and Crevat, A. 1986. In vitro inhibition of microtubule assembly by disulfiram. *International Journal of Clinical Pharmacology, Therapy, and Toxicology* 24(9), p. 499.

Raiborg, C. and Stenmark, H. 2009. The ESCRT machinery in endosomal sorting of ubiquitylated membrane proteins. *Nature* 458(7237), p. 445-52.

Raisz, L. G. 1999. Physiology and pathophysiology of bone remodeling. *Clinical Chemistry* 45(8), p. 1353-8.

Rakha, E. A., Reis-Filho, J. S., Baehner, F., Dabbs, D. J., Decker, T., Eusebi, V., Fox, S. B., Ichihara, S., Jacquemier, J. and Lakhani, S. R. 2010. Breast cancer prognostic classification in the molecular era: the role of histological grade. *Breast Cancer Research* 12(4), p. 207.

Rappoport, J. Z. and Simon, S. M. 2009. Endocytic trafficking of activated EGFR is AP-2 dependent and occurs through preformed clathrin spots. *Journal of Cell Science* 122(9), p. 1301-5.

Razandi, M., Oh, P., Pedram, A., Schnitzer, J. and Levin, E. R. 2002. ERs associate with and regulate the production of caveolin: implications for signaling and cellular actions. *Molecular Endocrinology* 16(1), p. 100-15.

Razandi, M., Pedram, A., Park, S. T. and Levin, E. R. 2003. Proximal events in signaling by plasma membrane estrogen receptors. *Journal of Biological Chemistry* 278(4), p. 2701-12.

Rennstam, K., Ahlstedt-Soini, M., Baldetorp, B., Bendahl, P. O., Borg, Å., Karhu, R., Tanner, M., Tirkkonen, M. and Isola, J. 2003. Patterns of chromosomal imbalances defines subgroups of breast cancer with distinct clinical features and prognosis. A study of 305 tumors by comparative genomic hybridization. *Cancer Research* 63(24), p. 8861.

Rimawi, M. F., Shetty, P. B., Weiss, H. L., Schiff, R., Osborne, C. K., Chamness, G. C. and Elledge, R. M. 2010. Epidermal growth factor receptor expression in breast cancer association with biologic phenotype and clinical outcomes. *Cancer* 116(5), p. 1234-42.

Ring, A. and Dowsett, M. 2004. Mechanisms of tamoxifen resistance. *Endocrine-Related Cancer* 11(4), p. 643-58.

Roger, P., Sahla, M. E., Mäkelä, S., Gustafsson, J. Å., Baldet, P. and Rochefort, H. 2001. Decreased expression of estrogen receptor β protein in proliferative preinvasive mammary tumors. *Cancer Research* 61(6), p. 2537-41.

Sakane, A., Hatakeyama, S. and Sasaki, T. 2007. Involvement of Rabring7 in EGF receptor degradation as an E3 ligase. *Biochemical and Biophysical Research Communications* 357(4), p. 1058-64.

Schneider, M.R. and Yarden, Y. 2014. Structure and function of epigen, the last EGFR ligand. Seminars in Cell & Developmental Biology 28, p.57-61.

Schnitt, S. J. 2010. Classification and prognosis of invasive breast cancer: from morphology to molecular taxonomy. *Modern Pathology* 23, p. S60-S64.

Sentis S, Le Romancer M, Bianchin C and Rostan MC and L., C. 2005. Sumoylation of the estrogen receptor alpha hinge region regulates its transcriptional activity. *Molecular Endocrinology*. 19(11), p. 2671-84.

Shen, F., Lin, Q., Childress, C. and Yang, W. 2013. Identificati*on of the domain in ErbB2 that restricts ligand-induced degradation. Cell Signalling* 20(4), p.779-89.

Schenck, A., Goto-Silva, L., Collinet, C., Rhinn, M., Giner, A., Habermann, B., Brand, M. and Zerial, M. 2008. The endosomal protein Appl1 mediates Akt substrate specificity and cell survival in vertebrate development. *Cell* 133(3), p. 486-97.

Shi, F., Telesco, S. E., Liu, Y., Radhakrishnan, R. and Lemmon, M. A. 2010. ErbB3/HER3 intracellular domain is competent to bind ATP and catalyze autophosphorylation. *Proceedings of the National Academy of Sciences* 107(17), p. 7692.

Shiau, A. K., Barstad, D., Loria, P. M., Cheng, L., Kushner, P. J., Agard, D. A. and Greene, G. L. 1998. The structural basis of estrogen receptor/coactivator recognition and the antagonism of this interaction by tamoxifen. *Cell* 95(7), p. 927-37.

Shou, J., Massarweh, S., Osborne, C. K., Wakeling, A. E., Ali, S., Weiss, H. and Schiff, R. 2004. Mechanisms of tamoxifen resistance: increased estrogen receptor-HER2/neu cross-talk in ER/HER2–positive breast cancer. *Journal of the National Cancer Institute* 96(12), p. 926-35.

Sigismund, S., Algisi, V., Nappo, G., Conte, A., Pascolutti, R., Cuomo, A., Bonaldi, T., Argenzio, E., Verhoef, L. G. and Maspero, E. 2013. Threshold-controlled ubiquitination of the EGFR directs receptor fate. *The EMBO Journal* 32(15), p. 2140-57.

Sigismund, S., Argenzio, E., Tosoni, D., Cavallaro, E.,Polo, S. and Di Fiore, P. P. 2008. Clathrin-mediated internalization is essential for sustained EGFR signaling but dispensable for degradation. *Developmental cell* 15(2), pp. 209-19.

Sigismund, S., Woelk, T., Puri, C., Maspero, E., Tacchetti, C., Transidico, P., Di Fiore, P. P. and Polo, S. 2005. Clathrin-independent endocytosis of ubiquitinated cargos. *Proceedings of the National Academy of Sciences of the United States of America* 102(8), pp. 2760-5.

Singh, R. R. and Kumar, R. 2005. Steroid hormone receptor signaling in tumorigenesis. *Journal of Cellular Biochemistry* 96(3), p. 490-505.

Skliris, G. P., Munot, K., Bell, S. M., Carder, P. J., Lane, S., Horgan, K., Lansdown, M. R., Parkes, A. T., Hanby, A. M. and Markham, A. F. 2003. Reduced expression of oestrogen receptor β in invasive breast cancer and its re-expression using DNA methyl transferase inhibitors in a cell line model. *The Journal of Pathology* 201(2), p. 213-20.

Smith, C. J., Berry, D. M. and McGlade, C. J. 2013. The E3 ubiquitin ligases RNF126 and Rabring7 regulate endosomal sorting of the epidermal growth factor receptor. *Journal of Cell Science* 126(6), p. 1366-80.

Steeg, P. S. 2003. Metastasis suppressors alter the signal transduction of cancer cells. *Nature Reviews Cancer* 3(1), p. 55-63.

Stockmeyer, B., Beyer, T., Neuhuber, W., Repp, R., Kalden, J. R., Valerius, T. and Herrmann, M. 2003. Polymorphonuclear granulocytes induce antibody-dependent apoptosis in human breast cancer cells. *The Journal of Immunology* 171(10), p. 5124-9.

Teixeira, C., Reed, J. C. and Pratt, M. C. 1995. Estrogen promotes chemotherapeutic drug resistance by a mechanism involving Bcl-2 proto-oncogene expression in human breast cancer cells. *Cancer Research* 55(17), p. 3902-7.

Tiseo, M., Bartolotti, M., Gelsomino, F. and Bordi, P. 2010. Emerging role of gefitinib in the treatment of non-small-cell lung cancer (NSCLC). *Drug Design, Development and Therapy* 4, p. 81.

Torres, V. A., Mielgo, A., Barbero, S., Hsiao, R., Wilkins, J. A. and Stupack, D. G. 2010. Rab5 Mediates Caspase-8–promoted Cell Motility and Metastasis. *Molecular Biology of the Cell* 21(2), p. 369-76.

Trang, S. H., Joyner, D. E., Damron, T. A., Aboulafia, A. J. and Randall, R. L. 2009. Potential for functional redundancy in EGF and TGFα signaling in desmoid cells: a cDNA microarray analysis. *Growth Factors* 28(01), p. 10-23.

Tzukerman, M. T., Esty, A., Santiso-Mere, D., Danielian, P., Parker, M. G., Stein, R. B., Pike, J. W. and McDonnell, D. P. 1994. Human estrogen receptor transactivational capacity is determined by both cellular and promoter context and mediated by two functionally distinct intramolecular regions. *Molecular Endocrinology* 8(1), p. 21-30.

Umebayashi, K., Stenmark, H. and Yoshimori, T. 2008. Ubc4/5 and c-Cbl continue to ubiquitinate EGF receptor after internalization to facilitate polyubiquitination and degradation. *Molecular Biology of the Cell* 19(8), p. 3454-62.

Vaccari, T., Lu, H., Kanwar, R., Fortini, M.E. and Bilder, D. 2008. Endosomal entry regulates Notch receptor activation in Drosophila melanogaster. *Journal of Cell Biology* 180(4), p. 755-62.

Van Damme, N., Goff, D., Katsura, C., Jorgenson, R. L., Mitchell, R., Johnson, M. C., Stephens, E. B. and Guatelli, J. 2008. The interferon-induced protein BST-2 restricts HIV-1 release and is downregulated from the cell surface by the viral Vpu protein. *Cell Host & Microbe* 3(4), p. 245-52.

Vanlandingham, P. A. and Ceresa, B. P. 2009. Rab7 regulates late endocytic trafficking downstream of multivesicular body biogenesis and cargo sequestration. *Journal of Biological Chemistry* 284(18), p. 12110-24.

Vieira, A. V. and Lamaze, C. and Schmid, S. L. 1996. Control of EGF receptor signaling by clathrin-mediated endocytosis. *Science* 274(5295), p. 2086-9.

Wang, Y. and Pennock, S. and Chen, X. and Wang, Z. 2002. Endosomal signaling of epidermal growth factor receptor stimulates signal transduction pathways leading to cell survival. *Molecular and cellular biology* 22(20), p. 7279-90.

Wang, T., Zhang, M., Ma, Z., Guo, K., Tergaonkar, V., Zeng, Q. and Hong, W. 2011a. A role of Rab7 in stabilizing EGFR-Her2 and in

sustaining Akt survival signal. *Journal of Cellular Physiology*. 227(6), p. 2788-97.

Wang, Y.-C., Morrison, G., Gillihan, R., Guo, J., Ward, R. M., Fu, X., Botero, M. F., Healy, N. A., Hilsenbeck, S. G. and Phillips, G. L. 2011b. Different mechanisms for resistance to trastuzumab versus lapatinib in HER2-positive breast cancers–role of estrogen receptor and HER2 reactivation. *Breast Cancer Research* 13(6), p. R121.

Weinberg, R. A. 2006. *The Biology of Cancer*. Garland Science.

Welcsh, P. L. and King, M. C. 2001. BRCA1 and BRCA2 and the genetics of breast and ovarian cancer. *Human Molecular Genetics* 10(7), p. 705-13.

Wheeler, D. L., Huang, S., Kruser, T. J., Nechrebecki, M. M., Armstrong, E. A., Benavente, S., Gondi, V., Hsu, K.-T. and Harari, P. M. 2008. Mechanisms of acquired resistance to cetuximab: role of HER (ErbB) family members. *Oncogene* 27(28), p. 3944-56.

WHO. 2011. Cancer Fact Sheet No. 297. [Online]. Available at: http://www.who.int/mediacentre/factsheets/fs297/en/index.html [Accessed: 10th October 2011].

WHO. 2012. World Health Statistics 2012. Geneva, Switzerland: WHO Press.

WHO. 2014. *Breast cancer: prevention and control* [Online]. Available at: http://www.who.int/cancer/detection/breastcancer/en/ [Accessed.

Wickramasinghe, D. and Kong-Beltran, M. 2005. Met activation and receptor dimerization in cancer: a role for the Sema domain. *Cell Cycle* 4(5), p. 683-5.

Wiechmann, L. and Kuerer, H. M. 2008. The molecular journey from ductal carcinoma in situ to invasive breast cancer. *Cancer* 112(10), p. 2130-42.

Wieffer, M., Maritzen, T. and Haucke, V. 2009. SnapShot: endocytic trafficking. *Cell* 137(2).

Wiggins, H., Hiscox, S., Westwell, A., Taylor, K. and Jones, A.T. 2014. 753: Disulfiram-induced cytotoxicity and endolysosomal sequestration of zinc in breast cancer cell models. *European Journal of Cancer* 50(Supplement 5).

Wiggins, H.L., Wymant, J.M., Solfa, F., Hiscox, S.E., Taylor, K.M., Westwell, A.D. and Jones, A.T. 2015. Disulfiram-induced cytotoxicity and endo-lysosomal sequestration of zinc in breast cancer cells. *Biochemical Pharmacology* 93(3), p. 332-42.

Wu, X., Yen, L., Irwin, L., Sweeney, C. and Carraway, K. L. 2004. Stabilization of the E3 ubiquitin ligase Nrdp1 by the deubiquitinating enzyme USP8. *Molecular and Cellular Biology* 24(17), p. 7748-57.

Zhang, M. H., Man, H. T., Zhao, X. D., Dong, N. and Ma, S. L. 2014. Estrogen receptor-positive breast cancer molecular signatures and therapeutic potentials (Review). *Biomedical Reports* 2(1), p. 41-52.

Zhang, Y. and Xiong, Y. 2001. Control of p53 ubiquitination and nuclear export by MDM2 and ARF. *Cell Growth & Differentiation: the Molecular Biology journal of the American Association for Cancer Research* 12(4), p. 175.

Chapter 2: Materials and Methods

2.1 Materials

Details of specific experimental materials and their suppliers are listed in Appendix A. Otherwise: tissue culture plasticware was manufactured by Corning® and supplied by Fisher Scientific (Loughborough, UK). Laboratory disposables and organic solvents were also obtained from Fisher Scientific. General usage chemicals and reagents were supplied by Sigma-Aldrich (Poole, UK) unless otherwise indicated in Appendix A. Cell lines and plasmids that were gifts to the laboratory are indicated in the text, along with the source. Antibodies are listed in Tables 2-3 and 2-6.

2.2 *In silico* procedures

To gain a better understanding of the role of BCA2 in breast cancer, publically-available, Affymetrix microarray datasets were interrogated. The datasets ranged from large patient cohorts, where the effects of gene expression on survival could be examined, to data from *in vitro* studies where the experimental conditions were pertinent to examining BCA2 expression levels.

Expression of BCA2 (mRNA) was primarily determined by the signal intensity of the "JetSet" probe Affymetrix ID 212742_at. JetSet probes provide the most reliable gene expression estimates based on assessment of gene specificity, splice variant coverage and resistance to degradation (Li *et al.* 2011). JetSet scores are between 0 and 1, and the closer the score to 1, the better the predicted probe performance. The JetSet scores

for the 212742_at probe set are given in Table 2-1. The 212742_at probe set scored highly for specificity and coverage and moderately for robustness. The overall score was sub-optimal but adequate for use.

Table 2-1: JetSet scores (out of a maximum of 1) for the 212742_at probe set for BCA2

Probe set	Specificity	Coverage	Robustness	Overall
212742_at	0.818181818	1	0.327884	0.268269

Where expression data from another probe set (226468_at) were also available they were examined alongside the JetSet probe data. Using information from multiple probes meant increased confidence in the reliability of findings i.e. trends in expression change that were detected with both probe sets were considered more likely to reflect true changes in BCA2 expression.

Patient numbers for the KM Plotter and GOBO data subsets examined are presented in Appendix J.

2.2.1.1 KM Plotter

The KM Plotter online biomarker analysis tool (http://www.kmplot.com/) was used to produce Kaplan-Meier plots for relapse free survival (RFS) based on BCA2 expression in 3458 patients. The median expression of BCA2 mRNA was used to split the dataset into high and low expressing groups and survival curves were generated across all breast cancers and for analyses restricted according to ER status and molecular subtype. The hazard ratio for RFS with 95% confidence intervals and logrank P value were calculated by the software for low vs. high BCA2 expression.

2.2.1.2 GOBO: gene expression-based outcome

The online biomarker assessment tool GOBO (http://co.bmc.lu.se/gobo) was also used to generate Kaplan-Meier survival plots based on Affymetrix ID 212742_at (BCA2) signal intensity. Association with breast cancer outcome was investigated in the 1881-sample dataset which was stratified into high, medium and low BCA2 expressing disease. Kaplan-Meir plots were created across all samples and for subgroups defined by: ER-status, molecular subtype (basal-like, HER2-enriched, luminal A, luminal B, normal-like), histological grade, and lymph-node status. Logrank P values were calculated by the software across the three expression quartiles.

The expression levels of BCA2 across different subgroups were also analysed using the GOBO patient samples and panel of 51 breast cancer cell lines. Mean log2 expression levels were displayed by the software in box-plots for each of the groups and analysis of variance (ANOVA) statistics was used to assess differences between them.

2.2.2 Gene co-expression analysis

2.2.2.1 MEM: Multi experiment matrix

Forty-eight genes, whose expression correlated most highly with BCA2 across 1794 human transcriptome datasets, were identified using the MEM online tool (http://biit.cs.ut.ee/mem/). The MEM tool ranks genes according to expression similarity using a novel algorithm that allows expression levels to be compared between different datasets (Adler *et al.* 2009). Similarity ranking is mainly informed by Pearson's correlation

and takes into account inverse-expression. The output of the MEM algorithm is a set of genes with P values that represent the degree of expression similarity with the gene of interest. For the BCA2 analysis a standard deviation cut-off filter of 0.29 was applied; 0.29 being the MEM creator's recommended level for eliminating the noise generated by experimental variability, as established by computational simulation. As in other *in silico* experiments, the BCA2 probeset used in the analysis was the Affymetrix ID 212742_at.

2.2.2.2 DAVID: database for annotation, visualization, and integrated discovery

DAVID (http://david.abcc.ncifcrf.gov/) is an online tool that enables a gene list input to be interrogated and clustered by functional keyword associations (Alvord *et al.* 2007). The co-expressed gene list generated by MEM (2.2.2.1) was subjected to functional annotation clustering analysis with DAVID using the default (medium) stringency setting.

2.2.3 Gene expression changes: BioGPS

BioGPS (http://www.biogps.org/) is an online gene annotation portal that provides access to gene expression information from a vast number of published datasets. The deposited expression data have been normalised, background corrected and summarised using the GeneChip Robust Multiarray Averaging (GC-RMA) procedure.

BCA2 mRNA expression (as measured by the Affymetrix ID 212742_at probeset) were obtained from the following Gene Expression Omnibus (GEO) datasets: GSE15192, GSE5116, GSE4668, GSE20361, GSE14986, GSE10696, GSE14987, GSE13274, and GSE3151. More

information on the individual datasets is provided in Chapter 3. Microsoft Excel was used for analysis and graphical presentation of the BioGPS data. In the absence of expression call information, log2 BCA2 expression was first calculated and tabulated. Positive log2 expression values were considered to indicate sufficient levels of gene expression for further analysis. Where BCA2 expression was suppressed by experimental conditions, log2 was calculated for the lowest expression data point to ensure the mRNA levels did not fall below detectable levels.

Mean log2 fold changes in BCA2 expression were determined by first converting the fluorescence intensity values to fold-change relative to control. These values were then log2 transformed and means were calculated and plotted graphically. Where possible/ applicable 95% confidence intervals were generated and T-Tests or ANOVA plus Tukey post-hoc tests were performed as appropriate.

2.3 *In vitro* procedures

2.3.1 General cell culture

2.3.2 Cell lines

Low-passage (P9) MCF-7, MDA-MB-231, BT474 and T47D human breast cancer cells were a gift from the Breast Cancer Molecular Pharmacology Group (BCMPG), Cardiff University. The authenticated cells were donated to the group by Astrazeneca or purchased from the American Type Culture Collection (ATCC). The passage number relates to the number of times the cells have been split by researchers in the BCMPG. Cell stocks were produced by freezing down 70% confluent

cells in media containing 20% serum, 5% DMSO, ~2.5 x 10^6 cells were aliquotted into each cryovial. The vials of cells were first stored at -20°C for 5 hr, then at -80°C overnight before being transferred to liquid nitrogen for long-term storage.

New, authenticated "near-normal" MCF-10A breast cells were purchased from the ATTC's approved UK supplier LGC Standards. Stocks of the MCF-10A cells were produced by freezing down 70% confluent cells in complete media (recipe in section Media 2.3.3) containing 7.5% DMSO. The cryovials of cells were frozen in a Mr. Frosty™ freezing container filled with ispropanol to allow cooling at the rate of 1°C per minute. The freezing protocol was as follows: -20°C for 1 hr, then at -80°C overnight then transfer to liquid nitrogen for long-term storage.

HeLa cells were obtained from the *European Molecular Biology Laboratory* (Simpson *et al.* 2004). Low passage cell stocks (P14) were made by freezing down 70% confluent cells in media containing 20% serum, 5% DMSO. The cryovials in the Mr. Frosty container were first frozen at -20°C for 5 hr, then at -80°C overnight before being transferred to liquid nitrogen for long-term storage.

All cell lines were used up to a maximum passage number of 28 and were subject to regular mycoplasma testing (section 2.3.5).

2.3.3 Media

MCF-7, MDA-MB-231, BT474 and T47D breast cancer cells were cultured in Roswell Park Memorial Institute media (RPMI) containing phenol red and supplemented with 10% Foetal Bovine Serum (FBS).

MCF-10A cells were grown in Dulbecco's Modified Eagle Medium: Nutrient mixture F12 (DMEM/F12) supplemented with 5% horse serum, 20 ng/mL EGF, 0.5 µg/mL hydrocortisone, 100 ng/mL cholera toxin and 10 µg/mL insulin. HeLa were grown in DMEM supplemented with 10% FBS. No antibiotics were used in routine cell culture.

2.3.4 Routine maintenance

All cells were cultured at 37^{o}C with 5% CO_2 in a humidified atmosphere. The cells were passaged every 3-5 days by washing with phosphate buffered saline (PBS) then incubating with 0.05% trypsin ethylenediaminetetraacetic acid (EDTA) for 3 min to detach the cells. After trypsinisation the cells were collected in 10 mL of culture media then centrifuged at 900 x *g* for 3 min. The supernatant was then removed and the pellet was resuspended in the appropriate volume of media for the cell line's required split ratio (see Table 2-2). 1 mL of cells was then transferred to a new T-75 flask.

Table 2-2 Split ratios for the routine maintenance of different cell lines used throughout the project. Ratios are for the passage of cells every 3-5 days.

Cell line	Split ratio
MCF-7	1:5
MDA-MB-231	1:7
MCF-10A	1:5
HeLa	1:6
T47D	1:5
BT474	2:7

2.3.5 Mycoplasma testing

All cell lines were subjected to quarterly mycoplasma testing by PCR. 1 mL of media was extracted from confluent cells and transferred to a sterile Eppendorf. The media was then centrifuged at 250 x g for 30 s to

sediment cells and debris. The supernatant was then transferred to a new sterile Eppendorf and centrifuged at 20,000 x g for 10 min to sediment mycoplasma (if present). The supernatant was then discarded and the pellet was resuspended in 50 µL of resuspension buffer (supplied with EZ-PCR kit). The resuspended pellet was heated for 3 min at 95^{o}C then 5 µL of this sample was added to a pre-prepared PCR tube. The PCR tube contained 35 µL of sterile dH_2O to and 10 µL of EZ-PCR reaction mix (containing primers, nucleotides and thermostable polymerase). The positive control was prepared by adding 39 µL of dH_2O to 10 µL of reaction mix and adding 1 µL of positive template (supplied with the kit). The tubes were gentle tapped to remove bubbles then transferred to a thermocycler where they were subjected to the following programme:

- **Initial denaturation**: 94^{o}C … 30s
- **Cycles (x36):**
  - 94^{o}C … 30s ***denaturation***
  - 60^{o}C … 120s ***annealing***
  - 72^{o}C … 60s ***elongation***
- **Final elongation step:** 72^{o}C … 4 min

Results were analysed by agarose gel electrophoresis of the post-PCR solution.

2.3.5.1 Agarose Gel electrophoresis

2.3.5.1.1 Agarose gel preparation

A 2% agarose gel was prepared by dissolving 1g of agarose in sterile TAE buffer (40 mM Tris, 20 mM acetic acid, 1 mM EDTA) to give a

final volume of 100 mL. To dissolve the agarose and destroy any nucleases the agarose-TAE mixture was microwaved for 6x 30 s on full power. The mixture was gently swirled between each heating interval to ensure even heating and mixing. After microwaving the agarose solution was allowed to cool for 3 min before 50 µL of 5 µg/mL ethidium bromide was mixed in and the solution was poured into the clean gel box. A well comb was placed into the liquid agarose and the gel was left for 40 min to solidify. Once the gel had set, the electrophoresis tank was filled with sterile 1x TAE buffer and the comb was removed.

2.3.5.1.2 Gel loading and running

2 µL of the DNA was mixed with 3 µL of dH_2O and 1 µl of 6x sample loading buffer (30% glycerol, 0.2% bromophenol blue in dH_20). Samples were loaded onto the agarose gel alongside 1 µL of DNA ladder. The gel was run at 80 V for 4 hr to achieve the required band separation before the gel was transferred to cling film and imaged on the Biorad Chemidoc imaging system.

2.4 Immunofluorescence microscopy (IF)

2.4.1 Cell culture

Cells were seeded onto glass coverslips in 12-well plates and grown in antibiotic-free, serum supplemented media (complete media). Cells were incubated at 37^oC in a 5% CO_2 humidified atmosphere until reaching 70-80% confluence on the day of fixation. Seeding densities (12 well plate; per well) were as follows:

- MCF-7: 150,000
- MDA-MB-231: 75,000
- MCF-10A: 150,000
- HeLa: 67,000 (for transfection)

2.4.2 Fixation and permeabilisation

2.4.2.1 Standard fixation & permeabilisation protocol: paraformaldehyde & Triton X-100

The media was aspirated and the cells were washed three times in PBS before being fixed in 3% paraformaldehyde for 15 min. The cells were washed again x3 in PBS and free aldehyde groups were blocked with 50 mM ammonium chloride for 10 min. The cells were washed x3 in PBS then permeabilised for 5 min with 0.2% Triton X-100: 2% bovine serum albumin (BSA). The cells were then washed a further x3 in PBS.

2.4.2.2 PFA fixation: saponin permeabilisation

The media was aspirated and the cells were washed 3 times in PBS before being fixed in 3% paraformaldehyde for 15 min. The cells were washed again x3 in PBS then incubated with 50 mM ammonium chloride for 10 min. The cells were washed x3 in PBS then permeabilised with 0.4% saponin in PBS for 5 min before being washed a further x3 in PBS.

2.4.2.3 Acetone fixation/permeabilisation

The media was aspirated and the cells were washed x1 in ice-cold PBS. The cells were then fixed and permeabilised in 80% acetone at -20^{o}C for 10 min. After fixation the cells were washed x3 in room temperature PBS.

2.4.2.4 Methanol fixation/permeabilisation

The media was aspirated and the cells were washed x1 in ice-cold PBS. The cells were then fixed and permeabilised in 100% methanol at -20^{o}C for 10 min. After fixation the cells were washed x3 in room temperature PBS.

2.4.2.5 Ethanol fixation/permeabilisation

The media was aspirated and the cells were washed once in ice-cold PBS. The cells were then fixed and permeabilised in 95% ethanol: 5% acetic acid at -20^{o}C for 10 min. After fixation the cells were washed x3 in room temperature PBS.

2.4.3 Immunolabelling

2.4.3.1 Antibodies

Table 2-3 contains a list of the different proteins analysed by immunofluorescence microscopy and antibodies used in their detection. Where available, journal article references for immunofluorescence are given, though the datasheets for the antibodies were the primary source of information used for method development.

Table 2-3: Primary antibodies, dilutions and associated fixation method used for IF. Including references for antibody use in IF.

Target	Primary Antibodies	Dilution	Fixation
Haemagglutinin tag (HA) *Transiently/stably expressed HA-tagged proteins*	- Mouse anti-HA HA.11 clone 16B12 (#MMS-101P, Covance) Scotter *et al.* 2014 - Mouse anti-HA (#H9658, Sigma Aldrich) Bijsmans *et al.* 2012 - Mouse anti-HA (#2362. Cell Signalling) Faux *et al.* 2008	1:1,000	PFA
BCA2	- Goat anti-BCA2 (#SAB2500854, Sigma Aldrich) - Rabbit anti-BCA2 (#HPA019130, Sigma Aldrich)	1:200 (endogenous) 1:5,000 (over-expressed)	**PFA** acetone methanol ethanol*
Early Endosome Antigen 1 (EEA1) *Early endosomes*	- Goat anti-EEA1 (#SC-6415, Santa-Cruz) Clementz *et al.* 2013 - Mouse anti-EEA1 (#610457, BD Bioscience) Sato *et al.* 2014	1:200	PFA
***Trans*-Golgi Network 46** *Golgi apparatus*	Sheep anti-TGN46 (#AHP500, AbD Serotec) Cornfine *et al.* 2011	1:750	PFA
Transferrin Receptor *Recycling endocytic pathway*	Mouse anti-Transferrin receptor (#13-6800, Life Technologies) Simpson *et al.* 2004	1:300	PFA
EGFR	- Mouse anti-EGFR (#Ab-10, Neo-Markers) Xu *et al.* 2006 - Rabbit anti-EGFR (#HPA018530, Sigma) Luke *et al.* 2014	1:100	PFA
Lysosomal-Associated Membrane Protein 2 (LAMP2) *Late endosomes & lysosomes*	Mouse anti-LAMP2 (#H4B4, Developmental studies hybridoma bank [DSHB]) Orenstein *et al.* 2013	1:200	Methanol
Tubulin *Microtubule cytoskeleton*	Mouse anti-tubulin (#T9026, Sigma Aldrich) Jin *et al.* 2008	1:2,000	Methanol
LAMP1** *Late endosomes & lysosomes*	Rabbit anti-LAMP1 (#L1418, Sigma Aldrich) Yogalingam and Pendergast 2008	1:100	PFA
Rab7 ** *Late endosomes & lysosomes*	Rabbit anti-Rab7 (#9367, Cell Signalling) Pacheco-Quinto and Eckman 2013	1:100	PFA
LC3B** *Autophagosomes*	Rabbit anti-LC3B (#2775, Cell Signalling) Bejarano *et al.* 2014	1:100	PFA

* Multiple methods are given to demonstrate the various techniques trialled in optimising the antibodies for immunofluorescence. The method in bold indicates the optimal method.

**Indicates that a non-standard immunofluorescence procedure was used for these antibodies. *See sections 2.4.3.4 and 2.4.3.5.*

2.4.3.2 Standard, single antibody immunolabelling

After fixation and permeabilisation the cell-coated coverslips were blocked in 150 µL of 2% FBS, 2% BSA blocking solution for 1 hr. The cells were then incubated for 1 hr with 100 µL of primary antibody diluted in blocking solution (see Table 5 for dilutions). The coverslips were washed 2x 5 min in 0.05% Triton X-100 in PBS and 1x in PBS before being incubated with species-specific Alexa labelled secondary antibodies (diluted 1:400) and Hoechst (1 µg/mL) for 1 hr. The cells were washed a final 2x 5 min in 0.05% Triton X-100 in PBS and 1x in PBS. After washing, the coverslips were dipped once into PBS, once into dH_2O then mounted onto glass slides with 12 µL of Dako oil and after half an hour were sealed with clear nail varnish.

Secondary antibody only controls were performed alongside IF experiments and unless stated otherwise in the text were all confirmed to be negative.

2.4.3.3 Double antibody immunolabelling

The protocol for double immunolabelling followed the protocol for single labelling until after the three PBS washes following the secondary antibody incubation. At this point the cells were blocked for a second time in 150 µL blocking buffer for 30 min before being incubated with 100 µL of the second diluted primary antibody (raised in a different species from either of the previously applied antibodies). After incubation for one hour at room temperature the coverslips were washed twice for 5 min in 0.05% Triton X-100 in PBS and once in PBS. The

cells were then incubated with the appropriate species of Alexa labelled secondary antibody (1:400) for 1 hr. The coverslips were washed a final 2x 5 min in 0.05% Triton X-100 in PBS and once more with PBS. Following the washing steps, the coverslips were treated as described for single antibody labelling.

2.4.3.4 Immunolabelling with anti-LAMP1 antibody

LAMP1 immunolabelling was performed in a 12-well plate. Following PFA fixation and saponin permeabilisation (2.4.2.2) the cells were blocked in 350 µL 2% FBS, 2% BSA, 0.4% saponin blocking solution for 1 hr. The cells were then incubated overnight with primary antibodies diluted 1:100 in 350 µL of blocking solution. Antibody incubation was performed at 4ºC with gentle agitation and in a humidified chamber. On the second day cells were washed 3x 5 min in PBS before being incubated with Alexa labelled secondary antibodies (1:400) and Hoechst (1 µg/mL) for 30 min. The cells were washed a final 3x 5 min in PBS. After washing the coverslips were washed and mounted as for single antibody labelling.

2.4.3.5 Immunolabelling with anti-LC3B and anti-Rab7 antibodies

The cells were fixed in PFA and the autofluorescence was quenched with ammonium chloride as in 2.4.2.1 but the separate cell permeabilisation step was omitted. After the three PBS washes post-quenching the cells were blocked in 150 µL of 5% BSA, 0.3% (v/v) Triton X-100 blocking solution for 1 hr. The cells were then incubated overnight with primary antibodies at 4^{o}C with gentle agitation and in a humidified chamber. The

antibody diluent was 1% BSA, 0.3% (v/v) Triton X-100, 350 µL of solution was used per well and the concentrations of antibody are listed in table 2-3. On the second day cells were washed 3x 5 min in PBS before being incubated with Alexa labelled secondary antibodies (1:400) and Hoechst (1 µg/mL) for 1 hr. The cells were washed a final 3x 5 min in PBS. Following the washing steps, the coverslips were washed and mounted as described for single antibody labelling.

2.4.3.5.1 Chloroquine positive control for LC3B antibody labelling

As a positive control for autophagy/LC3B immunolabelling: cells were incubated with 100 µM chloroquine for 6 hr prior to IF for LC3B. Chloroquine treatment induces the accumulation of LC3B in autophagic vacuoles (Lichtenstein *et al.* 2011).

2.5 Direct fluorescence methods

2.5.1 EGF-Alexa 488 and EGF-Tetramethylrhodamine

Cells were pre-incubated in 1 mL serum-free media (SFM) for 1 hr at 37°C, 5% CO_2. The SFM was then replaced with 500µL of SFM containing Alexa-labelled EGF (0.5 µg/mL) or EGF-Rhd (1 µg/mL) diluted in SFM. The cells were incubated in uptake media for time periods between 0 and 120 min at 37°C, 5% CO_2. The culture plates were placed on ice and rinsed twice with ice-cold PBS. The cells were then ready for fixation and IF.

2.5.2 Transferrin-Alexa 488 / 647

Cells were pre-incubated in 1 mL SFM for 60 min at 37°C, 5% CO_2. After 60 min the media was replaced with 500µL of uptake media

comprising 100 nM Alexa-488/647 transferrin diluted in SFM. The cells were incubated in uptake media for time points between 0 and 120 min at 37°C, 5% CO_2. The culture plates were then placed on ice and rinsed 2x1 min with ice-cold SFM and 2x with ice-cold PBS. The cells were then ready for fixation and IF.

2.5.3 Mitotracker Red

The growth medium of cells grown on coverslips in 12-well plates was replaced with 500 µL of complete media containing 100 nM of Mitotracker red. The cells were incubated with the Mitotracker media for 30 min at 37°C, 5% CO_2. The cells were washed x1 in room temperature PBS and were then ready for IF.

2.5.4 Rhodamine phalloidin

Actin filaments in PFA fixed, Triton X-100 permeabilised cells were labelled by incubation with 2µg/ml rhodamine phalloidin. Where used, rhodamine phalloidin incubation was incorporated into the secondary antibody step of IF experiments. Drug treatment and growth factor stimulation

2.6 Drug treatments and growth factor stimulation

2.6.1 Cell treatment with disulfiram

70% confluent MDA-MB-231 and MCF-7 cells were treated for 3 hr with 1μM DSF (Brahemi *et al.* 2010). DSF stocks were 1 mM reconstituted in DMSO and were diluted to working concentrations in cell media.

2.6.2 EGF stimulation

Cells were incubated for 1 hr in SFM before being stimulated with EGF (20 ng/mL SFM) for time periods up to 120 min. In the experiment using low-dose EGF, 1 ng/mL of the ligand was used (Sigismund *et al*. 2005; 2008 and 2013).

2.7 Microscopy

2.7.1 Confocal microscopy

Confocal fluorescence microscopy analysis was conducted on a Leica SP5 inverted confocal laser scanning microscope. The microscope was equipped with a 65x oil-immersion objective and different combinations of the 405, 488, 453 and 633 nm lasers. Gain and offset settings were optimised for each fluorescent channel within an experiment. Images were recorded using the sequential scanning mode to prevent fluorescence channel crosstalk/bleedthrough. Images were scanned at 100 Hz with a line average of three to reduce noise.

2.7.2 Epifluorescence microscopy

Epifluorescence microscopy analysis was performed using a Leica DMIRB inverted microscope equipped with a 40x oil immersion objective.

2.7.3 Differential interference contrast microscopy

Differential interference contrast (DIC) microscopy was performed using a Leica DMIRB inverted microscope equipped with 10x objective and using the brightfield mode with a "Ph1" setting on the phase selector ring.

2.8 Western blotting

2.8.1 Cell culture

Cells were seeded in 6-well plates and grown in complete media at 37^{o}C in a 5% CO_2 humidified atmosphere. Cells were subjected to various experimental procedures, such as transfection and EGF stimulation before lystates were collected. Cells were 70-80% confluent on the day of lysate collection. Seeding densities (per well) were as follows:

MCF-7: 220,000
MDA-MB-231: 160,000
BT474: 300,000
T47D: 300,000
MCF-10A: 250,000
HeLa: 160,000

2.8.2 Lysate collection and preparation

2.8.2.1 Lysate collection

The cell culture plates were placed on ice, the media was removed from the wells and the cells were washed twice with ice-cold PBS. 100 µL of lysis buffer (150 mM NaCl, 50 mM Tris base pH 8, 1% Nonidet p-40 [NP-40] including protease and phosphatase inhibitors) was added to each well. The well plates (on ice) were placed on a lateral, circular shaker for 5 min before lyates were scraped and transferred to pre-cooled eppendorfs. Samples were then centrifuged at 4^{o}C, 13,800 x g for 10 min. The supernatants were finally transferred to fresh, pre-cooled eppendorfs.

2.8.2.2 Bicinchoninic acid assay

The protein concentration of each sample was determined by bicinchoninic acid (BCA) assay. BSA protein standards were prepared in lysis buffer at concentrations from 0 to 1 mg/mL. In order for the sample absorbance measurements to fit in the linear range of the assay, cell lysate samples were diluted 1:6 in lysis buffer. The BCA working solution was then prepared by mixing 49 parts biochoninic acid with 1 part copper sulphate pentahydrate. 200 µL of working BCA solution was pipetted into a flat-bottomed 96 well plate. Enough wells were prepared to take duplicate measurements for BSA standards and triplicate for samples. 1 µL of the standards/samples was added to the appropriate number of measurement wells. The plate was incubated 37ºC for 30 min before the absorbance was measured at 562 nm on a plate reader.

A calibration curve was created by plotting the absorbance measurements against the known BSA standard concentrations. The equation of the line of best fit for the calibration graph was then used to determine unknown sample concentrations (taking into account the dilution factor).

2.8.2.3 Standard lysate sample preparation

Sample concentrations were equalised by addition of appropriate volumes of lysis buffer. Appropriate volumes of 4x loading buffer (2% sodium dodecyl sulphate [SDS], 10% glycerol, 0.02% bromophenol blue, 62.5 mM Tris-HCL) were added to each of the samples which were then denatured by heating at 98^{o}C for 5 min. Samples were returned to ice to cool then centrifuged at room temperature at 13,800 x g for 30 s. Samples were stored at -20^{o}C.

2.8.3 Standard SDS-PAGE gel preparation

The gels were cast and run using a BioRad Mini-Protean II SDS-PAGE kit. The front and back plates were assembled in the clamp frame and secured into the casting stand. The resolving gel was prepared using the following recipe table (the TEMED was added last):

Table 2-4: Resolving gel recipes for 10% and 12% acrylamide gels

	10% gel		12% gel	
Total volume of gel /	**10**	**20**	**10**	**20**
40% acrylamide/Bis	**2.5**	**5**	**3**	**6**
3M Tris pH 8.8 / mL	**1.25**	**2.5**	**1.25**	**2.5**
10% SDS / µL	**100**	**200**	**100**	**200**
dH_20 / mL	**6.10**	**12.2**	**5.6**	**11.2**
10% APS (freshly	**75**	**150**	**75**	**150**
TEMED /µL	**7.5**	**15**	**7.5**	**15**

Once the TEMED had been added the liquid gel was quickly mixed by inverting the capped universal tube. The mixture was then poured into

the casting mould, leaving a 2.5 cm gap at the top which was then filled with 100% isopropanol. The resolving gel was then left to set for 45 min. Once the gel had solidified the isopropanol was poured away and the gap at the top of the resolving gel was gently washed eight times with dH_2O. The stacking gel was then made according to the following recipe table:

Table 2-5: Stacking gel recipes for 2 or 4 gels.

	4% stacking **gel**	
Total volume of gel / mL	**10**	**15**
40% acrylamide/Bis / mL	**1**	**1.5**
1M Tris pH 6.8 / mL	**1.3**	**1.95**
10% SD / µL	**100**	**150**
dH_20 / mL	**7.22**	**10.82**
0.1% Bromophenol blue / µL	**300**	**450**
10% APS (freshly made) / µL	**75**	**112.5**
TEMED	**10**	**15**

Again the TEMED was added last and the liquid gel was mixed by inverting. The stacking gel mixture was poured on top of the set resolving gel and the well comb was inserted. The stacking gel was left to set for 30 min before the comb was removed and the gels (in their casting plates and clamps) were transferred to the running tank and immersed in running buffer (385 mM glycine, 250 mM Tris base, 0.5% SDS) ready for sample loading.

2.8.4 Native PAGE and non-reducing conditions

The majority of the Western blotting experiments were performed in denaturing, reducing conditions, as described in Section 2.8.2.3 and 2.8.3). However, for one experiment investigating the effect of Western

blotting conditions on immunoblotting results, native and non-reducing PAGE were carried out. The experimental procedures for these were very similar to the standard Western blotting protocol but with some minor adjustments. For non-reducing PAGE/SDS-PAGE, DTT was omitted from the sample buffer. For native PAGE, SDS was excluded from the sample buffer, the resolving and stacking gels and the running buffer. The heat denaturing step following addition of the sample buffer was also omitted. With the exception of these changes samples were otherwise treated as per the standard Western blotting procedure.

2.8.5 Sample loading and SDS-PAGE

18 µg of protein from each sample was loaded onto a 4% acrylamide stacking gel alongside 10 µL of protein standard molecular weight marker. The proteins were separated by SDS-PAGE at 100 V on a 10% acrylamide resolving gel for 80-100 min, typically for 85 min. The separation time depended on the molecular weight of the target protein, the desired resolution, and the percentage of acrylamide in the gel.

2.8.6 Protein transfer and ponceau staining

Proteins were transferred to a Polyvinylidene fluoride (PVDF) membrane at 100 V for 1 hr at 4^{o}C. The membrane was then washed briefly in dH_2O before being placed in ponceau S solution for 1 min. The membrane was returned to dH_2O and the staining was checked to ensure even transfer and sample loading. The membrane was cut into three strips of lighter (<100 kDa) and heavy weight (>100 kDa) proteins. The

ponceau solution was recycled and the membrane strips were washed 4 x 5 min in PBS to remove all traces of the red stain.

2.8.7 Protein detection by immunoblotting

The standard protocol for immunoblotting with most antibodies was as follows: the membrane strips were blocked for 1 hour at room temperature in 5% milk in PBS containing 0.025% Tween20 (PBST). Each strip was incubated for 1 hour with the primary antibodies, listed in Table 2-6, diluted in 2% milk in PBST.

The membranes were then washed 3x 15 min in PBST before being incubated for 1 hour at room temperature with the appropriate secondary antibody diluted in 2% milk in PBST (complimentary secondary antibodies listed in Table 2-6).

The membrane was washed a further 3 x 5 min in PBST before development. Equal volumes of enhanced chemiluminescence (ECL) reagents were mixed, applied to the PVDF membrane and left for 5 min. Clarity™ Western ECL was used for most standard Western blotting procedures but for low level expression (where indicated) SuperSignal West Femto was used. Following incubation with the ECL mixture, excess solution was shaken from the membrane which was subsequently wrapped in cling film. The membranes were then either imaged using a BioRad ChemiDoc system or were placed inside a developer cassette and transferred to the dark room for imaging with ECL hyperfilm that was then processed in an x-ray developer.

Antibody protocols that deviated from the methods outlined above were for: antibodies against phosphoproteins (where BSA was substituted for milk and used at the same concentrations), goat anti-BCA2 which was diluted in 3% or 5% milk (for endogenous or overexpressed protein respectively) and mouse anti-β-tubulin HRP which was diluted in 5% milk and for which no secondary antibody was required.

Table 2-6: Primary and secondary antibodies and dilutions for Western blotting. Including references for antibody use in immunoblotting.

Primary Antibodies	Dilution	Secondary antibodies (all Pierce)	Dilution
Goat anti-BCA2 (#SAB2500854, Sigma Aldrich)	1:500	**Rabbit anti-goat HRP**	1:8,000
Mouse anti-HA HA.11 clone 16B12 (#MMS-101P, Covance) Wolken *et al.* 2014	1:4,000	**Goat anti-mouse HRP**	1:2,000
Mouse anti-Transferrin Receptor (#13-6800, Life Technologies) Malik *et al.* 2011	1:500	**Goat anti-mouse HRP**	1:2,000
Mouse anti-c-Met (#3127, Cell Signalling) Cen *et al*. 2014	1:500	**Goat anti-mouse**	1:2,000
Rabbit anti-EGFR (#HPA018530, Sigma) Arabi *et al*. 2012	1:1,000	**Goat anti-rabbit HRP**	1:2,000
Rabbit anti-pEGFR *Tyr1068* (#3777, Cell Signalling) *Katayama et al.* 2012	1:1,000	**Goat anti-rabbit HRP**	1:2,000
Rabbit anti-AKT (#9272, Cell Signalling) Masiello *et al.* 2014	1:1,000	**Goat anti-rabbit HRP**	1:2,000
Rabbit anti-pAKT *Ser473* (#9271, Cell Signalling) Masiello *et al.* 2014	1:500	**Goat anti-rabbit HRP**	1:2,000
Rabbit anti-ERK 1/2 (#9102, Cell Signalling) Baek *et al.* 2014	1:500	**Goat anti-rabbit HRP**	1:2,000
Rabbit anti-pERK 1/2 *Thr202/Tyr204* (#9101, Cell Signalling) Baek *et al*. 2014	1:500	**Goat anti-rabbit HRP**	1:2,000
Mouse anti-Flotillin 1 (#610820, BD Biosciences) Al Soraj *et al.* 2012	1:500	**Goat anti-mouse HRP**	1:2000
Mouse anti-β-actin (#A5441, Sigma) Ciucci *et al*. 2014	1:1,000	**Goat anti-mouse HRP**	1,2000
Mouse anti-β-tubulin HRP conjugated (#AB21058, Abcam) Castro-Diaz *et al*. 2014	1:50,000	-	-

2.8.8 Antibody stripping procedure for membrane reprobing

Where proteins of similar molecular weights needed to be detected e.g. for phospho- and total protein, a stripping and reprobing protocol was employed. After the first immunoblotting procedure had been completed and imaged, the membrane was washed 2x 5 min in PBS then 2 x 5 min in dH_2O. The membrane was then stripped in 0.2M NaOH for 10 min

before being washed twice more for 5 min in dH_20 and 2 x 5min in PBS. The membrane was then ready for the blocking step of the second immunoblotting procedure.

2.8.9 Band intensity quantification using ImageJ

Band intensities were quantified from digital images using ImageJ software. The analysis began by using the **Rectangular selection** tool to draw a tall, narrow box around the first band representing the expression level of a protein of interest. The **Analyze>Gels>Select First Lane** command was then used to highlight the box and identify it as lane "1". Subsequent lanes were outlined with equally sized rectangles which were highlighted and assigned lane numbers using the following command: **Analyze>Gels>Select Next Lane** (Fig. 2-1 A). Profile plots were then drawn by using **the Analyze>Gels>Plot Lanes** command. The resulting plots showed the relative density within each of the highlighted lanes. The width of the peaks represented the size/area of the bands and the peak height represented the shade/darkness of the bands. The **Straight Line** tool was used to draw a line across the base of each peak so that the area under each one could be measured with little/no background noise (Fig. 2-1 B). Once each peak was enclosed the **Wand** tool was used to select and highlight the peaks. Measurements for the area under each peak then appeared in a pop up **Results** window (Fig. 2-1 C). These measurements for the band densities of the protein of interest were then exported to Excel. The process was repeated for bands representing housekeeping/loading control proteins. Figure 2-1 D demonstrates the

calculations involved for determining the relative density of a protein of interest, normalised to the loading control.

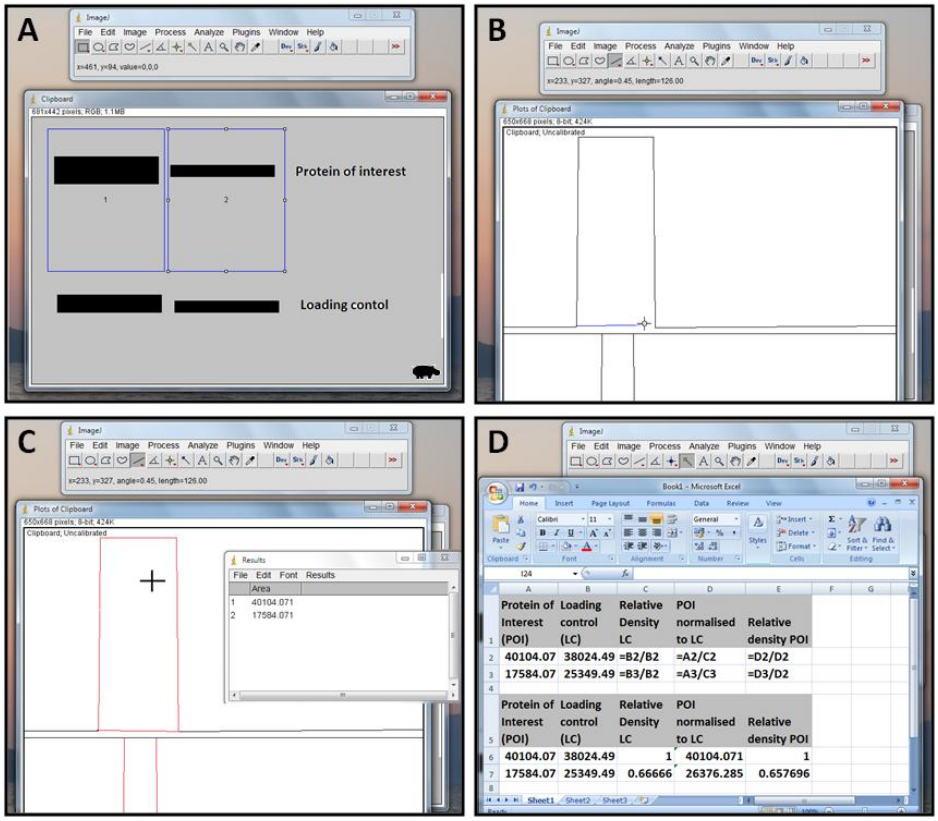

Figure 2-1: ImageJ quantification of immunoblotting data

2.9 Statistical methods

In the results chapters, either all the data from three independent experiments are shown or representative images/immunoblots are presented. Where replicates were performed (and data was quantitative) separate means were calculated for each independent experiment. These independent means were then averaged to give an estimate of the true mean (μ) and 95% confidence intervals. Quantitative data are presented as means ± 95% confidence intervals as outlined and recommended by (Cumming *et al.* 2007).

Prior to conducting statistical analyses to compare means, F-tests for heteroscedasticity were performed. P values ≥ 0.05 returned by an F-test indicate populations with equal variance (homoscedastic) which is a basic assumption of the one-way analysis of variance (ANOVA) test. F-test scores were also used to determine whether a T-test for equal or unequal variance should be used.

Student's independent T-tests were performed when determining the significance of differences between two groups/means. For comparisons between ≥ 3 groups: one-way ANOVA for independent samples was carried out. If the overall difference between groups was determined to significant by ANOVA, Tukey's post-hoc testing was then conducted to identify specifically which groups were different from each other.

2.10 HA-BCA2 plasmid extraction from filter paper, amplification and purification

2.10.1 Plasmid extraction from filter paper

The pCMV-HA plasmid containing the BCA2 insert was a kind gift from Naoki Yamamoto at the AIDS Research Centre, National Institute of Infectious Diseases, Tokyo. The plasmid had been previously used in the 2009 publication by (Miyakawa *et al.*). The vector map is included in Appendix D.

A sterile scalpel was used to cut out the marked circle area containing dried plasmid DNA. Using clean forceps, the filter paper was then inserted into a 1.5 mL eppendorf. 400 µL of sterile dH_2O was added to the filter paper and the eppendorf was vortexed for 10 s. The sample was then incubated at room temperature for 5 min to allow plasmid DNA to

leach into the water. The sample was then vortexed for another 10 s. The sample was centrifuged at 800 x g for 2 min to sediment loose filter paper etc. The supernatant, containing the plasmid DNA solution was then transferred to a new eppendorf.

2.10.2 Plasmid amplification and purification

2.10.2.1 Transformation of competent *E.coli*

400 µL of competent DH5α cells were defrosted on ice. 90 µL of cells were added to four separate, sterile eppendorfs containing 0.1, 1 and 10 µL of the extracted HA-BCA2 DNA. The cells and DNA were incubated for 20 min on ice then heat-shocked for 90 s at 42^{o}C before being returned to ice for 2 min. 600 µL of SOC medium* was added to each eppendorf and the cells and DNA were incubated at 37^{o}C for 1 hr with constant agitation (150 RPM shaking).

The transformed cells were then cultured for 24 hr on 100µg/mL ampicillin LB-agar plates.

*SOC medium: liquid medium containing 2% tryptone, 0.5% yeast extract, 10 mM NaCl, 2.5 mM KCl, 10 mM MgCl2, 10 mM MgSO4, and 20 mM glucose.

2.10.3 Stocks of transformed bacteria cultures

Single, transformed bacteria colonies were picked from the selection plates with a sterile pipette tip. The inoculated tip was then stirred into a vial of Cryobank™ ceramic beads. After thorough mixing, the fluid was drained from the vial which was then stored at -80^{o}C. When more stocks of the plasmid needed to be made: single beads were removed from the

frozen vials and rubbed across the surface of a fresh antibiotic selection plate. After overnight incubation the plasmids could then be extracted and purified as described below.

2.10.4 Plasmid amplification, extraction and purification

Colonies grown on selection plates were picked with sterile pipette tips and cultured at 37^{o}C/150 RPM in LB broth (containing 100 μg/mL ampicillin). The volume of broth, duration of the incubation and subsequent purification protocol used depended on the amount of plasmid DNA required. For the initial testing, that a plasmid of the correct molecular weight had been amplified, only a small amount of plasmid was required. In the first instance therefore only 5 mL of broth was needed for a small culture; grown in a sterile universal with the cap loosely screwed on. After an overnight incubation the Qiagen Mini-prep procedure was then performed, following the manufacturer's instructions (Section 2.10.4.1). A restriction digest followed by agarose gel electrophoresis was carried out to check that a plasmid of the correct size had been produced before scaling up the amplification and purification protocol. Agarose electrophoresis was performed as described in 2.3.5.1 but using a 1% gel. For large-scale/batch cultures to make plasmid stocks: 5 mL of inoculated broth was cultured as for the mini-prep but, initially, for a shorter time of 7 hr. After 7 hr incubation, 500 μL of this starter culture was then transferred to large conical flask containing 100 mL of the LB/ampicillin broth for overnight culture at 37^{o}C with constant agitation of 150 RPM. The plasmids were extracted and

purified from the batch cultures using the Qiagen Maxi-prep kit, according to manufacturer's instructions (Section 2.10.4.2).

2.10.4.1 Plasmid mini-prep

Bacteria were harvested by centrifuging 1.5 mL of culture in a large Eppendorf tube at 6,800 x g for 3 min. The supernatant was discarded and a further 1.5 mL of culture was added on top of the pellet. These steps were repeated once more until a bacterial pellet from a total of 4.5 mL of culture was produced. The supernatant from the final harvesting step was discarded and the pellet was then thoroughly resuspended in 250 µL of buffer P1. 250 µL of lysis buffer P2 was then added to the bacterial suspension and the tube was gently inverted 5 times to fully mix the solutions without damaging the plasmid DNA. The tube was incubated at room temperature for 4 min 45 s before 350 µL of neutralisation buffer N3 was added and mixed by inverting 4-6 times until the blue colour of the lyse blue indicator had completely disappeared. The sample was centrifuged at 17,900 x g for 10 min to sediment the precipitated cell debris. The supernatant was then carefully decanted into a QIAprep spin column and centrifuged for 60 s at 17,900 x g; all centrifugation steps after this point were performed at this speed. The flow-through from the column was discarded and 750 µL of wash buffer PE was added to the top reservoir. The column was centrifuged for 60 s, the flow through discarded and then the column was centrifuged "dry" for a further 60 s to remove residual wash buffer. The column was then transferred to a sterile Eppendorf tube and 25 µL of elution buffer EB was gently pipetted onto the top of the column and incubated for 60 s.

The column was centrifuged for 60 s before another 25 µL of buffer EB was added to the top, incubated for 60 s and centrifuged for 120 s. The eluted plasmid DNA was then stored at -80 ^{o}C for long-term storage or at 4 ^{o}C for quantification and use in experiments.

2.10.4.2 Plasmid maxi-prep

After overnight incubation, half of the 100 mL batch culture was transferred into a 50 mL falcon tube and centrifuged at 6000 x g, 4^{o}C for 15 min. The supernatant was discarded and the remaining half of the batch culture was poured into the falcon tube. The sample was again centrifuged at 6000 x g, 4^{o}C for 15 min. The supernatant was discarded and the bacterial pellet was thoroughly resuspended in 10 mL of buffer P1. 10 mL of lysis buffer P2 was then added the tube was gently inverted 5 times to mix the buffer into the bacterial suspension without causing shearing of the DNA. The lysing bacteria were incubated at room temperature for 4 min 45 s before 10 mL of neutralisation buffer P3 was added and thoroughly mixed by inverting 6 times. The sample was then incubated on ice for 20 min to allow the cell debris to precipitate. The solution and precipitate were transferred to high-speed centrifuge tubes and centrifuged at 20,000 x g for 15 min at 4^{o}C. While the sample was being centrifuged, a Qiagen-tip 500 column was equilibrated by applying 10 mL of buffer QBT. The column emptied by gravity flow and the flow through was discarded. After centrifugation the sample supernatant containing the plasmid DNA was quickly transferred to the top of the equilibrated column. The sample passed through the resin of the column by gravity flow and once the column had emptied the flow

through was discarded. The column was washed twice, each time with 30 mL of wash buffer QC which was discarded after passing through the resin. After washing, the column was transferred to a new 50 mL centrifuge and taped in place at the top of the tube. The plasmid DNA was eluted by applying 15 mL of elution buffer QF to the column; the flow through was retained and the column discarded. 10.7 mL of isopropanol was mixed with the eluate to precipitate the DNA. The sample was the centrifuged at 5000 x g, 4^{o}C for 60 min to pellet the DNA precipitate. The supernatant was carefully discarded and the plasmid pellet was washed with 70% ethanol. The sample was centrifuged for a final time at 5000 x g, 4^{o}C for 60 min. After carefully decanting the supernatant the DNA pellet was left to air dry for 10 min before it was resuspended in 750 µL of sterile Tris-EDTA (TE) buffer.

2.10.4.3 Determining DNA concentration

The concentration of DNA in the purified plasmid solution was determined using the nanodrop spectrophotometer. A sample of approximately 1 µL was taken from the plasmid solution using a thin-walled quartz capillary tube. The end of the capillary tube was sealed with cork and the sample concentration was measured relative to a TE buffer only reference using the spectrophotometer's DNA concentration setting. Once the DNA concentration had been determined the sample was diluted in additional sterile TE buffer to produce plasmid stocks with a concentration of 0.5 mg/mL.

2.10.4.4 Agarose electrophoresis

2 µl of each of the plasmid eluate produced by mini-prep and their corresponding maxi-prep plasmid solutions were analysed by agarose electrophoresis using a 2% gel (Fig. 2-2).

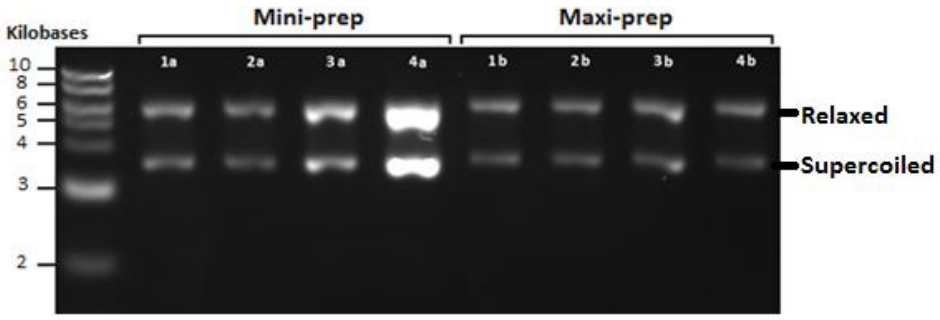

Figure 2-2: Agarose gel electrophoresis of amplified and purified pCMV-HA-BCA2. 2 µL of plasmid product amplified and purified from 4 colonies/cultures of transformed *E.coli* first by mini-prep (1a-4a) then by maxi-prep (1b-4b).

The HA-BCA2 construct consisted of a pCMV-HA-N vector of ~3.8 kb (Appendix D) into which a ~1 kb BCA2 sequence had been cloned. The size of the complete HA-BCA2 vector was therefore ~4.8 kb.

Separation by agarose gel electrophoresis (Fig. 2-2) indicated that a plasmid of the correct size had been produced by the transformation, extraction and amplification process.

2.11 Subcloning of BCA2 from pCMV-HA into EGFP –N1 and -C1 plasmids

2.11.1 EGFP-N1 and EGFP-C1 destination vector preparation

2 µg of each destination vector were digested with EcoR1 and PspOMI restriction enzymes. For each restriction reaction 5 µL NEBuffer 4 was mixed with 37 µL of sterile dH_2O and 4 µL of DNA. 2 µL of EcoR1 and 2 µL of PspOMI were added to give a total volume of 50 µL and each reaction mixture was incubated at 37^{o}C for 1 hr. The linearized plasmids

were then dephosphorylated by adding 5.7 µL of 10X reaction buffer and 1 µL of Antarctic Phosphatase to each completed digest and incubating at 37^{o}C for 30 min. The phosphatase and restriction enzymes were then inactivated by heating the reaction mixture at 65^{o}C for 20 min.

2.11.2 BCA2 insert preparation

2 µg of the HA-BCA2 pCMV parental vector was digested with EcoR1 and Not1 restriction enzymes. Four times the amount of Not1 enzyme was used compared with EcoR1 as a greater excess of this restriction enzyme is needed to cut supercoiled plasmids. 5 µL NEBuffer 3 was mixed with 30.5 µL of sterile dH_2O, 0.5 µL of 10X (100µg/mL) BSA and 4 µL of DNA. 2 µL of EcoR1 and 8 µL of Not1 were added to give a total volume of 50 µL and each reaction mixture was incubated at 37^{o}C for 1 hr. The restriction enzymes were then inactivated by heating the reaction mixture at 65^{o}C for 20 min.

2.11.3 Gel preparation

A 1% agarose gel was formed as described in 2.3.5.1 but the ethidium bromide was omitted from the agarose solution before being poured into the clean gel box to set. A larger-well comb was prepared by taping together two adjacent teeth of a standard comb and this was placed into the unset gel. After 40 min the gel had solidified, the electrophoresis tank was then filled with sterile 1x TAE buffer and the comb was removed.

2.11.4 Gel loading and running

50µL of the digested parental and destination vectors were each mixed with 10 µL of 6x sample loading buffer. The samples were loaded onto the agarose gel alongside 1 µL of 1 kB DNA ladder. The gel was run at 80 V for 4 hr to achieve the required band separation. The gel was then stained in 100 mL of 5 µg/mL ethidium bromide in TAE buffer for 10 min. The gel was then transferred to cling film and placed on a UV transluminator. The required bands were visible at approximately 4.7 kb (EGFP-C1 and –N1) and 1 kb (BCA2 insert). The bands were excised from the gel using sharp, sterile scalpels and were transferred to sterile eppendorfs. The gel excision was performed in <40 s to minimise DNA damage from the UV light and ethidium bromide.

2.11.5 Gel extraction – DNA purification

The DNA was extracted from the agarose gel using the QIAquick gel extraction kit according to the manufacturer's instructions. The gel slices were weighed and 3 uL of Buffer QG per 1 mg of gel was added to each eppendorf. The samples were then incubated at 50^{o}C for 10 min and were vortexed every 2 min to aid dissolution. The resulting solutions were yellow which indicated that the pH was in the desired range and did not need to be adjusted. To each sample: 1 µL isopropanol was added per 1 mg gel and mixed. The samples were then added to QIAquick spin columns in 2 mL collection tubes. The loaded columns were centrifuged at 17,900 x g for 1 min to bind the DNA to the column. The flow-throughs were then discarded and the columns were returned to the collection tubes. 500 µL of Buffer QG was added to each of the columns

which were then centrifuged again at 17,900 x g for 1 min. The flow-throughs were discarded, the columns returned to the collection tubes and 750 µL of wash buffer PE was added. The columns were centrifuged for a third time at 17,900 x g for 1 min after which the flow-throughs were discarded and the columns were centrifuged again in empty collection tubes to remove the residual wash buffer. The columns were transferred to sterile 1.5m l eppendorfs and the DNA was eluted by applying 30 µL of buffer EB to the centre of each column and incubating for 2 min before centrifuging a final time at 17,900 x g for 1 min.

2.11.6 Ligation reaction

The purified BCA2 insert and EGFP destination vector DNA was quantified so that a 3:1 molar ratio of insert:vector DNA could be prepared for the ligation reaction.

The following calculation was performed:

$$\boldsymbol{ng\ of\ insert\ required}$$

$$= ng\ vector\ required\ \ X\ \frac{kb\ size\ of\ insert}{kb\ size\ of\ vector}\ \ X\ \frac{moles\ of\ insert\ required}{moles\ of\ vector\ reqired}$$

Substituting in values for HA-BCA2 and EGFP vectors:

ng vector required = 100
kb size of insert = 1
kb size of vector = 4.7
moles of insert required = 3
moles of vector required = 1

$$= 100\,ng\ \ X\ \frac{1\,kb}{4.7\,kb}\ \ X\ \frac{3\,mol}{1\,mol}$$

$$= 63.8\,ng$$

Two ligation reactions were set up, each containing 63.8 ng of BCA2 DNA and 100 ng of either EGFP-N1 or EGFP-C1. 2 µL of 10x reaction buffer was added to each DNA mix and the volume was brought to 19 µL with sterile dH_2O. 1 µL of T4 DNA ligase was added and the reaction was left to proceed at room temperature for 10 min.

2.11.7 Transformation of competent *E.coli* / amplification of EGFP-BCA2 and BCA2-EGFP

400 µL of competent DH5α cells were defrosted on ice. 90 µL of cells were added to four separate, sterile eppendorfs containing 0.1 µL and 1 µL of either EGFP-BCA2 (C1) or BCA2-EGFP (N1) DNA. The cells and DNA were incubated for 20 min on ice then heat-shocked for 90 s at 42^{o}C before being returned to ice for 2 min. 600 µL of SOC medium was added to each eppendorf and the cells and DNA were incubated at 37^{o}C for 1 hr with constant agitation (150 RPM shaking). The transformed cells were then cultured for 24 hr on 30 µg/mL kanamycin LB-agar before colonies were selected and cultured for 16 hr in LB broth (containing 30 µg/mL kanamycin). The cultures were then maxi-prepped (as in Section 2.10.4.2). To check that BCA2 gene had been successfully inserted, the plasmid subclones were separated by agarose gel electrophoresis in parallel with the empty EGFP vectors. Prior to separation on a 1% gel, all the plasmids were digested with EcoR1 restriction enzyme so that a single band would be produced by electrophoresis. Results are shown in Figure 2-3.

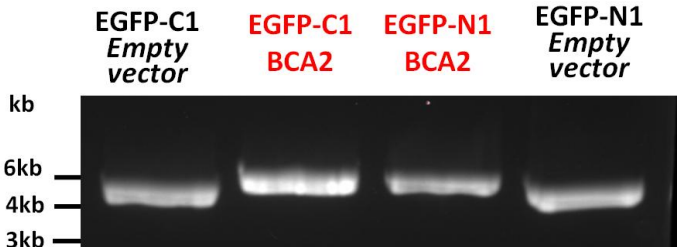

Figure 2-3: Agarose gel electrophoresis verification of BCA2 subcloning into EGFP vectors. Purified EGFP-BCA2 (C1) and BCA2-EGFP (N1) constructs were linearised along with the insert-free EGFP-N1 and C1 vectors.

Successful incorporation of BCA2 was apparent in both EGFP N1 and C1 vectors. The molecular weight increase in the BCA2 constructs was approximately 1 kb which matches the size of the BCA2 gene.

2.12 BCA2 insert sequencing in pCMV-HA and EGFP –N1 and -C1 plasmids

Sequencing was performed in Cardiff University Central Biotechnology Services (CBS) facility under the supervision of Dr. Keith Hart and Andrew Francis.

2.12.1 PCR – Insert amplification

PCR reactions were set up by mixing 5 µL of Better Buffer with 1 µL of BigDye® 3.1 RRM, 3.2 µL of 1 µM primer solution, 1 µL of 250 ng/µL DNA and 4.8 µL of dH_2O. Table 2-7 describes DNA and primers used.

Table 2-7: Sequencing primers

Sample	DNA	Primer
A	HA-BCA2 pCMV	Forward - pCMV 631-657: 5'-ATCCGGTACTAGAGGAACTGAAAAAC-3'
B	HA-BCA2 pCMV	Reverse - M13 reverse: 5'-AAACAGCTATGACCATG-3'
C	EGFP-BCA2 (C1)	Forward - pEGFPC1for: 5'-GATCACTCTCGGCATGGAC-3'
D	EGFP-BCA2 (C1)	Reverse - pEGFPC1rev: 5'-CATTTTATGTTTCAGGTTCAGGG-3'
E	BCA2-EGFP (N1)	Forward - pEGFPN1for: 5'-GTCGTAACAACTCCGCCC-3'
F	BCA2-EGFP (N1)	Reverse - pEGFPN1rev: 5'-GTCCAGCTCGACCAGGATG-3'

The reaction mixtures were placed on a Veriti Thermocycler and amplified using the following programme:

1. Initial denaturation step: 96°C for 1min
2. Denaturation cycle step: 96°C, for 10 s
3. Primer annealing step: 50°C, for 5 s
4. Strand elongation step: 60°C, for 4min

Repeat – 25 cycles

2.12.2 Dynabeads® sequencing clean-up

20 µL of homogenous Dynabeads® solution was added to each completed PCR reaction sample and was thoroughly mixed by pipetting. The samples were then incubated at room temperature for 15 min before being placed on a magnetic PCR plate. The supernatants were carefully removed with clean pipette tips and 30 µL of 85% ethanol was added to each tube. The samples were returned to the PCR plate for 1min before the supernatants were again removed and discarded. The samples were air-dried for 5 min then 30 µL of sterile dH_2O was added to each tube and mixed by pipetting till homogenous. The samples were left for 2 min to allow the cleaned PCR products to leach into the water then 25 µL of the eluted DNA was transferred into new eppendorfs for sequencing.

2.12.3 Sequencing preparation

The cleaned PCR products were dried for 15 min in a centrifugal evaporator before being resuspended in 10 µL of formamide and sequenced on an ABI PRISM® 3100.

2.12.4 Sequencing analysis

The .seq results files generated by sequencing were analysed using open source Chromas Lite software (http://technelysium.com.au/)

2.13 Transfection

2.13.1 DNA transfection

Plasmid constructs

- pCMV-HA-BCA2 (HA-BCA2; (Miyakawa et al. 2009) was used in BCA2 over-expression experiments.

- pCMV6-AC-HA with no insert DNA was used as a vector control in HA-BCA2 transfection experiments.

- pEGFP-C1 containing Rab7, Rab5 and Rab21 (Simpson *et al.* 2004) were used in the double-transfection / co-localisation experiments.

Methods

The following methods all describe volumes and quantities per well of a 12-well plate (quantities were multiplied by 2.4 for transfections in 6-well plates and divided by 10 for 96-well plates to account for differences in surface area):

2.13.1.1 Fugene 6 transfection – HA-BCA2

100,000 MCF-7, 100,000 MCF-10A, 67,000 HeLa or 70,000 MDA-MB-231 cells were seeded onto coverslips in a 12-well plate and incubated for 24 hr (37^{o}C, 5% CO_2) in complete media. After 24 hr the cells were 50-60% confluent. The Fugene 6 transfection mixture was prepared by mixing 3 μL of Fugene 6 with 97 μL of SFM and incubating at room temperature for 5 min. The diluted Fugene 6 was then added to 1 μg of

plasmid DNA in 98 μL of SFM. The mixture was incubated at room temperature for 30 min then 200 μL of the FuGENE 6:DNA complex was added dropwise cells. The media was changed for fresh complete media after 5 hr. The transiently transfected cells were fixed and labelled with antibodies and probes 24 hr later.

2.13.1.2 Lipofectamine 2000 transfection

140,000 MCF-7 or 90,000 MDA-MB-231 cells were seeded onto coverslips in a 12-well plate and incubated for 24 hr (37^{o}C, 5% CO_2) in RPMI supplemented with 10% FBS. After 24 hr the cells were ≈80% confluent. The Lipofectamine 2000 transfection mixture was prepared by mixing 3 μL of Lipofectamine 2000 with 97 μL of SFM and incubating at room temperature for 5 min. The diluted Lipofectamine 2000 was then added to 1 μg of plasmid DNA in 98 μL of SFM. The mixture was incubated at room temperature for 30 min then 200 μL of the Lipofectamine 2000:DNA complex was added dropwise to the cells. The media was changed for fresh RPMI after 4 hr. The transiently transfected cells were fixed and and labelled with antibodies and probes after 24 hr.

2.13.2 siRNA Transfection

The following method describes volumes and quantities per well of a 6-well plate.

2.13.2.1 Single-siRNA sequence depletion method for BCA2 and flotillin 1

250,000 MCF-7 cells were seeded in 6-well plates and grown to 60% confluence in RPMI supplemented with 10% FBS. Cells were

transfected 24 hr after plating with siRNA (sequences below). The transfection reagent was prepared by mixing 4.8 μL of oligfectamine in 19.2 μL Opti-MEM to a final volume of 24 μL. 1.2 μL of a 50 μM siRNA solution was diluted in 214.8 μL of Opti-MEM® I to a final volume of 216 μL. The siRNA and oligofectamine were mixed gently and incubated at room temperature for 30 min. During this time the culture media in the well plates was aspirated, the cells were washed once with SFM then the media was replaced with 960 μL of SFM. 240 μL of the oligfectamine:siRNA complex was then added to each well to transfect the cells. After 4 hr incubation (37ºC, 5%CO_2): 600μL of 30% serum RPMI was added to the culture medium without removing the transfection mixture. Lysates of the siRNA depleted cells were collected after 48 hr total transfection.

siRNA sequences

Non-targeting siRNA control (GFP)

Sense sequence 5′-GGCUACGUCCAGGAGCGCAdTdT-3′

Flotillin-1 siRNA – *published sequence*

Sense sequence 5'-AGAUGCACGGAUUGGAGAA-dTdT-3′

BCA2-1 siRNA – *standard MWG sequence*

Sense sequence 5′-CUACCGGAAUAUAUAUGUC-dTdT-3′

BCA2-K siRNA – *published sequence*

Sense sequence 5′-CGUCUGAAUAGAAUUAAUU-dTdT-3′

2.13.2.2 SMARTPOOL siRNA depletion of BCA2

250,000 MCF-7 cells were seeded into 6 well plates. After 24 hr the cells were ≈40% confluent. The transfection mixture was prepared by mixing:

2.4 µL Dharmafect1 transfection reagent in 237.6 µL of SFM and incubating at room temperature for 5 min. Meanwhile 12 µL of 5 µM siRNA (either non-targeting GFP siRNA or BCA2 Dharmacon ON-TARGET plus SMARTpool siRNA) was mixed into 228 µL SFM. The diluted Dharmafect1 was then added to the diluted siRNA and the mixture was incubated at room temperature for 30 min at room temperature. The cell media was aspirated and replaced with 1920 µL of compete media. After 30 min incubation 480 µL transfection mixture was added to each well, giving a final siRNA concentration of 25 nM. Cells were incubated with the siRNA at 37°C in 5 % CO_2 for 48 hr before further experiments were performed.

2.14 Cell viability assay

Cell viabilities were determined using the CellTiter-Blue® assay in accordance with manufacturer's instructions. 3,500 HeLa cells were seeded into black 96-well plates and incubated overnight at 37ºC, 5% CO_2. The following day cells were transfected with 0.1 µg HA-BCA2 or empty vector control using 0.3 µL of Fugene 6 (see 2.13.1.1). 24 hr after transfection cells were serum starved in SFM for 1 hr then incubated for 48 hr with 100 µL of either: complete media, reduced-serum (0.5% FBS) media or reduced-serum media containing 20 ng/ml EGF. After 44 hr incubation, 20 µL of CellTiter-Blue reagent was added to each of the wells and the plates were returned to the incubator. After 4 hr incubation with the CellTiter-Blue reagent, the fluorescence ($544_{Ex}/590_{Em}$) was analysed using a Fluostar Optima fluorescent plate reader.

2.15 Generation of stable cell lines

2.15.1 Preparation of vector constructs

2.15.1.1 Truncation mutant design

Truncation mutants were designed for BCA2 based on the location of key domains predicted by the HHPred online bioinformatics software: Homology detection & structure prediction by HMM-HMM comparison. *http://toolkit.tuebingen.mpg.de/hhpred*. A truncation mutant lacking the N-terminal zinc finger was designed (-Zn-BCA2) along with a mutant lacking the C-terminal RING-H2 domain (-RING-BCA2). The results of the homology detection and structure prediction by HMM-HMM comparison are presented in Appendix I. Diagrams of truncation mutants that were designed based on the domain prediction results are presented in Figure 2-4.

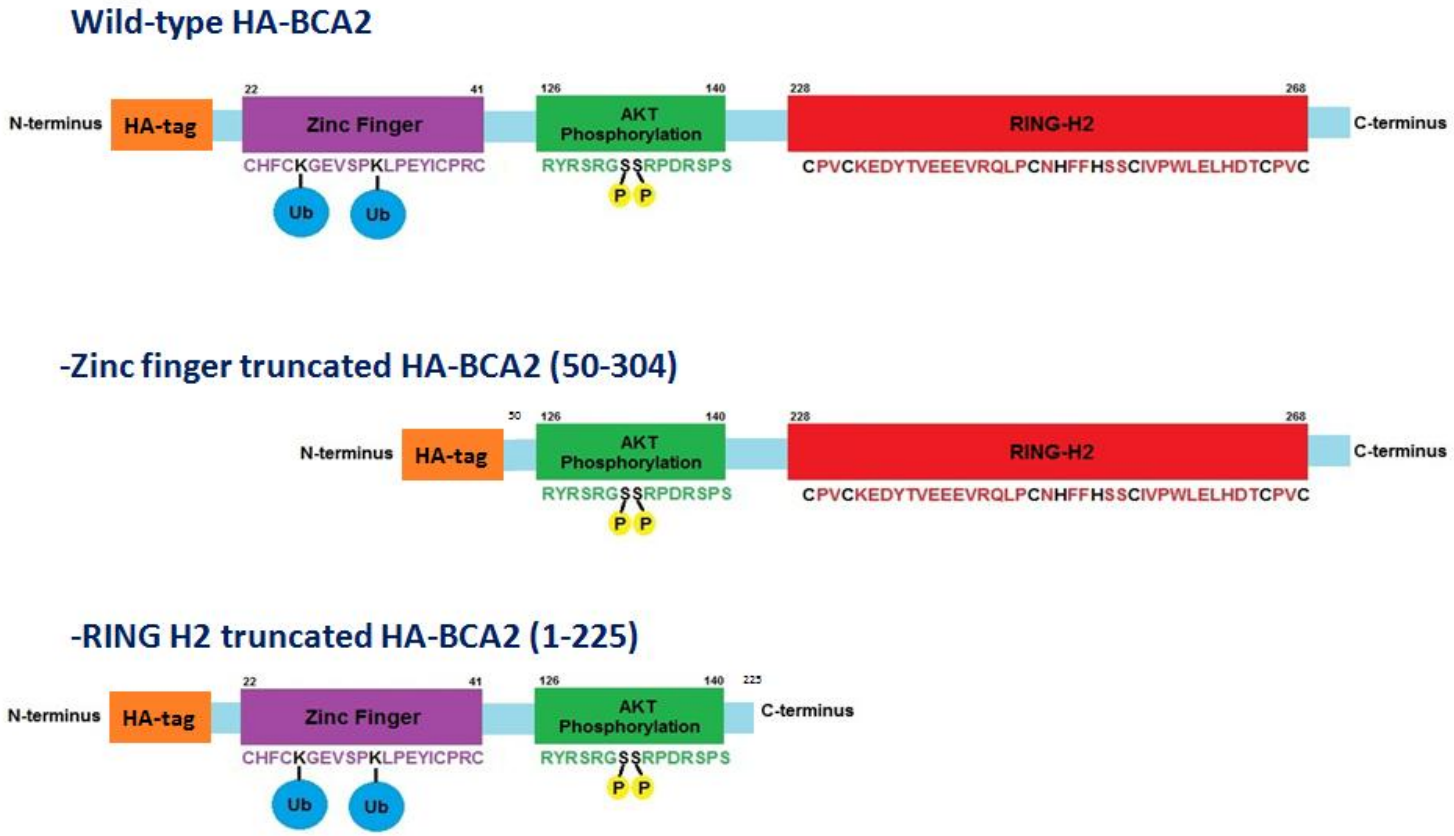

Figure 2-4: Schematic diagram of BCA2, functional truncation mutants developed based on predicted domains

2.15.1.2 PCR primer design

PCR primers were then designed to amplify wild-type HA-BCA2 and the two truncation mutants from the pCMV-HA-BCA2 plasmid. To enable directional cloning into the pEF5/FRT/V5-D-TOPO® vector, "CACC" was added to the 5' end of the forward PCR primers. To prevent the vector's optional V5 C-terminal tag from being added to the translated protein, reverse primers were designed with TGA stop codons at the 5' end. The HA-sequence was reintroduced to the N-terminal truncation mutant by including the HA-sequence in the forward primer for this partial gene. The primers and their target sites in the HA-BCA2 sequence are presented in Figure 2-5.

HA-BCA2 sequence & primer sites

A

ATGTACCCATACGATGTTCCAGATTACGCTCTTATGGCCATGGAGGCCCGAATTCGGTC
GACCGAGATCCGGATGGCGGAGGCTTCGGCGGCCGGGGCGGACTCGGGCGCCGCTGTAG
CCGCCCACCGGTTTTTCTGCCACTTTTGCAAGGGCGAGGTCAGCCCCAAACTACCGGAA
TATATATGTCCCAGATGTGAATCAGGCTTTATTGAAGAAGTGACAGATGATTCCAGTTT
TTTAGGTGGTGGCGGCAGTCGGATAGACAATACCACAACAACACATTTTGCAGAGCTTT
GGGGCCATTTGGATCACACGATGTTTTTTCAAGATTTTAGACCCTTTCTAAGTAGCAGT
CCACTGGACCAAGATAATAGAGCCAATGAAAGGGGTCACCAGACTCACACTGACTTCTG
GGGAGCAAGACCTCCACGGTTGCCATTGGGTCGGAGATACAGATCTCGAGGAAGTTCTC
GTCCTGACAGATCTCCAGCTATTGAAGGAATACTACAACACATCTTTGCAGGATTCTTT
GCAAATTCTGCCATTCCTGGATCTCCACACCCTTTTTCCTGGAGCGGGATGCTGCACTC
CAACCCTGGGGACTATGCCTGGGGTCAGACAGGGCTTGATGCCATTGTAACCCAGCTTT
TAGGACAACTGGAAAACACAGGCCCTCCCCCAGCTGACAAGGAAAAGATCACATCTCTT
CCAACAGTGACAGTAACTCAGGAACAAGTTGATATGGGTTTAGAGTGTCCAGTATGCAA
AGAAGATTACACAGTTGAAGAGGAAGTCCGGCAGTTACCTTGCAATCACTTCTTTCACA
GCAGTTGTATTGTGCCGTGGCTAGAACTGCATGACACATGTCCTGTATGTAGGAAGAGC
TTAAATGGTGAGGACTCTACTCGGCAAAGCCAGAGCACTGAGGCCTCTGCAAGCAACAG
ATTTAGCAATGACAGTCAGCTACATGACCGATGGACTTTCTGA

Key:

HA-Tag	CACC-HA-BCA2-50for primer site
BCA2	HA-BCA2-225rev primer site
CACC-HA-BCA2for primer site	HA-BCA2rev primer site

B

Primers for WT-BCA2

CACC-HA-BCA2for

5′-**CACC**ATGTACCCATACGATGTTCC-3′ T_m = 64.6°C

HA-BCA2rev

5′-TCAGAAAGTCCATCGGTCATGTAGC-3′ T_m = 64.6°C

C

Primers for –Zn-BCA2 (a.a. 50 – 304)

CACC-HA-BCA2-50for

5′-**CACC**ATGTACCCATACGATGTTCCAGATTACGCTACAGATGATTCCAGTTT-
TTTAGGTGG-3′ T_m = 61.5°C

HA-BCA2rev

5′-TCAGAAAGTCCATCGGTCATGTAGC-3′ T_m = 64.6°C

D

Primers for -RING truncation mutant (a.a. 1-225)

CACC-HA-BCA2for

5′-**CACC**ATGTACCCATACGATGTTCC-3′ T_m = 64.6°C

HA-BCA2-225rev

5′- **TCA**ACCCATATCAACTTGTTCCTGAG-3′ T_m = 63°C

Figure 2-5: Primers for PCR subcloning of wild-type and truncation mutant BCA2. A) HA-BCA2 sequence with colour coded primer binding sites. Primers for PCR amplification of B) HA-BCA2 Wild-Type. C) -Zn-finger mutant and D) –RING mutant HA-BCA2.

2.15.1.3 Insert generation by PCR

In order to amplify the wild-type HA-BCA2 and the truncation mutants, the following mixture was set up for each PCR reaction:

PCR reaction mixture	***Volume***	***Final concentration***
5x Hot star PCR buffer	10 µL	1x
100 µM Fwd primer*	0.5 µL	1 µM
100 µM Rev primer*	0.5 µL	1 µM
HotStar Hifidelity Polymerase	1 µL	2.5 units
Nuclease-free dH_2O	37 µL	-
50 ng/ µL HA-BCA2 template	1 µL	1ng/µL
Total volume 50 µL		

*The following forward and reverse primer combinations were used:

For WT-BCA2:
CACC-HA-BCA2for
HA-BCA2rev

For –Zn mutant-BCA2:
CACC-HA-BCA2-50for primer site
HA-BCA2rev

For –RING H2 mutant-BCA2:
CACC-HA-BCA2for
HA-BCA2-225rev

The PCR reaction was then performed according to the following protocol:

Thermocycler protocol

- **Initial denaturation:** 95°C ... 5min
- **Cycles (x30):**
  - 94°C … 15s ***denaturation***
  - 55 °C …60s ***annealing***
  - 72°C … 60s ***elongation***
- **Final elongation step:** 72°C … 10 min

Following PCR amplification 500ng of DNA was then loaded onto a 1% agarose gel and separated at 80 V for 2 hr in TBE. The resulting gel was imaged and is presented in Figure 2-6. Single bands at the appropriate molecular weight for wild-type HA-BCA2 (~1 kb), the two truncation mutants (~0.75 kb) were clearly visible.

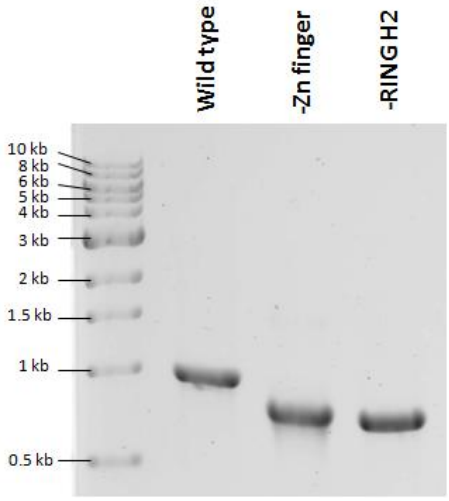

Figure 2-6: Agarose gel separation of wild-type and mutant HA-BCA2 PCR products.

2.15.1.4 TOPO cloning

The PCR products were TOPO cloned into the pEF5/FRT/V5-D-TOPO® using a 1:1 molar ratio of insert:vector DNA. The following values and calculations were used:

kb size of vector = 5.831
kb size of W.T. HA-BCA2 = 0.987
kb size of –Zn HA-BCA2 = 0.777
kb size of –RING H2 HA-BCA2 = 0.768
ng of vector used = 20

$$\textit{ng of insert needed} = \textit{ng of vector used} \times \frac{\textit{kb size of insert}}{\textit{kb size of vector}} \times \frac{\textit{mol. insert required}}{\textit{mol. vector required}}$$

W.T. HA-BCA2

$$\text{ng of insert needed} = 20 \times \frac{0.987}{5.831} \times \frac{1}{1}$$

= 3.39 ng

-Zn HA-BCA2

$$\text{ng of insert needed} = 20 \times \frac{0.777}{5.831} \times \frac{1}{1}$$

= 2.67 ng

-RING HA-BCA2

$$\text{ng of insert needed} = 20 \times \frac{0.768}{5.831} \times \frac{1}{1}$$

= 2.63 ng

The PCR products were diluted in nuclease-free water to the following concentrations:

W.T. HA-BCA2	**= 3.39 ng/ µL**
-Zn HA-BCA2	**= 2.67 ng/ µL**
-RING H2 HA-BCA2	**=2.63 ng/ µL**

The TOPO cloning was performed by setting up the following reaction mixture and incubating for 20 min at room temperature:

TOPO reaction mixture

PCR product	1 µL
Salt solution	1 µL
Nuclease-free dH_2O	3 µL
TOPO vector	1 µL
Final vol.	**6 µL**

2.15.1.5 Transformation of One Shot® TOP10 competent cells

2 µL of the TOPO cloning reaction mixture was added to a 50 µL vial of One Shot® TOP10 competent cells and mixed by gentle stirring before incubation on ice for 30 min. The cells were then heat-shocked in a water bath at 42^{o}C for 30 s and transferred to ice for 2 min. SOC media (250 µL) was added to each of vials which were then tightly sealed and transferred to the shaking incubator for 1 hr at 37^{o}C, 200 RPM. 50 µL and 200 µL of each transformed cell suspension were spread onto separate pre-warmed LB agar plates containing 100 µg/mL ampicillin. Untransformed cells and cells previously transformed with HA-BCA2 were also spread onto ampicillin-plates to act as negative and positive controls respectively. The inoculated selection plates were incubated overnight at 37^{o}C, 5% CO_2.

The following day, 30-50 colonies were seen on the plate for WT-BCA2 and both mutants. No growth was observed on the selection media inoculated with untransformed bacteria (negative control) and lawn of bacterial growth was present on non-selective LB agar (positive control).

2.15.1.6 Amplification and purification of plasmids

Half of an isolated colony was lifted with a sterile pipette tip and placed into 5 mL of antibiotic-containing LB broth in a sterile universal with the lid loosely screwed on. The other half of the isolated colony was then used to check the presence and orientation of the insert by PCR (see section 2.15.1.7 for method).

The plasmids were amplified by incubating the 5 mL cultures overnight at 37^{o}C with 200RPM shaking. Plasmid extraction and purification was performed via a miniprep procedure, according to manufacturer's instructions and as described previously in section 2.10.4.1. The inoculated universals were stored at 4^{o}C for later Maxiprep amplification of successful transformants.

2.15.1.7 PCR analysis of Transformants

In order to determine the presence and orientation of the inserts in the transformants, PCR analysis was performed. In PCR verification of insert orientation two reactions are set up. One PCR reaction contains a T7 primer and an insert sequence-specific forward primer. The second PCR reaction contains T7 primer and a sequence specific reverse primer. Figure 2-7 shows how correct and incorrect insert orientations would appear following PCR and agarose electrophoresis of samples. The figure demonstrates how results are interpreted: a correctly orientated insert would only be amplified with the T7 primer and a reverse primer.

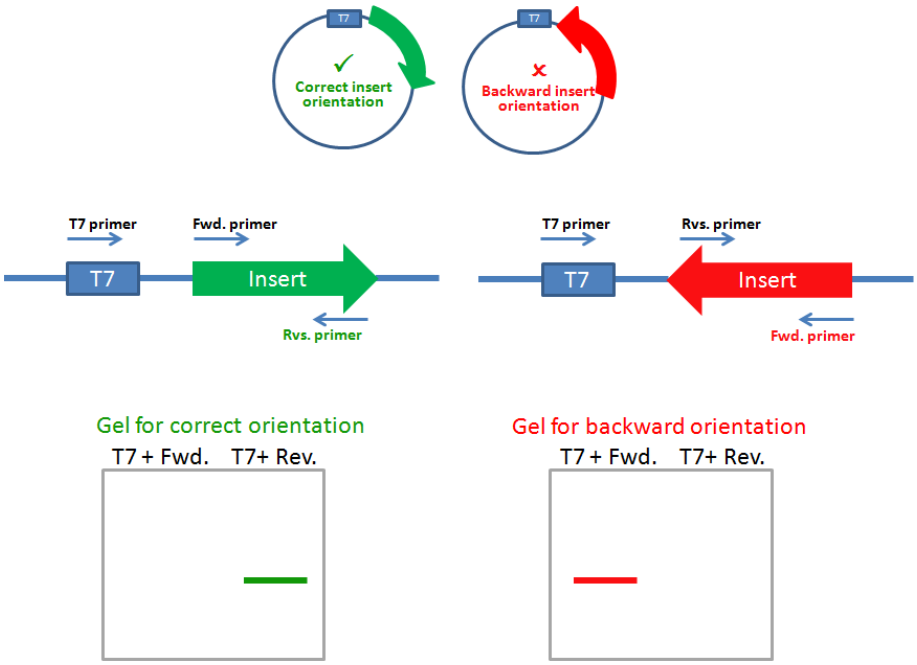

Figure 2-7: The principle of PCR verification of insert orientation

Two PCR reactions were performed on the half-colonies (from section 2.15.1.6). Half-colonies from the previous section were resuspended in the following PCR reaction mix:

Hot star PCR buffer	10 µL	Add ½ colony
T7 primer	1 µL	
Fwd or Rev insert primer	1 µL	
HotStar Polymerase	1 µL	
Nuclease-free water	37 µL	

The thermocyler was set up and the samples were run using the following PCR programme:

Thermocycler protocol

- **Initial denaturation**: 94^{o}C ... 10min (lyses cells & deactivates nucleases)

- **Cycles (x30):**
  - 94^{o}C … 15s *denaturation*
  - 55 ^{o}C …60s *annealing*
  - 72^{o}C … 60s *elongation*

- **Final elongation step**: 72^{o}C … 10 min

The PCR products were mixed with loading buffer separated by electrophoresis on a 1% agarose gel for 3 hr (80 V) alongside a DNA ladder to enable band size determination. The results of the PCR analysis are presented in Figure 2-8.

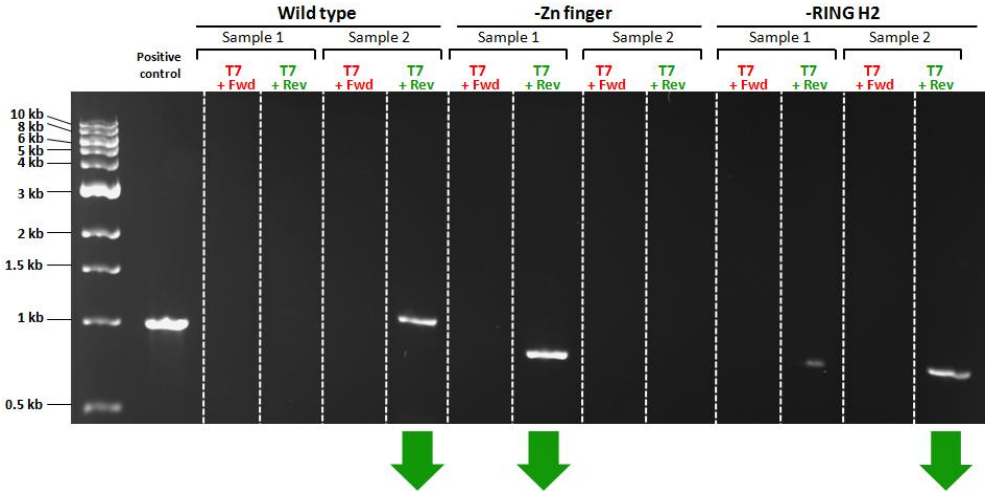

Figure 2-8: Agarose gel of PCR transformant analysis. The presence of a band in the "T7 + Fwd" primer lane indicates a correctly orientated insert. Samples from the lanes indicated by green arrows were selected for batch culture amplification

PCR verification of HA-BCA2 and mutant constructs confirmed that the TOPO cloning had been successful.

2.15.1.8 Batch Culture and Purification of Plasmids

Add 5 mL of ampicillin-containing LB broth was added into the previously inoculated universal tubes containing the successful transformants. The lid was screwed on loosely and the cultures were incubated for 4 hr at 37^{o}C with 200 RPM shaking. The starter cultures were transferred to large (1 L flasks) containing 100 mL ampicillin LB-broth. Sterilised sponge bungs were placed in flask openings and the batch cultures were then incubated overnight at 37^{o}C with 200 RPM shaking.

Plasmid extraction and purification was performed via the maxiprep procedure (previously described in 2.10.4.2) according to manufacturer's instructions.

2.15.1.9 Restriction analysis of transformants

Following maxi-prep, restriction analysis was performed to re-verify the presence and correct orientation of the insert.

For restriction analysis two restriction enzymes were selected: one to cut the vector and one to cut the insert. The first enzyme to be chosen was one that cut at a **single site**, **only** in the destination vector. The second enzyme to be chosen was one that cut **once, asymmetrically** and **only** in the insert. The vector information sheet (Appendix G) and the online "NEB cutter" tool (*http://tools.neb.com/NEBcutter2/index.php*) were used to identify suitable sites for restriction analysis of the HA-BCA2 and mutant constructs. The information used in restriction enzyme selection is summarised in Figure 2-9. Not1 was chosen as the first

(vector) restriction enzyme and BstEII was identified as a suitable candidate for the second enzyme (to cut the insert).

Figure 2-9: Restriction enzyme selection for restriction analysis validation of correct insert orientation.

The predicted band sizes that would be generated by correctly and incorrectly orientated inserts were calculated using the vector map and the insert sequence. This process is described and summarised in Figure 2-10.

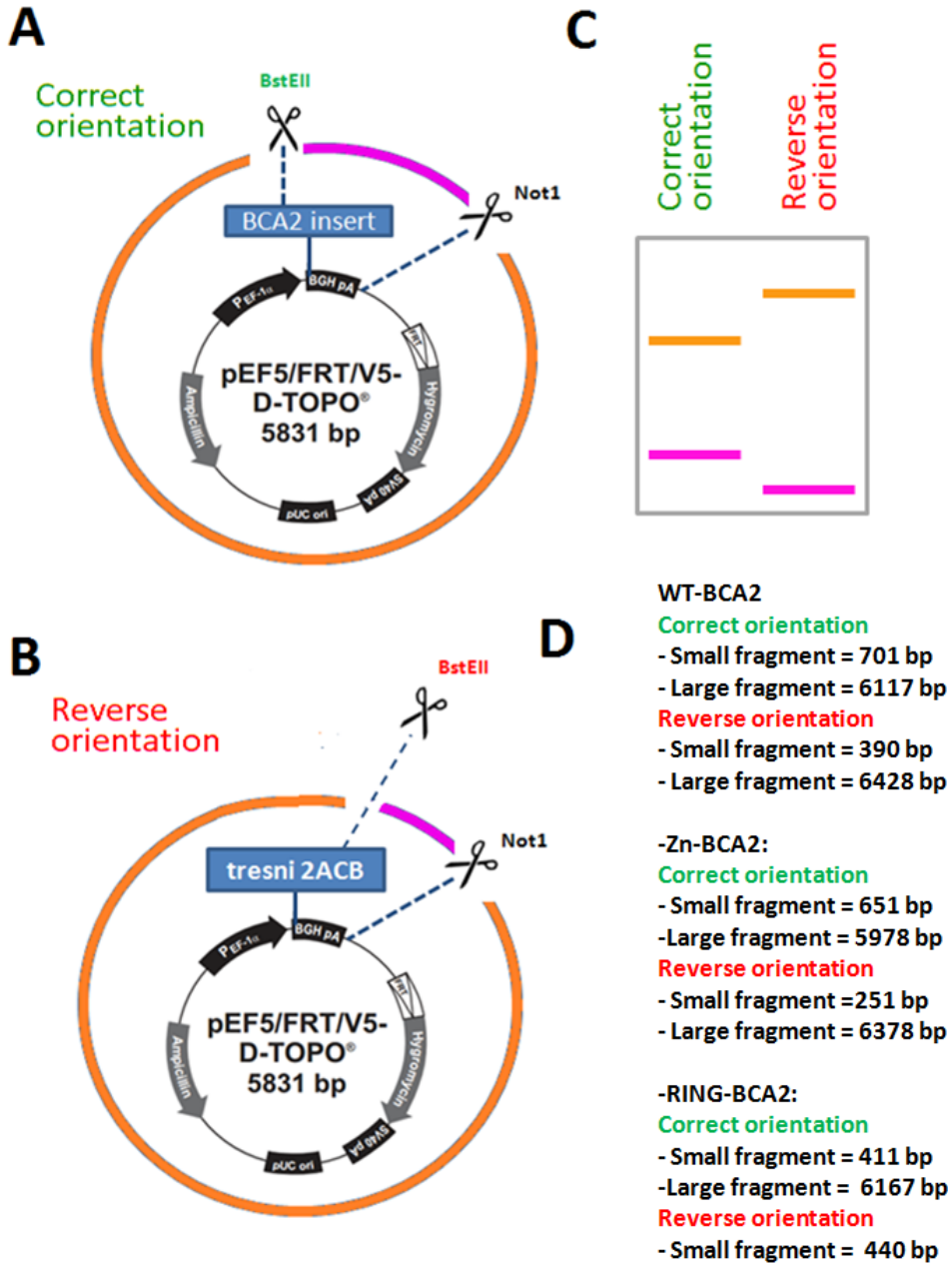

Figure 2-10: Predicted relative and absolute band sizes for restriction analysis of HA-BCA2, –Zn and –RING mutant constructs. A) The relative band sizes created by restriction analysis of a correctly orientated insert. B) The relative band sizes for an incorrectly orientated insert. C) The predicted pattern produced by agarose electrophoresis of differently orientated inserts. D) The calculated sizes for wild-type and truncation mutants of HA-BCA2.

The approximate sizes of the small fragments produced by correctly orientated insets were ~0.7 kb, ~0.65 kb and ~ 0.4 kb for the WT-BCA2, -Zn-BCA2 and -RING-BCA2 respectively.

Sequential double digests of the HA-BCA2, -Zn and-RING mutant constructs were performed as follows: 2 μg of vector construct was digested with an eighty-fold excess of Not1 at 37^{o}C followed by an eighty-fold excess of BstEII at 60^{o}C. For each restriction reaction 5 μL NEBuffer 3.1 was mixed with 31 μL of sterile dH2O and 4 μL of DNA. 8 μL of Not1 was added to give a total volume of 48 μL and each reaction mixture was incubated in a water bath set to 37^{o}C for 1 hr. After 1 hr, 2 μL of BstEII were added and the reaction mixtures were transferred to a water bath set to 60^{o}C for a further hour.

The complete digest was then mixed with loading buffer and separated on a 1% agarose gel at 80 V for 3 hr alongside a DNA ladder to enable band size determination (Fig. 2-11). The banding pattern produced by the separated digest products was compared with predicted band sizes (Fig. 2-10).

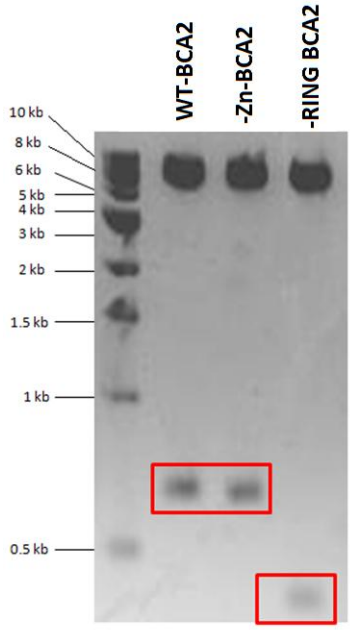

Figure 2-11: Restriction analysis of HA-BCA2 (wild-type), –Zn and –RING mutant constructs separated by agarose gel electrophoresis. Verification of insert orientation was determined by the size of the small, highlighted fragments.

The results of the restriction analysis confirmed that the inserts were correctly orientated in all the constructs. The constructs could therefore be used to produce stable cell lines.

2.15.2 Producing the stable cells

Due to the intensiveness of the tissue culture stages in terms of labour, time and resources, only one of the constructs could be developed into a stable cell line at a time. The wild-type HA-BCA2 construct was selected for the first stable cell line development work.

2.15.2.1 Parental cell line

Flp-In HeLa S3 parental cells (along with the pOG44 vector) were a kind gift from Prof. Michael Clague and Prof. Sylvie Urbé from the Department Cellular and Molecular Physiology at Liverpool University.

Flp-In HeLa were cultured in complete media (DMEM, 10% FBS supplemented with 250 µg/mL Zeocin selection antibiotic).

2.15.2.2 Genejuice transfection of Flp-In HeLa with Wild Type BCA2

400,000 Flp-In S3 HeLa cells were seeded into 5 wells of a 6-well plate and incubated for 24hr (37ºC, 5% CO_2) in 2 mL DMEM supplemented with 10% FBS and 250 µg/mL of Zeocin. After 24 hours the cells were ≈60% confluent. The Genejuice transfection mixture was prepared by adding 3 µL of Genejuice to 100 µL of SFM, vortexing on medium speed for 10s then incubating at room temperature for 5 min. The diluted Genejuice was then added to 0.5 µg of WT construct and 0.5 µg of pOG44 in SFM to 100 µl. The mixture was incubated at room temperature for 30min before 200 µL of the Genejuice:DNA complex was used to transfect the cells in 3 of the wells. After 4 hr the media was changed for fresh complete media. After 24 hours, the cells in each well were split 1/6 and plated onto two 10 cm dishes containing 10 mL of complete, Zeocin-free media. 1/6 splits were also made from a well of untransfected cells to act as negative (i.e. hygromycin sensitive) controls. The cells were incubated for 3 hr at 37ºC, 5% CO_2 before the media was replaced with hygromycin (400 µg/mL) supplemented, complete media.

2.15.2.3 Growth and maintenance of cells

The cells were maintained in complete selection media (DMEM containing 10% FBS and 400 µg/mL Hygromycin B) which was changed every 3 days till day 18 of the experiment. During the media changes the cells were periodically imaged to document their progress. Cells were imaged with a digital camera adapted to fit an inverted light microscope. Untransfected, non-resistant cells were gradually killed by the hygromycin and resistant clone colonies began to form. After nineteen days were picked and transferred to 24 well plates as described below.

2.15.2.4 Colony picking

Marker pen was used to circle usable colonies (those with a diameter large enough to fill most of a 10x objective field of view and with good separation margins from other colonies). The colonies on plates that were too dense to allow individual colonies to be picked were discarded. Before starting: 500 µL of hygromycin media (400 µg/mL) was added to the wells of a 24 well plate and the plate was placed in the incubator at 37ºC. The trypsin was kept cool in an ice bath in the tissue culture hood. One 10 cm dish was processed at a time: stable colonies were washed in 10 mL autoclaved and pre-warmed PBS. All traces of PBS were removed and 1.5 mL of ice-cold trypsin was added to and swirled across the dish. 1 mL of trypsin was then removed, leaving a thin film across the cells. The pipette was set to 10 µL, ~5 µL of trypsin was taken up into a filter tip pipette. Approximately 2 µL of trypsin were then added directly onto a colony which was then quickly scratched off with the pipette tip. The colony was then transferred to the 24-well plate and

gently mixed into to the hygromycin media. After 6 colonies had been picked and transferred to wells a 1 mL pipette (set at 350 µL to avoid bubbles) was used to pipette the cells up and down in order to break up large cell aggregates into smaller clumps. This was repeated for all the remaining cell dishes. All the plated cells were then incubated at 37^{o}C, 5% CO_2. The colony picking procedure is summarised in Figure 2-12.

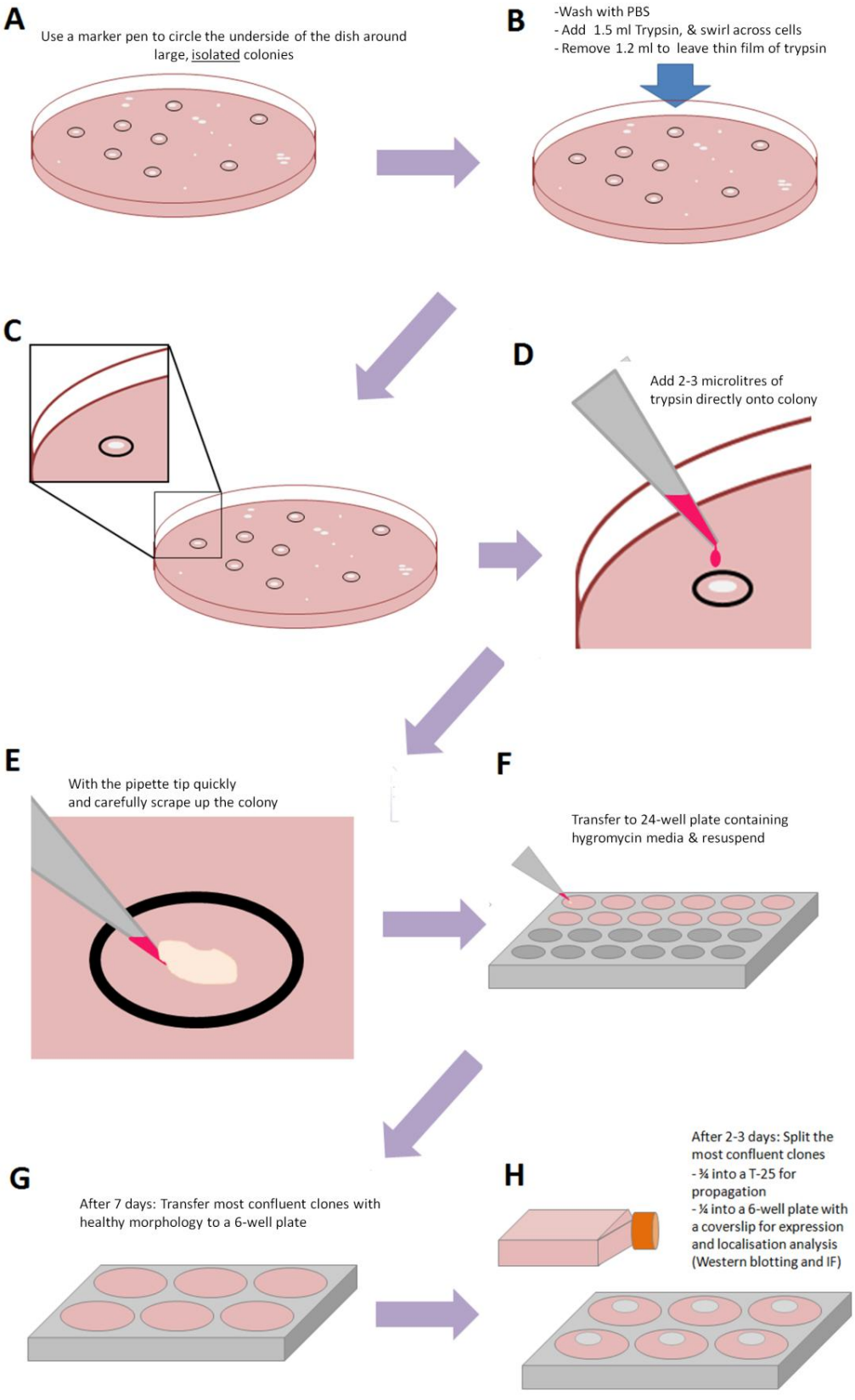

Figure 2-12: Illustration of procedure for colony picking of stable Flp-in clones.

2.15.2.5 Growth and maintenance of stable cell lines

The cells were left to grow for 7 days in the 24 well plates. The cell density was monitored and recorded and the media was changed every 2-3 days. After 7 days the cells in wells that were >60% confluent were split 1:2 into two wells of 12-well plates. Once the 12-well plate clones became70% confluent, one well was used for lysate collection and the second well was split into two wells of separate 6-well plates (one well for freezing cells down, one for Zeocin sensitivity testing).

2.15.2.6 Cell freezing

Once the clones in the 6 well plate had reached 70% confluency the hygromycin media was aspirated and the cells were washed with 1 mL of PBS. The PBS was removed and the cells were incubated with 450 µL of trypsin EDTA at 37^{o}C for 3 min. 1 mL of media was then used to inactivate the trypsin and the cells in the media suspension were then transferred to Eppendorf tubes and centrifuged for 3 min at 900g. The supernatants were aspirated and the cell pellets were gently resuspended in 750 µL of freezing medium (10% DMSO, 10% FBS DMEM) and transferred to cryovials. The cryovials were placed in a Mr. Frosty^{TM} freezing container at -80^{o}C to ensure the cells froze at a slow and steady rate of approximately -1^{O}C per minute.

2.15.3 Testing the success of the stable cells

2.15.3.1 Zeocin sensitivity

Zeocin sensitivity testing was performed on the clones by seeding at low confluency (~10%) into a 6-well plate alongside two wells of HeLa Flp-

In S3 cells. The cells were grown in 250 µg/mL Zeocin media for 7 days. The media was changed on day 2 and day 5 after seeding.

Clones were classified according to observed changes in growth rate and morphology:

- ***Resistant:*** cells appear healthy and grow at a normal rate, no apparent sensitivity
- ***Some sensitivity***: some cells showing morphological changes (blebbing, cytoplasmic granulation, cell enlargement, increased heterogeneity. Slower growth rate.
- ***Sensitive:*** Extensive changes to cell size, morphology and/or growth rate
- ***Highly sensitive:*** Extensive cell death.

Sensitive Zeocin clones were then tested for HA-BCA2 expression by Western blotting for HA.

2.15.3.2 HA-BCA2 expression analysis

Lysates were made of the 18 clones growing in T25 flasks by seeding the cells in 6-well plates and collecting lysates on ice in 100 µL of NP-40 lysis buffer containing protease inhibitor cocktail. Lysates containing 50 µg of total protein were separated on a 10% acrylamide gel by SDS-PAGE. Lysates of untransfected Flp-In HeLa and HeLa cells transiently transfected with HA-BCA2 were run alongside the clone lysates to act as a negative and positive control respectively. After separation the samples were transferred to PVDF. After Ponceau S staining to verify even loading and transfer the the PVDF membrane was blocked for 1 hr at room temperature in 5% milk in PBS containing 0.025% Tween (PBST). The membrane was incubated with mouse anti ~HA was diluted 1:500 in 2% milk in PBST. This primary antibody incubation step was performed

overnight in a humidified chamber at 4^{o}C. After 3x 5 min washes in PBST the PVDF strips were incubated at room temperature for 1 hr with anti mouse secondary antibody diluted 1:5000 in 2% milk in PBST. The strips were washed a further 3x 5 min in PBST before Clarity ECL reagent was applied for 5 min and the resulting signal was detected using the Chemi-doc imaging system.

2.15.3.3 Further HA-BCA2 expression analysis

Three passages after resurrecting the cells lysates were taken of the clones that had indicated positive BCA2 expression. Lysates were collected from 6-well plates by scraping into 100 µL lysis buffer (including protease and phosphatase inhibitors) on ice. As previously described lysates were prepared, separated by SDS-PAGE, transferred to PVDF then blotted for HA.

2.15.3.4 Induction/enhancement of HA-BCA2 expression

150,000 clone cells were plated into 6-well plates and incubated at 37^{o}C/5% CO_2 overnight. The following morning cells were treated either with diluents controls or the following promoter enhancing drugs for 48 hr:

- 100 µM Butyric acid – 48 hr treatment (Tsubaki *et al.* 2002)
Diluent control = dH_2O

- 1 µM 5-azacytidine – 48 hr treatment (Escher *et al.* 2005)
Diluent control = acetic acid:water (1:1 v/v)

After 40 hours incubation a third (as yet untreated) set of wells were treated with 10 µM of the proteasome inhibitor MG132 or a DMSO diluent control. Incubation with MG132 was for 8 hr (Wang *et al*. 2013)

2.16 References

Adler, P., Kolde, R., Kull, M., Tkachenko, A., Peterson, H., Reimand, J. and Vilo, J. 2009. Mining for coexpression across hundreds of datasets using novel rank aggregation and visualization methods. *Genome Biology* 10(12), p. R139.

Al Soraj, M., He, L., Peynshaert, K., Cousaert, J., Vercauteren, D., Braeckmans, K., De Smedt, S. and Jones, A. T. 2012. siRNA and pharmacological inhibition of endocytic pathways to characterize the differential role of macropinocytosis and the actin cytoskeleton on cellular uptake of dextran and cationic cell penetrating peptides octaarginine (R8) and HIV-Tat. *Journal of Controlled Release* 161(1), p. 132-141.

Alvord, G., Roayaei, J., Stephens, R., Baseler, M. W., Lane, H. C. and Lempicki, R. A. 2007. The DAVID Gene functional classification tool: a novel biological module-centric algorithm to functionally analyze large gene lists. *Genome Biology* 8, p. R183.

Arabi, A., Ullah, K., Branca, R.M., Johansson, J., Bandarra, D., Haneklaus, M., Fu, J., Ariës, I., Nilsson, P., Den Boer, M.L., Pokrovskaja, K., Grandér, D, Xiao, G., Rocha, S., Lehtiö, J. and Sangfelt, O. 2012. Proteomic screen reveals Fbw7 as a modulator of the NF-κB pathway. *Nature Communications* 3, p. 976.

Baek, J,M., Kim, J.Y., Cheon, Y.H., Park, S.H., Ahn, S.J., Yoon, K.H., Oh, J. and Lee, M.S. 2014. Aconitum pseudo-laeve var. erectum inhibits receptor activator of nuclear factor kappa-B ligand-induced osteoclastogenesis via the c-Fos/nuclear factor of activated T-cells, cytoplasmic 1 signaling pathway and prevents lipopolysaccharide-induced bone loss in mice. *Molecules* 19(8) p. 11628-44.

Bejarano, E., Yuste, A., Patel, B., Stout, R.F. Jr., Spray, D.C. and Cuervo, A.M. 2014. Connexins modulate autophagosome biogenesis. *Nature Cell Biology* 16(5), p. 401-14.

Bijsmans, I.T., Bouwmeester, R.A., Geyer, J., Faber, K.N. and van de Graaf, S.F. 2012. Homo- and hetero-dimeric architecture of the human liver Na^+-dependent taurocholate co-transporting protein. *Biochemical Journal* 441(3), p. 1007-15.

Brahemi, G., Kona, F. R., Fiasella, A., Buac, D., Soukupová, J., Brancale, A., Burger, A. M. and Westwell, A. D. 2010. Exploring the structural requirements for inhibition of the ubiquitin E3 ligase breast cancer associated protein 2 (BCA2) as a treatment for breast cancer. *Journal of Medicinal Chemistry* 53(7), p. 2757-65.

Castro-Diaz, N., Ecco, G., Coluccio, A., Kapopoulou, A., Yazdanpanah, B., Friedli, M., Duc, J., Jang, S.M., Turelli, P. and Trono, D. 2014. Evolutionally dynamic L1 regulation in embryonic stem cells. *Genes and Development* 28(13), p. 1397-1409.

Cen, B., Xiong, Y., Song, J.H., Mahajan, S., DuPont, R., McEachern, K., DeAngelo, D.J., Cortes, J.E., Minden, M.D., Ebens, A., Mims, A., LaRue, A.C. and Kraft, A.S. 2014. The Pim-1 protein kinase is an important regulator of MET receptor tyrosine kinase levels and signaling. *Molecular and Cellular Biology* 34(13), 2517-32

Ciucci, A., Meco, D., De Stefano, I., Travaglia, D., Zannoni, G.F., Scambia, G., Riccardi, R., Saran, A., Mancuso, M. and Gallo, D. 2014. Gender effect in experimental models of human medulloblastoma: does the estrogen receptor β signaling play a role? *PLoS One* 9(7), p. e101623.

Clementz. A.G., Mutolo, M.J., Leir, S.H., Morris, K.J., Kucybala, K., Harris, H. and Harris, A. 2013. Collagen XV inhibits epithelial to mesenchymal transition in pancreatic adenocarcinoma cells. *PLoS One* 8(8), e72250.

Cornfine, S., Himmel, M., Kopp, P., El Azzouzi, K., Wiesner, C., Krüger, M., Rudel, T. and Linder, S. 2011. The kinesin KIF9 and reggie/flotillin proteins regulate matrix degradation by macrophage podosomes. *Molecular Biology of the Cell*. 22(2), p.202-15.

Cumming, G., Fidler, F. and Vaux, D. L. 2007. Error bars in experimental biology. *The Journal of Cell Biology* 177(1), pp. 7-11.

Escher, G., Hoang, A., Georges, S., Tchoua, U., El-Osta, A., Krozowski, Z. and Sviridov D. 2005. Demethylation using the epigenetic modifier, 5-

azacytidine, increases the efficiency of transient transfection of macrophages. *The Journal of Lipid Research* 46(2), p. 356-65.

Faux, M.C., Coates, J.L., Catimel, B., Cody, S., Clayton, A.H., Layton, M.J. and Burgess, A.W. 2008. Recruitment of adenomatous polyposis coli and beta-catenin to axin-puncta. *Oncogene* 27(44), p. 5808-20.

Jin, J., Pastrello, D., Penning, N. A. and Jones, A. T. 2008. Clustering of endocytic organelles in parental and drug-resistant myeloid leukaemia cell lines lacking centrosomally organised microtubule arrays. *The International Journal of Biochemistry & Cell Biology* 40(10), p. 2240-52.

Katayama, R., Shaw, A.T., Khan, T.M., Mino-Kenudson, M., Solomon, B.J., Halmos, B., Jessop, N.A., Wain, J.C., Yeo, A.T., Benes, C., Drew, L., Saeh, J.C., Crosby, K., Sequist, L.V., Iafrate, A.J. and Engelman, J.A. 2012. Mechanisms of acquired crizotinib resistance in ALK-rearranged lung Cancers. *Science Translational Medicine* 4(120) p. 120ra17.

Li, Q., Birkbak, N. J., Gyorffy, B., Szallasi, Z. and Eklund, A. C. 2011. Jetset: selecting the optimal microarray probe set to represent a gene. *BMC Bioinformatics* 12(1), p. 474.

Lichtenstein, A., Minogue, P. J., Beyer, E. C. and Berthoud, V. M. 2011. Autophagy: a pathway that contributes to connexin degradation. *Journal of Cell Science* 124(6), pp. 910-20.

Luke, G.P., Myers, J.N., Emelianov, S.Y. and Sokolov, K.V. 2014. Sentinel lymph node biopsy revisited: ultrasound-guided photoacoustic detection of micrometastases using molecularly targeted plasmonic nanosensors. *Cancer Research* 74(19), p. 5397-408.

Malik, I.A., Naz, N., Sheikh, N., Khan, S., Moriconi, F., Blaschke, M. and Ramadori, G. 2011. Comparison of changes in gene expression of transferrin receptor-1 and other iron-regulatory proteins in rat liver and brain during acute-phase response. *Cell Tissue Research* 344(2), p. 299-312.

Masiello, M.G., Cucina, A., Proietti, S., Palombo, A., Coluccia, P., D'Anselmi, F., Dinicola, S., Pasqualato, A., Morini, V. and Bizzarri. M. 2014. Phenotypic switch induced by simulated microgravity on MDA-MB-231 breast cancer cells. *Biomed Research International* 2014, p. 652434

Miyakawa, K.,Ryo, A., Murakami, T., Ohba, K., Yamaoka, S., Fukuda, M., Guatelli, J. and Yamamoto, N. 2009. BCA2/Rabring7 promotes tetherin-dependent HIV-1 restriction. *PLoS Pathogens* 5(12), p. e1000700.

Orenstein, S.J., Kuo, S.H., Tasset, I., Arias, E., Koga, H., Fernandez-Carasa, I., Cortes, E., Honig, L.S., Dauer, W., Consiglio, A., Raya, A., Sulzer, D. and Cuervo, A.M. 2013. Interplay of LRRK2 with chaperone-mediated autophagy. *Nature Neuroscience*16(4), p. 394-406.

Pacheco-Quinto, J. and Eckman, E.A. 2013. Endothelin-converting enzymes degrade intracellular β-Amyloid produced within the endosomal/lysosomal pathway and autophagosomes. *The Journal of Biological Chemistry* 288(8), p. 5606-15.

Sato, J., Kinugasa, M., Satomi-Kobayashi, S., Hatakeyama, K., Knox, A.J., Asada, Y., Wierman, M.E., Hirata, K. and Rikitake, Y. 2014. Family with sequence similarity 5, member C (FAM5C) increases leukocyte adhesion molecules in vascular endothelial cells: implication in vascular inflammation. *PLoS One* 9(9), e107236.

Scotter, E.L., Vance, C., Nishimura, A.L., Lee, Y.B., Chen, H.J., Urwin, H., Sardone, V., Mitchell, J.C., Rogelj, B., Rubinsztein, D.C. and Shaw, C.E. 2014. Differential roles of the ubiquitin proteasome system and autophagy in the clearance of soluble and aggregated TDP-43 species. *Journal of Cell Science* 127(Pt 6), p. 1263-78.

Sigismund, S., Algisi, V., Nappo, G., Conte, A., Pascolutti, R., Cuomo, A., Bonaldi, T., Argenzio, E., Verhoef, L. G. and Maspero, E. 2013. Threshold-controlled ubiquitination of the EGFR directs receptor fate. *The EMBO Journal* 32(15), pp. 2140-2157.

Sigismund, S., Argenzio, E., Tosoni, D., Cavallaro, E.,Polo, S. and Di Fiore, P. P. 2008. Clathrin-mediated internalization is essential for sustained EGFR signaling but dispensable for degradation. *Developmental Cell* 15(2), pp. 209-219.

Sigismund, S., Woelk, T., Puri, C., Maspero, E., Tacchetti, C., Transidico, P., Di Fiore, P. P. and Polo, S. 2005. Clathrin-independent endocytosis of ubiquitinated cargos. *Proceedings of the National Academy of Sciences of the United States of America* 102(8), pp. 2760-2765.

Simpson, J. C., Griffiths, G., Wessling-Resnick, M., Fransen, J. A., Bennett, H. and Jones, A. T. 2004. A role for the small GTPase Rab21 in the early endocytic pathway. *Journal of Cell Science* 117(26), p. 6297-6311.

Tsubaki, J., Hwa, V., Twigg, S.M. and Rosenfeld, R.G. 2002. Differential activation of the IGF binding protein-3 promoter by butyrate in prostate cancer cells. *Endocrinology.* 143(5), p.1778-88.

Wang, Z., Nie, Z., Chen, W., Zhou, Z., Kong, Q., Seth, A. K., Liu, R. and Chen, C. 2013. RNF115/BCA2 E3 ubiquitin ligase promotes breast cancer cell proliferation through targeting p21Waf1/Cip1 for ubiquitin-mediated degradation. *Neoplasia* 15(9), p. 1028.

Wolken, D.M., McInnes, J. and Pon, L.A. 2014. Aim44p regulates phosphorylation of Hof1p to promote contractile ring closure during cytokinesis in budding yeast. *Moecular Biology of the Cell* 25(6), p.753-62.

Xu, Y., Shao, Y., Voorhees, J.J. and Fisher, G.J. 2006. Oxidative Inhibition of Receptor-type Protein-tyrosine Phosphatase κ by Ultraviolet irradiation activates epidermal growth factor receptor in Human Keratinocytes. *The Journal of Biological Chemistry* 281(37), p. 27389-97.

Yogalingam, G. and Pendergast, A.M. 2008. Abl kinases regulate autophagy by promoting the trafficking and function of lysosomal components. *The Journal of Biological Chemistry* 283(51), p. 35941-53.

Chapter 3: *In silico* studies of BCA2 in Breast Cancer and Identification of Co-expressed Genes

3.1 Biomarker and survival analysis

The expanding research use of microarray technology has lead to the creation of online repositories for gene expression data. Microarray databases are free, searchable resources that allow users to access large quantities of experimental data for analytical purposes. In this project publically available gene microarray databases were used for three main objectives. Firstly, clinical gene expression data was used to evaluate the impact of BCA2 on patient survival in breast cancer, importantly also according to subtype. Secondly, coexpression analysis was performed to identify genes which may be coregulated with BCA2 and/or have similar cellular functions. Thirdly, microarray data from specific experiments were examined in order to identify changes in BCA2 expression that may be biologically relevant and warrant further study. The experimental datasets examined were primarily those pertaining to breast cancer development, oestrogen stimulation, therapeutic resistance and oncogene overexpression (including RTKs).

3.1.1 KM Plotter

The KM Plotter (http://www.kmplot.com/) is an online analysis tool that integrates microarray expression data with clinical information from 4,142 breast tumours. Users can examine the impact on survival of different levels of gene expression for over 22 thousand target genes (Gyorffy *et al.* 2010). Median gene expression is used to split the data into high and low expressing groups and survival curves are generated

across all breast cancers or for analyses restricted according to different parameters such as oestrogen receptor (ER) status, molecular subtype, grade etc. The hazard ratio for RFS with 95% confidence intervals and logrank P value are automatically calculated for low vs. high expression. The effect of BCA2 expression was analysed using the optimal "JetSet" probe: AffymetrixID 212742_at (Li *et al*. 2011). Results of the survival analyses performed as part of this project are shown in Figure 3-1.

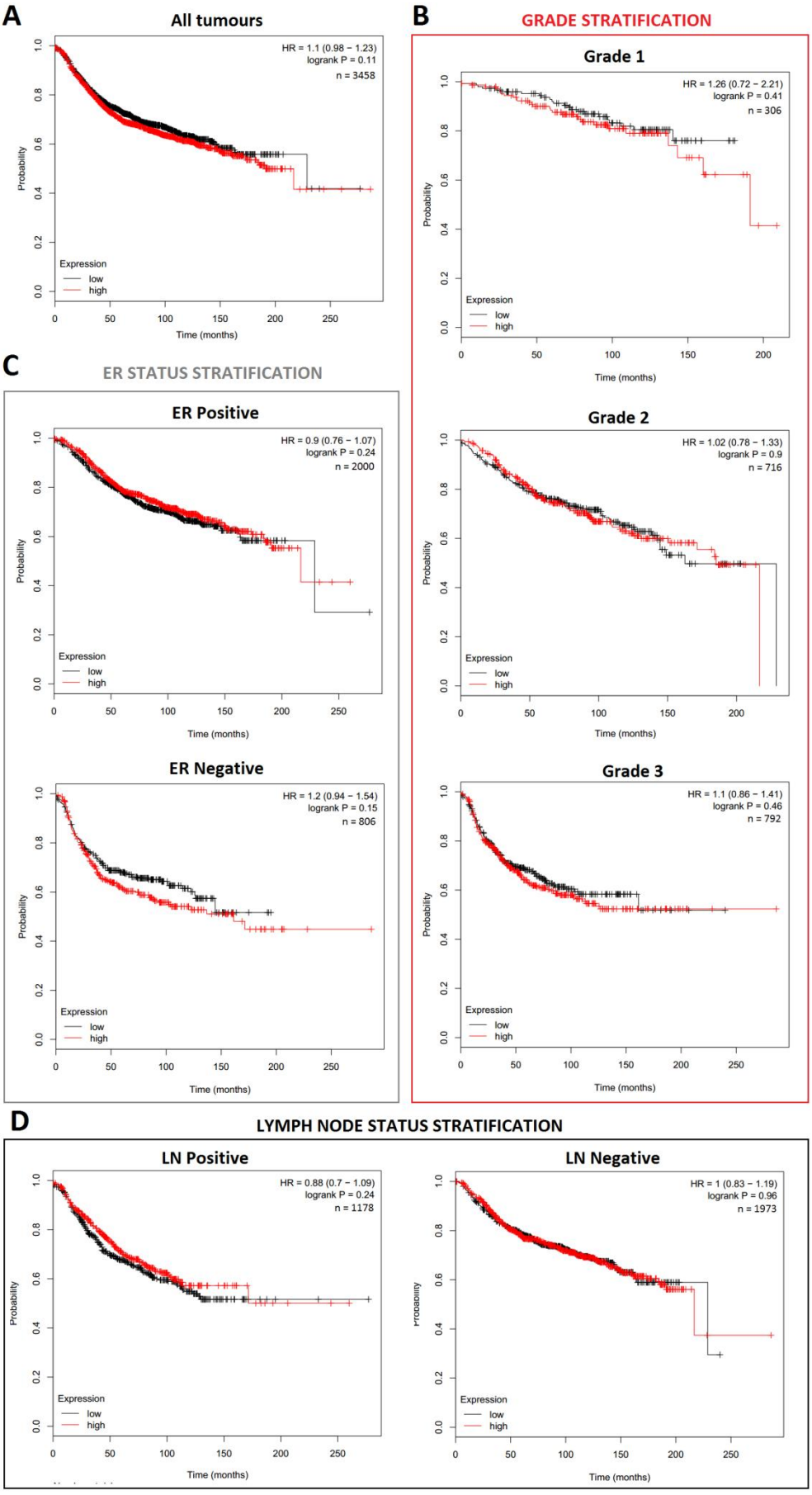
A
All tumours
HR = 1.1 (0.98 − 1.23)
logrank P = 0.11
n = 3458
B
GRADE STRATIFICATION
Grade 1
HR = 1.26 (0.72 − 2.21)
logrank P = 0.41
n = 306
Grade 2
HR = 1.02 (0.78 − 1.33)
logrank P = 0.9
n = 716
Grade 3
HR = 1.1 (0.86 − 1.41)
logrank P = 0.46
n = 792
C
ER STATUS STRATIFICATION
ER Positive
HR = 0.9 (0.76 − 1.07)
logrank P = 0.24
n = 2000
ER Negative
HR = 1.2 (0.94 − 1.54)
logrank P = 0.15
n = 806
D
LYMPH NODE STATUS STRATIFICATION
LN Positive
HR = 0.88 (0.7 − 1.09)
logrank P = 0.24
n = 1178
LN Negative
HR = 1 (0.83 − 1.19)
logrank P = 0.96
n = 1973
Probability
Expression
low
high
Time (months)

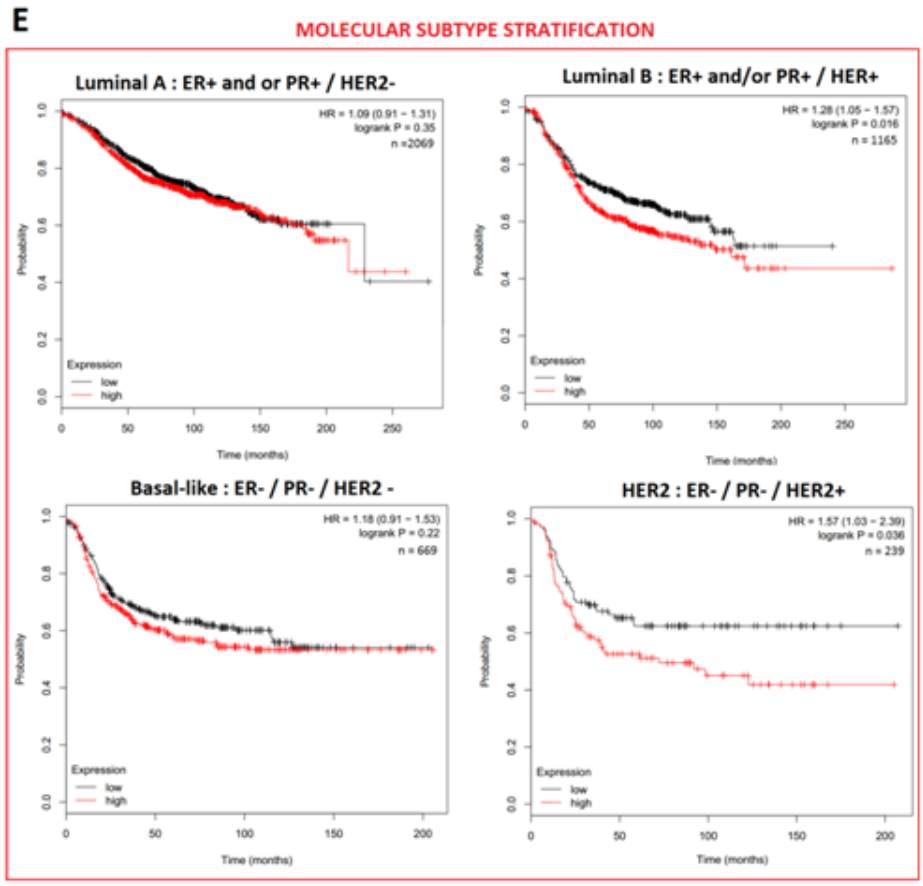

Figure 3-1: Kaplan-Meier survival curves for high vs. low BCA2 mRNA expression created using KM Plotter (Gyorffy *et al.* 2010). Probability of relapse free survival in high (red) or low (black) BCA2 expressing breast cancer is compared. A) Survival across all tumours. B) Survival stratified according to tumour grade C) Survival in ER+ vs. ER- disease. D) Survival in lymph node (LN)+ vs. LN- disease. E) Survival stratified according to molecular subtype.

Kaplan-Meier plots for high versus low BCA2 expression show that BCA2 only significantly impacts on relapse free survival in luminal B and HER2 subtypes of breast cancer (Fig. 3-1 E). High levels of BCA2 in luminal B disease are associated with poorer prognosis, with a hazard ratio (HR) for RFS of 1.28 and a P value of 0.016. Significantly reduced relapse free survival was also demonstrated in high BCA2 expressing HER2-type disease (HR = 1.57, P = 0.036).

3.1.2 GOBO: Gene expression-based outcome

The online biomarker assessment tool GOBO (http://co.bmc.lu.se/gobo) was also used to generate Kaplan-Meier relapse free survival plots based on BCA2 mRNA expression with the 212742_at Jetset probes (Li *et al*. 2011). GOBO is fundamentally similar to KM Plotter: microarray data and associated clinical information enable the user to investigate the potential prognostic significance of genes of interest (Ringnér *et al*. 2011). The GOBO analytical tool uses a smaller patient data set (1881 samples) than KM Plotter but has the advantage that it can be subdivided into >2 groups for outcome analysis, based on magnitude of gene expression. The greater expression stratification capability of GOBO means that graded relationships between gene expression and survival can be explored.

For the BCA2 survival analyses, relapse free patient survival was compared for samples separated into high, medium and low BCA2 expressing tumours. Kaplan-Meier plots were created across all tumours and for groups subdivided according to: ER-status, molecular subtype, histological grade, and lymph-node status. Logrank P values were calculated across the three expression levels. Survival curves for graded BCA2 expression are shown in Figure 3-2.

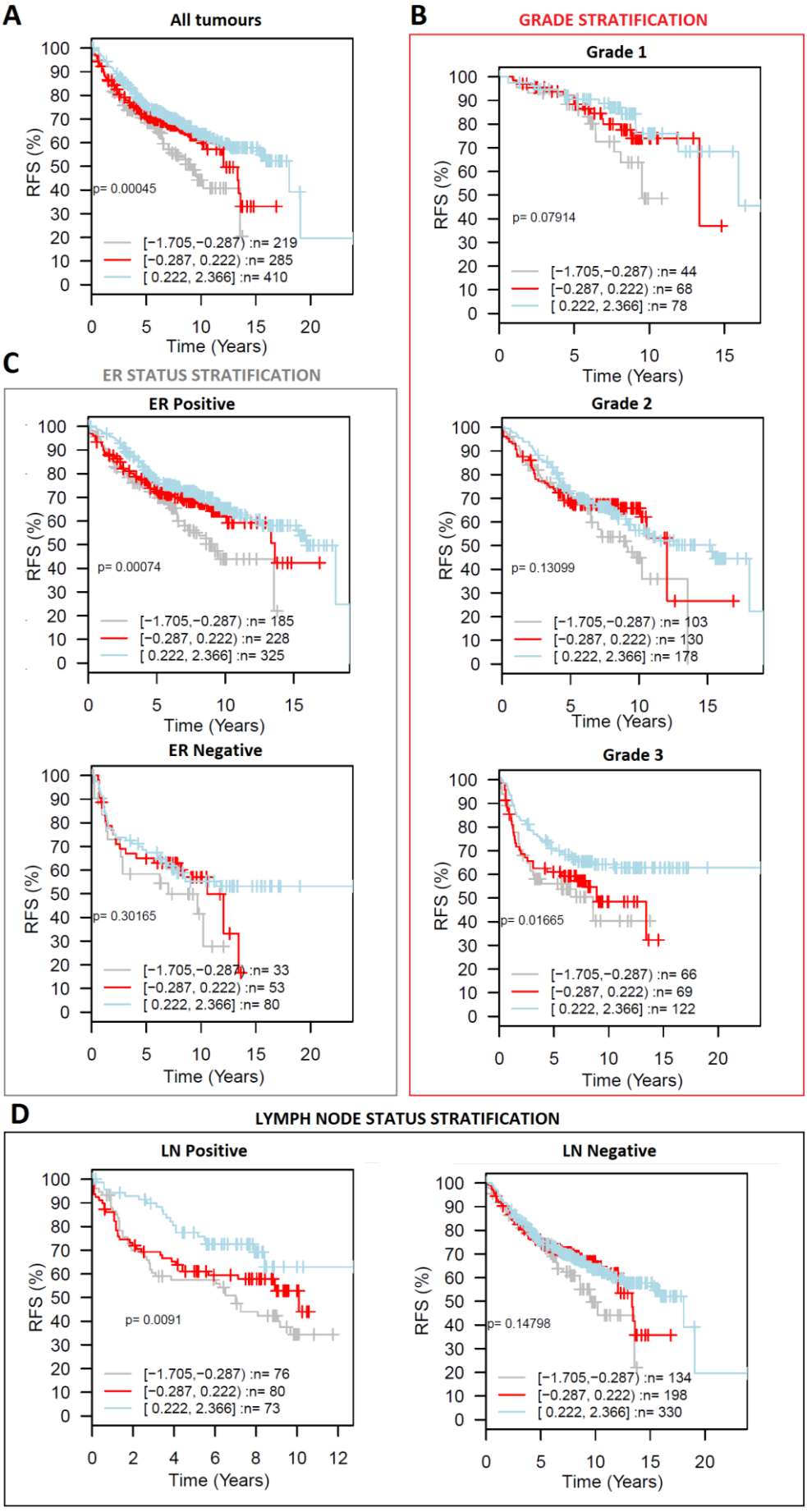
A
All tumours
RFS (%)
p= 0.00045
[−1.705,−0.287) :n= 219
[−0.287, 0.222) :n= 285
[0.222, 2.366] :n= 410
Time (Years)
B
GRADE STRATIFICATION
Grade 1
p= 0.07914
[−1.705,−0.287) :n= 44
[−0.287, 0.222) :n= 68
[0.222, 2.366] :n= 78
Grade 2
p= 0.13099
[−1.705,−0.287) :n= 103
[−0.287, 0.222) :n= 130
[0.222, 2.366] :n= 178
Grade 3
p= 0.01665
[−1.705,−0.287) :n= 66
[−0.287, 0.222) :n= 69
[0.222, 2.366] :n= 122
C
ER STATUS STRATIFICATION
ER Positive
p= 0.00074
[−1.705,−0.287) :n= 185
[−0.287, 0.222) :n= 228
[0.222, 2.366] :n= 325
ER Negative
p= 0.30165
[−1.705,−0.287) :n= 33
[−0.287, 0.222) :n= 53
[0.222, 2.366] :n= 80
D
LYMPH NODE STATUS STRATIFICATION
LN Positive
p= 0.0091
[−1.705,−0.287) :n= 76
[−0.287, 0.222) :n= 80
[0.222, 2.366] :n= 73
LN Negative
p= 0.14798
[−1.705,−0.287) :n= 134
[−0.287, 0.222) :n= 198
[0.222, 2.366] :n= 330

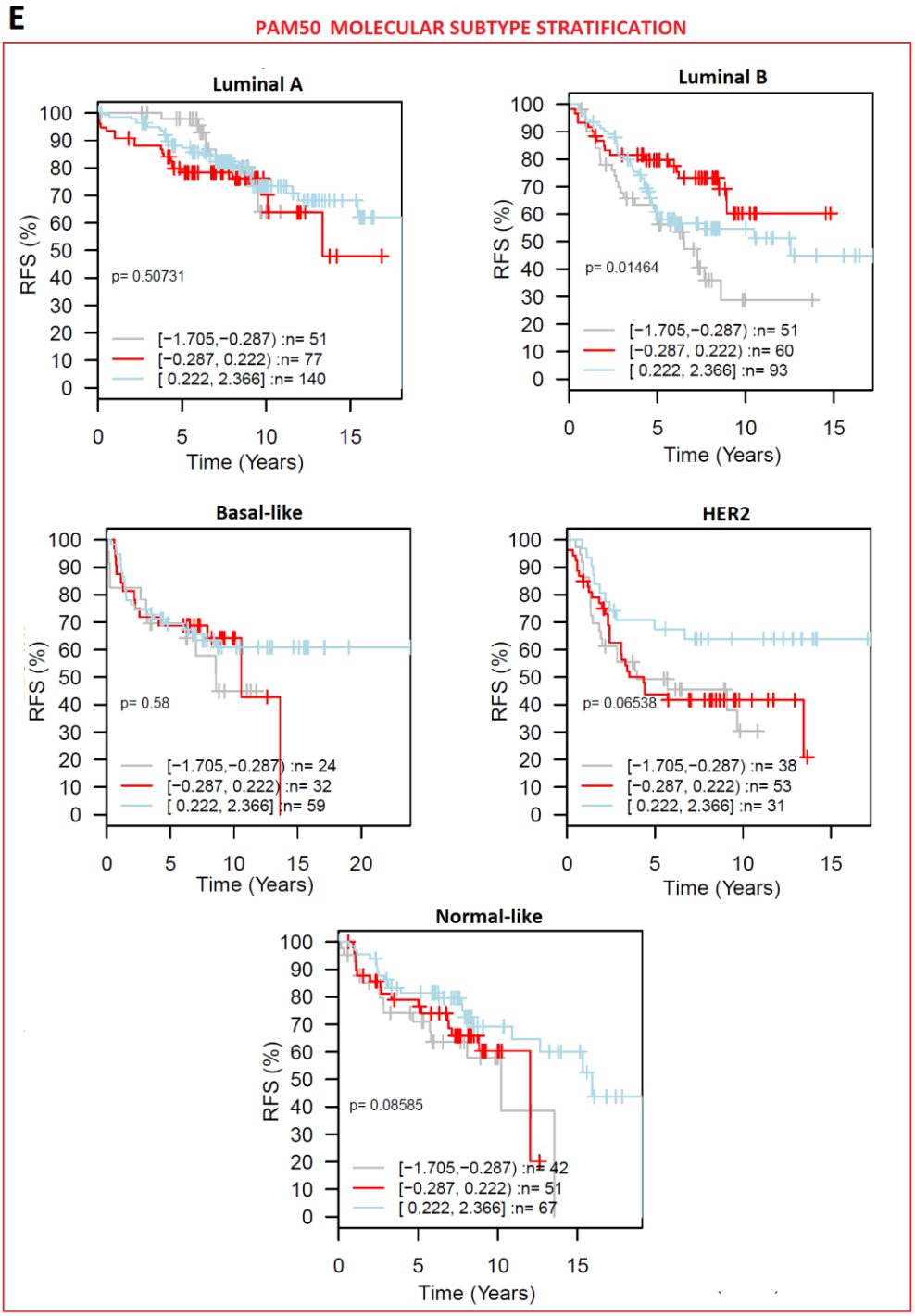

Figure 3-2: Kaplan-Meier survival curves for high vs. low BCA2 mRNA expression created using GOBO (Ringnér et al. 2011). Probability of relapse free survival in high (blue), medium (red) or low (grey) BCA2 expressing breast cancer is compared. A) Survival across all tumours. B) Survival stratified according to tumour grade C) Survival in ER+ vs. ER- disease. D) Survival in LN+ vs. LN- disease. E) Survival stratified according to molecular subtype.

The GOBO expression data indicated that higher BCA2 expression was associated with better prognosis in breast cancer (Fig. 3-2 A, p = 0.00045).

Significantly improved relapse free survival was also demonstrated in higher BCA2 expressing disease of tumour grade 3 (Fig. 3-2 B, p = 0.01665), ER positive status (Fig. 3-2 C, p = 0.00074) and LN positive status (Fig. 3-2 D, p = 0.00910). Intermediate BCA2 expression was associated with better prognosis in luminal B type disease with high and low expression being associated with poorer prognosis (Fig. 3-2 E, p = 0.01464).

In addition to producing Kaplan-Meier curves, GOBO also allows comparisons of gene expression between different molecular subtypes of breast cancer. Expression levels are compared using box-plots and analysis of variance (ANOVA) statistics. Average BCA2 expression levels were compared in patient breast tumours stratified according to molecular subtype, ER status and tumour grade (Fig. 3-3).

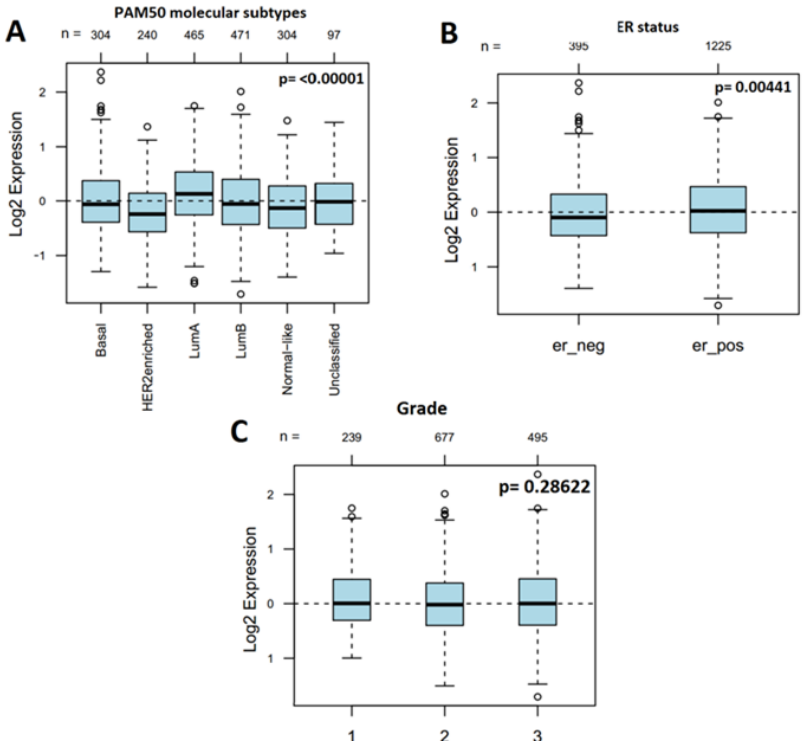

Figure 3-3: Comparative BCA2 expression analysis in GOBO datasets of patient tumours categorised according to molecular and clinical features. Relative BCA2 expression levels in patient data subdivided into A) different molecular subtypes of breast cancer, B) ER+ vs. ER- disease and C) tumour grade.

BCA2 was expressed at statistically significantly different levels across patient breast tumours of different molecular subtype ($p < 0.00001$, Fig. 3-3 A), and ER-status ($p = 0.00441$, Fig. 3-3 B) but not grade ($p = 0.28622$, Fig. 3-3 C). Higher BCA2 levels were associated with the luminal A subtype (Fig. 3-3 A) and with ER+ breast cancer (Fig. 3-3 B). There was no significant difference in expression levels between tumour grades (Fig. 3-3 C, $p = 0.28622$).

Mean BCA2 expression in a publically available dataset from a panel of 51 cell lines was analysed using GOBO (Fig. 3-4 A). A statistical comparison was also made between groups of cell lines divided according to basal or luminal type (Fig. 3-4 B). A third analysis looked at BCA2 expression across cell line groups defined by HER2 positivity, hormone receptor positivity and triple negative-type (Fig. 3-4 C).

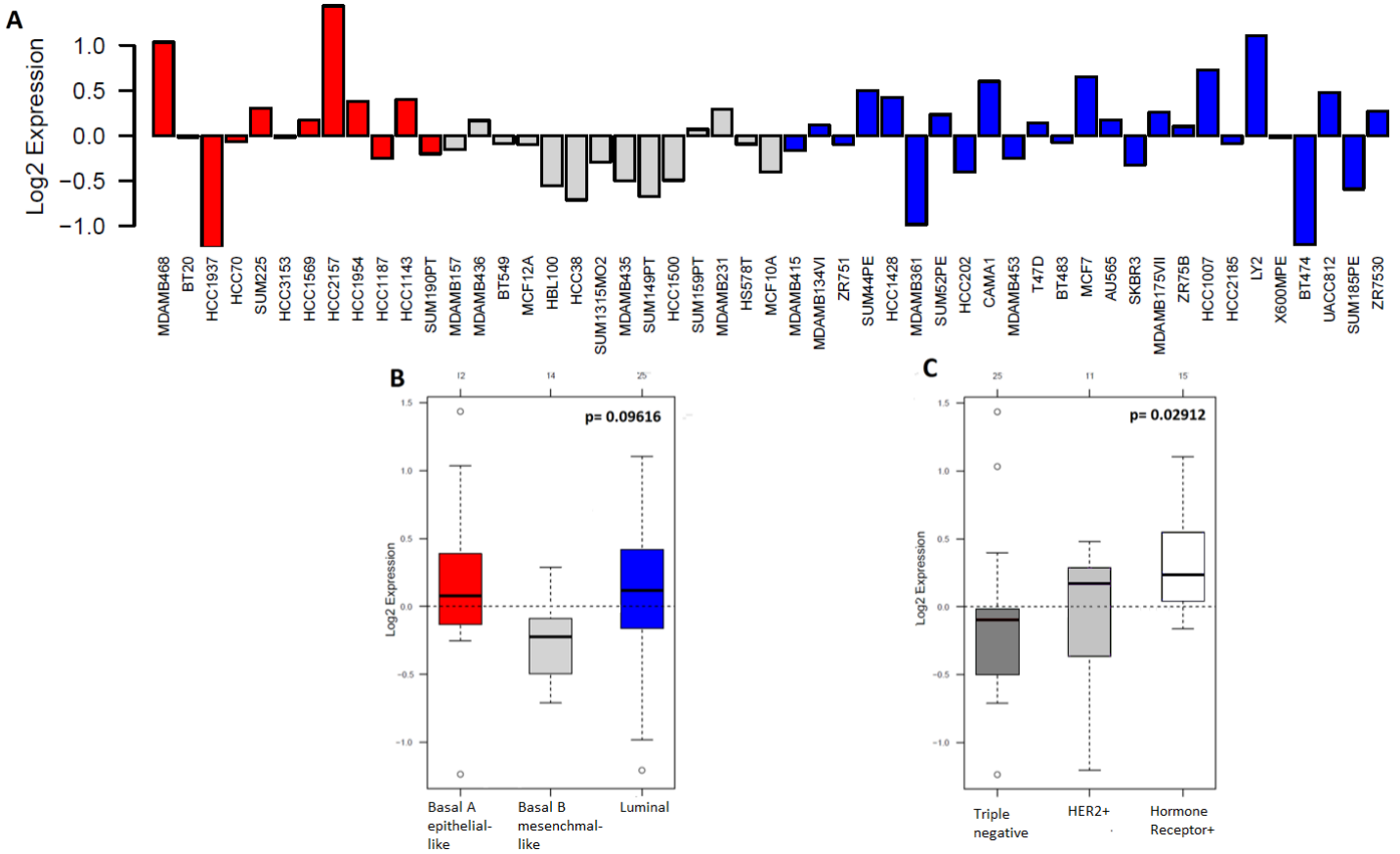

Figure 3-4: Comparative BCA2 expression analysis in GOBO dataset of 51 normal and malignant breast cell lines categorised according to subtype. A) Log2 BCA2 expression levels across individual cell lines. B) Mean Log2 BCA2 expression compared between basal A, B and luminal A subtypes. C) Mean Log2 BCA2 expression compared between triple negative, HER2 positive and hormone receptor positive disease. In A and B: Red = Basal A, Grey = Basal B and Blue = Luminal.

Mean BCA2 levels appeared to be higher in breast/breast cancer cell lines categorised as luminal (e.g. MCF-7 and T47D) though the difference in expression compared with basal A (e.g. MDA-MB-468) and basal B (e.g. MDA-MB-231) types was non-significant ($p = 0.09616$). Highest mean BCA2 expression was associated with hormone receptor positivity and lower mean BCA2 expression levels were seen in the triple negative and $HER2^+$ cell lines. The difference in BCA2 expression between triple negative, HER2 and hormone receptor positive cell line classes was statistically significant ($p = 0.02912$).

3.1.3 Gene co-expression using MEM: Multi experiment matrix

Co-expression is an important principle of gene expression analysis and relates to the theory that genes which are co-expressed may have shared transcriptional control mechanisms and/or similar functional roles. The usefulness of this rationale has been demonstrated in a number of studies on gene co-expression and function (Stuart *et al.* 2003; Wolfe *et al.* 2005).

Based on the "guilt by association" theory, genes whose expression was highly correlated with BCA2 were identified using the MEM tool (http://biit.cs.ut.ee/mem/). The MEM ranks genes according to expression similarity across 1794 human microarray datasets using an algorithm based on Pearson's correlation (Adler *et al.* 2009).

The full list of 48 genes whose expression was most highly correlated with BCA2 can be found in Appendix B. Chromosome locations of the co-expressed genes were researched using Genecards

(http://www.genecards.org/). The purpose of describing gene loci was to identify genes that were potentially co-expressed with BCA2 due to cytogenetic aberrations such as increased copy number. Of the 48 co-expressed genes, 6 were localised to the same chromosome arm as BCA2 (Chr.1q) and 7 were from Chr.7q (Table 3-1). The remaining genes were distributed fairly evenly among the other chromosome arms.

Table 3-1: Genes co-expressed with BCA2 from the long arm of chromosome 1 (grey) or the long arm of chromosome 7 (white)

Chr1q gene	Gene locus	Full gene name
POLR3C	1q21.1	Polymerase (RNA) III (DNA directed) polypeptide C (62kD)
TIMM17A	1q32.1	Translocase of inner mitochondrial membrane 17 homolog A (yeast)
TMCO1	1q22-q25	Transmembrane and coiled-coil domains 1
UBE2Q1	1q21.3	Ubiquitin-conjugating enzyme E2Q family member 1
TROVE2	1q31	TROVE domain family, member 2
HAX1	1q21.3	HCLS1 associated protein X-1
SBDS	7q11.21	Shwachman-Bodian-Diamond syndrome pseudogene 1
BCAP29	7q22.3	B-cell receptor-associated protein 29
AP2B1	17q11.2-q12	Adaptor-related protein complex 2, beta 1 subunit
ANKIB1	7q21.2	Ankyrin repeat and IBR domain containing 1
DLD	7q31-q32	Dihydrolipoamide dehydrogenase
METTL2B	7q32.1	Methyltransferase like 2A
PSMD12	17q24.2	Proteasome (prosome, macropain) 26S subunit, non-ATPase, 12

Functional annotation clustering analysis of the 48 co-expressed genes was performed using DAVID (http://david.abcc.ncifcrf.gov/). The strongest gene ontology (keyword) associations were primarily functions

relating to intracellular protein and vesicle transport (see Table 3-2). A more detailed table of results from the DAVID functional clustering analysis is also included in Appendix C.

Table 3-2: Genes co-expressed with, and ontologically related to, BCA2. Gene loci and protein names and functions were compiled from the Genecards database.

Gene	Locus	Protein	Function
BCAP29	7q22.3	B-cell receptor-associated protein 29	Transport of membrane proteins from endoplasmic reticulum to Golgi. May be involved in caspase-8 mediated apoptosis.
RAB18	10p12.1	Rab18	Transport of proteins from endoplasmic reticulum to Golgi.
COPB1	11p15.2	Coatomer protein complex, subunit beta	Part of the coatamer complex. Involved in protein transport from Golgi to endoplasmic reticulum.
TIMM17A	1q32.1	Mitochondrial inner membrane translocase	Protein translocation across inner mitochondrial membrane.
TRAM1	8q13.3	Translocation associated membrane protein 1	Glycosylation and translocation of secretary proteins across the endoplasmic reticulum
TNPO1	5q13.2	Transportin 1	Receptor for nuclear localisation signals. Nuclear import of proteins.
VPS37A	8p22	Vacuolar protein sorting associated protein 37A	Part of the ESCRT-I complex, required for sorting of ubiquitinated, endocytosed receptors into internal vesicles of MVBs.
VAMP7	Xq28 / yq12	Vesicle-associated membrane protein 7	Targeting, fusion and transport of vesicles with late endolysosomes.
ARL1	12q23.2	ADP-ribosylation factor-like 1	Regulation of Golgi structure and function.
AP2B1	17q11.2-q12	Adaptor-related protein complex 2, beta 1 subunit	Part of assembly protein complex 2 (AP2), which links clathrin to receptors in coated vesicles.
YWHAQ	2p25.1	14-3-3 θ / τ	Adaptor protein, binds to phosphoserine/threonine motifs and modulates protein activity and localisation. E.g. Protein kinase C θ.
VIMP	15q26.3	Selenoprotein S	Transfer of misfolded proteins from the endoplasmic reticulum to the cytosol for proteasomal degradation.
HAX1	1q21.3	HCLS1 associated protein X-1	Clathrin mediated endocytosis of integrin αvβ6.
SLC25A32	8q22.3	Mitochondrial folate carrier	Transports folate across the inner membranes of mitochondria

3.2 Gene expression changes: BioGPS

BioGPS (http://www.biogps.org/) is an open-access, online portal that allows users to find and extract gene expression information from a large selection of publically available datasets. BCA2 expression information was obtained via the BioGPS portal from the following datasets:

- **GSE15192**: Differences between CD44+/CD24- and CD44-/CD24+ subpopulation of immortalized human mammary epithelial cells
- **GSE5116**: Genomic Pathways of 17-beta-Estradiol Induced Malignant Cell Transformation in Human Breast Epithelial Cells
- **GSE4668**: Expression data from hormone-starved MCF7/BUS cell culture
- **GSE20361**: Dynamic changes during adaptation to estrogen deprivation in MCF7 cell line
- **GSE14986**: Antiestrogen-resistant subclones of MCF-7 human breast cancer cells are derived from a common clonal drug-resistant progenitor
- **GSE10696**: Expression analysis in A431_wt vs A431_GR cells
- **GSE14987**: Expression data from ERBB2 over-expression and EGF stimulation in MCF10A cells
- **GSE13274**: Ad-HER-wt and Ad-HER2-ki infected HMECs
- **GSE3151:** Oncogenic signalling dataset

The gene expression values in BioGPS datasets were generated in Affymetrix microarray experiments and relate to probe set fluorescence intensity. Gene expression data used in this chapter were obtained with Human Genome U133A (HG-U133 plus 2.0) arrays (GPL570 platform) and the 212742_at (JetSet) probe for optimal RNF115/BCA2 detection. Where available, data using the 226468_at probe set were also analysed to determine whether a consistent direction of expression change was

detected. This afforded further confidence that observed changes in BCA2 expression were robust and reliable.

In place of expression call data, log2 BCA2 expression was calculated and positive values were deemed "present". If in the experimental conditions BCA2 expression fell below control levels then log2 was calculated for the lowest data point to ensure the mRNA levels were still detectable (present).

Fluorescence intensity values were converted to relative expression ratios (fold-change) compared to control. The fold-change values were then log2 transformed and means and 95% confidence intervals were calculated. The statistical significance of differences between groups was assessed by one of two approaches. For analyses comparing two sample populations/means, the student's independent T-test was chosen to determine significance. For groups of three or more, one-way analysis of variance (ANOVA) for independent samples was carried out. ANOVA was followed, where appropriate, by Tukey's post-hoc testing. The log2 fold-change data and statistical test results are presented graphically in section 3.2.1 onwards.

A standard threshold of 1.5 (absolute) fold-change between the control and the test groups was considered the cut-off for biological relevance. Absolute fold-change values are presented in table format; red values indicate ≥1.5 fold induction, green values denote ≥ 1.5 fold suppression.

3.2.1 BCA2 expression in CD44+/CD24- and CD44-/CD24+ subpopulations of immortalized human mammary epithelial cells

A subpopulation of normal and malignant breast epithelial cells have been implicated in tumour initiation and have demonstrated stem cell like properties (Al-Hajj *et al*. 2003). This subpopulation is defined by a $CD44^{+}/CD24^{-/low}$ phenotype and in breast cancer is most often found in basal breast cancers that have undergone a degree of epithelial to mesenchymal transition (Sheridan et al. 2006; Honeth et al. 2008).

In order to determine whether BCA2 was differentially expressed in putative stem cells, the GSE15192 dataset was examined. This dataset was generated by gene expression profiling of $CD44^{+}/CD24^{-}$ and $CD44^{-}/CD24^{+}$ subpopulations of MCF-10A cells. The subpopulations were identified and sorted by flow cytometry in 4 independent experiments. More detailed descriptions of the methods employed are provided in the source publication (Bhat-Nakshatri *et al.* 2010). BCA2 expression data were extracted from the dataset, detectable expression was confirmed, then mean relative log2 fold-change between the cellular subpopulations was calculated and statistically compared. This fold-change in BCA2 expression in $CD44^{+}/CD24^{-}$ versus $CD44^{-}/CD24^{+}$ subpopulations are presented and compared in Figure 3-5.

A

Log2 BCA2 expression	
Probe set	CD44-/CD24+
212742_at	10.64
226468_at	10.17

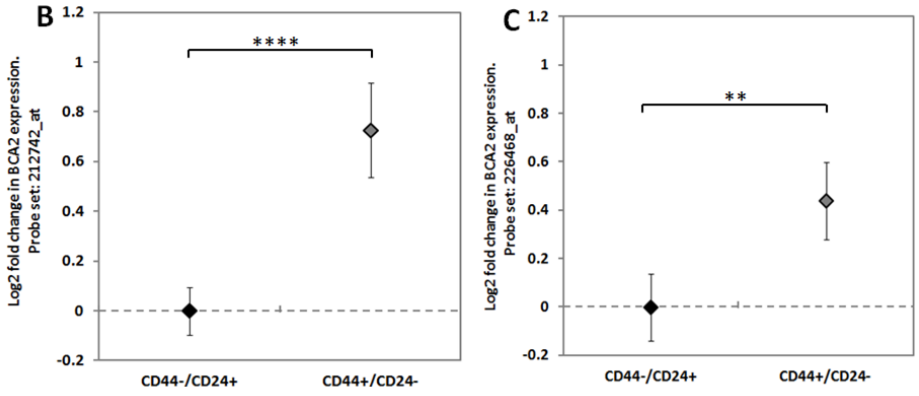

D

Fold-change in BCA2 expression relative to CD44-/CD24+	
Probe set	CD44+/CD24-
212742_at	1.66
226468_at	1.36

Figure 3-5: BCA2 mRNA expression in CD44-/CD24+ and progenitor-like CD44+/CD24- subpopulations in human mammary epithelial cells. Global gene expression in MCF-10A subpopulations was measured by microarray (Bhat-Nakshatri *et al*. 2010) and deposited online (GSE15192). A) Log2 mRNA expression analysis of controls confirmed detectable BCA2 expression with both probesets. Mean log2 fold change in BCA2 expression between the cell subpopulations was determined from B) the 212742_at probe set data and C) 226468_at set. *Error bars represent 95% confidence intervals* **** *Statistical significance* $p \leq 0.0001$. ** *Statistical significance* $p \leq 0.01$. D) Absolute fold change in BCA2 expression in the stem cell subpopulation. *Red values indicate fold induction* ≥ 1.5.

BCA2 expression was confirmed by log2 analysis (Fig. 3-5 A). Students independent T-test of the two subpopulation means IN Fig 3-5 B revealed that the CD44+/CD24- (stem-like) cells expressed significantly higher BCA2 levels than the CD44-/CD24+ cells when measured with both the 212742_at probe set ($p = 0.0001$) and the 226468_at set ($p = 0.0012$, Fig. 3-5 C). BCA2 expression measured with the JetSet probe showed a fold increase of 1.66 in the putative stem cell population (Fig. 3-5 D). The fold induction indicated by the 226468_at probe set was 1.36, below the threshold for biological significance but the directional trend (i.e. increase) in BCA2 expression was still apparent.

3.2.2 BCA2 expression during oestradiol induced oncogenic transformation of human breast epithelial cells

17β-oestradiol (E2) has been demonstrated to induce malignant transformation in human breast epithelial cells (Fernandez *et al*. 2005). The GSE5116 dataset is comprised of gene expression profiling of MCF-10F cells that were progressively transformed by E2 supplementation in 3 independent experiments (Huang *et al*. 2007). MCF-10F cells are an ER negative, immortalised, non-tumourigenic breast epithelial cell line. After 7-9 passages with bi-weekly E2 supplementation cells were subjected to further testing and selection and were classified according to their malignant properties. Cells that demonstrated high colony forming efficiency and spheroid (rather than duct) formation in collagen-matrix were categorised as transformed (trMCF). trMCF cells that were then able to cross the membrane in Matrigel invasion assays were classified as invasive bsMCF cells. Clones derived from the bsMCF cells were classed as bcMCF cells. The final classification of cell transformation was caMCF. These were cells harvested from tumours that had formed after injection of bsMCF and bcMCF cells into severe combined immunedeficient (SCID) mice. RNA was extracted from MCF-10F, trMCF, bcMCF and caMCF cells at three different passages and global gene expression was assessed by microarray. Using the GSE5116 dataset generated by these studies, BCA2 expression changes during malignant transformation were examined and results are presented in Figure 3-6.

A

Log2 BCA2 expression	
	MCF-10F control
212742_at	6.28
226486_at	5.17

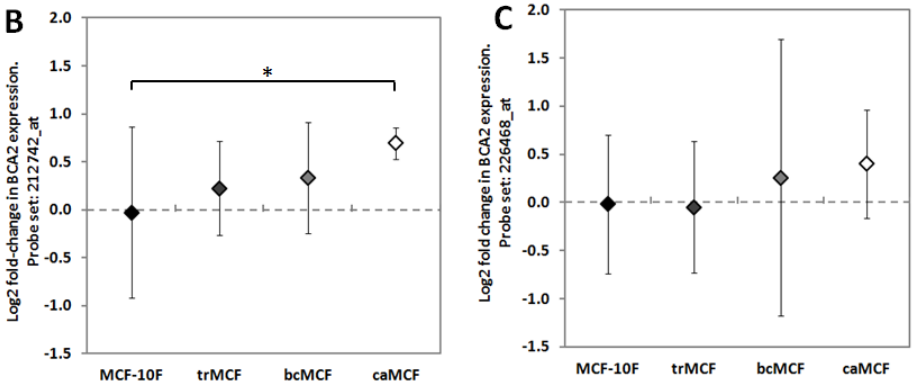

D

Fold-change in BCA2 expression relative to control			
Probe set	trMCF	bcMCF	caMCF
212742_at	1.18	1.27	1.62
226468_at	-1.02	1.26	1.33

Figure 3-6: BCA2 mRNA expression in progressively transformed mammary epithelial cells. Global gene expression in MCF-10F and derived cell lines was measured by microarray (Huang *et al.* 2007) and deposited online (GSE5116). A) Log2 mRNA expression analysis of controls confirmed detectable BCA2 expression with both probesets. Mean log2 fold change in BCA2 expression was determined from data obtained with B) the 212742_at probe set and C) the 226468_at probe set. * *Statistical significance $p \leq 0.05$. Error bars represent 95% confidence intervals.* D) Absolute fold change in BCA2 expression in the transformed cell lines relative to MCF-10F control. *Red values indicate fold induction ≥ 1.5*

BCA2 expression was confirmed by log2 analysis (Fig. 3-6 A). BCA2 fold-change measured with both probe sets exhibited a general trend of increasing BCA2 expression with increasing malignant transformation. The difference between groups measured using the 212742_at probe set (Fig. 3-6 B) was statistically significant by one-way ANOVA $F(3, 8) = 4.76$, $p = 0.0345$. Tukey post-hoc tests revealed that the increase in BCA2 expression was only statistically significant between the MCF-10F control cells and caMCF breast cancer cells ($p < 0.05$). The increase was above the threshold for biological relevance as the caMCF cells were associated with a 1.62 fold induction in BCA2 expression (Fig. 3-6 D). Although BCA2 fold-change measured with the 226468_at probe set

appeared to follow a similar trend of increasing BCA2 expression with increasing transformation (Fig. 3-6 C), the difference between groups was not statistically significant by one-way ANOVA ($F(3, 8) = 1.04$, $p = 0.4257$). The lack of statistical significance may relate to the increased variability of the expression data obtained with the 226468_at probe set compared with 212742_at.

3.2.3 Response of BCA2 expression to oestrogen deprivation and supplementation.

BCA2 expression has been shown to be regulated by the oestrogen receptor and by E2 stimulation in breast cancer cells (Kona *et al*. 2012). To analyse BCA2s transcriptional responsiveness to E2, two datasets from oestrogen stimulation and/or deprivation were examined from the BioGPS portal. Data from the GSE4668 set were obtained from 5 independent experiments in which MCF7/BUS cells (clonal cells derived from the MCF-7 cell line) were stimulated with sub-saturating concentrations (0-100 pM) of E2 for 48 hr. E2 induced changes in gene expression compared to unstimulated cells were evaluated by microarray (Coser *et al.* 2003). Levels of BCA2 expression following different E2 doses are presented in Figure 3-7 A. Also included in the GSE4668 dataset are the results of three independent microarray experiments in which cells were deprived of oestrogen for 0, 24, and 48 hr. BCA2 relative expression data for hormone starved MCF-7/BUS cells is shown in Figure 3-7 B.

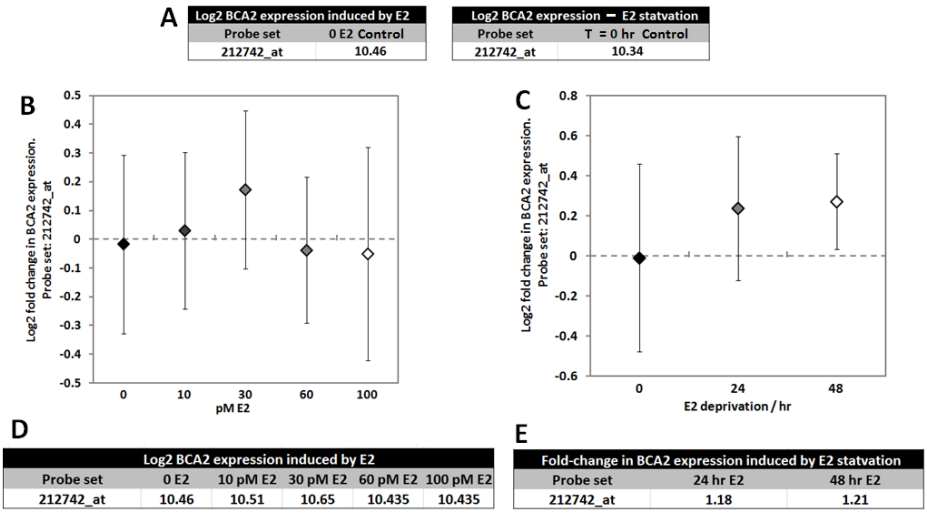

Figure 3-7: BCA2 mRNA expression in oestrogen stimulated and oestrogen deprived MCF-7/BUS cells. Global gene expression was determined by microarray (Coser *et al.* 2003) and deposited online (GSE4668). A) Log2 mRNA expression analysis of controls confirmed detectable BCA2 expression in both experiments. Mean log2 fold change in BCA2 expression was calculated. B) BCA2 expression in MCF-7/BUS cells treated with increasing dose of E2. C) BCA2 expression over an E2 deprivation time course of 0 – 48 hours. D and E) Associated absolute fold-changes in BCA2 expression are shown below resepective experiment graphs.

BCA2 expression was confirmed by log2 analysis (Fig. 3-7 A) expression was also checked and confirmed for the lowest expression point (100 pM E2). The data in Figure 3-7 B and C indicate that BCA2 mRNA levels are not significantly altered by either oestrogen stimulation or starvation. There was no significant difference between MCF-7/BUS cell groups stimulated by different oestrogen concentrations (Fig. 3-7 B). Statistical significance was evaluated by one-way ANOVA $F(4, 20) = 0.71$, $p = 0.5946$. There was also no significant difference in the mRNA levels of BCA2 after 24 or 48 hours of hormone starvation (Fig. 3-7 C): one-way ANOVA $F(2, 6) = 3.21$, $p = 0.1127$. None of the absolute fold-changes indicated a biologically significant alteration in BCA2 expression (Fig. 3-7 D and E).

Data in Figure 3-8 were extracted from the GSE20361 data set. The data in this set come from microarray analysis of a series of RNA extracts taken from long-term oestrogen deprived (LTED) MCF-7 cells over a 180 day period (Aguilar *et al*. 2010).

A

Log2 BCA2 expression	
Probe set	0 days (control)
212742_at	3.52
226468_at	3.56

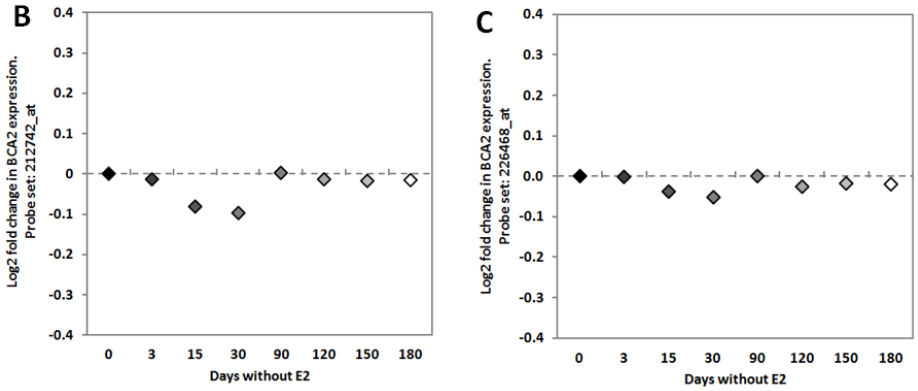

D

Fold-change in BCA2 expression following E2 deprivation							
Probe set	3 days	15 days	30 days	90 days	120 days	150 days	180 days
212742_at	-1.01	-1.06	-1.07	1.00	-1.01	-1.01	-1.01
226468_at	1.00	-1.03	-1.04	1.00	-1.02	-1.01	-1.01

Figure 3-8: BCA2 mRNA expression in long term oestrogen deprived MCF-7 cells. Global gene expression was determined by microarray (Aguilar *et al.* 2003) and deposited online (GSE20361). A) Log2 mRNA expression analysis of controls confirmed detectable BCA2 expression with both probesets. Mean log2 fold change in BCA2 expression over a time course of oestrogen deprivation in MCF-7 cells was calculated from the: B) the 212742_at probe set and C) the 226468_at probe set. D) Associated absolute fold-changes in BCA2 expression are shown below resepecive experiment graphs.

BCA2 expression was confirmed by log2 analysis of controls (Fig. 3-8 A) and expression was also checked and confirmed for the lowest expression point (day 30). Statistical testing could not be performed on the LTED culture as only single experiment values were given. The amount of BCA2 appeared to be decreasing up to 30 days but then returned to baseline levels between 30 and 90 days. Overall there was relatively little variation in BCA2 expression detected by either the 212742_at or 226468_at probe sets over the time course (Fig. 3-8).

3.2.4 BCA2 expression in tamoxifen and fulvestrant resistant breast cancer cell lines

BCA2 regulation by E2 and the ER has been shown to be impaired *in vitro* by tamoxifen anti-oestrogen treatment (Kona *et al*. 2012). It was therefore hypothesised that levels of the E3 ligase may be altered in cell lines with acquired anti-oestrogen therapeutic resistance. To investigate this hypothesis, the GSE14986 dataset was interrogated. This dataset contains microarray data for the MCF-7 cell line along with MCF-7 derived cell lines with acquired resistance to anti-E2 (tamoxifen) and anti-ER (fulvestrant) therapies. Details of the production and selection process of the drug resistant clonal cell lines are given in the source publication (Coser *et al*. 2009). Mean relative BCA2 levels in MCF-7, low cell density control, tamoxifen resistant (TAMR) and fulvestrant resistant (FASR) cells are presented and compared in Figure 3-9.

A

Log2 BCA2 expression	
Probe set	MCF-7
212742_at	9.18
226468_at	8.23

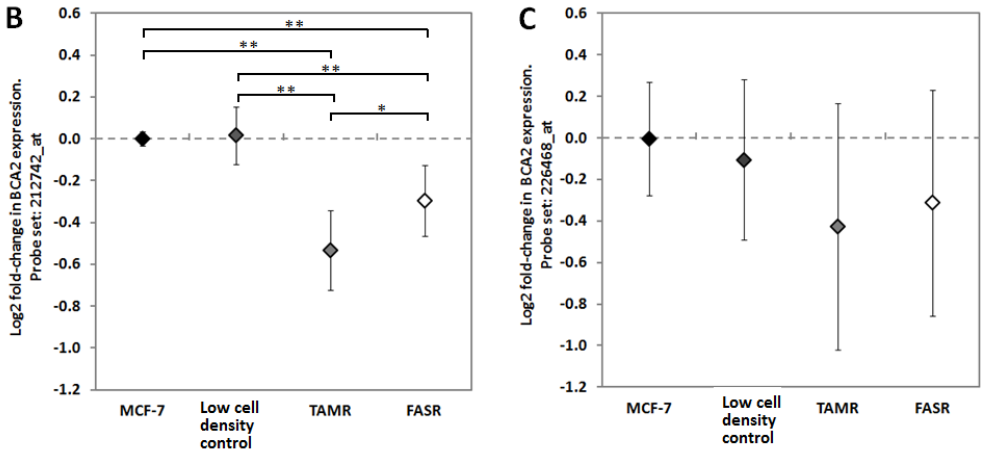

D

Fold-change in BCA2 expression relative to MCF-7 control			
Probe set	Low density control	TAMR	FASR
212742_at	1.01	-1.44	-1.23
226468_at	-1.12	-1.21	-1.21

Figure 3-9: BCA2 mRNA expression in MCF-7 breast cancer cells and derived cell lines with acquired hormone therapy resistance. Global gene expression profiles of MCF-7 and hormone refactory celll lines were obtained by microarray (Coser *et al.* 2009) and deposited under the dataset identifier GSE14986. A) Log2 mRNA expression analysis of controls confirmed detectable BCA2 expression with both probesets. Mean log2 fold change in BCA2 expression was compared between the cell lines using (B) the 212742_at probe set data and C) the 226468_at set. ** *Statistical significance $p \leq 0.01$. Error bars represent 95% confidence intervals.* D) Absolute fold change in BCA2 expression in the resistant cell lines relative to MCF7 control.

BCA2 expression was confirmed by log2 analysis of controls (Fig. 3-9 A) and expression was also checked and confirmed for the lowest expression point (TAMR). Both tamoxifen and fulvestrant resistant cell lines demonstrated slight reductions in BCA2 expression levels, though the suppression appeared to be greater in the TAMR cells. The differences between the MCF-7 cells and the resistant cell lines were statistically significant for the 212742_at probe set (Fig. 3-9 A): one-way ANOVA $F(3, 11) = 29.01$, $p < 0.0001$. Tukey post-hoc testing indicated that the difference in BCA2 expression was statistically significant between the MCF-7 cells and the cell lines resistant to tamoxifen

(TAMR, $p < 0.01$) and to fulvestrant (FASR, $p < 0.01$). Despite the differences being statistically significant however, the fold suppression of 1.44 in the TAMR and 1.23 in the FASR cells were below the 1.5 threshold for biological relevance (Fig. 3-9 C).

None of the differences between groups tested with the 226468_at probe set (Fig. 3-9 B) were statistically significant as determined by one-way ANOVA $F(3, 11) = 1.52$, $p = 0.2640$.

3.2.5 BCA2 expression in EGFR overexpressing and derived gefitinib resistant cell lines

There is literature to suggest that BCA2 has a functional role in EGFR endocytosis and downregulation (Mizuno *et al.* 2003; Sakane *et al.* 2007; Smith *et al*. 2013). However, reports are conflicting in terms of the protein's mechanism of action and the ultimate effects on receptor trafficking. In light of BCA2's putative endocytic function and the known association between EGFR inhibitor resistance and altered endocytosis (Hopper-Borge *et al*. 2009), changes in BCA2 expression were examined in a dataset of EGFR inhibitor (gefitinib) sensitive and resistant cell lines. The GSE10696 dataset was generated from a study comparing the EGFR overexpressing A431 skin epithelial cell line with a model of acquired resistance (A431_GR). The A431_GR cell line was developed from parental A431 cells by chronic gefitinib exposure and resistant cell selection. More methodological details are described in (Guix *et al.* 2008). The results of the BCA2 expression analyses are presented in Figure 3-10.

A

Log2 BCA2 expression	
Probe set	A431
212742_at	10.18
226468_at	9.18

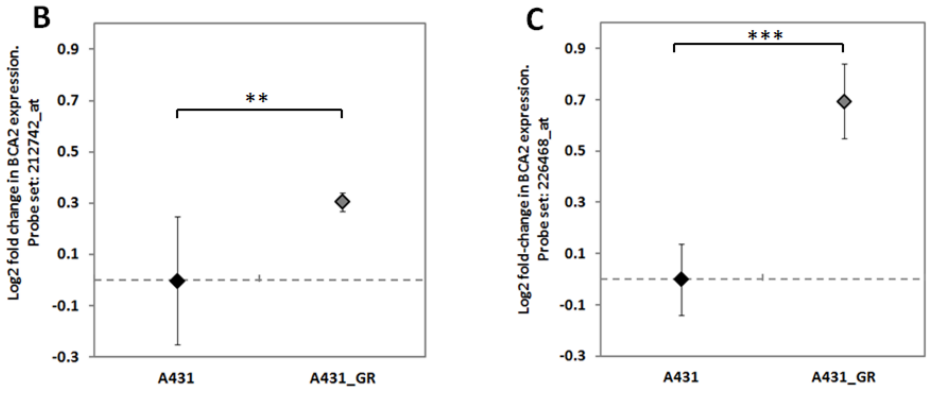

D

Fold-change in BCA2 expression relative to A431 control	
Probe set	A431_GR
212742_at	1.24
226468_at	1.62

Figure 3-10: BCA2 mRNA expression levels in parental (naturally EGFR overexpressing) cancer cells and a derived cell line model of gefitinib resistance. Global gene expression in A431 and acquired gefitinib resistant A431 cells was measured by microarray (Guix *et al*. 2008). A) Log2 mRNA expression analysis of controls confirmed detectable BCA2 expression with both probesets. Mean log2 fold change BCA2 expression from B) the 212742_at probe set and C) the 226468_ was compared between the EGFR inhibitor sensitive (parental) cell line and the acquired resistance model. *** *Statistical significance* $p \leq 0.001$. ** *Statistical significance* $p \leq 0.01$. *Error bars represent 95% confidence intervals.* D) Absolute fold change in BCA2 expression in the gefitinib resistant cell lines relative to A431 control. *Red values indicate fold induction* ≥ 1.5

BCA2 expression was confirmed by log2 analysis (Fig. 3-10A). For both BCA2 probe sets an elevation of BCA2 expression was evident in the gefitinib resistant cells compared with wild type A431 cells. Student's independent T-tests indicated the difference in expression between the two cell types was statistically significant for 242742_at probe set (Fig. 3-10 B, p = 0.0062) and for the 226468_at (Fig. 3-10 C, p = 0.0001).

The 242742_at probes indicated an absolute fold induction of 1.24 of BCA2 in the resistant compared with wild type cells, the 226468_at probes on the other hand showed a 1.62 fold increase (Fig. 3-10 D).

3.2.6 BCA2 expression following HER2 overexpression in mammary epithelial cells

Despite strong evidence for a role in breast cancer and literature to indicate that BCA2 has a regulatory role in EGFR endocytosis, no published work to date has explored possible effects of BCA2 on HER2. Trafficking of HER2 is poorly characterised but the receptor is known to form heterodimers with other ErbB family receptors such as EGFR. Heterodimerisation with HER2 has been shown to modulate the downregulation and trafficking of EGFR (Hendriks *et al*. 2003). HER2 is an internalisation resistant receptor, a property that gives rise to sustained activity of downstream signalling pathways (Hommelgaard *et al*. 2004). Identifying proteins that influence HER2 downregulation may therefore potentially provide therapeutic opportunities.

BCA2 expression data was analysed from two separate microarray studies of HER2 overexpression in breast epithelial cells. The GSE14987 dataset examines transcriptional effects of HER2 over-expression and EGF stimulation in MCF10A cells from 3 independent experiments (Wolfer *et al*. 2010). The GSE13274 microarray data is from human mammary epithelial cells (HMECs) and HMECs transfected with HER2 or a kinase inactivated HER2 mutant (Hartman *et al*. 2010). Five independent experiments were performed.

Comparative BCA2 expression data from the GSE14987 and GSE13274 datasets are presented in Figure 3-11.

A

Log2 BCA2 expression in MCF-10A cells	
Probe set	Vector control
212742_at	8.64
226468_at	7.32

Log2 BCA2 expression in HMEC cells	
Probe set	GFP control
212742_at	10.21
226468_at	8.35

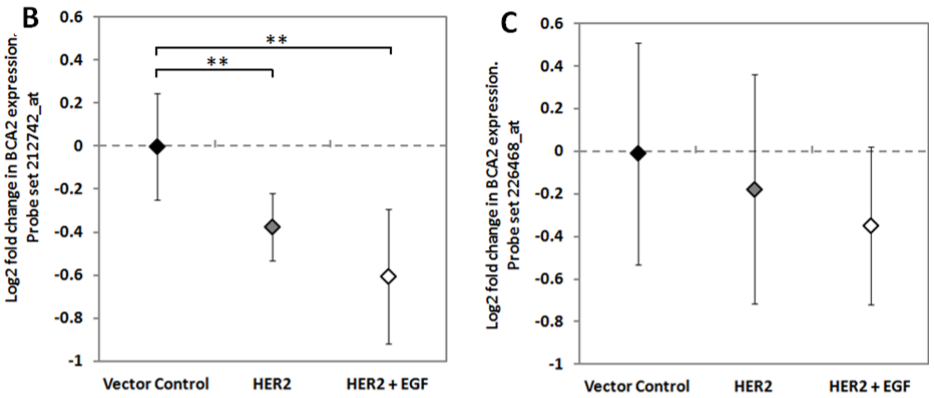

D

Fold-change in BCA2 expression relative to control		
Probe set	HER2	HER2 + EGF
212742_at	-1.30	-1.52
226468_at	-1.12	-1.27

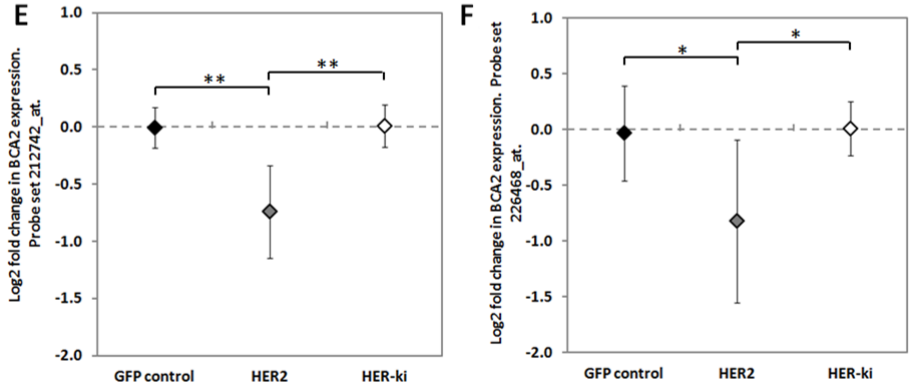

G

Fold-change in BCA2 expression relative to control		
Probe set	HER2	HER2-ki
212742_at	-1.64	1.01
226468_at	-1.65	1.01

Figure 3-11: BCA2 mRNA expression levels in HER2 overexpressing mammary epithelial cell lines. BCA2 expression data, measured by two probe sets, 212742_at probe and 226468_at, were extracted from two datasets. A) Log2 mRNA expression analysis of controls confirmed detectable BCA2 expression with both probesets and in both datasets. B and C were taken from GSE14987 and depict mean log2 fold change in BCA2 expression in MCF-10A and HER2 transfected cells ± EGF stimulation (Wolfer *et al*. 2010). E and F) Mean log2 fold change BCA2 expression from the GSE13274 dataset of HMEC cells transfected with GFP control, HER2 or a kinase-dead HER2 mutant (Hartman *et al*. 2010). ** *Statistical significance* $p \leq 0.01$. * *Statistical significance* $p \leq 0.05$. *Error bars represent 95% confidence intervals.* D and G) Associated absolute fold-changes in BCA2 expression are shown below respective experiment graphs. *Green values indicate fold suppression* ≥ 1.5

BCA2 expression was confirmed by log2 analysis of controls (Fig. 3-11 A and D) and expression was also checked and confirmed for the lowest

expression points for each experiment (HER2 + EGF in the GSE14987 dataset and C and HER2 in the GSE13274 dataset).

Both probe sets and both experiments displayed small but statistically significant downregulation of BCA2 following HER2 overexpression. In the HER2 overexpressing MCF-10A cells BCA2 mRNA levels measured by 212742_at suggested a 1.30 fold downregulation (Fig. 3-11 D). Further reduction in BCA2 was apparent in the HER2 transfected cells stimulated with EGF: BCA2 expression was reduced by 1.52 fold relative to the GFP control transfected cells (Fig. 3-11 B). One-way ANOVA of the 212742_at data (Fig. 3-11 B) indicated that the differences in BCA2 expression between the groups were statistically significant $F(2, 6) = 28.37$, $p = 0.0009$. Tukey post-hoc testing returned significant differences between the GFP control and HER2 transfected cells, with and without EGF stimulation ($p < 0.01$). Though the trend seen in Figure 3-11 B was mirrored in the 226468_at probe set data (Fig. 3-11 C), the results of the one-way ANOVA indicated the differences between groups were not statistically significant $F(2, 6) = 2.30$, $p = 0.1813$.

BCA2 expression in the transfected HMECs was only modulated by overexpression of the kinase-competent HER2, suggesting the decrease in BCA2 may be linked with HER2 function. The difference between the three transfected groups, as detected with probe set 212742_at (Fig. 3-11 E), was statistically significant: one-way ANOVA $F(2, 12) = 18.49$, $p = 0.0002$. Tukey post-hoc tests revealed that the difference in expression was statistically significant between HER2 transfected HMECs and the

GFP transfected controls ($p<0.01$). Post hoc tests also showed that BCA2 expression in the kinase dead HER2 overexpressing cells was not significantly different from the GFP control but was significantly different from the HER2 overexpressing cells ($p<0.01$). Similar results were obtained from analysis of the 226468_at probe data (Fig. 3-11 F). One-way ANOVA showed a significant difference in expression across the transfected groups $F(2, 12) = 6.51$, $p = 0.0122$. Post-hoc tests showed that the expression differences were statistically significant between the HER2 transfected HMECs and the GFP control and HER2-ki transfected groups ($p < 0.05$).

The absolute fold changes in BCA2 expression in the HER2 transfected cells were above the threshold for biological relevance for both probe sets. The 212742_at probe set indicated a 1.64 fold suppression of BCA2 expression and the 226468_at probset showed 1.65 fold downregulation compared with the GFP control and any change in expression was lost with the kinase dead mutant (Fig. 3-11 G).

3.2.7 BCA2 expression following overexpression of selected oncogenes in mammary epithelial cells

BCA2 stability has previously been shown to be enhanced by Akt phosphorylation (Bacopulos *et al*. 2012). Since BCA2 expression also appeared to be altered by HER2 overexpression (Fig. 3-11), the effect of overexpressing oncogenic signalling proteins on BCA2 levels was examined. BCA2 expression data was extracted from the GSE3151 set containing samples of GFP control, c-Myc, Src and H-Ras transfected HMEC cells. The samples were taken from 7-10 independent

experiments. For more details regarding the transfection and RNA extraction methods see the source publication (Bild *et al*. 2005). Fold-changes in BCA2 between GFP transfected control and oncogene overexpressing cells are presented in Figure 3-12.

A

Log2 BCA2 expression	
Probe set	GFP control
212742_at	9.72
226468_at	8.70

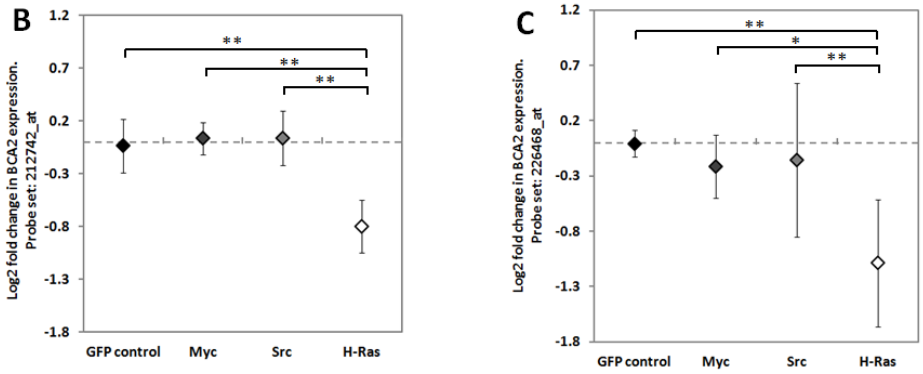

D

Fold-change in BCA2 expression relative to control			
Probe set	Myc	Src	H-Ras
212742_at	1.04	1.04	-1.69
226468_at	-1.12	1.01	-1.86

Figure 3-12: BCA2 mRNA expression levels in breast epithelial cells transfected with GFP (control) and selected oncogenes. Global gene expression in HMEC cells transfected with GFP, Myc, Src or H-Ras was measured by microarray (Bild *et al*. 2005). A) Log2 mRNA expression analysis of controls confirmed detectable BCA2 expression with both probesets. Mean relative expression data from B) the 212742_at probe set and C) the 226468_ was comparing BCA2 levels in the GFP control cells and the oncogene transfects. ** *Statistical significance* $p \leq 0.01$. * *Statistical significance* $p \leq 0.05$. *Error bars represent 95% confidence intervals.* D) Absolute fold change in BCA2 expression in the oncocgene overexpressing cells relative to control. *Green values indicate fold suppression* ≥ 1.5.

BCA2 expression was confirmed by log2 analysis of controls (Fig. 3-12 A) and expression was also checked and confirmed for the lowest expression points for each experiment (H-Ras).

H-Ras was the only overexpressed oncogene to induce a statistically and (potentially) biologically significant change in BCA2 expression. The H-

Ras induced reduction in BCA2 levels was observed with both probe sets. One-way ANOVA of the 212742_at probe set data (Fig. 3-12 B) demonstrated the difference in fold-change between groups was significant: $F(3, 33) = 16.72$, $p < 0.0001$. Post-hoc tests showed that only the H-Ras transfected cells expressed significantly lower levels of BCA2 than the GFP transfected HMECs ($p < 0.01$). The results with second probe set demonstrated a similar trend: the one-way ANOVA was significant $F(3, 33)$ 7.08, $p = 0.00084$ and BCA2 levels in the H-Ras transfected cells were significantly reduced (Fig. 3-12 C, $p < 0.01$).

The absolute fold suppression in BCA2 levels (Fig. 3-12 D) was above the biological significance threshold of ≥ 1.5 fold for both the 212742_at probe set (fold reduction = 1.69) and the 226468_at set (fold reduction = 1.86).

3.3 Discussion

Presented in Figure 3-2, is evidence that high levels of BCA2 may be associated with improved relapse-free survival and novel findings of better outcome with higher BCA2 expression in ER-positive, grade 3, and LN-positive disease. One previous study linked high levels of BCA2 to increase in disease-free survival for regional recurrence and reduced lymph node metastasis (Burger *et al*. 2005). The relationship between BCA2 and the positive prognostic indicators was not thought to be functional consequence of BCA2 expression. BCA2's association with reduced recurrence and metastasis was attributed to the high incidence of BCA2 upregulation in ER+ breast cancer, the most readily treatable form

of the disease. The data created using the GOBO online tool (Fig. 3-2) suggest that BCA2 may in fact have an independent functional impact on breast cancer prognosis rather than simply bystander correlation with other positive prognostic indicators. This can be inferred as the relationship between BCA2 expression and good prognosis is retained in the ER+ group following stratification.

The association of BCA2 expression with increased relapse free survival in breast cancer has not been previously reported by subtype but is examined here. A potential relationship between BCA2 and HER2 is indicated by a number of figures presented in this chapter. The KM Plot data in Figure 3-1 E indicate that high levels of BCA2 adversely affect relapse free survival in the HER2-type and luminal B type breast cancers. This finding was not however fully replicated in the GOBO data (Fig. 3-2 E). Luminal B is a subtype of breast cancer that is itself comprised of different disease subtypes: some are positive for HER2 expression while others are highly proliferative (high Ki67). The GOBO data may reflect the complexity of luminal B breast cancer as moderate BCA2 expression was associated with better prognosis but the highest and lowest BCA2 expressing groups were associated with reduced RFS. In the HER2 subtype, high BCA2 expression was associated with improved prognosis but moderate and low BCA2 expressing disease were both associated with reduced RFS. Overall, the survival data in Figures 3-1 and 3-2 indicate a complex, context dependent, relationship between BCA2 and breast cancer outcome.

It is worth noting that the differences in survival impact of BCA2 between the GOBO and KM Plotter biomarker tools, in particular with respects to luminal B and HER2+ disease, could be due to the difference in sizes of the data sets analysed. GOBO has just under half the number of patient samples as KM Plotter overall, but for the expression studies in the luminal B subtype over 1000 samples were used in the KM Plotter analysis compared with ~200 from the GOBO database (Figs. 3-1 E and 3-2 E). It may be that with more samples a statistically significant effect would be seen in the GOBO cohort.

Elevated BCA2 expression and adverse impact on survival in HER2 positive breast cancers may relate more to BCA2's putative role in EGFR regulation than to a specific HER2 effect. EGFR overexpression is most commonly seen in basal-type breast cancer (Nielsen *et al*. 2004) but elevated levels of EGFR and other RTKs are also seen in HER2+ and luminal B subtypes (see Table 1-1). However, in general BCA2 is most prevalent in ER^+ / luminal A cancers with no HER2 or EGFR suggesting generally an inverse association. Interestingly the data from the microarray in Fig. 3-11 also suggest that BCA2 levels may be negatively regulated by HER2. Figure 3-11 shows data from two separate studies that show a modest (~1.3-1.6 fold) decrease in BCA2 levels following HER2 overexpression. The decrease is, however, statistically significant, possibly enhanced by EGF stimulation (Fig. 3-11 B) and appears to require HER2 kinase activity (Fig. 3-11 E). Experiments to directly analyse BCA2 protein levels in response to HER2 overexpression would

need to be performed to verify the effect. The data in Figure 3-11 therefore suggest a potentially interesting investigative avenue.

The reduction in BCA2 expression following HMEC transfection with H-Ras (Fig. 3-12) is also in keeping with the data showing a decrease in BCA2 following HER2 overexpression and EGF stimulation (Fig. 3-11). This also offers a potential insight into how HER2 may exert influence on BCA2 levels: via enhanced Ras activity. Specific experiments examining downstream transcription factor activity and BCA2 expression would need to be conducted to confirm these effects and to elucidate a mechanism.

The small molecule drug gefitinib (IRESSA®) has exhibited activity against EGFR overexpressing breast cancers but therapeutic resistance remains a significant problem (Normanno *et al*. 2009). The development of therapeutic resistance has been linked to alterations in the endocytic downregulation of EGFR (Hopper-Borge *et al*. 2009). BCA2 has also been associated with changes in EGFR degradation (Mizuno *et al.* 2003; Smith *et al.* 2013; Wymant *et al.* 2014). The data in Figure 3-10 showing modest but significant upregulation of BCA2 mRNA in gefitinib resistant epithelial cells is therefore potentially significant. If the changes in BCA2 levels were also evident at the protein level siRNA depletion studies of BCA2 could then be carried out in the resistant cells. These investigations might then reveal whether a) the resistance was, in part, a functional consequence of increased BCA2 levels and b) if drug sensitivity could be restored by inhibiting BCA2. The data showing an increase in BCA2 in acquired gefitinib resistance provides further

evidence for EGFR/BCA2 inverse association. The resistant cell model was produced by long-term gefitinib exposure and since the drug inhibits EGFR signalling this blockade may be the cause of the increase in BCA2 levels, potentially via activation of alternative signalling pathways e.g. IGF-1R (van der Veeken *et al*. 2009). The data add weight to the hypothesis suggested by data in Figures 3-11 and 12 that BCA2 levels are inversely proportional to ErbB expression/signalling.

The relationship between BCA2 and the oestrogen receptor was examined in a few of the studies presented in this chapter. In line with previously published findings, elevated BCA2 levels were seen in hormone receptor positive clinical breast cancer subtypes and cell lines (Figs. 3-3 B, 3-4 B and C). Unexpectedly however, the data from the E2 stimulation and starvation experiments shown in Figure 3-7 and 3-8 all demonstrated no significant change in BCA2 levels with either probe set or any of the experimental conditions. This might suggest that while the BCA2 may be transcriptionally modulated by the oestrogen receptor (Kona *et al*. 2012), it may not be the only BCA2 regulating factor. A number of other transcription factor binding sites have been predicted in the BCA2 promoter region, including NFκB, AP-1 and the progesterone receptor (Burger *et al*. 2010). This may explain how BCA2 levels could be maintained in the absence of E2 and in ER- cell lines. Another explanation for the null effect of E2 on BCA2 expression seen in Figure 3-7 may be the suboptimal hormone dose used in the experiment. Experiments previously showing transcriptional regulation of BCA2 by the ER involved stimulation with 10 nM of E2 (Kona *et al*. 2012),

considerably higher than the maximum dose of 100 pM used by Coser *et al.* (2003). The data in Figure 3-7 may therefore reflect the fact that BCA2 is transcriptionally regulated by ER but is not highly oestrogen-sensitive i.e. a larger stimulating E2 dose is required to induce an effect on BCA2 levels.

The limited effects of long-term oestrogen withdrawal on BCA2 mRNA expression (Fig. 3-8) may reflect that fact that E2 withdrawal can promote the development of resistance. Resistance developed at 90 days (Aguilar *et al*. 2010) and endocrine resistance is a phenomenon associated with upregulation of ER and increased RTK expression and signalling (Gee and Hutcheson 2005). In light of other findings, increase in ER would increase BCA2 expression (Kona *et al.* 2012) while upregulation of RTKs and downstream signalling would reduce BCA2 levels (Fig. 3-10 to 3-12) thus (potentially) producing a net null-effect on BCA2 expression.

BCA2 appeared to be slightly downregulated in tamoxifen and fulvestrant resistant cell lines (Fig. 3-9). However, the reductions of ~1.22-1.44 fold (depending on the probe used) were below the 1.5 fold-change cut off for biological significance/relevance. Nonetheless this may still be worth exploring at the protein level given BCA2's well documented relationship with the oestrogen receptor (Burger *et al*. 2005; Burger *et al*. 2010; Kona *et al*. 2012). Investigation of BCA2 in the TAMR and FASR models of acquired resistance may also be warranted since increased growth factor signalling has a role in the development of anti-oestrogen resistance (Gee *et al.* 2005; Nicholson *et al*. 2007) and

since BCA2 is shown here to be suppressed by HER2/EGFR expression and signalling (Figs. 3-10 to 3-12).

The steady increase of BCA2 levels seen in increasingly transformed mammary epithelial cells (Fig. 3-6) could point to a role for BCA2 in breast cancer development. However, the results could also be explained by the E2 supplementation used to induce the oncogenic transformation. The MCF-10F cells are ER^- but BCA2 induction has been previously demonstrated in an E2 stimulated, triple negative cell line (Kona *et al*. 2012). The mechanism of BCA2 upregulation in E2 treated, ER^- cells has not been identified.

The data in Figure 3-5 potentially suggest a role for BCA2 in cancer epithelial to mesenchymal transition (EMT). EMT is the process by which epithelial cells lose their terminally differentiated characteristics and acquire/revert to those of stem-like mesenchymal cells (Mani *et al*. 2008). EMT is a key feature of cancer cell invasion and metastasis (Chaffer and Weinberg 2011). The spontaneous development of a $CD44^+/CD24^-$ subpopulation in MCF-10A cells in Figure 3-5 is shown to be accompanied by a statistically significant increase in BCA2 expression. BCA2 mRNA levels are increased ~1.36-1.66 fold in the stem-like cells which is a modest elevation but may suggest a role in EMT. If the BCA2 induction was also present at the protein level, the findings would support published data showing that BCA2 overexpression promotes cell migration while siRNA depletion reduces invasiveness (Burger *et al*. 2005; Amemiya *et al*. 2008).

The BCA2 gene locus is 1q21.1, on a chromosome arm associated with increased copy number in over half of all primary breast cancers (Bièche *et al*. 1995; Rennstam *et al.* 2003). Six of the twenty genes co-expressed with BCA2 (Table 3-1) were also from the long arm of chromosome 1, more than would be expected by chance. This could be an indication that BCA2 overexpression may in some instances relate to transcriptional upregulation in this chromosome region. Alterations in chromosome 7 are among the most frequent cytogenetic aberrations found in breast cancer (Bièche *et al*. 1997). The enriched co-expression of BCA2 with chromosome 7q genes may simply be an indirect consequence of their respective involvements in breast cancer or may be indicative of an underlying co-regulatory mechanism that is disrupted in mammary carciongenesis.

The presence of 14-3-3θ/τ in the co-expressed gene list (Table 3-2) was notable since another 14-3-3 family member (14-3-3σ) has been shown to be a BCA2 effector (Bacopulos *et al*. 2012). 14-3-3 family members are conserved adaptor/scaffold proteins that recognise common motifs containing phospho- serine or threonine idues (Tzivion *et al*. 2001). *In vitro* data previously demonstrated that 14-3-3σ was able to bind to and stabilise BCA2 and that the interaction was dependent upon Akt activity (Bacopulos *et al.* 2012). The evidence of co-expression between BCA2 and 14-3-3θ/τ may potentially indicate that BCA2 can also be regulated by a second 14-3-3 family member.

The ontological investigation conducted into the co-expressed genes (Table 3-2) revealed an enrichment of genes relating to membrane

transport, particularly to and from the Golgi apparatus. BCAP29, RAB18, COPB1, TRAM1, ARL1, VIMP and VAMP7 all have roles associated with anterograde and retrograde Golgi trafficking. BCA2 has no documented association with the Golgi body but has been shown to associate with late endosomes and lysosomes via an interaction with Rab7 (Mizuno *et al.* 2003). There are several examples of other late-endolysosome associated proteins that have additional roles at the Golgi body. VAMP7 for example, forms part of the SNARE complex that mediates fusion between late endocytic organelles and other membranes (Kent *et al.* 2012). VAMP7 also functions at the *trans*-Golgi Network (TGN) where it coordinates trafficking of proteins to the cell surface. Through this role VAMP7 has been reported to inhibit endocytosis of EGFR (Danglot *et al*. 2010). Depletion of VAMP7 was shown to prevent transport of the tetraspanin protein CD82 to the plasma membrane. The loss of CD82 from the cell-surface enhanced recruitment of AP-2 and the CME machinery which in turn promoted EGFR endocytosis.

A number of Rab proteins have dual endosomal-TGN functions. One of principal functions of Rab7b is thought to be co-ordination of retrograde transport from endosomes to the Golgi (Progida *et al.* 2010). Rab7a and Rab5 have also been shown to be involved in retrograde trafficking via endosomal recruitment of the retromer complex (Rojas *et al*. 2008). The retromer complex facilitates the vesicular transport of transmembrane cargo such as the mannose 6-phosphate receptor (M6PR) from late endosomes to the TGN. Return of the M6PR to the TGN is important for

efficient delivery of acid hydrolases to the lysosomes and as such is critical to lysosome function (Arighi *et al*. 2004). Rab7 directly binds the retromer complex recruiting it to late endosomes and lysosomes. Rab5 however, is thought to indirectly promote retromer membrane association via PI3K activation (Rojas *et al*. 2008). Loss of Rab7 or Rab5 activity can inhibit retrograde transport from late endolysosomes to the TGN. BCA2 has been shown to interact with Rab7 and is thought to have a role in co-ordinating the late stages of receptor endocytosis (Mizuno *et al.* 2003; Sakane *et al.* 2007; Smith *et al.* 2013). It is therefore possible that through Rab7, and like a number of its co-expressed genes, BCA2 may also have a function in, or an effect on, retrograde transport.

BCA2 was originally discovered by subtractive hybridization cloning in breast cancer cell lines. The protein has since been shown to increase breast cancer cell proliferation and invasiveness *in vitro* and its overexpression has been demonstrated in 56% of invasive mammary tumours (Burger *et al*. 2005). BCA2 has been linked to two receptors of major significance in breast cancer: EGFR and the ER (Mizuno *et al*. 2003; Burger *et al*. 2010).

Through *in silico* studies in this chapter BCA2's relationship with breast cancer outcome and clinical features has been extended beyond the existing literature in the context of breast cancer subtype with both positive and negative associations with outcome according to subtype. Results of preliminary investigations with publically available microarray data also indicate a potential role for altered BCA2 during breast cancer

development and in acquired therapeutic resistance to EGFR or ER blockade. These studies additionally suggest a possible functional relationship between BCA2 and the HER2 and EGFR oncoproteins and their downstream signalling. Co-expression and ontological studies have highlighted the possibility of a connection between BCA2 and protein transport from late-endosomes and lysosomes to the TGN.

While these preliminary *in silico* findings do not provide robust evidence of BCA2-mediated effects, they offer some insight into potentially productive avenues for further research. Analyses to study BCA2 expression changes at the protein level and to explore the effects of localisation (e.g. nuclear versus cytoplasmic BCA2) would add weight and depth to the data presented in this chapter.

3.4 References

Adler, P., Kolde, R., Kull, M., Tkachenko, A., Peterson, H., Reimand, J. and Vilo, J. 2009. Mining for coexpression across hundreds of datasets using novel rank aggregation and visualization methods. *Genome Biology* 10(12), p. R139.

Aguilar, H., Sole, X., Bonifaci, N., Serra-Musach, J., Islam, A., Lopez-Bigas, N., Mendez-Pertuz, M., Beijersbergen, R., Lazaro, C. and Urruticoechea, A. 2010. Biological reprogramming in acquired resistance to endocrine therapy of breast cancer. *Oncogene* 29(45), p. 6071-83.

Al-Hajj, M., Wicha, M. S., Benito-Hernandez, A., Morrison, S. J. and Clarke, M. F. 2003. Prospective identification of tumorigenic breast cancer cells. *Proceedings of the National Academy of Sciences* 100(7), p. 3983-8.

Amemiya, Y., Azmi, P. and Seth, A. 2008. Autoubiquitination of BCA2 RING E3 ligase regulates its own stability and affects cell migration. *Molecular Cancer Research* 6(9), p. 1385.

Arighi, C. N., Hartnell, L. M., Aguilar, R. C., Haft, C. R. and Bonifacino, J. S. 2004. Role of the mammalian retromer in sorting of the cation-

independent mannose 6-phosphate receptor. *The Journal of Cell Biology* 165(1), p. 123-3.

Bacopulos, S., Amemiya, Y., Yang, W., Zubovits, J., Burger, A., Yaffe, M. and Seth, A. K. 2012. Effects of partner proteins on BCA2 RING ligase activity. *BMC Cancer* 12(1), p. 63.

Bhat-Nakshatri, P., Appaiah, H., Ballas, C., Pick-Franke, P., Goulet, R., Badve, S., Srour, E. F. and Nakshatri, H. 2010. SLUG/SNAI2 and tumor necrosis factor generate breast cells with CD44+/CD24-phenotype. *BMC Cancer* 10(1), p. 411.

Bild, A. H., Yao, G., Chang, J. T., Wang, Q., Potti, A., Chasse, D., Joshi, M.-B., Harpole, D., Lancaster, J. M. and Berchuck, A. 2005. Oncogenic pathway signatures in human cancers as a guide to targeted therapies. *Nature* 439(7074), p. 353-7.

Bièche, I., Champème, M. H. and Lidereau, R. 1995. Loss and gain of distinct regions of chromosome 1q in primary breast cancer. *Clinical Cancer Research* 1(1), p. 123-7.

Bièche, I., Khodja, A., Driouch, K. and Lidereau, R. 1997. Genetic alteration mapping on chromosome 7 in primary breast cancer. *Clinical Cancer Research* 3(6), p. 1009-16.

Burger, A. M., Gao, Y., Amemiya, Y., Kahn, H. J., Kitching, R., Yang, Y., Sun, P., Narod, S. A., Hanna, W. M. and Seth, A. K. 2005. A novel RING-type ubiquitin ligase breast cancer-associated gene 2 correlates with outcome in invasive breast cancer. *Cancer Research* 65(22), p. 10401.

Burger, A. M., Kona, F., Amemiya, Y., Gao, Y., Bacopulos, S. and Seth, A. K. 2010. Role of the BCA2 ubiquitin E3 ligase in hormone responsive breast cancer. *The Open Cancer Journal* 3(1), p. 116.

Chaffer, C. L. and Weinberg, R. A. 2011. A perspective on cancer cell metastasis. *Science* 331(6024), p. 1559-64.

Coser, K. R., Chesnes, J., Hur, J., Ray, S., Isselbacher, K. J. and Shioda, T. 2003. Global analysis of ligand sensitivity of estrogen inducible and suppressible genes in MCF7/BUS breast cancer cells by DNA microarray. *Proceedings of the National Academy of Sciences* 100(24), p. 13994-9.

Coser, K. R., Wittner, B. S., Rosenthal, N. F., Collins, S. C., Melas, A., Smith, S. L., Mahoney, C. J., Shioda, K., Isselbacher, K. J. and Ramaswamy, S. 2009. Antiestrogen-resistant subclones of MCF-7 human breast cancer cells are derived from a common monoclonal drug-resistant progenitor. *Proceedings of the National Academy of Sciences* 106(34), p. 14536-41.

Danglot, L., Chaineau, M., Dahan, M., Gendron, M.-C., Boggetto, N., Perez, F. and Galli, T. 2010. Role of TI-VAMP and CD82 in EGFR cell-surface dynamics and signaling. *Journal of Cell Science* 123(5), p. 723-35.

Fernandez, S. V., Russo, I. H., Lareef, M., Balsara, B. and Russo, J. 2005. Comparative genomic hybridization of human breast epithelial cells transformed by estrogen and its metabolites. *International Journal of Oncology* 26(3), p. 691-6.

Gee, J.M.W and Hutcheson, I.R. 2005. Understanding endocrine resistance: the critical need for sequential samples from clinical breast cancer and novel in vitro models. *Breast Cancer Research* 7(5), p. 187-89.

Gee, J., Robertson, J., Gutteridge, E., Ellis, I., Pinder, S., Rubini, M. and Nicholson, R. 2005. Epidermal growth factor receptor/HER2/insulin-like growth factor receptor signalling and oestrogen receptor activity in clinical breast cancer. *Endocrine-Related Cancer* 12(Supplement 1), p. S99-S111.

Guix, M., Faber, A. C., Wang, S. E., Olivares, M. G., Song, Y., Qu, S., Rinehart, C., Seidel, B., Yee, D. and Arteaga, C. L. 2008. Acquired resistance to EGFR tyrosine kinase inhibitors in cancer cells is mediated by loss of IGF-binding proteins. *The Journal of Clinical Investigation* 118(7), p. 2609-19.

Gyorffy, B., Lanczky, A., Eklund, A., Denkert, C., Budczies, J., Li, Q. and Szallasi, Z. 2010. An online survival analysis tool to rapidly assess the effect of 22,277 genes on breast cancer prognosis using microarray data of 1809 patients. *Breast Cancer Research and Treatment* 123(3), p. 725-31.

Hartman, Z. C., Wei, J., Osada, T., Glass, O., Lei, G., Yang, X.-Y., Peplinski, S., Kim, D.-W., Xia, W. and Spector, N. 2010. An adenoviral vaccine encoding full-length inactivated human Her2 exhibits potent immunogenicity and enhanced therapeutic efficacy without oncogenicity. *Clinical Cancer Research* 16(5), p. 1466-77.

Hendriks, B. S., Wiley, H. S. and Lauffenburger, D. 2003. HER2-mediated effects on EGFR endosomal sorting: analysis of biophysical mechanisms. *Biophysical Journal* 85(4), p. 2732-45.

Hommelgaard, A. M., Lerdrup, M. and van Deurs, B. 2004. Association with membrane protrusions makes ErbB2 an internalization-resistant receptor. *Molecular Biology of the Cell* 15(4), pp. 1557-67.

Honeth, G., Bendahl, P.-O., Ringnér, M., Saal, L. H., Gruvberger-Saal, S. K., Lovgren, K., Grabau, D., Ferno, M., Borg, A. and Hegardt, C. 2008. The CD44+/CD24-phenotype is enriched in basal-like breast tumors. *Breast Cancer Research* 10(3), p. R53.

Hopper-Borge, E. A., Nasto, R. E., Ratushny, V., Weiner, L. M., Golemis, E. A. and Astsaturov, I. 2009. Mechanisms of tumor resistance to EGFR-targeted therapies. *Expert Opinion on Theraputic Targets* 13(3), p. 339-62.

Huang, Y., Fernandez, S. V., Goodwin, S., Russo, P. A., Russo, I. H., Sutter, T. R. and Russo, J. 2007. Epithelial to Mesenchymal Transition in Human Breast Epithelial Cells Transformed by 17β-Estradiol. *Cancer Research* 67(23), p. 11147-57.

Kent, H. M., Evans, P. R., Schäfer, I. B., Gray, S. R., Sanderson, C. M., Luzio, J. P., Peden, A. A. and Owen, D. J. 2012. Structural basis of the intracellular sorting of the SNARE VAMP7 by the AP3 adaptor complex. *Developmental Cell* 22(5), p. 979-88.

Kona, F. R., Stark, K., Bisoski, L., Buac, D., Cui, Q., Dou, Q. P. 2012. Transcriptional activation of breast cancer-associated gene 2 by estrogen receptor. *Breast Cancer Research and Treatment*, p. 1-9.

Li, Q., Birkbak, N. J., Gyorffy, B., Szallasi, Z. and Eklund, A. C. 2011. Jetset: selecting the optimal microarray probe set to represent a gene. *BMC Bioinformatics* 12(1), p. 474.

Mani, S. A., Guo, W., Liao, M. J., Eaton, E. N., Ayyanan, A., Zhou, A. Y., Brooks, M., Reinhard, F., Zhang, C. C. and Shipitsin, M. 2008. The epithelial-mesenchymal transition generates cells with properties of stem cells. *Cell* 133(4), p. 704-15.

Mizuno, K., Kitamura, A. and Sasaki, T. 2003. Rabring7, a novel Rab7 target protein with a RING finger motif. *Molecular Biology of the Cell* 14(9), p. 3741-52.

Nicholson, R., Hutcheson, I., Jones, H., Hiscox, S., Giles, M., Taylor, K. and Gee, J. M. W. 2007. Growth factor signalling in endocrine and anti-growth factor resistant breast cancer. *Reviews in Endocrine & Metabolic Disorders* 8(3), p. 241-53.

Nielsen, T. O., Hsu, F. D., Jensen, K., Cheang, M., Karaca, G., Hu, Z., Hernandez-Boussard, T., Livasy, C., Cowan, D. and Dressler, L. 2004. Immunohistochemical and clinical characterization of the basal-like subtype of invasive breast carcinoma. *Clinical Cancer Research* 10(16), p. 5367-74.

Normanno, N., Morabito, A., De Luca, A., Piccirillo, M. C., Gallo, M., Maiello, M. R. and Perrone, F. 2009. Target-based therapies in breast cancer: current status and future perspectives. *Endocrine-Related Cancer* 16(3), p. 675-702.

Progida, C., Cogli, L., Piro, F., De Luca, A., Bakke, O. and Bucci, C. 2010. Rab7b controls trafficking from endosomes to the TGN. *Journal of Cell Science* 123(9), p. 1480-91.

Rennstam, K., Ahlstedt-Soini, M., Baldetorp, B., Bendahl, P. O., Borg, Å., Karhu, R., Tanner, M., Tirkkonen, M. and Isola, J. 2003. Patterns of chromosomal imbalances defines subgroups of breast cancer with distinct clinical features and prognosis. A study of 305 tumors by comparative genomic hybridization. *Cancer Research* 63(24), p. 8861.

Ringnér, M., Fredlund, E., Häkkinen, J., Borg, Å. and Staaf, J. 2011. GOBO: gene expression-based outcome for breast cancer online. *PloS One* 6(3), p. e17911.

Rojas, R., van Vlijmen, T., Mardones, G. A., Prabhu, Y., Rojas, A. L., Mohammed, S., Heck, A. J., Raposo, G., van Der Sluijs, P. and Bonifacino, J. S. 2008. Regulation of retromer recruitment to endosomes by sequential action of Rab5 and Rab7. *The Journal of Cell Biology* 183(3), p. 513-26.

Sakane, A., Hatakeyama, S. and Sasaki, T. 2007. Involvement of Rabring7 in EGF receptor degradation as an E3 ligase. *Biochemical and Biophysical Research Communications* 357(4), p. 1058-64.

Sheridan, C., Kishimoto, H., Fuchs, R. K., Mehrotra, S., Bhat-Nakshatri, P., Turner, C. H., Goulet Jr, R., Badve, S. and Nakshatri, H. 2006. CD44+/CD24-breast cancer cells exhibit enhanced invasive properties: an early step necessary for metastasis. *Breast Cancer Research* 8(5), p. R59.

Smith, C. J., Berry, D. M. and McGlade, C. J. 2013. The E3 ubiquitin ligases RNF126 and Rabring7 regulate endosomal sorting of the epidermal growth factor receptor. *Journal of Cell Science* 126(6), p. 1366-80.

Stuart, J. M., Segal, E., Koller, D. and Kim, S. K. 2003. A gene-coexpression network for global discovery of conserved genetic modules. *Science* 302(5643), p. 249-55.

Tzivion, G., Shen, Y. H. and Zhu, J. 2001. 14-3-3 proteins; bringing new definitions to scaffolding. *Oncogene* 20(44), p. 6331-8.

van der Veeken, J., Oliveira, S., Schiffelers, R.M., Storm, G., van Bergen En Henegouwen, P.M. and Roovers, R.C. 2009. Crosstalk between epidermal growth factor receptor- and insulin-like growth factor-1 receptor signaling: implications for cancer therapy. *Current Cancer Drug Targets* 9(6), p. 749-60.

Wolfe, C. J., Kohane, I. S. and Butte, A. J. 2005. Systematic survey reveals general applicability of. *BMC Bioinformatics* 6(1), p. 227.

Wolfer, A., Wittner, B. S., Irimia, D., Flavin, R. J., Lupien, M., Gunawardane, R. N., Meyer, C. A., Lightcap, E. S., Tamayo, P. and Mesirov, J. P. 2010. MYC regulation of a “poor-prognosis” metastatic cancer cell state. *Proceedings of the National Academy of Sciences* 107(8), p. 3698-703.

Wymant, J., Hiscox, S., Westwell, A., Urbé, S., Clague, M. and Jones, A. 2014. 479: The role of Breast Cancer Associated gene 2 in EGFR endocytosis, downregulation and breast cancer survival. *European Journal of Cancer* 50(Supplement 5).

Chapter 4: Method Development for Endocytic Profiling and BCA2 Subcellular Localisation in Breast Cell Lines

BCA2 is thought to be involved in endocytosis in a number of ways. Through its interaction with Rab7, BCA2 has been shown to alter EGFR endocytosis, though depending on the publication, the interaction has been shown to both accelerate and impair degradation of the receptor. Mizuno *et al.* (2003) demonstrated that overexpressed, His-tagged BCA2 was recruited to late endosomes and lysosomes by EGFP-Rab7. Overexpression led to late endosomes and lysosomes becoming clustered in the perinuclear region and EGF degradation was shown to be inhibited. The same group then studied the interaction between BCA2 and Rab7 in a different cell line and examined rates of EGFR degradation rather than EGF. Under these experimental conditions, it was reported BCA2 overexpression promoted receptor degradation (Sakane *et al.* 2007). A second group of researchers recently found that BCA2 depletion inhibited EGFR (and c-Met) degradation by destabilisation of the ESCRT-II complex which decreased the number of MVBs (Smith *et al.* 2013).

BCA2 has also been implicated in regulating HIV infection via alterations in endocytosis. By interacting with tetherin, BCA2 was revealed to inhibit HIV particle release and promote lysosomal trafficking and degradation of the virions (Miyakawa *et al.* 2009). A more recent paper demonstrated tetherin-independent anti-viral BCA2 activity. Here BCA2 was able to interact directly with a critical viral protein, HIV-1 Gag, promoting its ubiquitination and lysosomal

degradation. The resulting reduction in HIV-1 Gag protein levels prevented virion assembly and release (Nityanandam and Serra-Moreno 2014).

Details regarding BCA2's subcellular localisation and its spatial and functional relationship with components of the endocytic pathway are limited. Our initial studies therefore focused on trying to better describe the subcellular localisation of BCA2 and to explore differences in structure and/or subcellular localisation of endocytic organelles between cells thought to express different levels of the protein.

4.1 The Subcellular Localisation of BCA2

4.1.1 Endocytic profiling of breast cancer and non-tumourigenic breast cell lines

The endocytic profiles of breast cancer and "near normal" breast cell lines were initially determined (Fig. 4-1 to 4-7). Profiling entailed the labelling of key endocytic proteins/organelles with fluorescent probes and antibodies. The aim was to identify any differences in the subcellular localisation of key endocytic components between cancerous and non-cancerous cell lines and between cell lines expressing different levels of BCA2. MCF-7 and MDA-MB-231 breast cancer cells were examined as they have been previously described in literature as "BCA2 overexpressing" and "BCA2 negative/low" respectively (Brahemi *et al.* 2010). MCF-10A cells were also selected for study as it was demonstrated in Figure 3-4 that at the mRNA level this cell line expressed lower BCA2 levels than the MDA-MB-231 cells.

MCF-10A cells are an immortalised, non-tumourigenic, mammary gland epithelial cell line and as such were used as a model of normal breast tissue. MCF-7 cells are a model of luminal A breast cancer while MDA-MB-231 cells represent basal or "triple negative" disease.

Actin is a highly abundant cellular protein that exists in two forms: globular actin (G-actin) monomers and polymerised actin filaments (F-actin). In addition to having critical roles in cell structure, adhesion and migration, actin is thought to have a diverse range of roles in endocytosis. In mammalian cells for example there is data to support a role for actin in the internalisation of clathrin-coated vesicles (Merrifield *et al.* 2002) and in vesicle scission (Merrifield *et al.* 2005). There is also experimental evidence which implicates actin in intracellular vesicle transport: vesicles have been shown to shuttle along actin cables in budding yeast (Toshima *et al.* 2006).

F-actin can be visualised in cells with the fluorescent phallotoxin: rhodamine-phalloidin. Phalloidin binds to actin filaments with high affinity and the attached tetramethyl rhodamine (TMR) fluorophore emits an orange-red fluorescence that is proportional to the amount of actin present (Huang *et al.* 1992).

Early endosomes are critical sorting compartments where multiple endocytic pathways intersect. Endocytic cargo such as receptors and their ligands may be trafficked from the early endosome directly back to the cell surface, to recycling compartments for slower return to the cell surface or into lysosomes for degradation (See Fig. 1-6). Early Endosome Antigen 1 (EEA1) is a marker of early endosomes and is a protein that is

essential for the tethering and fusing of endocytic vesicles with the early endosome (Mu *et al.* 1995; Simonsen *et al.* 1998).

PFA fixed MCF-7, MDA-MB-231 and MCF-10A cells were stained with rhodamine phalloidin and labelled for the early endosome marker EEA1 by IF, the nuclei were counterstained with Hoechst (Fig. 4-1).

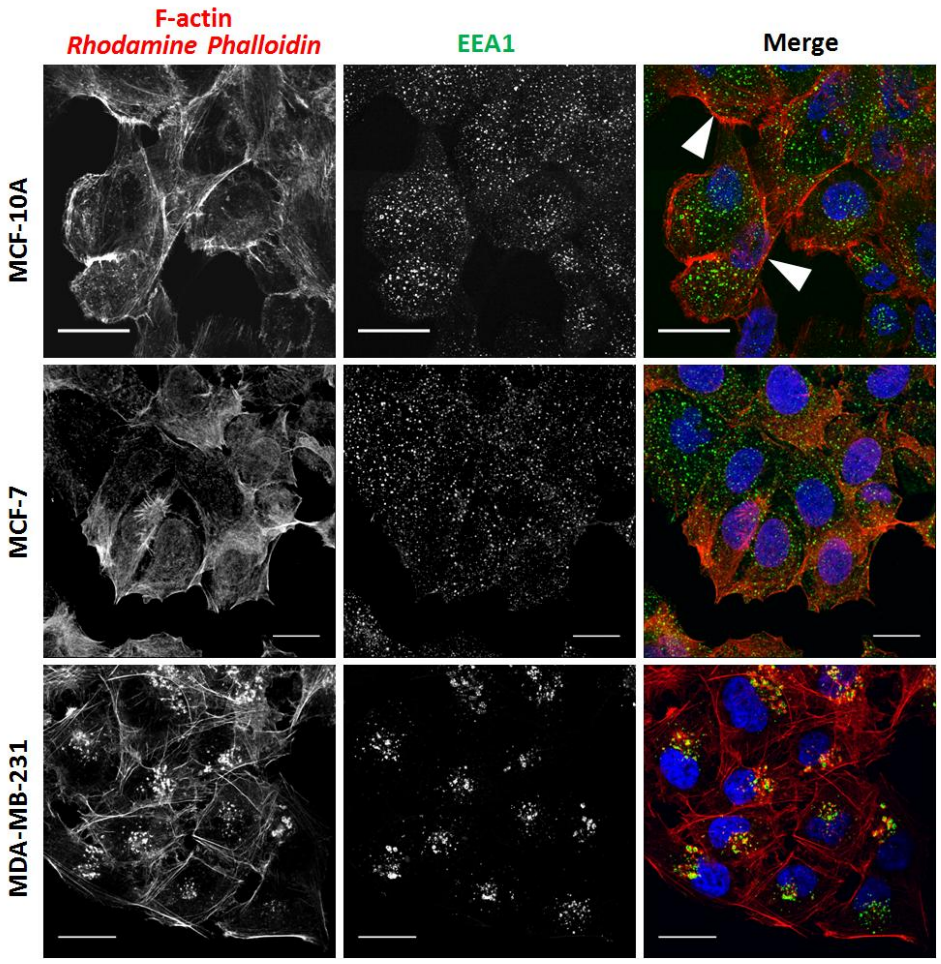

Figure 4-1: Actin and early endosome localisation in breast and breast cancer cells. Rhodamine phalloidin (red) labelled actin filaments and (green) immunolabelled EEA1. Nuclei are stained blue with Hoechst. *Arrowheads indicate cortical actin. Scale bars = 25 µm.*

Figure 4-1 demonstrates considerable similarities between the MCF-7 and MCF-10A cell lines with respect to the structure and distribution of F-actin and early endosomes. The MDA-MB-231 cells showed notable differences in their actin and EEA1 labelling.

Rhodamine phalloidin staining indicated that the vast majority of the F-actin in the MCF-10A and MCF-7 cell lines was contained in sub-membranous pools of cortical actin (indicated by arrowheads in Fig. 4-1). In addition to their cortical actin however, MDA-MB-231 cells contained prominent actin stress fibres. MDA-MB-231 cells also featured several pericentral actin foci that showed some colocalisation with EEA1.

The early endosomes in MDA-MB-231 cells were concentrated in polar, perinuclear regions of the cell. The ubiquitous early endosomes in the MCF-7 and in MCF-10A cells however were distributed evenly throughout the cells.

Microtubules are formed from polymerised heterodimers of α and β tubulin called protofilaments that assemble into long, hollow fibres. Microtubules form part of the cellular cytoskeleton and are involved in cell structure, division and motility. Microtubules also have a role in endocytosis: lysosomal clustering occurs around the centrosome/ microtubule organising centre (MTOC) and endolysosomal translocation has been shown to be microtubule dependent (Matteoni and Kreis 1987).

MCF-7, MDA-MB-231 and MCF10A cells were fixed and permeabilised with -20ºC methanol, a protocol which has been shown to optimally preserve microtubule structure (Wheatley and Wang 1998). Fixed cells were fluorescently immunolabelled for β-tubulin and the nuclei were counterstained with Hoechst (Fig. 4-2).

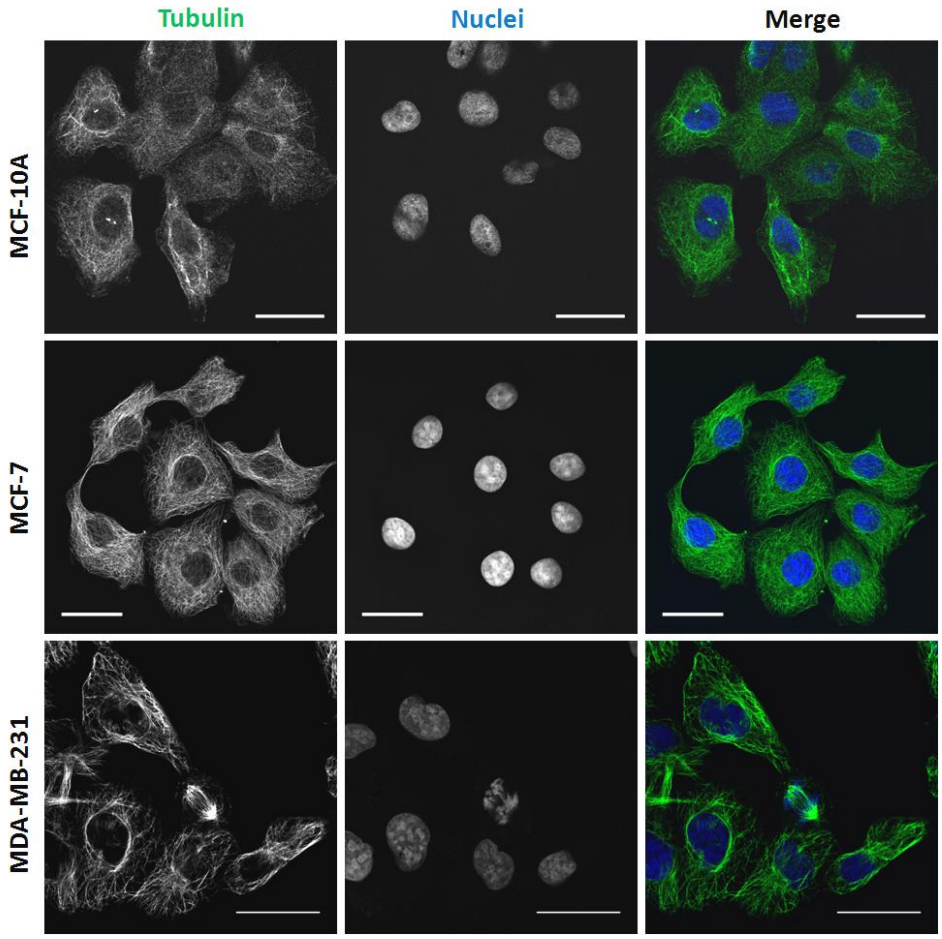

Figure 4-2: Microtubule cytoskeleton structure in breast and breast cancer cells. Cells were immunolabelled against tubulin (green) and nuclei were counterstained blue with Hoechst. *Scale bars = 25 µm.*

In all cell lines the microtubules formed a nest-like mesh of interwoven microfilaments (Fig.4-2). The microtubules in the MDA-MB-231 cells however appeared less densely fibrous than the cytoskeleton in MCF-7 and MCF-10A cells. There were also many more mitotic cells evident in the MDA-MB-231 cell line.

Late endosomes and lysosomes are respectively responsible for the sorting and proteolysis of endocytic cargo targeted for lysosomal degradation. These endocytic structures are critically important for the cessation of signalling by activated and internalised cell surface receptors.

A number of antibodies against different late endolysosomal markers such as the mannose-6-phosphate receptor (M6PR) and beta-Galactosidase-1 were tested with different fixation protocols before the optimal antibody and method were identified. Ultimately a protocol for LAMP2 IF was successfully created (Fig. 4-3). LAMP2 is a glycoprotein that is enriched on the limiting membranes of both late endosomes and lysosomes. LAMP2 is believed to be an important receptor for the selective uptake and degradation of cargo by lysosomes (Cuervo and Dice 1996). This protein is also thought to have roles in lysosome biogenesis and autophagy (Eskelinen *et al.* 2002).

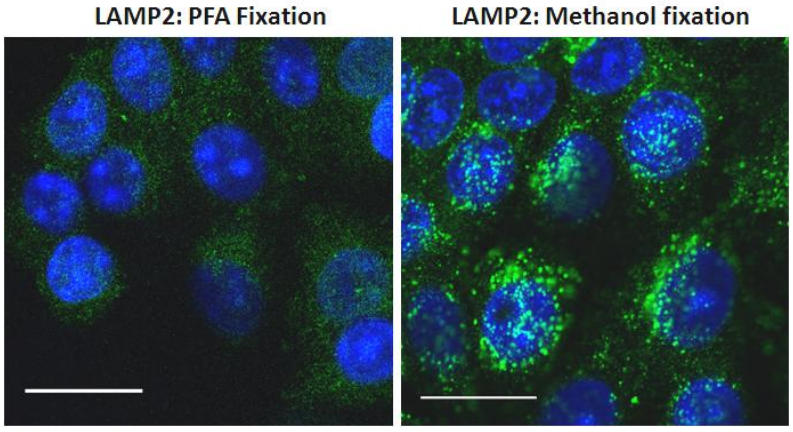

Figure 4-3: LAMP2 immunofluorescence with different fixation methods. MCF-7 cells were either fixed with PFA and permeabilised with Triton x-100 or were fixed and permeabilised with -20ºC methanol. IF for LAMP2 was then performed. Nuclei were counterstained blue with Hoechst. *Scale bars = 25 µm.*

Late endolysosomal labelling with the anti-LAMP2 antibody was sucessfully achieved through the implementation of a -20ºC methanol fixation protocol (Fig. 4-3). The development of an effective LAMP2 IF protocol enabled the method to be used in a small collaboration between Cardiff University laboratories (Webber *et al.* 2015). This is discussed in more detail in Section 4.3.

For the endocytic profiling, methanol fixed MCF-10A, MCF-7 and MDA-MB-231 cells were fluorescently immunolabelled for LAMP2 and the nuclei were counterstained with Hoechst (Fig. 4-4).

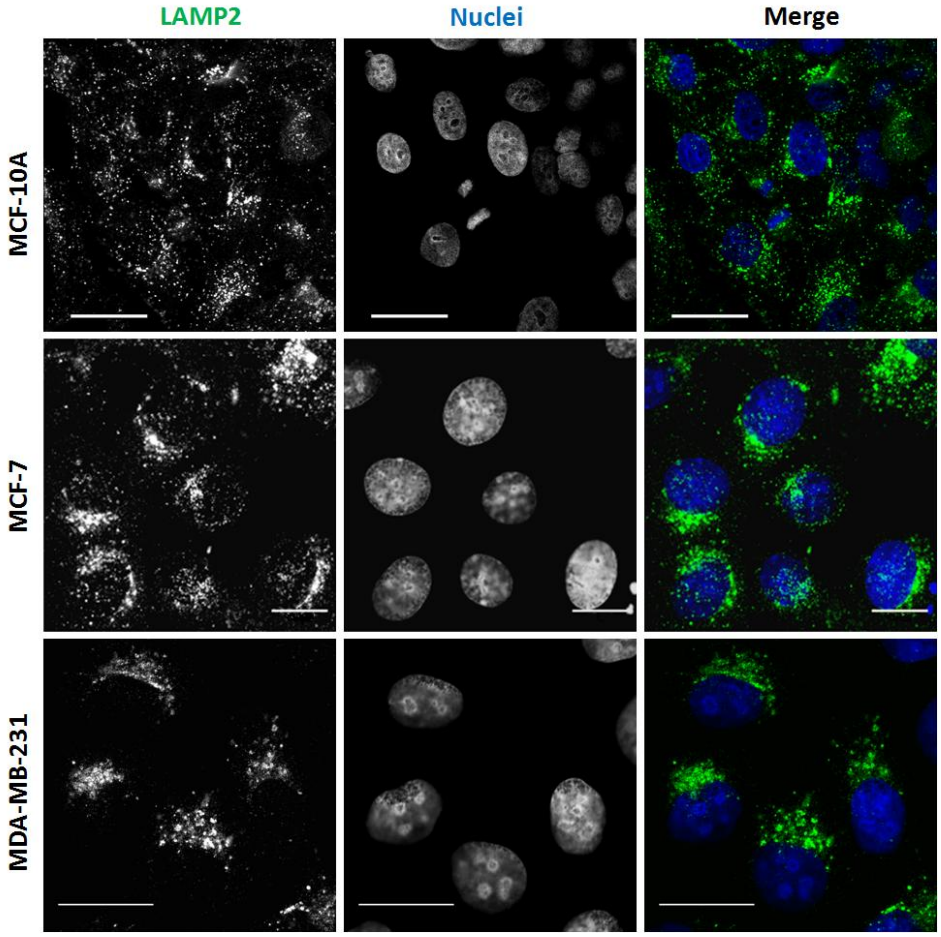

Figure 4-4: Subcellular localisation of late endosomes and lysosomes in breast and breast cancer cells. Cells were fluorescently immunolabelled for LAMP2 (green). Nuclei were counterstained blue with Hoechst**.** *Scale bars = 25 µm.*

The late endosomes and lysosomes in both MDA-MB-231 and MCF-7 cells were localised in polar perinuclear clusters. In the MCF-7 cells these endocytic organelles were more densely clustered than in the MDA-MB-231 cells where individual endolysosomal structures were more clearly visible. The late endosomes and lysosomes in the MCF-10A cells were enriched in the perinuclear region but there were

also more small structures scattered throughout the cytoplasm in these cells.

The *trans*-golgi-network (TGN) has links to endocytosis via a process known as retrograde transport. Retrograde transport is the trafficking of proteins from the early endosome to the TGN via recycling endosomes (Bonifacino and Rojas 2006). The process is coordinated by Rab11 and is a key pathway in promoting recycling of endocytic cargo and inhibiting its lysosomal degradation (Wilcke *et al.* 2000). The TGN also has an integral role in lysosome function as this compartment organises the transport of newly synthesised enzymes such as cathepsin D to the lysosomes (Press *et al.* 1998; Rojas *et al.* 2008). The TGN was also of interest due to the *in silico* research which demonstrated co-expression of Golgi-associated genes with BCA2 (Table 3-2).

PFA fixed MCF-7, MDA-MB-231 and MCF10A cells were subjected to immunofluorescence for TGN46 and the nuclei were counterstained with Hoechst (Fig. 4-5).

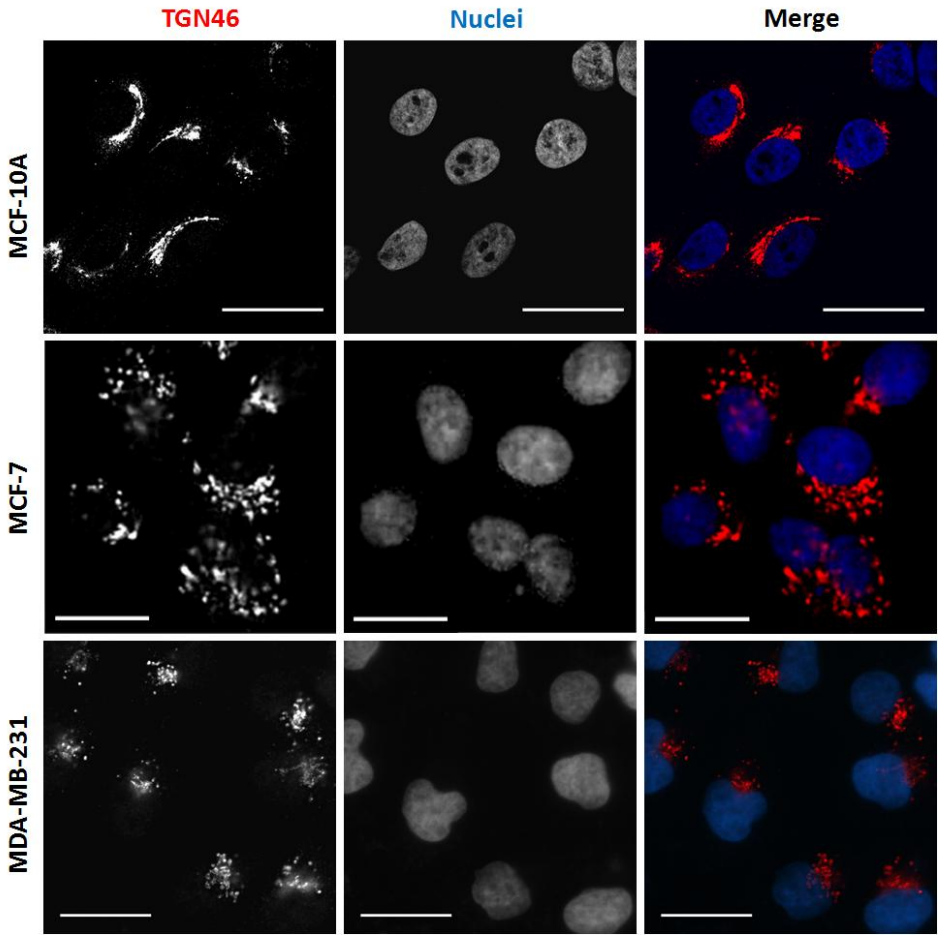

Figure 4-5: *Trans*-Golgi network structure and localisation in breast and breast cancer cells. Immunofluorescence was performed for TGN46 (red) in the three cell lines. Nuclei were counterstained blue with Hoechst. *Scale bars = 25 µm.*

The TGN in the MDA-MB-231 cells was highly condensed and polarised in the perinuclear area. In the MCF-10A cells the TGN was also perinuclear however the morphology indicated a more layered, tubular configuration. The TGN in the MCF-7 cells appeared to be more fragmented and dispersed than in the other cell lines.

The transferrin receptor (TfR) is carrier protein responsible for the cellular uptake of iron via transferrin (Tf). Tf protein, complexed with Ferric (FE^{3+}) iron, binds to TfRs on the cell surface. The receptor-transferrin complex is imported into cells via endocytosis following clustering of TfRs and clathrin pit formation at the membrane (Liu *et al.*

2010). Upon reaching the early endosomes TfR-Tf complexes are either recycled directly back to the cell surface or they enter the network of recycling endosomes that form the recycling compartment of the cell. The recycling compartment is usually found in the perinuclear region of the cell and from here TfR-Tf complexes may either be recycled to the cell surface or be transported to the TGN (van Dam *et al.* 2002; Maxfield and McGraw 2004). Tf and the TfR are often used as proxy markers for the recycling endocytic pathway, early endosomes and CME.

MCF-7, MDA-MB-231 and MCF-10A cells were fixed with PFA, labelled for TfR by immunofluorescence, and nuclei were counterstained with Hoechst (Fig. 4-6). Secondary antibody only controls were also performed and were confirmed to be negative.

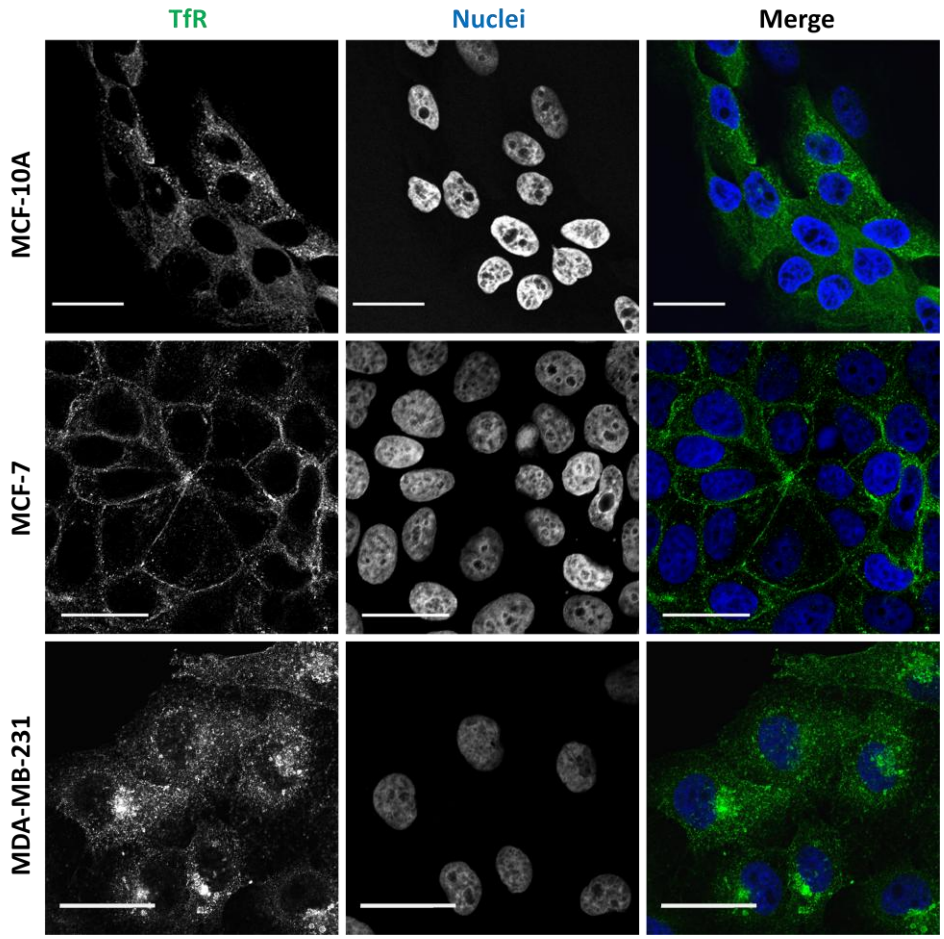

Figure 4-6: Subcellular localisation of the transferrin receptor in breast cancer cells. Immunofluorescence was performed for TfR (green) in the three cell lines. Nuclei were counterstained blue with Hoechst. *Scale bars = 25 µm.*

Figure 4-6 demonstrates that in MCF-7 cells the TfR was primarily localised on the cell membrane. In MCF-10A and MDA-MB-231 cells however the majority of the TfR was contained in intracellular vesicles. In MDA-MB-231 cells there was perinuclear enrichment of the receptor suggesting that a large portion of the receptor pool was contained within the recycling compartment.

EGFR is an important oncoprotein in many cancers and alterations in the endocytosis of this receptor have been linked to resistance to EGFR inhibitors (see 1.2.7). Following internalisation and trafficking to the early endosome EGFR may be recycled or degraded depending on a

number of conditions. Factors influencing receptor fate once endocytosed include: the stimulating ligand (Roepstorff *et al.* 2009), the dimerisation partner receptor i.e. homodimerisation versus heterodimerisation, in particular with HER2 (Hendriks *et al*. 2009), receptor ubiquitination (Longva *et al.* 2002) and the internalisation pathway i.e. CME or NCME (Sigismund *et al.* 2008).

PFA fixed MCF-7, MDA-MB-231 and MCF10A cells labelled for EGFR by immunofluorescence and nuclei were counterstained with Hoechst (Fig. 4-7). Secondary antibody only controls were also performed and were confirmed to be negative.

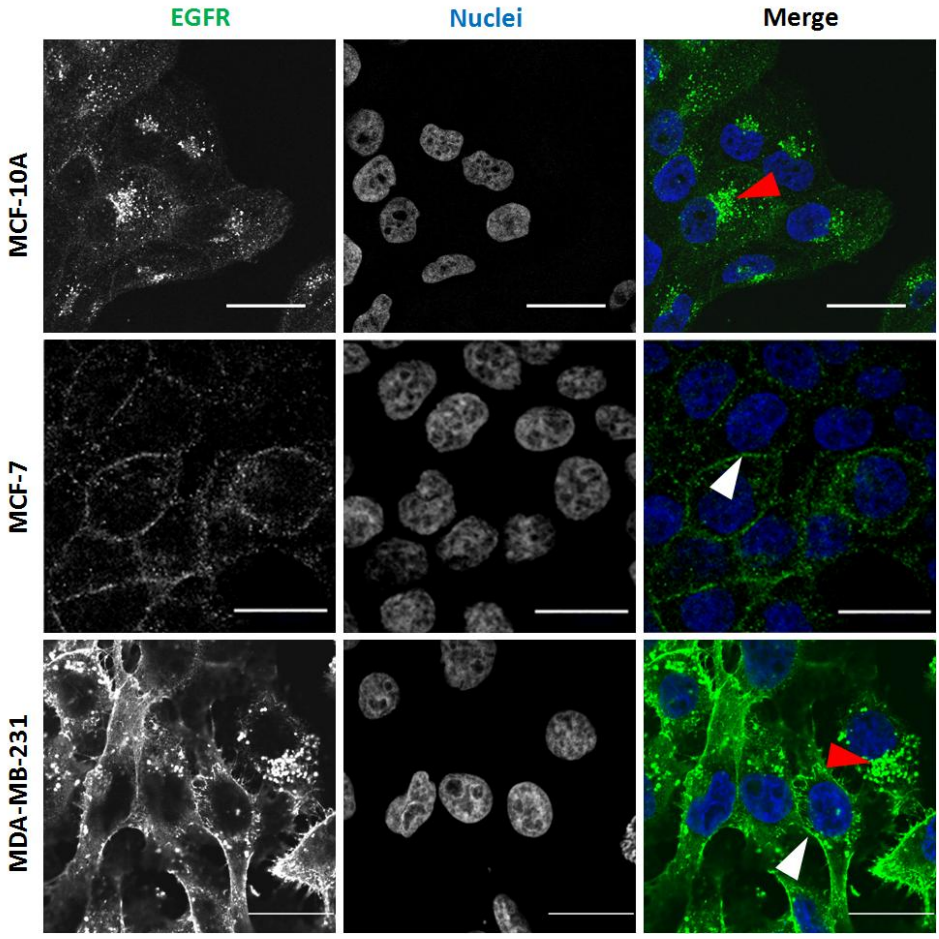

Figure 4-7: EGFR expression and localisation in breast and breast cancer cells. Cells were immunolabelled against EGFR (green) and nuclei were counterstained blue with Hoechst. *White arrowheads indicate membranous EGFR, red arrowheads indicate vesicular EGFR. Scale bars = 25 µm.*

MDA-MB-231 cells highly overexpress EGFR and this was reflected in the bright, abundant labelling in this cell line: EGFR was enriched on the plasma membrane (white arrowheads, Fig. 4-7) and in large intracellular vesicle structures (red arrowheads, Fig. 4-7). MCF-7 cells express very low EGFR levels and so only faint labelling was detected and this was largely limited to the cell membrane. MCF-10A cells express moderate levels of EGFR and since their growth medium contains EGF (which stimulates endocytosis), this may explain why majority of the EGFR in these cells was confined to intracellular vesicles.

4.2 Effect of Disulfiram treatment on BCA2 and EGFR expression and Trafficking in MCF-7 cells

Dilsulfiram (DSF) has previously been shown to reduce BCA2 levels in breast cancer cells and to inhibit BCA2's ubiquitination activity (Brahemi *et al.* 2010; Burger and Westwell 2011). Experiments were conducted to determine whether DSF treatment affected the subcellular localisation of early and late endocytic organelles. MCF-7 cells were incubated with 1 μM DSF for three hours before fixation and IF for EEA1 and LAMP2 were carried out.

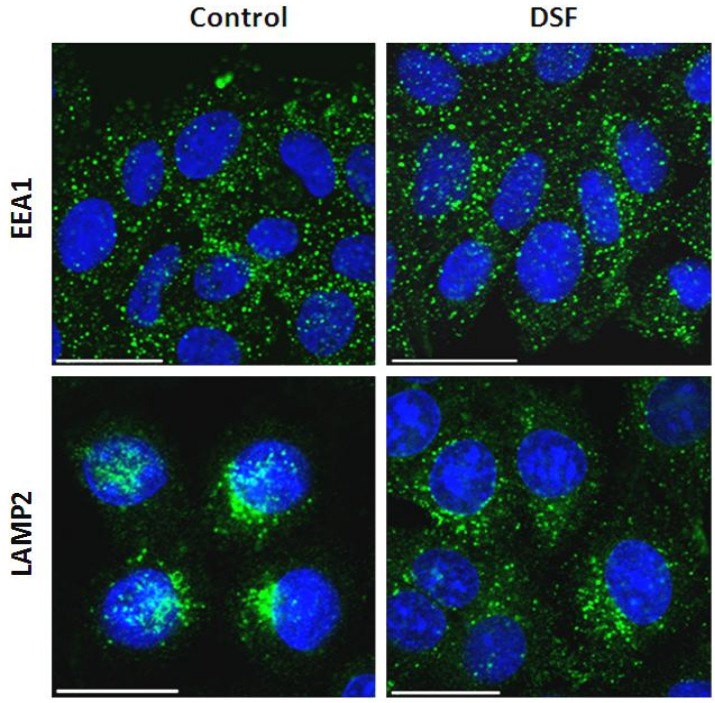

Figure 4-8: Effect of disulfiram on the subcellular localisation of early endosomes and late endosolysosomes in MCF-7 cells. Cells were treated with 1 µM DSF for 3 hr before IF was performed for EEA1or LAMP2. Nuclei were labelled blue with Hoechst. *Scale bars = 25 µm.*

Figure 4-8 demonstrates that while no effect on early endosomes was detected after DSF treatment, the drug caused relocalisation of late endolysosomes from perinuclear clusters to a more scattered distribution throughout the cytoplasm (Fig. 4-8). This work has been extended as part of a co-running breast cancer PhD project in the laboratory. The focus of the second project is the effect of DSF on cell viability and on endolysosomal zinc sequestration. A publication from the DSF project is being prepared for submission and incorporates the data, from Figure 4-8.

4.3 Application of methods utilised in endocytic profiling to a separate collaborative project

Some of the IF methods developed and practiced in the endocytic profiling work were shared with researchers from Velindre Cancer

Hospital, Cardiff. Dr. Aled Clayton works in the field of exosomes in cancer immunology. The information and advice shared allowed researchers in the Clayton laboratory to perform IF to examine changes in endocytic organelles following ribozyme silencing of Rab27. Methods developed for endocytic profiling here were then utilised in collaboration with Dr. Clayton to identify specific changes in late endosome/ lysosome distribution associated with Rab27 depletion in Du145 prostate cancer cells (Fig. 4-9). The data showed Rab27 depletion led to a dramatic cell phenotype with clustered late endolysosomes and has been published in Oncogene (Webber *et al.* 2015).

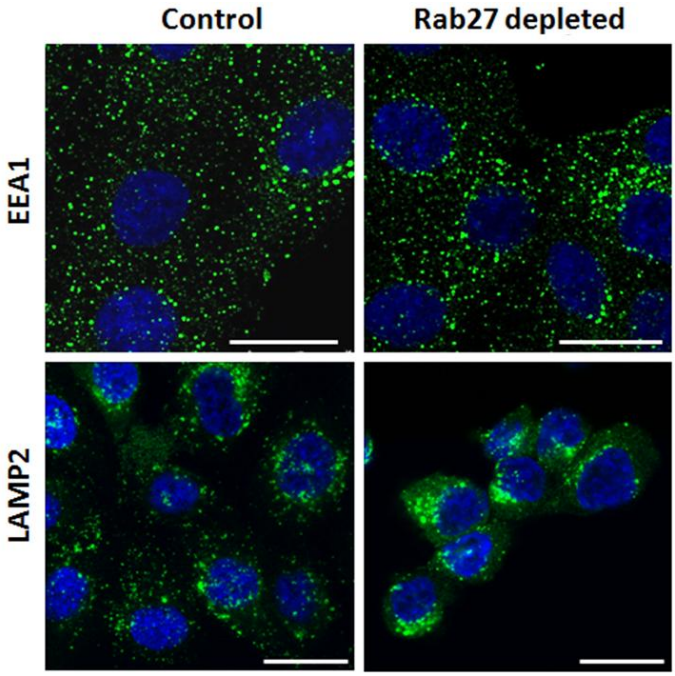

Figure 4-9: Effect of Rab27 depletion on the subcellular localisation of early and late endocytic organelles in Du145 cells. Rab27 depletion with ribozymes was performed by Dr. J. Webber who then performed IF according to protocols developed by J. Wymant. Confocal microscopy was performed by J. Wymant. *Scale bars = 25µm*

4.4 Investigating the subcellular localisation of endogenous BCA2 with immunofluorescence

The subcellular localisation of BCA2 is somewhat poorly illustrated in the literature and little detail beyond "cytoplasmic" and "nuclear" has

been described. In order to determine and clearly image the endogenous distribution of BCA2, a variety of different IF techniques were tested. The methods developed were subjected to validation checks so that the optimum protocol for BCA2 IF could be identified.

Alcohol and ketone fixative/permeabilisers were assessed for BCA2 IF compatibility alongside the more commonly used PFA and Triton X-100 reagents. PFA is a cross-linking fixative, so called because it generates covalent bonds between cellular proteins that fix them in place. Alcohols and ketones are precipitating/dehydrating fixatives that work by disrupting the hydrophobic bonds of cellular proteins causing denaturation of their tertiary structure (Jamur and Oliver 2010a). Precipitating fixatives can be particularly useful for IF with antibodies directed against the internal regions of proteins. Cross-linking fixatives can sometimes cause proteins to become rigidly fixed in a conformation that does not allow antibodies to reach their target epitopes. In these instances precipitating fixatives can be utilised in order to expose the antibody binding sites (Schnell *et al.* 2012).

A commercially available but un-validated goat anti-BCA2 antibody as a starting point, various fixative and permeabilisation agents were tested (Fig. 4-10). MCF-7 cells were used as they have been described as high BCA2 expressing in the literature as a high BCA2 expressing cell line (Brahemi *et al*. 2010) and this is supported by mRNA data in Figure 3-4.

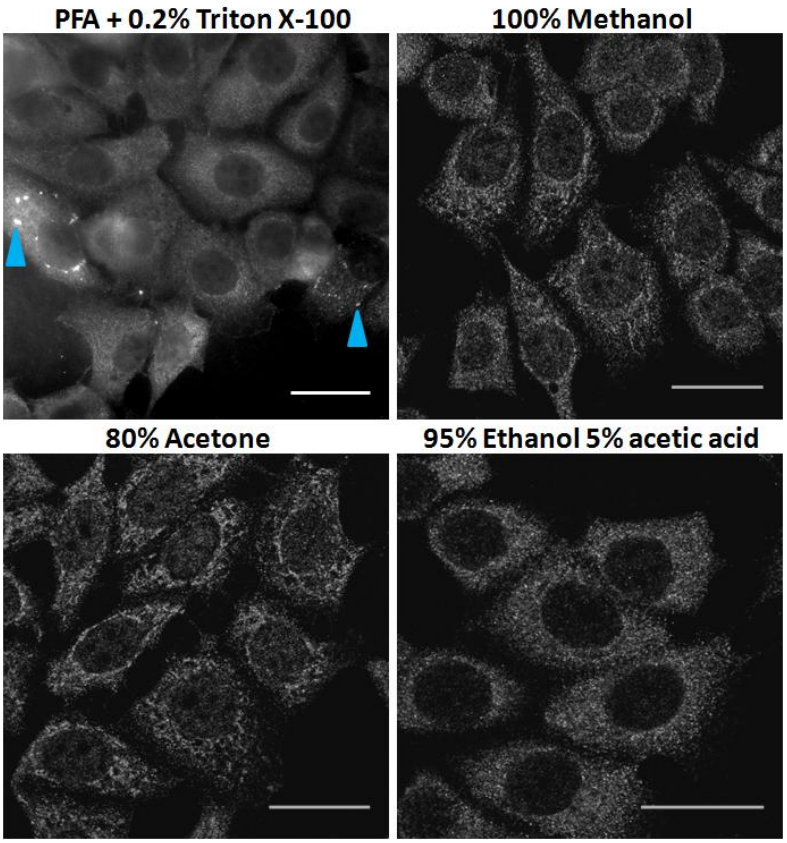

Figure 4-10: Comparison of fixative/permeabilisation agents for BCA2 IF with goat~BCA2 antibody (Sigma). MCF-7 cells were fixed and permeabilised with a range of techniques as indicated above. IF was performed for BCA2 using goat~BCA2. (1:200). *Blue arrowheads indicate regions BCA2 enrichment. Scale bars = 25 µm.*

PFA and Triton X-100 gave predominantly diffuse cytoplasmic labelling though some very faint nuclear fluorescence was also detected (Fig. 4-10). In some cells (~1%) there were regions of apparent BCA2 enrichment (indicated by blue arrowheads in Fig. 4-10). Vesicular-like structures of varying size and staining intensity were evident in these cells but they were not representative of the typical staining pattern. The dehydrating and protein precipitating fixatives such as acetone and methanol appeared to indicate that BCA2 was enriched in the perinuclear region. With these fixatives a reticular staining pattern was evident that was indicative of localisation on filamentous structures. At the time of performing the experiments (2012) this localisation was in-keeping with

the BCA2 IF staining pattern depicted in A431 cells in the Human Protein Atlas (HPA; http://www.proteinatlas.org/). However, the subcellular localisation images have since been removed from the HPA website.

The primary antibody being used was against an internal region of the protein which indicated the potential suitability of a precipitating fixative. In support of this, acetone and methanol fixation both produced similar patterns of fluorescence which suggested that the labelling produced by these methods was a reflection of true BCA2 localisation. In light of this, and the fact that acetone protocol produced the clearest labelling, the acetone fixation method was investigated further.

Anti-BCA2 labelling in acetone-fixed MCF-7 and MDA-MB-231 cells was performed along with secondary controls (Fig. 4-11). Since the two cell lines had been described in the literature as high and low BCA2 expressers (Brahemi *et al.* 2010) their combined use was intended to determine whether differential BCA2 expression could be demonstrated with IF.

The reticular labelling in the BCA2 overexpressing MCF-7 cells and filamentous staining in the MDA-MB-231 cells suggested BCA2 was possibly localising to the mitochondria. However, although the data was initially promising, there did not appear to be a difference in staining intensity between the two cell lines which was a possible indication that the staining might not be specific for BCA2. Also disquieting were the secondary only controls which showed similar (but fainter) staining patterns (right hand column, Fig 4-11).

Further investigation revealed that FBS and BSA may not be suitable for use in blocking solutions with anti-goat secondaries due to contamination from bovine IgG. Cross-reactivity between goat secondary antibodies and bovine IgG can lead to the formation of immune complexes which can increase background staining and potentially produce false positive results (Buchwalow *et al.* 2011). Rabbit serum was tested in place of FBS and this reduced but did not eradicate the background staining (bottom row of each cell line montage in Fig. 4-11).

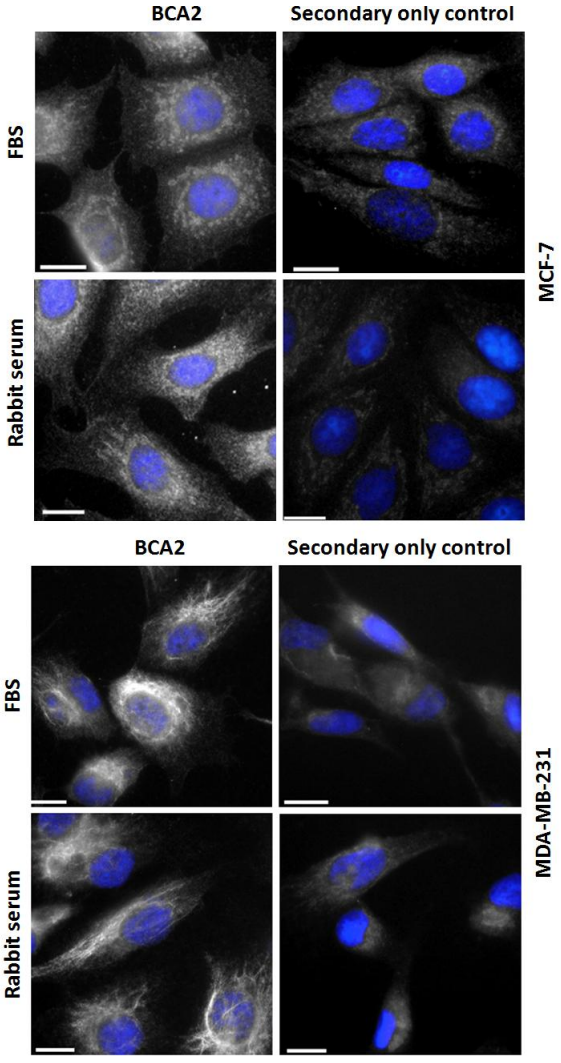

Figure 4-11: Comparing different serums in blocking solutions and antibody diluents for BCA2 immunolabelling. MCF-7 and MDA-MB-231 cells were fixed with 80% acetone and IF was performed for BCA2 using the goat anti-BCA2 antibody (1:200). Either 2% FBS + 2% BSA or 5% rabbit serum were used as blocking and diluents solutions as indicated. Negative controls were performed by omitting the primary antibody (third column of images). *Scale bars = 15 µm.*

The lack of BCA2 staining specificity was ultimately confirmed by using a different fluorescent anti-goat secondary antibody. With a different secondary antibody, the BCA2 labelling was fairly diffuse throughout the cell and there was little/no sign of the structures that were visualised when using the original anti-goat antibody (Fig.4-12).

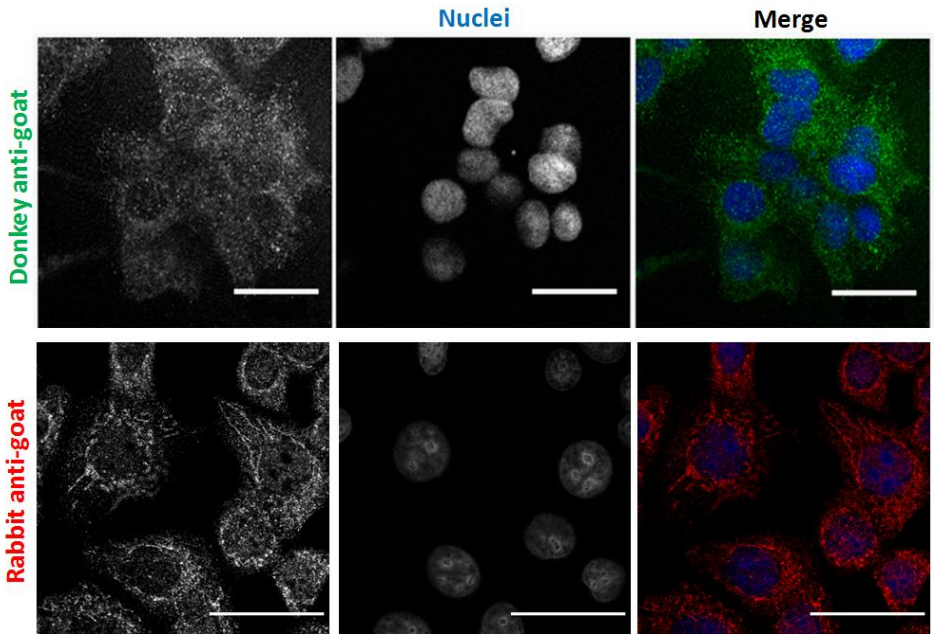

Figure 4-12: Comparing fluorescent anti-goat secondary antibodies for BCA2 labelling in acetone fixed MCF-7 cells. Nuclei are counterstained blue with Hoechst. *Scale bars = 25 µm.*

A second anti-BCA2 antibody raised in rabbit was subsequently investigated in MCF-7 and MDA-MB-231 cells. Experiments were initially performed solely with the PFA/Triton X-100 protocol.

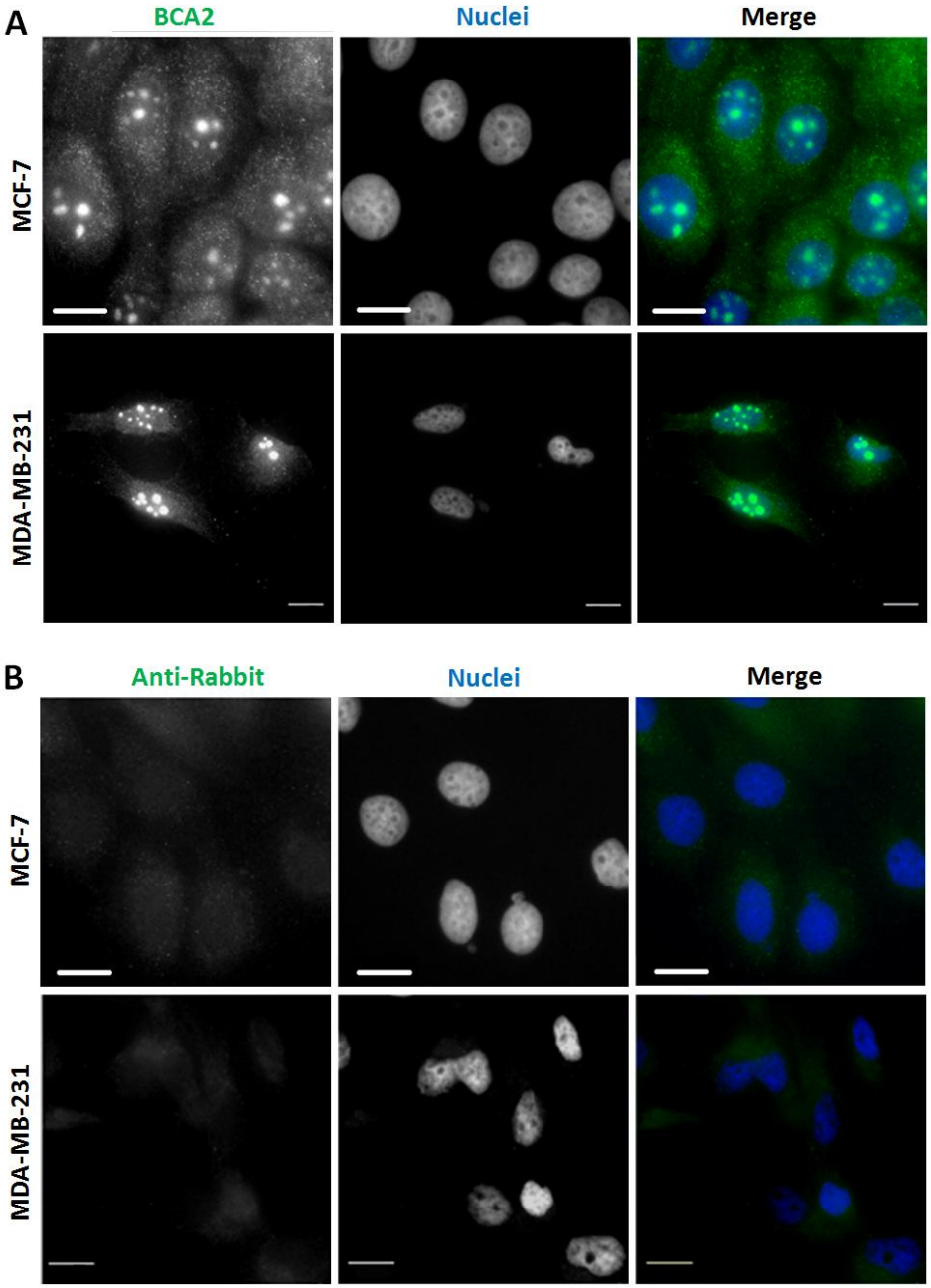

Figure 4-13: Testing the suitability of a rabbit anti-BCA2 primary antibody for IF. PFA fixed breast cancer cells were subjected to IF for BCA2 using the rabbit anti-BCA2 antibody diluted 1:200 A) Localisation in MCF-7 and MDA-MB-231 cells. B) Secondary only controls. *Scale bars = 15 µm.*

The staining produced using the rabbit anti-BCA2 antibody indicated cytoplasmic and nuclear BCA2 localisation with enrichment in the nucleoli (Fig. 4-13 A). The nuclear and cytoplasmic labelling was in line with previous literature (Burger *et al.* 2005). The prominent nucleolar

staining had also been demonstrated in a BCA2 publication (Kona *et al.* 2012) and matched some localisation data shown on the HPA.

However, nucleoli are a common site for off-target immunofluorescence labelling. Non-specific nucleolar labelling has been reported for various primary antibodies including #2626 (Cell Signalling), ab78517 and ab27171 (Abcam). A study by Sangale *et al.* (2011) described the limitations of a number of optimised anti-PTEN antibodies from Abcam, Millipore and Novus that all produced off-target, nucleolar fluorescence.

Encouragingly the secondary-antibody-only controls in Figure 4-13 B were all negative, though further tests were necessary to validate the labelling. For this a plasmid encoding an epitope tagged version of BCA2 was acquired and tested. Overexpression of epitope tagged BCA2 would enable dual detection by IF against the tag and the protein. This would demonstrate whether an antibody could detect different cellular levels of the protein and would determine its suitability for IF.

4.5 Subcellular localisation of HA-BCA2

In view of the problems experienced in investigating the subcellular localisation of endogenous BCA2, transient overexpression was identified as an alternative means of characterising BCA2 localisation.

4.5.1 pCMV-HA-BCA2 vector

The pCMV-HA plasmid containing a BCA2 insert was a generous gift from Naoki Yamamoto at the National Institute of Infectious Diseases in Tokyo (Miyakawa *et al.* 2009). For the plasmid map see Appendix D.

The plasmid was extracted from filter paper, amplified and purified as described in Chapter 2 (Section 2-10) for use in transient transfection experiments.

4.5.2 Subcellular localisation of HA-BCA2 in breast cancer cells

HA-BCA2 was transfected into MCF-7 cells which, after 24 hrs of transfection, were then PFA fixed and immunolabelled for the human influenza haemagglutinin (HA) protein tag. Using an anti-HA primary antibody from Cell Signalling there initially appeared to be evidence of intermittent cell membrane labelling, with particular enrichment at focal adhesions. There also seemed to be filamentous labelling within the cells. Such localisation of BCA2 had not been previously described in literature and upon examination of the untransfected controls the reason for this became clear. The untransfected controls displayed the same localisation pattern as the supposedly HA-BCA2 transfected cells (Fig. 4-14). The labelling artefacts related to a problem with the primary rather than secondary antibody as two different secondary antibodies were tried without success. The antibody (#2362) has been discontinued by Cell Signalling.

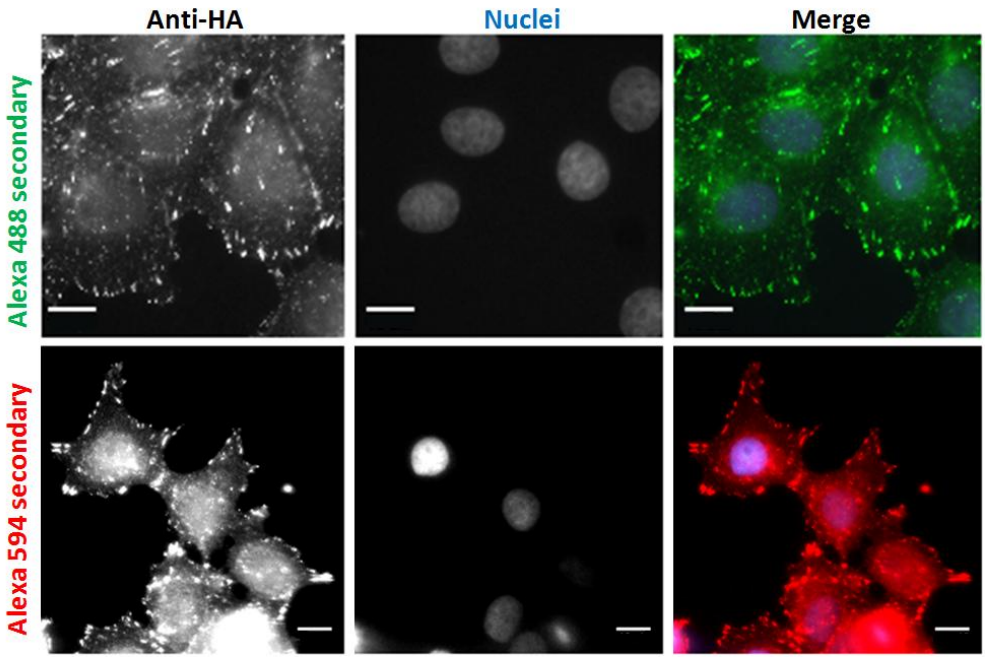

Figure 4-14: Labelling artefacts for IF with the Cell Signalling anti-HA primary antibody in untransfected controls. Nuclei were counterstained with Hoechst.. *Scale bars = 10 µm*

Having experienced problems with high background staining with the Cell Signalling antibody, a different anti-HA was tried from Sigma. Even at relatively high dilutions the background staining in untransfected cells, particularly in the MDA-MB-231 cells, was very high (Fig. 4-15 A). Under specific microscope settings it was possible to identify high HA-BCA2 expressing cells from the transfected MCF-7 population (Fig. 4-15 B). However, the high background staining made it very difficult distinguish the transfected but low/moderate BCA2 overexpressing cells.

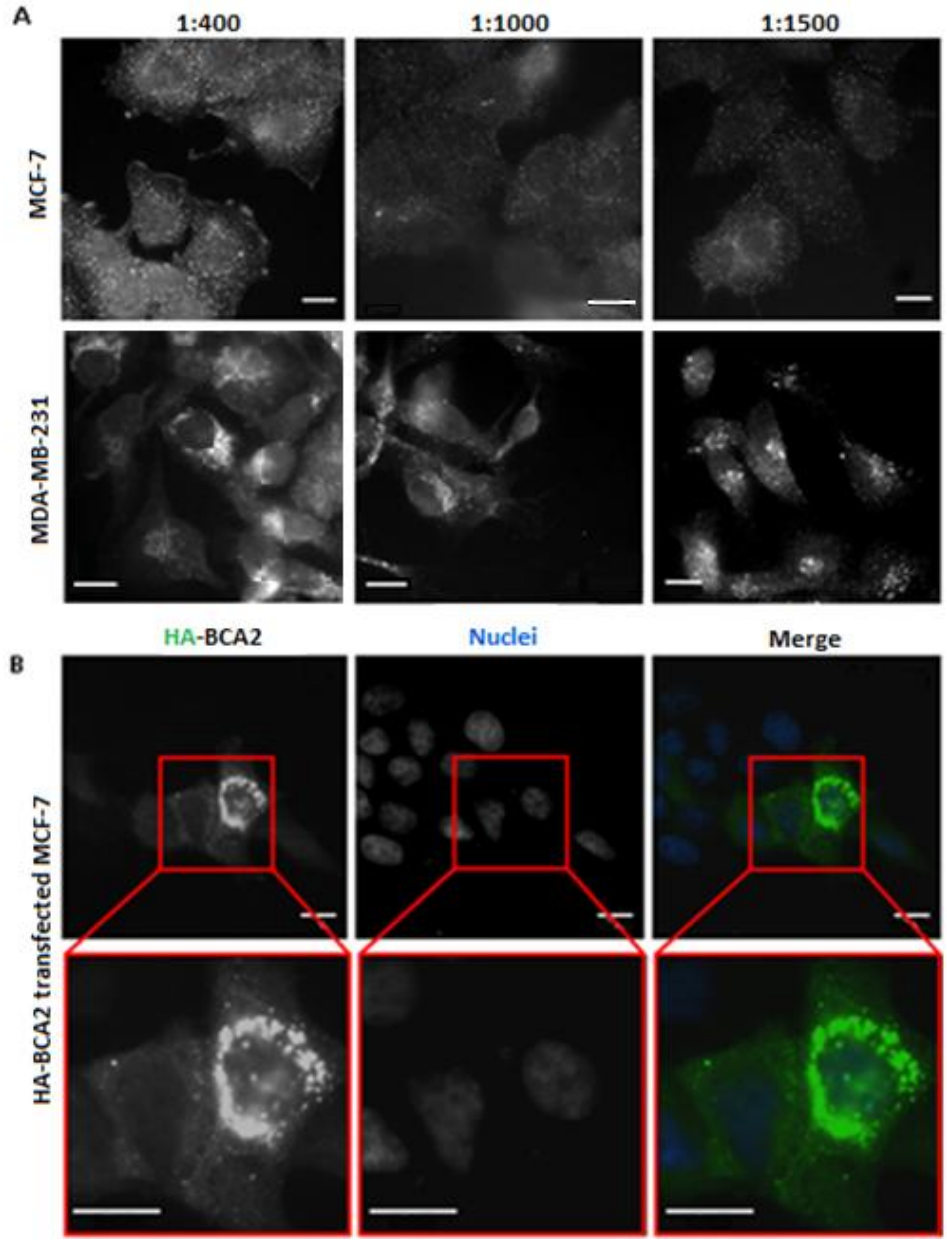

Figure 4-15: Anti-HA labelling with the Sigma primary antibody. A) In untransfected MCF-7 and MDA-MB-231 cells, even at high dilutions, the anti –HA background staining was unworkably high, particularly in the MDA-MB-231 cells. B) In transfected MCF-7 cells, using an highly diluted primary antibody (1:5000) and altering the microscope settings, it was possible to distinguish transfected cells that were very highly expressing BCA2. Nuclei were counterstained blue with Hoechst. *Scale bars = 10 µm*

A third anti-HA primary antibody was tested and the mouse anti-HA from Covance proved to be by far the most effective. Figure 4-16 shows that there was no background staining in untransfected cells and Figure

4-17 demonstrates how clearly the transfected, HA-BCA2 expressing cells can be identified.

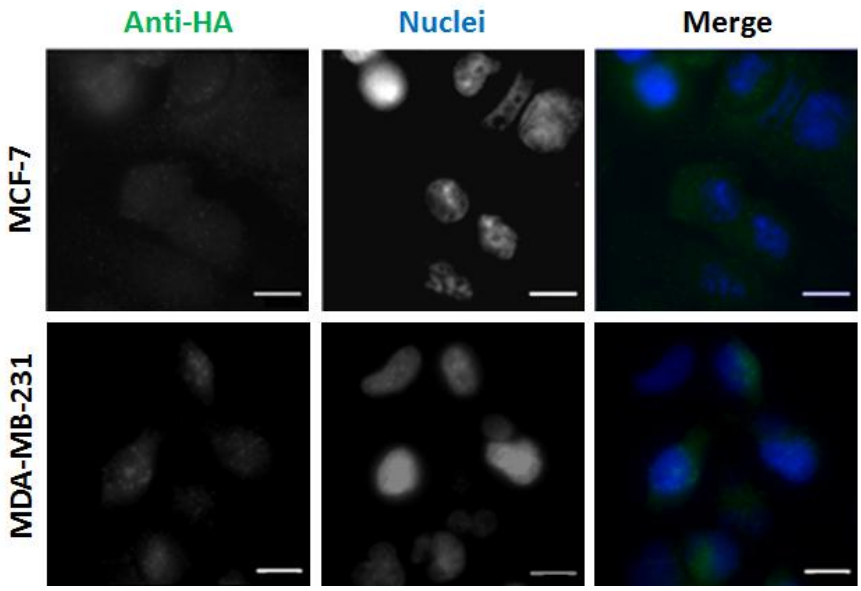

Figure 4-16: Negative (untransfected) controls for mouse anti-HA (Covance). Cells were fixed in PFA and IF was performed with the mouse anti-HA antibody from Covance (1:1000). Nuclei were counterstained blue with Hoechst. *Scale bars = 10 µm*

Fugene 6 and Lipofectamine 2000 are widely used transfection reagents: ~33,400 and ~62,500 literature references respectively. The two reagents were tested and compared in order to determine the optimum method for HA-BCA2 transfection and expression. Figure 4-17 demonstrates that MCF-7 cells had much higher HA-BCA2 transfection efficiency than MDA-MB-231 cells, irrespective of the transfection reagent used. Fugene 6 provided higher transfection efficiency in MCF-7 cells (~60%) compared with Lipofectamine 2000 (~40%). In MDA-MB-231 cells the transfection efficiency with Lipofectamine 2000 appeared to be slightly higher than with Fugene 6 but both efficiencies were very low (< 5%).

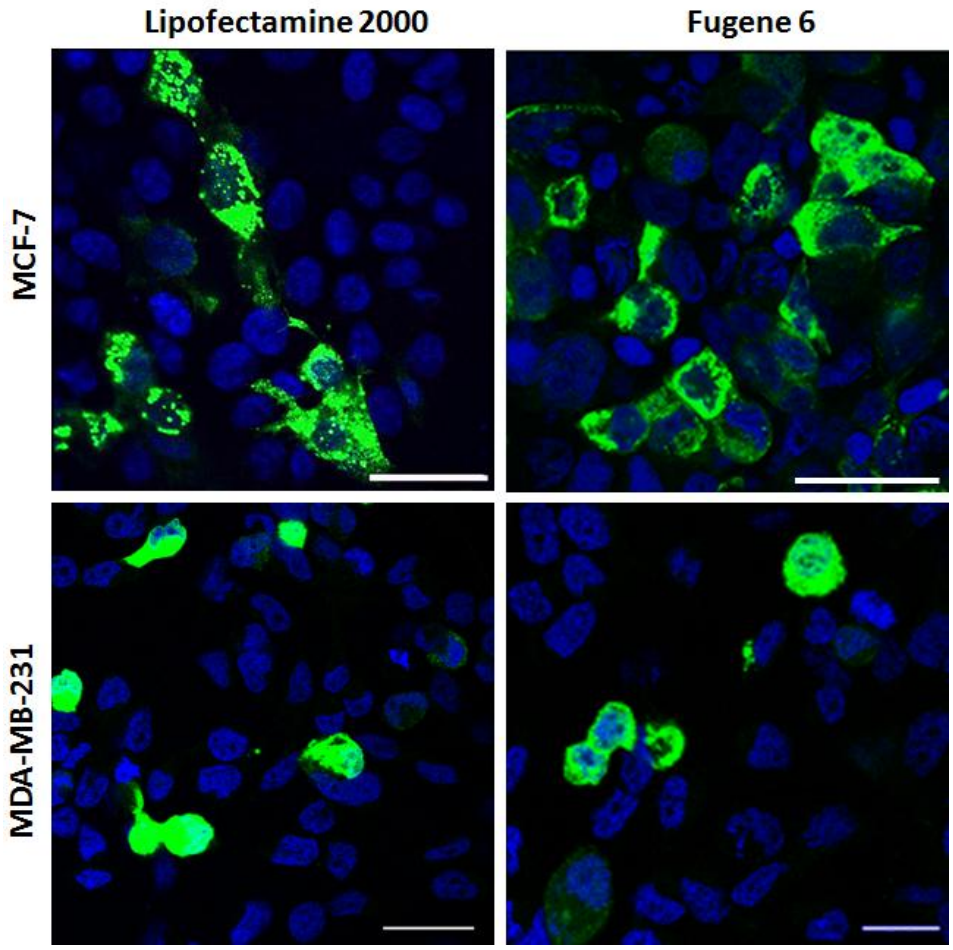

Figure 4-17: Optimising HA-BCA2 transfection and Covance anti-HA immunolabelling in MCF-7 and MDA-MB-231 cells. Cells were transfected with HA-BCA2 using either Fugene 6 or Lipofectamine 2000. After 24 hours cells were PFA fixed and immunolabelled for HA (Mouse ~HA, Covance, 1:1000). Nuclei were counterstained blue with Hoechst. *Scale bars = 25 µm*

HA-BCA2 transfected MCF-7 cells display a number of different, seemingly expression-dependent phenotypes (Fig. 4-18, top row). High expressers tended to display ubiquitous small, uniform vesicles which were closely packed throughout the cytoplasm or they contained large, dense perinuclear vesicles and/or large cytoplasmic structures. The moderate expressing cells tended to have diffuse cytoplasmic staining with some, more sparsely distributed vesicles. Low HA-BCA2 expressing cells had faint, diffuse cytoplasmic labelling. There was some evidence of nuclear labelling in the transfected cells but it was more

rarely seen than the cytoplasmic structures (~5% of transfected cells). There was no evidence of nucleolar labelling.

HA-BCA2 overexpressing MDA-MB-231 cells (Fig. 4-18, bottom row) showed signs of poor viability: most of the transfected cells appeared to be rounded or demonstrated cytoplasmic vacuolation. Owing to the poor transfection efficiency and viability of the MDA-MB-231 cells it was decided that further experimentation would be performed using the MCF-7 cell line.

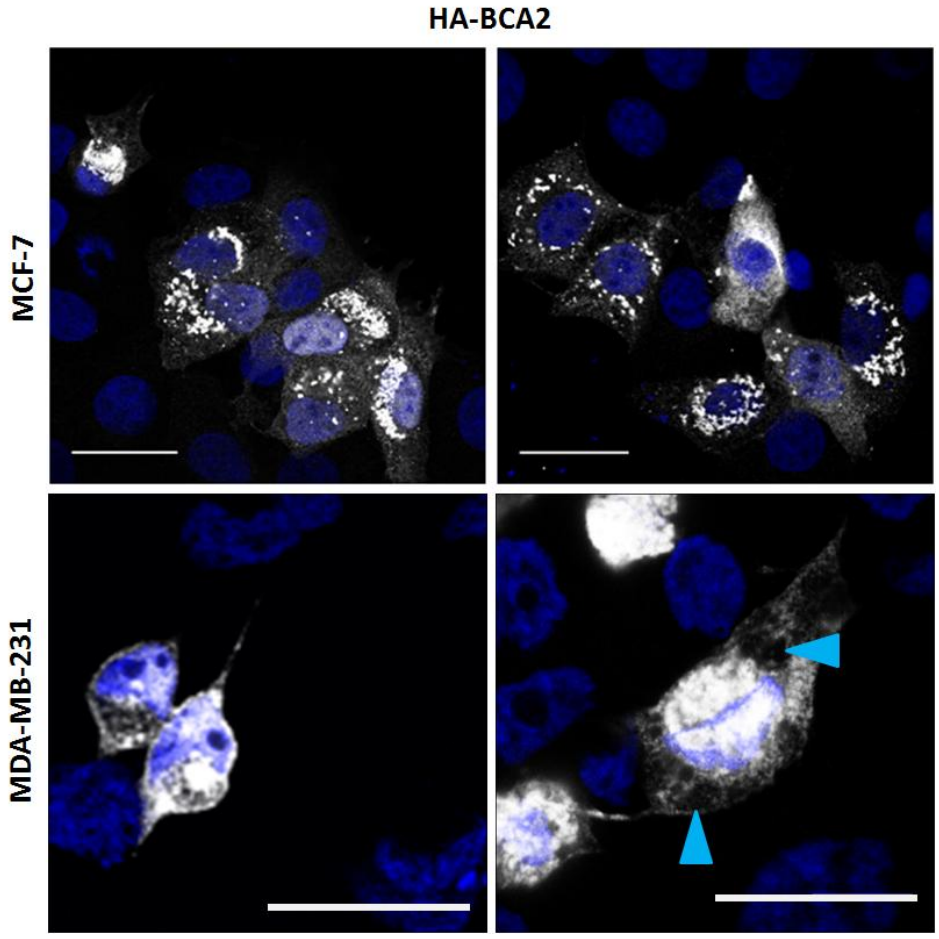

Figure 4-18: Subcellular localisation of HA-BCA2 in MCF-7 and MDA-MB-231 cells determined by immunofluorescence. Cells were transfected with HA-BCA2, PFA fixed and immunolabelled for HA (Mouse~HA, Covance, 1:1000). Nuclei were counterstained blue with Hoechst. *Blue arrowheads indicate vacuoles*. *Scale bars = 25 µm*

In order to verify that the subcellular localisation related to HA-tagged BCA2 (i.e. that the protein was expressed and the HA-tag was uncleaved): double-immunolabelling was performed for BCA2 and HA. The goat anti-BCA2 primary antibody was used at a relatively high dilution (1:5000) alongside the Covance anti-HA antibody. Colocalisation analysis confirmed that IF staining was specific to BCA2 and that the HA tag remained attached *in vitro* (Fig. 4-19 A). Single labelling was also performed for both BCA2 and HA (Fig. 4-19 B). The staining patterns seen in single-labelled cells were very similar, further indicating the structures/localisation seen were not artefacts of the double-labelling process. These findings also helped to validate the goat anti-BCA2 antibody for use in IF.

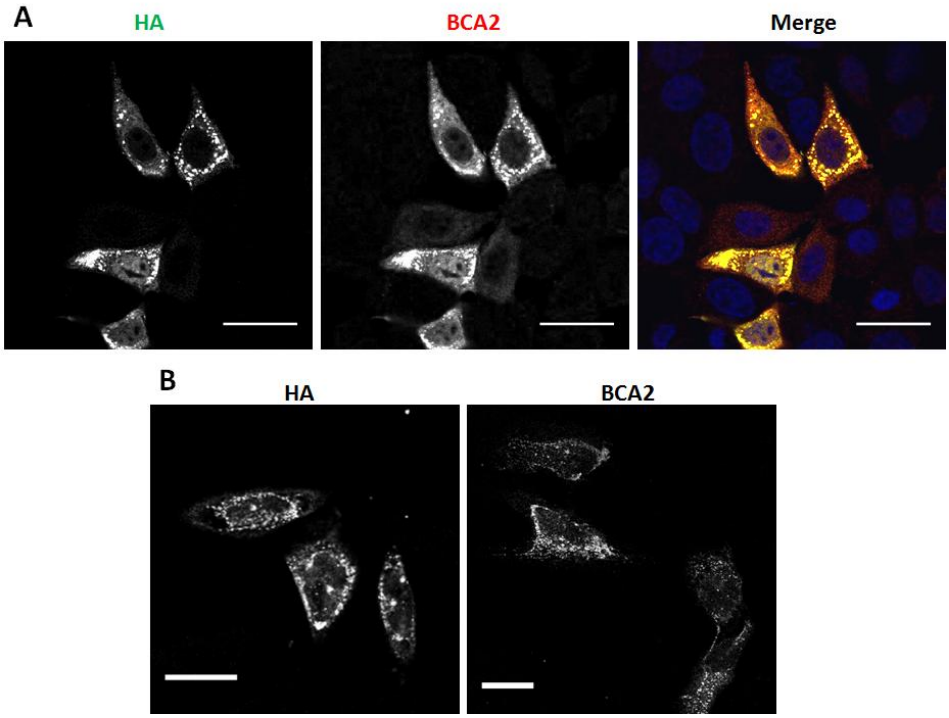

Figure 4-19: Anti-HA and Anti-BCA2 IF in HA-BCA2 Transfected MCF-7 cells. A) Sequential double IF was performed in HA-BCA2 transfected cells using the goat anti-BCA2 antibody and mouse anti-HA. Nuclei were counterstained with Hoechst. B) Separate anti-HA and anti-BCA2 IF was performed. *Scale bars = 25 µm*

The localisation patterns produced by high levels of HA-BCA2 overexpression were similar to those observed in a small subpopulation of MCF-7 cells when endogenous levels of BCA2 were examined (PFA fixation, Fig. 4-10). Comparative IF images of HA-BCA2 transfected MCF-7 cells and the subpopulation of MCF-7 cells containing vesicle-like cytoplasmic structures are presented in Figure 4-20.

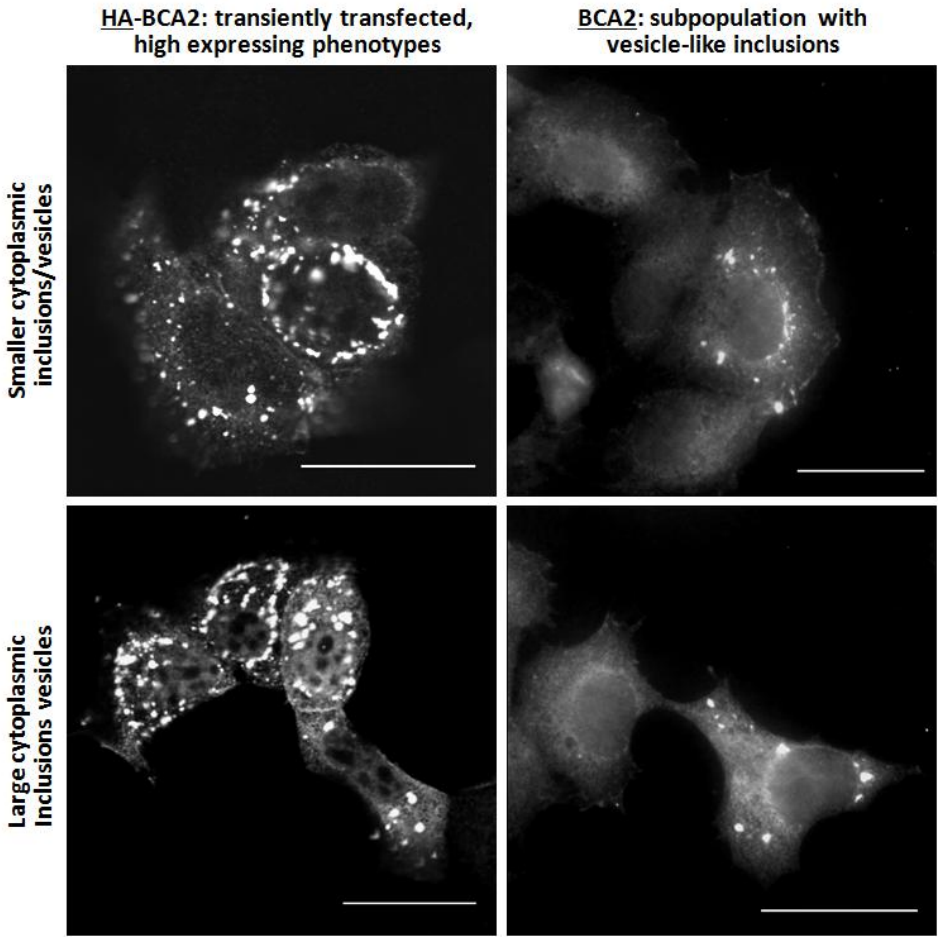

Figure 4-20: Comparison of HA-BCA2 localisation with endogenous BCA2 localisation in a subpopulation of MCF-7 cells. Cells were either transfected with HA-BCA2 and IF was performed for HA (PFA fixation, Mouse~HA, Covance, 1:200, *left column*) or cells were untransfected and IF was performed for BCA2 (PFA fixation, goat~BCA2, 1:200, *right column*). *Scale bars = 25 µm*

Figure 4-20 demonstrates the similarity in localisation between overexpressed HA-BCA2 in MCF-7 cells and endogenous BCA2 found in a small subpopulation of the (untransfected) cell line. The results

suggested that although expression levels were much higher in the transiently transfected cells, the cellular distribution of HA-BCA2 approximated a localisation pattern found endogenously in a small cell subpopulation of the MCF-7 cells.

A series of double-immunolabelling (colocalisation) experiments were performed in order to identify which cellular compartments could be said to house transfected BCA2. The experiments had a dual purpose as they also enabled exploration of possible HA-BCA2 induced effects on endocytic and metabolic organelles. Secondary antibody only controls were also performed and were all confirmed to be negative.

Figure 4-21 A shows that overexpressed HA-BCA2 neither altered nor co-localised with early endosomes in transfected MCF-7 cells that were fixed and immunolabelled for HA and EEA1.

Fluorescent transferrin probes such as transferrin Alexa-488 (Tf-488) can be used to visualise the recycling endocytic pathway in addition to early endosomes (see 1.2.8.1). HA-BCA2 overexpressing MCF-7 cells were serum-starved for one hour before being incubated with transferrin-488 for 20 min, fixed with PFA and immunofluorescence for HA was performed against direct visualisation of Tf. The results in Figure 4-21 B demonstrate that the localisation of Tf-488, and by proxy, the recycling pathway was minimally effected by BCA2 overexpression and BCA2 did not colocalise with Tf-488 suggesting that BCA2 does not localise to recycling compartments.

HA-BCA2 transfected MCF-7 cells immunolabelled for HA and stained with rhodmaine phalloidin indicated that BCA2 overexpression did not induce alterations in the actin cytoskeleton (Fig. 4-21 C). There was also no indication of colocalisation between the F-actin and HA-BCA2.

HA-BCA2 did not co-localise with or appear to alter the TGN in transfected MCF-7 cells that were fixed and immunolabelled for TGN46 and HA (Figure 4-21 D).

Mitochondria have numerous cellular functions including generation of ATP and regulation of apoptosis. Alterations in mitochondrial structure can therefore indicate changes in cell proliferation and viability. MitoTracker Red is a probe that accumulates and fluoresces in the mitochondria of viable cells and can be fixed with paraformaldehyde and/or acetone. Because the accumulation of MitoTracker Red depends on the membrane potential of the mitochondria, changes in mitochondrial activity can be visualised in addition to changes in structure. HA-BCA2 overexpressing MCF-7 cells were incubated for 30 min with MitoTracker Red, fixed in 80% acetone and immunofluorescently labelled for HA. The results in Figure 4-21 E demonstrate that overexpressed BCA2 does not co-localise with or alter the structure and activity of the mitochondria in MCF-7 cells.

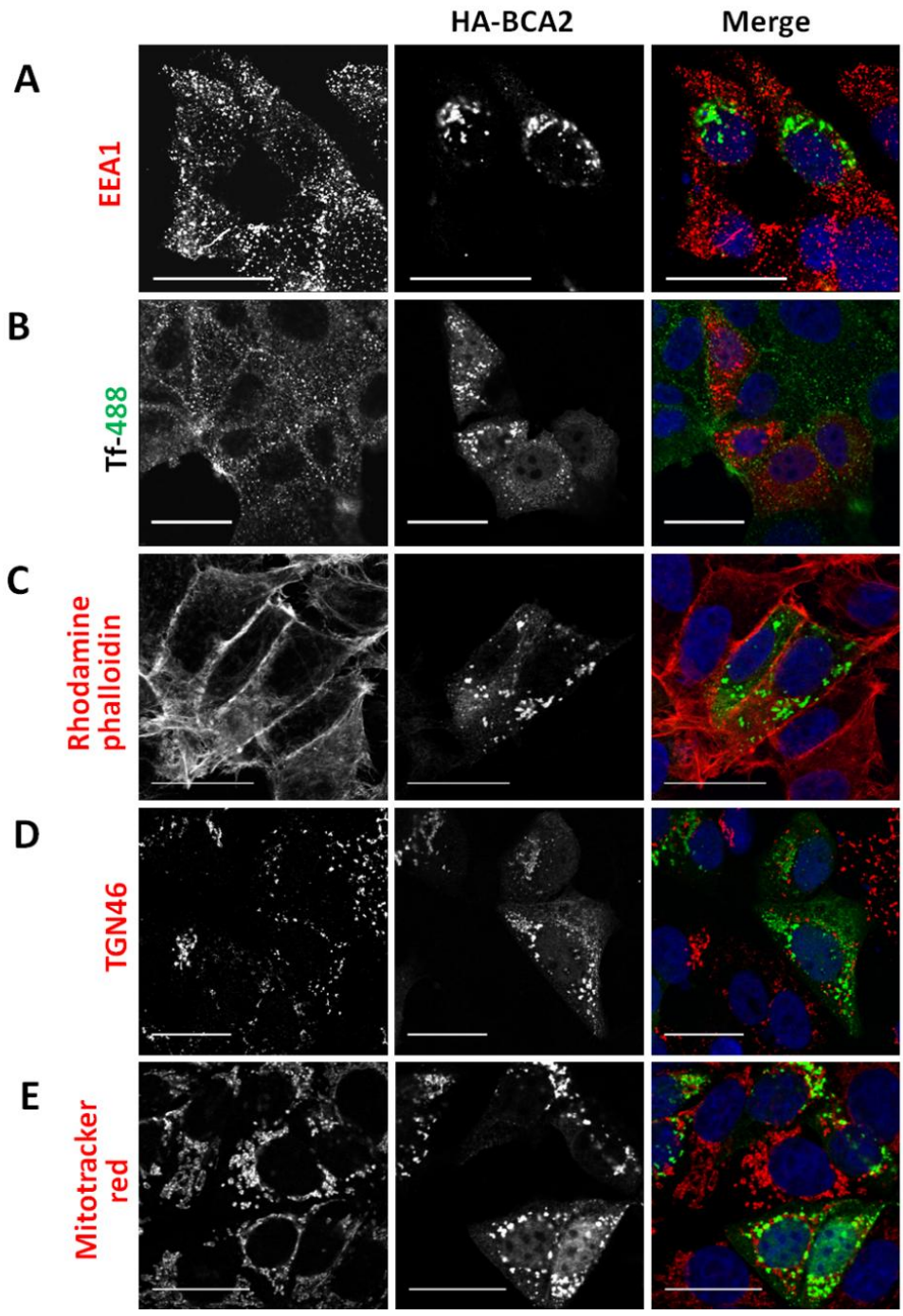

Figure 4-21: In MCF-7 cells HA-BCA2 does not co-localise with, or affect the distribution of A) EEA1, B) transferrin, C) actin D) the TGN or E) the mitochondria. Nuclei were counterstained blue with Hoechst. *Scale bar = 25 µm*

Both the primary antibody used for labelling late endosome/lysosomes (anti-LAMP2) and the anti-HA primary were produced in mice. For the purposes of double-labelling a new antibody (from a non-mouse host species) was therefore purchased against LAMP1. Like LAMP2,

LAMP1 is an integral lysosomal membrane protein that regulates lysosome biogenesis and maintenance of structural integrity (Eskelinen 2006).

An immunolabelling procedure for LAMP1 needed to be designed and optimised before colocalisation analysis with HA-BCA2 could be performed. The fully optimised protocol involved PFA fixation with 0.4% saponin permeabilisation. Primary antibody incubation was performed overnight at 4^{o}C in a humidified chamber. These conditions produced clear immunolabelling with the rabbit anti-LAMP1 antibody (Fig. 4-22). The polar, perinuclear clustering of the LAMP1 positive vesicles is typical of terminal endocytic organelles (Korolchuk *et al.* 2011).

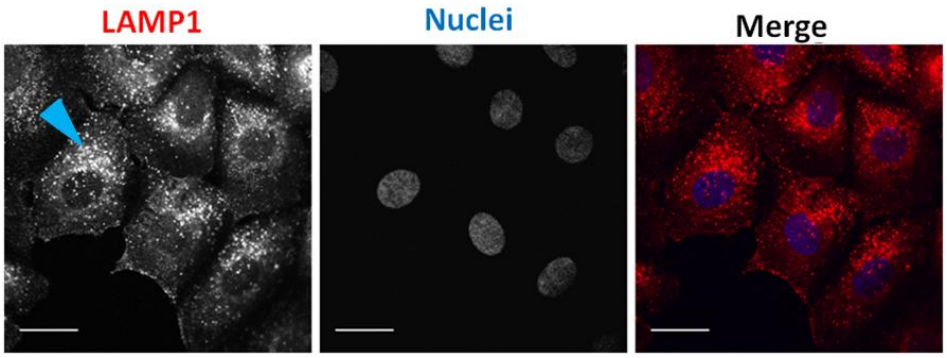

Figure 4-22: Optimised LAMP1 IF in MCF-7 cells. Cells were PFA fixed and IF was performed for LAMP1 (1:100). Nuclei were counterstained with Hoechst. *Arrowheads indicate perinuclear clusters. Scale bar = 25 µm.*

In spite of the of literature that suggests that BCA2 interacts with, and is recruited to the late endosomes by Rab7, double-IF with anti-LAMP1 and anti-HA gave no indication of co-localisation (Fig. 4-23). Also not apparent were any clear and significant effects of HA-BCA2 overexpression on late endosome/lysosome distribution. In some

transfected cells it seemed that there may have been slightly fewer and more sparsely arranged late endocytic organelles but this was by no means a universal trend (Fig. 4-23, bottom row).

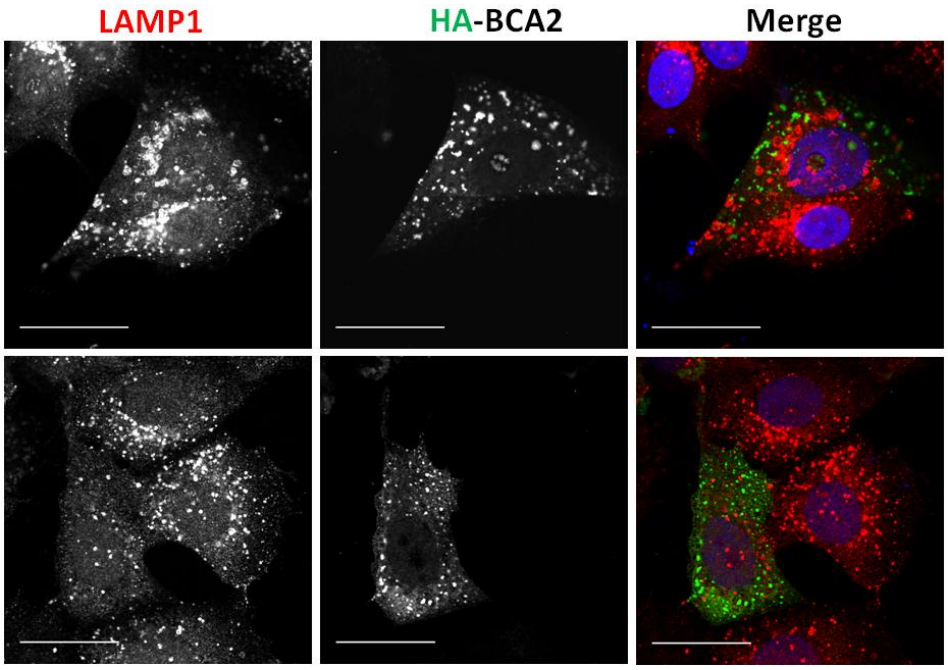

Figure 4-23: LAMP1 labelling in HA-BCA2 transfected MCF-7 Cells. Cells were PFA fixed and sequential IF was performed for LAMP1 (1:100) and HA (Mouse ~HA, Covance, 1:1000). Nuclei were counterstained blue with Hoechst. . *Scale bar = 25 µm.*

The morphology and distribution of some of the larger HA-BCA2 structures resembled that of autophagosomes (Jäger *et al*. 2004). Autophagosomes are large membrane bound organelles containing cell componenents that need to be broken down and recycled into new, essential proteins/structures. Autophagosomes fuse with lysosomes in order utilise their acid hydrolase enzymes to degrade cellular proteins. Autophagosomes often form when a cell is metabolically stressed as the recycling of cell components supports survival. Owing to the morphological similarity between autophagosomes and HA-BCA2 structures, possible co-localisation was investigated by dual-IF with the autophagosome marker LC3B. An assay for autophagy needed to be

developed first in order to validate the anti-LC3B antibody. To achieve this, cells were treated for 6 hrs with 100mM of chloroquine as a positive control for autophagy (Fig. 4-24). Chloroquine has been shown to inhibit lysosome acidification and prevent autophagosome-lysosome fusion, leading to accumulation of LC3B in autophagic vacuoles (Mizushima *et al*. 2010).

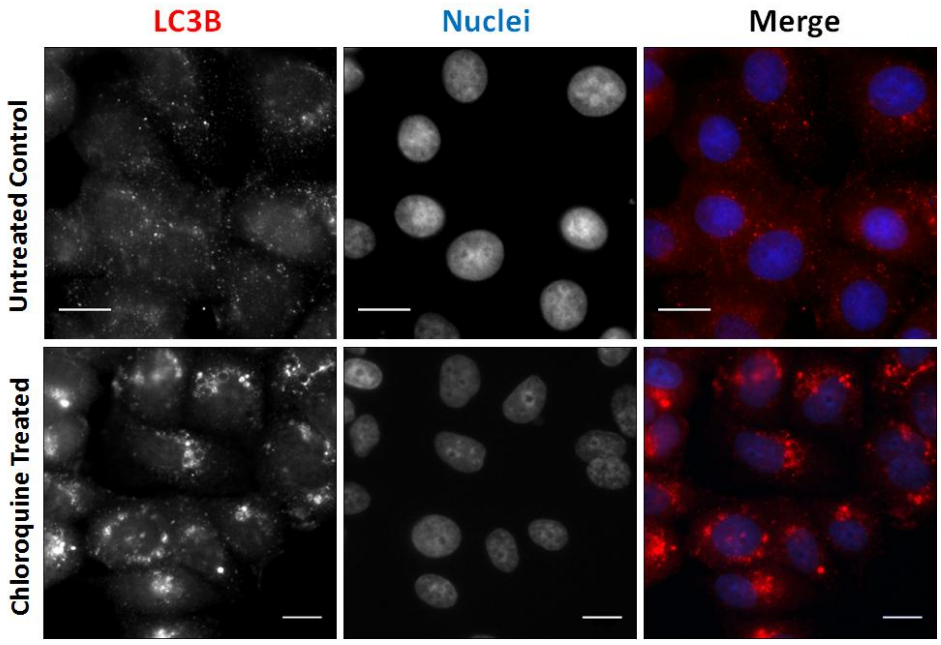

Figure 4-24: LC3B labelling in MCF-7 cells with and without chloroquine treatment to induce autophagy. Cells were treated for 6 hr ± 100 mM chloroquine then PFA fixed and IF for LC3B was performed (Rabbit~LC3B, 1:100). Nuclei were counterstained blue with Hoechst. *Scale bars = 15 µm.*

The results in Figure 4-24 demonstrate that the anti-LC3B antibody could be successfully employed in the detection of autophagy. Small cytoplasmic puncta were observed in the untreated control cells indicating that some autophagomes were present under normal cellular conditions. Chloroquine induced formation of large LC3B positive structures in the cytoplasm that were indicative of autophagic vacuoles.

The successful establishment of this assay allowed HA-BCA2 to be evaluated for possible localisation to autophagosomes and for a role in induction/regulation of autophagy. Double-labelling for LC3B then HA-BCA2 was performed.

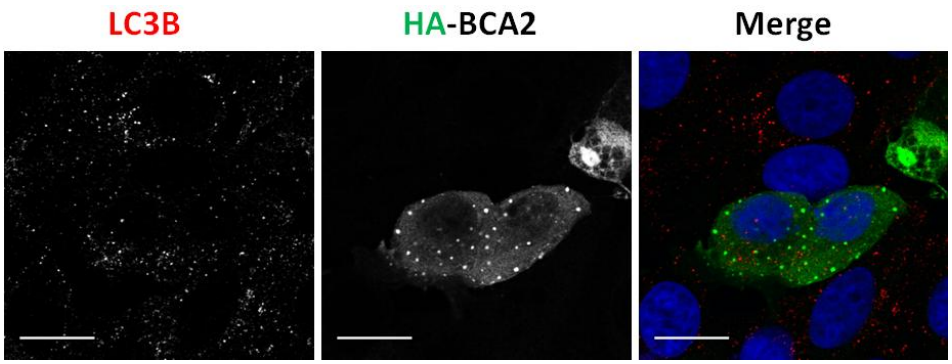

Figure 4-25: LC3B labelling in MCF-7 cells transfected with HA-BCA2. HA-BCA2 transfected cells were fixed with PFA and sequential IF was performed for LC3B (Rabbit~LC3B, 1:100) and HA (Mouse~HA, Covance, 1:1000) *Scale bars = 25 µm.*

The results in Figure 4-25 show that HA-BCA2 did not induce autophagy as no large accumulations of LC3B were detected in the transfected cells. HA-BCA2 also did not appear to suppress the normal autophagic process as transfected and untransfected cells contained similar numbers of the smaller L3CB positive puncta. There was no evidence of HA-BCA2 and LC3B colocalisation.

In order to further explore the documented interaction between HA-BCA2 and Rab7 (Mizuno *et al*. 2003), HA-BCA2 was co-transfected into MCF-7 cells with fluorescently tagged (EGFP) Rab7. As a control the MCF-7 cells were also transfected with HA-BCA2 and EGFP-Rab21. Rab21 is a protein that localises to early endosomes and has been shown to affect endocytosis of EGFR and TfR (Simpson *et al*. 2004). The results of the co-transfections were somewhat inconclusive, although co-localisation between HA-BCA2 and Rab7 was demonstrated; it was by

no means in all of the doubly-transfected cells (Fig. 4-26 A). Surprisingly, co-localisation between HA-BCA2 and Rab21 was also seen in a small number of cells (Fig. 4-26 B). It is unclear whether this is biologically significant, as interaction between BCA2 and Rab21 and early endosome localisation have not been previously reported.

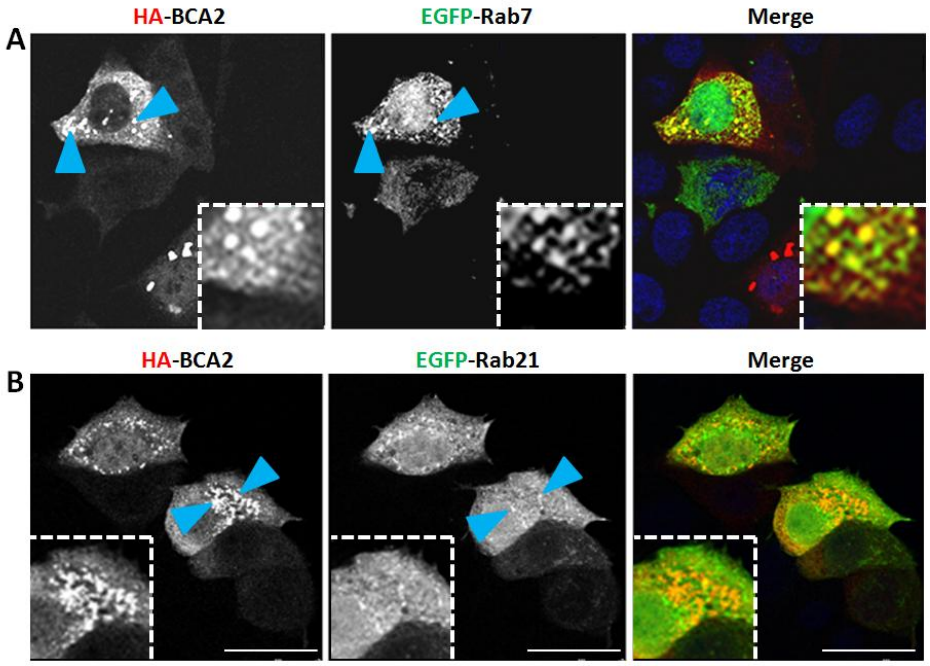

Figure 4-26: HA-BCA2 and EGFP-rab7 and 21 co-transfected MCF-7 cells. Cells were PFA fixed, and immunolabelled for HA (Mouse~HA, Covance, 1:1000). Nuclei were counterstained with Hoechst. *Blue arrowheads indicate co-localisation. Scale bars = 25 µm*

4.5.3 EGFP-tagged BCA2

In order to allow live-cell imaging of BCA2 and to rule out possible effects of the HA tag, BCA2 was subcloned into two EGFP vectors (C1 and N1) that enable *in vitro* expression of N and C terminally tagged proteins respectively. For the vector maps see Appendix E.

Following subcloning and amplification and purification, the EGFP-tagged BCA2 constructs (along with empty EGFP control vectors) were transfected into MCF-7 cells. Transfection was performed using

Lipofectamine 2000 transfection method that was optimised for the EGFP control vectors. Unfortunately the localisation of the EGFP-tagged BCA2 was indistinguishable from that of EGFP alone. EGFP, BCA2-EGFP and EGFP-BCA2 all saturated the cytoplasm and the nucleus of MCF-7 cells (Fig. 4-27).

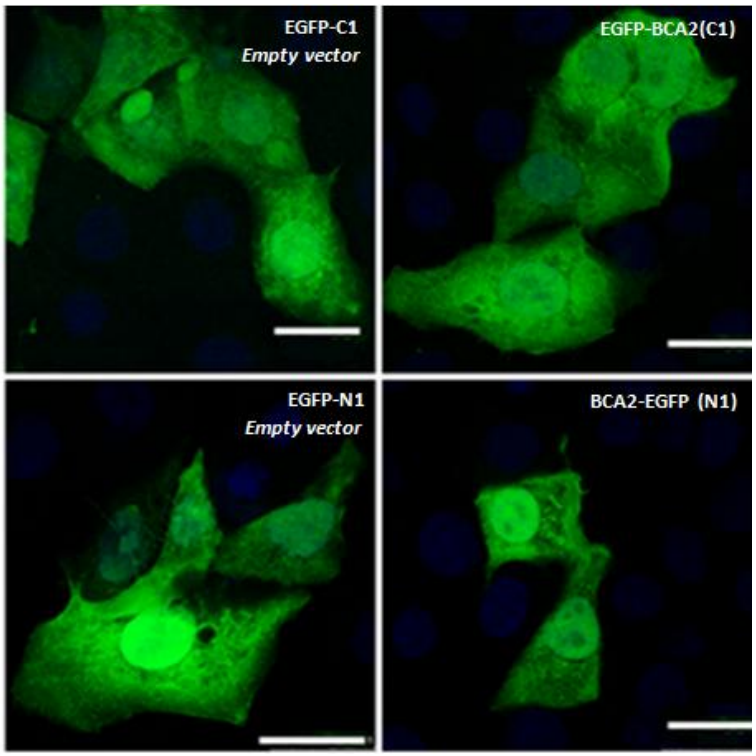

Figure 4-27: EGFP-BCA2 and BCA2-EGFP localisation in MCF-7 breast cancer cells compared with EGFP controls. *Scale bars = 25 µm.*

The transfection efficiency of the EGFP-tagged BCA2 clones was also observed to be markedly lower than the efficiency of the EGFP vectors alone (Fig. 4-28). The transfection efficiency was ~20% for the EGFP-tagged BCA2 clones and ~50% for the EGFP vector alone.

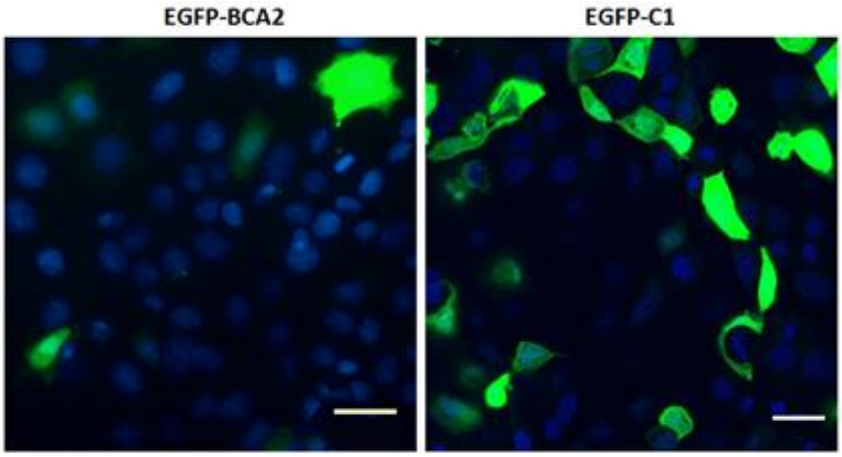

Figure 4-28: Comparison of transfection efficiency between EGFP-BCA2 and EGFP-C1 in MCF-7 cells. *Scale bars = 15 µm.*

Since EGFP fusion proteins can cause the protein of interest to misfold and also because BCA2 is an E3 ligase with known autoubiquitination activity, we thought it possible that the apparent low transfection efficiency was in fact a case of rapid protein degradation. To investigate this possibility, 10 µM of the proteasome inhibitor MG132 was used to treat the transfected cells for 6 hrs. The cells were then fixed, their nuclei stained with Hoechst and after mounting onto glass slides were analysed by fluorescence microscopy (Fig. 4-29) The percentage of transfected cells in the treated and untreated conditions from two independent experiments was determined by cell counting in three fields of view, selected at random (but containing approximately the same number of cells). Proteasome inhibition appeared to increase the average number of BCA2 expressing cells to levels in line with EGFP-vector alone.

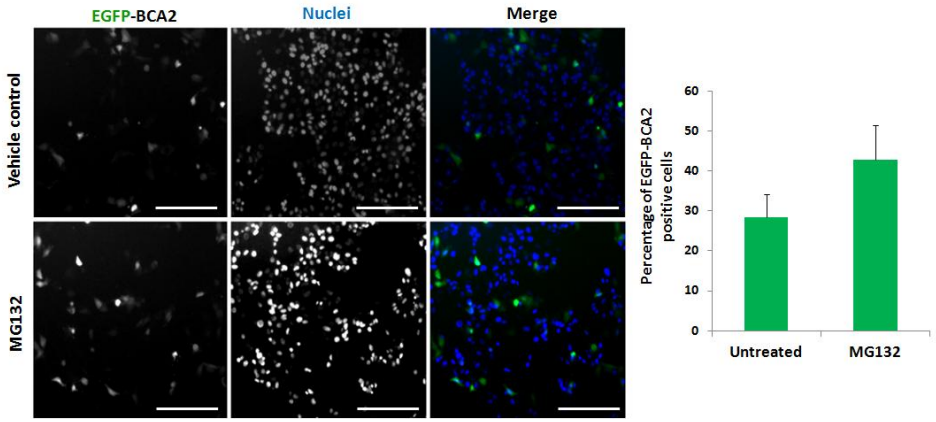

Figure 4-29: Proteasome inhibition with 10 µM MG132 for 6 hr enhances fluorescent expression in EGFP-BCA2 transfected MCF-7 cells. *Scale bars = 25 µm. Error bars represent standard deviation from a single experiment.*

From these results it was initially thought that BCA2 was either ubiquitinating itself, or one of the EGFP lysine residues, thus marking the fusion protein for proteasomal degradation. However, BCA2 could not be detected by Western blotting, indicating that the protein was not being produced. Sequencing data later confirmed this (Fig. 4-30). A frameshift between the BCA2 insert and the EGFP tag caused a 77 amino acid peptide to be attached to the fluorescent protein rather than BCA2. In light of this, the enhanced expression effect by MG132 can be explained in terms of a misfolded, frameshift protein product (fused with EGFP) being degraded by the proteasome. The experimental findings in Figure 4-30 were therefore deemed unrelated to BCA2 function and no further work was performed with the EGFP constructs during the course of this project.

Also revealed by the sequencing data was that within the BCA2 sequence there was a 209A>T point mutation that lead to an H70L amino acid substitution (Fig. 4-30 E). The mutation was detected in forward and

reverse sequencing and was also confirmed to be present in the parental HA-BCA2 plasmid that had been supplied by (Miyakawa *et al.* 2009).

A EGFP-BCA2 (C1) Insert Sequencing: Forward primer

Key

VECTOR
INSERT
BCA2

CCGAGCTGATCGCTAGATCTCGAGCTCAGCTTCGAATTCGGTCGACCGAGATCCGGATGGCGGAGGCTTCGGCGG
ATGGCGGAGGCTTCGGCGG

CCGGGGCGGACTCGGGCGCCGCTGTAGCCGCCCACCGGTTTTTCTGCCACTTTTGCAAGGGCGAGGTCAGCCCCA
CCGGGGCGGACTCGGGCGCCGCTGTAGCCGCCCACCGGTTTTTCTGCCACTTTTGCAAGGGCGAGGTCAGCCCCA

AACTACCGGAATATATATGTCCCAGATGTGAATCAGGCTTTATTGAAGAAGTGACAGATGATTCCAGTTTTTTAG
AACTACCGGAATATATATGTCCCAGATGTGAATCAGGCTTTATTGAAGAAGTGACAGATGATTCCAGTTTTTTAG

GTGGTGGCGGCAGTCGGATAGACAATACCACAACAACACTTTTTGCAGAGCTTTGGGGCCATTTGGATCACACGA
GTGGTGGCGGCAGTCGGATAGACAATACCACAACAACACATTTTGCAGAGCTTTGGGGCCATTTGGATCACACGA

TGTTTTTTCAAGATTTTAGACCCTTTCTAAGTAGCAGTCCACTGGACCAAGATAATAGAGCCAATGAAAGGGGTC
TGTTTTTTCAAGATTTTAGACCCTTTCTAAGTAGCAGTCCACTGGACCAAGATAATAGAGCCAATGAAAGGGGTC

ACCAGACTCACACTGACTTCTGGGGAGCAAGACCTCCACGGTTGCCATTGGGTCGGAGATACAGATCTCGAGGAA
ACCAGACTCACACTGACTTCTGGGGAGCAAGACCTCCACGGTTGCCATTGGGTCGGAGATACAGATCTCGAGGAA

GTTCTCGTCCTGACAGATCTCCAGCTATTGAAGGAATACTACAACACATCTTTGCAGGATTCTTTGCAAATTCTG
GTTCTCGTCCTGACAGATCTCCAGCTATTGAAGGAATACTACAACACATCTTTGCAGGATTCTTTGCAAATTCTG

CCATTCCTGGATCTCCACACCCTTTTTCCTGGAGCGGGATGCTGCACTCCAACCCTGGGGACTATGCCTGGGGTC
CCATTCCTGGATCTCCACACCCTTTTTCCTGGAGCGGGATGCTGCACTCCAACCCTGGGGACTATGCCTGGGGTC

AGACAGGGCTTGATGCCATTGTAACCCAGCTTTTAGGACAACTGGAAAACACAGGCCCTCCCCCAGCTGACAAGG
AGACAGGGCTTGATGCCATTGTAACCCAGCTTTTAGGACAACTGGAAAACACAGGCCCTCCCCCAGCTGACAAGG

AAAAGATCACATCTCTTCCAACAGTGACAGTAACTCAGGAACAAGTTGATATGGGTTTAGAGTGTCCAGTATGCA
AAAAGATCACATCTCTTCCAACAGTGACAGTAACTCAGGAACAAGTTGATATGGGTTTAGAGTGTCCAGTATGCA

AAGAAGATTACACAGTTGAAGAGGAAGTCCGGCAGTTACCTTGCAATCACTTCTTTCACAGCAGTTGTATTGTGC
AAGAAGATTACACAGTTGAAGAGGAAGTCCGGCAGTTACCTTGCAATCACTTCTTTCACAGCAGTTGTATTGTGC

CGTGGCTAGAACTGCATGACACATGTCCTGTATGTAGGA_GAGCTTAA_TGGTGAG_ACTCTACTCGGCAAAGCC
CGTGGCTAGAACTGCATGACACATGTCCTGTATGTAGGAAGAGCTTAAATGGTGAGGACTCTACTCGGCAAAGCC

AGAGCACTGAG_CCTCTGCA_GCA_CAGATTAAGCATTGACAGTCAGCTACATGACGGAATGACTTTCTGAAT
AGAGCACTGAGGCCTCTGCAAGCAACAGATTTAGCAATGACAGTCAGCTACATGACCGATGGACTTTCTGA

CACTAGTGCGCAGGCAATTCCACCGGATCTAGAATAACCTTGGAATTCATAAAC

B EGFP-BCA2 (C1) Insert Sequencing: Reverse primer

Key

VECTOR
INSERT
BCA2

GTGGATCCCGGGCCGCACTAGTGATTCAGAAAGTCCATCGGTCATGTAGCTGACTGTCATTGCTAAATCTGTTGC
TCAGAAAGTCCATCGGTCATGTAGCTGACTGTCATTGCTAAATCTGTTGC

TTGCAGAGGCCTCAGTGCTCTGGCTTTGCCGAGTAGAGTCCTCACCATTTAAGCTCTTCCTACATACAGGACATG
TTGCAGAGGCCTCAGTGCTCTGGCTTTGCCGAGTAGAGTCCTCACCATTTAAGCTCTTCCTACATACAGGACATG

TGTCATGCAGTTCTAGCCACGGCACAATACAACTGCTGTGAAAGAAGTGATTGCAAGGTAACTGCCGGACTTCCT
TGTCATGCAGTTCTAGCCACGGCACAATACAACTGCTGTGAAAGAAGTGATTGCAAGGTAACTGCCGGACTTCCT

CTTCAACTGTGTAATCTTCTTTGCATACTGGACACTCTAAACCCATATCAACTTGTTCCTGAGTTACTGTCACTG
CTTCAACTGTGTAATCTTCTTTGCATACTGGACACTCTAAACCCATATCAACTTGTTCCTGAGTTACTGTCACTG

TTGGAAGAGATGTGATCTTTTCCTTGTCAGCTGGGGGAGGGCCTGTGTTTTCCAGTTGTCCTAAAAGCTGGGTTA
TTGGAAGAGATGTGATCTTTTCCTTGTCAGCTGGGGGAGGGCCTGTGTTTTCCAGTTGTCCTAAAAGCTGGGTTA

CAATGGCATCAAGCCCTGTCTGACCCCAGGCATAGTCCCCAGGGTTGGAGTGCAGCATCCCGCTCCAGGAAAAAG
CAATGGCATCAAGCCCTGTCTGACCCCAGGCATAGTCCCCAGGGTTGGAGTGCAGCATCCCGCTCCAGGAAAAAG

GGTGTGGAGATCCAGGAATGGCAGAATTTGCAAAGAATCCTGCAAAGATGTGTTGTAGTATTCCTTCAATAGCTG
GGTGTGGAGATCCAGGAATGGCAGAATTTGCAAAGAATCCTGCAAAGATGTGTTGTAGTATTCCTTCAATAGCTG

GAGATCTGTCAGGACGAGAACTTCCTCGAGATCTGTATCTCCGACCCAATGGCAACCGTGGAGGTCTTGCTCCCC
GAGATCTGTCAGGACGAGAACTTCCTCGAGATCTGTATCTCCGACCCAATGGCAACCGTGGAGGTCTTGCTCCCC

AGAAGTCAGTGTGAGTCTGGTGACCCCTTTCATTGGCTCTATTATCTTGGTCCAGTGGACTGCTACTTAGAAAGG
AGAAGTCAGTGTGAGTCTGGTGACCCCTTTCATTGGCTCTATTATCTTGGTCCAGTGGACTGCTACTTAGAAAGG

GTCTAAAATCTTGAAAAAACATCGTGTGATCCAAATGGCCCCAAAGCTCTGCAAAAAGTGTTGTTGTGGTATTGT
GTCTAAAATCTTGAAAAAACATCGTGTGATCCAAATGGCCCCAAAGCTCTGCAAAATCTGTTGTTGTGGTATTGT

CTATCCGACTGCCGCCACCACCTAAAAAACTGGAATCATCTGTCACTTCTTCAATAAAGCCTGATTCACATCTGG
CTATCCGACTGCCGCCACCACCTAAAAAACTGGAATCATCTGTCACTTCTTCAATAAAGCCTGATTCACATCTGG

_ACATATATATTCCGGTAGTTTGGGGCTGACCTCGCCCT_GCAAA_GTGGCAGAAAAACCG_TGGACGCTTACGC
GACATATATATTCCGGTAGTTTGGGGCTGACCTCGCCCTTGCAAAAGTGGCAGAAAAACCGGTGGGCGGCTACAG

GA_CGCC_GAGTCCGCCCCGACCGCCGAAGCCTCCGCCAAAT
CGGCGCCCGAGTCCGCCCCGGCCGCCGAAGCCTCCGCCAT

C EGFP-C1 and multiple cloning site (MCS) sequence

EGFP…GAGTTCGTGACCGCCGCCGGGATCACTCTCGGCATGGACGAGCTGTACAAGTCCGGACTCAGATCTCGAG
CTCAAGCTTCGAATTC
EcoR1

D Frameshift mutation leading to aberrant/non-BCA2 translation

```
1   - CTGCTGGAGTTCGTGACCGCCGCCGGGATCACTCTCGGCATGGACGAGCTGTACAAGTCC - 60
1   - L  L  E  F  V  T  A  A  G  I  T  L  G  M  D  E  L  Y  K  S   - 20
61  - GGACTCAGATCTCGAGCTCAAGCTTCGAATTCGGTCGACCGAGATCCGGATGGCGGAGGC - 120
21  - G  L  R  S  R  A  Q  A  S  N  S  V  D  R  D  P  D  G  G  G   - 40
121 - TTCGGCGGCCGGGGCGGACTCGGGCGCCGCTGTAGCCGCCCACCGGTTTTTCTGCCACTT - 180
41  - F  G  G  R  G  G  L  G  R  R  C  S  R  P  P  V  F  L  P  L   - 60
181 - TTGCAAGGGCGAGGTCAGCCCCAAACTACCGGAATATATATGTCCCAGATGTGAATCAGG - 240
61  - L  Q  G  R  G  Q  P  Q  T  T  G  I  Y  M  S  Q  M  *         - 80
```

E **Translated BCA2 amino acid sequence**

Insert
BCA2

M A E A S A A G A D S G A A V A A H R F F C H F C K G E V S P K L P
M A E A S A A G A D S G A A V A A H R F F C H F C K G E V S P K L P

E Y I C P R C E S G F I E E V T D D S S F L G G G G S R I D N T T T
E Y I C P R C E S G F I E E V T D D S S F L G G G G S R I D N T T T

T **L** T A E L W G H L D H T M F F Q D F R P F L S S S P L D Q D N R A
T **H** T A E L W G H L D H T M F F Q D F R P F L S S S P L D Q D N R A

N E R G H Q T H T D F W G A R P P R L P L G R R Y R S R G S S R P D
N E R G H Q T H T D F W G A R P P R L P L G R R Y R S R G S S R P D

R S P A I E G I L Q H I F A G F F A N S A I P G S P H P F S W S G M
R S P A I E G I L Q H I F A G F F A N S A I P G S P H P F S W S G M

L H S N P G D Y A W G Q T G L D A I V T Q L L G Q L E N T G P P P A
L H S N P G D Y A W G Q T G L D A I V T Q L L G Q L E N T G P P P A

D K E K I T S L P T V T V T Q E Q V D M G L E C P V C K E D Y T V E
D K E K I T S L P T V T V T Q E Q V D M G L E C P V C K E D Y T V E

E E V R Q L P C N H F F H S S C I V P W L E L H D T C P V C R K S L
E E V R Q L P C N H F F H S S C I V P W L E L H D T C P V C R K S L

N G E D S T R Q S Q S T E A S A S N R F S N D S Q L H D R W T F Stop
N G E D S T R Q S Q S T E A S A S N R F S N D S Q L H D R W T F Stop

H70L Point mutation

Figure 4-30: Sequencing data demonstrating a reading frame shift between the EGFP tag and the BCA2 insert and point mutation in the BCA2 sequence. A) Forward sequencing and B) reverse sequencing data were combined with the vector sequence information in C) to produce the translational alignment in D) which shows that the BCA2 insert sequence (in red) is out of frame with the EGFP sequence (green). A fusion between EGFP an aberrant peptide is transcribed and translated. E) Translated BCA2 insert amino acid sequence showing H70L substitution mutation.

4.6 Discussion

The MDA-MB-231 cell line represents a highly invasive "triple negative" breast cancer cell type. MDA-MB-231 cells have a mesenchymal-like morphology in culture and the data from the endocytic profiling of these cells appear to reflect their aggressive, mesenchymal characteristics.

The abundance of actin stress fibres in MDA-MB-231 cells may relate to the high migratory and invasive capacity of this cell line. Actin stress fibres are believed to have a role in the generation of the contractile force needed for cell migration (Kreis and Birchmeier 1980; Hotulainen and Lappalainen 2006) and stress fibres are thought to be characteristic

features of migrating mesenchymal cells (Vallenius 2013). The greater abundance of stress fibres in the more motile and invasive MDA-MB-231 cells compared with MCF-7 and MCF-10A cells would seem to support these theories (Fig. 4-1).

Early endosomes are usually found throughout the cell cytoplasm, as seen in the MCF-10A and MCF-7 cells (Fig. 4-1). The perinuclear enrichment of early endosomes seen in the MDA-MB-231 cells is more typical of recycling endosomes (e.g. Fig. 4-6) or late endolysosomes (e.g. Fig. 4-4). The endocytic and broader cellular consequences of this clustered localisation of early endosomes is currently unknown. Clustering of early endosomes (and other endocytic organelles) has been reported as feature of multi-drug resistant myeloid leukaemia cells and in these studies was shown to occur concomitantly with extensive microtubule reorganisation (Jin *et al*. 2008). Figure 4-2 indicates that the microtubule cytoskeleton of the MDA-MB-231 cells was less densely fibrous than nest-like filament networks seen in other cell lines. This supports the idea that cytoskeletal reorganisation may be associated with the development/progression of some breast cancer types.

MDA-MB-231 cells have been shown by some researchers to be unable to degrade EGFR in response to ligand stimulation (Decker 1988; Tsai *et al.* 2012), though it should be noted that this is not a universally reported phenomenon (Sun *et al.* 2013). One explanation for a receptor degradation defect in these cells might be overexpression of EGFR leading to saturation of the lysosomal degradation machinery and redirection of internalised receptors to recycling pathway. An

alternative/supplementary hypothesis is that the capacity and/or activity of recycling pathway of the MDA-MB-231 cells may be enhanced.

To investigate the possible significance of the clustered early endosomes and (possible) receptor degradation defect in MDA-MB-231 cells, a small set of further experiments could be performed. The investigations would comprise pulse-chase experiments with fluorescent EGF and Tf ligands in cells that would subsequently be immunolabelled for different endocytic organelles. By performing these co-localisation experiments and following the progress of the ligands though the endocytic pathways it would be possible to gain a better understanding of the co-ordination of trafficking in the cell line.

The fragmentation of the TGN apparent in the MCF-7 cells in Figure 4-5 has been previously described (Schindler *et al.* 1996; Altan *et al.* 1998). The fragmentation reflects a defect in acidification of a number of intracellular compartments including the TGN and recycling compartments. A functional consequence of this is that MCF-7 cells have enhanced sensitivity to cytotoxic drugs: the cells are less able to sequester cytotoxic compounds in vesicles and so cannot remove them from the cell via the secretory pathway. Reduced recycling capacity may partly explain the low levels of EGFR and absence of TfR from a distinct recycling compartment in this cell line (Fig. 4-6 and 4-7).

The clarity of vesicular LAMP2 labelling produced by the methanol fixation protocol compared with PFA (Fig. 4-3) may relate this fixative's ability to preserve microtubule structure (Wheatley and Wang 1998).

Microtubule disruption has been shown to alter the subcellular localisation and morphology of late endosomes and lysosomes (Reaves *et al.* 1996). However, the lack of vesicular labelling in PFA fixed cells is more likely to be the result of impaired antibody access to the LAMP2 epitope caused by protein cross-linking (Schnell *et al.* 2012). Alternatively, the lack of distinct LAMP2 labelling in PFA fixed cells may be a consequence of Triton X-100 permeabilisation. Triton X-100 induces solubilisation of lipid bilayers, including endosomal membranes, and has been reported to cause extraction of proteins from cells (Jamur and Oliver 2010b). The absence of vesicular LAMP2 labelling in the PFA-fixed/Triton X-100 permeabilised cells may therefore be due to the detergent inducing leaching of LAMP2 protein.

A study by (Nishimura *et al.* 1998) indicated that malignant transformation of MCF-10A cells with a mutant ras potein led to redistribution of lysosomes from the perinuclear region to throughout the cytoplasm of cells. The lysosomal scattering was shown to be a result of reorganisation of the microtubule network. Using LAMP2 immunofluorescence, the late endosomes and lysosomes were slightly more dispersed in the MDA-MB-231 cells than in MCF-7s but contrary to Nishimura *et al.*'s findings the late-endosomes and lysosomes were *more* scattered in the normal MCF-10A cells (Fig. 4-4).

The endocytic profiling data was herein only discussed in the context of cell type rather than BCA2 status as too many other differences between the cells exist for any variance to be attributed to BCA2 effects. Recent publications (Buac *et al.* 2013; Wang *et al.* 2013) and our own data (Fig.

3-4 and 6-4) indicate that in actual fact the difference in BCA2 protein expression between these cell lines is fairly minimal. Differences in disulfiram sensitivity between MDA-MB-231 and MCF-7 cells have been attributed to differences in BCA2 levels (Brahemi *et al.* 2013). However, given the uncertainty of BCA2 expression differences, it may be that DSF activity against breast cancer is dependent on the cellular context of BCA2 expression rather than the level of expression. There are many differences between MCF-7 and MDA-MB-231 cells, as indicated by the endocytic profiles (Figs. 4-1 to 4-7), and there are many reported effects/targets of DSF so it may also be that differences in drug sensitivity are unrelated to or only partly involve BCA2. Other data from this lab suggests that the DSF induced scattering of the lysosomes observed in Figure 4-8 may relate to endolysosomal sequestration of extracellular zinc (Wiggins *et al.* 2015). Sequestration of zinc into endocytic structures was the mechanism proposed for DSF cytotoxicity, though the possible involvement of BCA2 in this was not explored.

During this initial methodological development phase difficulty was experienced in obtaining a validated siRNA and then further difficulties were encountered in achieving adequate (and detectable) BCA2 depletion. These siRNA problems were later resolved for Western blotting (see Chapter 6). Without an efficient siRNA knockdown procedure to fully validate the IF data it was difficult to draw reliable conclusions about the endogenous localisation of BCA2. The most promising localisation would appear to be that produced by the goat anti-BCA2 antibody. This antibody was able to detect and distinguish

elevated BCA2 levels in cells transiently transfected with the HA-tagged protein (Fig. 4-19). When used with a PFA fixation protocol to detect the endogenous protein, the goat anti-BCA2 antibody demonstrated strong cytoplasmic labelling (Fig. 4-10). Some heterogeneity of BCA2 expression levels between cells was evident and a small subpopulation was identified that contained vesicle-like regions of BCA2 enrichment that varied in size. Because these cells did not represent typical examples of BCA2 localisation they were not investigated in detail but may be of interest for future studies.

The results of experiments exploring the subcellular localisation of HA-BCA2 are extremely difficult to interpret. The data itself is clear: HA-BCA2 does not co-localise with actin, with the mitochondria, the TGN, the recycling pathway, early or late endosomes or lysosomes in MCF-7 cells. This poses the question, what are the BCA2 positive structures? Are they membrane bound? Are they aggregates? Transmission electron microscopy could be implemented to answer some of these questions but was beyond the scope of this project. The structures resembled those seen in the subpopulation of MCF-7 cells (Fig. 4-20). The similarity in labelling confers a degree of confidence that the HA-BCA2 structures may not simply be artefacts of transient transfection. The similarity also presents a possible explanation for the subpopulation of MCF-7 cells: that they represent a fraction of high BCA2 expressing cells. It may be that once BCA2 levels exceed a certain threshold, the protein accumulates in the currently unidentified

cytoplasmic structures. This hypothesis was not tested during the course of this project but could be examined as part of future investigations.

Another confounding aspect of the HA-BCA2 overexpression system is why such heterogeneity exists in the localisation of transfected cells. It may be that the different localisation patterns correlate with biological processes e.g. stage of the cell cycle. Culture synchronisation experiments may have been an experimental approach worth exploring to see if a more homogenous localisation pattern could be produced. However, the efficacy and validity of cell synchronisation methods is somewhat controversial (Pirkmajer and Chibalin 2011; Cooper 2004) so in the interests of minimising further confounding factors such approaches were avoided. Stable transfection is an experimental approach that can overcome the problems of heterogeneity produced by transient transfection. Chapter 5 details the process of generating a stable HA-BCA2 expressing cell line as a future tool to try and address the issue of intercellular heterogeneity.

The effect of the HA-tag and the H70L mutation (Fig. 4-30) on BCA2 localisation and function is still uncertain. The HA sequence is very short (9 amino acids) and such a small tag is unlikely to alter BCA2 localisation. However, it is worth noting that the HA tag is translated upstream of the BCA2 insert, such that extra amino acids are also fused to the N-terminus of BCA2; 24 in total. The BCA2 N-terminus is the Rab7 interacting domain so while the fused peptide may be small, it could potentially have functional consequences for BCA2.

The H70L mutation is located in a region with no known structural or functional features but since BCA2s crystal structure has not been solved the impact of the substitution is difficult to predict. The 209A>T point mutation was not listed in a database of single nucleotide polymorphisms (SNPs; http://www.ncbi.nlm.nih.gov/snp). In addition to this a protein sequence alignment performed using the Basic Local Alignment Search Tool (BLAST) revealed that the histidine is conserved (http://blast.ncbi.nlm.nih.gov/Blast). Taken together these facts suggest that the mutation could potentially be significant.

Though not conducted as part of this project, future experiments will be carried out using a sequence-corrected HA-BCA2 construct in order to evaluate possible effects of the point mutation. Further investigations will also explore the possible impact of epitope tagging on BCA2 biology. To this end, the EGFP-BCA2 construct will be subjected to site directed mutagenesis (SDM) to bring BCA2 into frame with the fluorescent tag. A (sequence corrected) HA-BCA2 plasmid will also be modified to encode BCA2 without an epitope tag (see Appendix H).

The apparently cytotoxic effect of overexpressing HA-BCA2 in MDA-MB-231 cells is interesting when compared with the minimal evidence of cytotoxicity seen in the MCF-7 cells (Fig. 4-17 and 4-18). The difference in tolerance of transient HA-BCA2 transfection between the cell lines may reflect context dependency of BCA2 expression. Evidence of context-dependence had been previously suggested by survival analyses (Figs. 3-1 and 3-2) and by conflict in the literature surrounding BCA2's function (Mizuno *et al.* 2003, Sakane *et al.* 2007).

Despite any limitations, the HA-BCA2 co-localisation data with the EGFP-tagged Rab7 and Rab21 proteins was of particular interest due to BCA2's documented effects on EGFR trafficking and interaction with Rab7. BCA2 colocalisation with another Rab protein has not been previously reported and may be a significant finding in terms of the function of the protein or in terms of appropriate experimental approaches for studying BCA2. The relationship between BCA2, EGFR and Rab7 is explored in more detail in Chapter 6.

4.7 References

Altan, N., Chen, Y., Schindler, M. and Simon, S. M. 1998. Defective acidification in human breast tumor cells and implications for chemotherapy. *The Journal of Experimental Medicine* 187(10), p. 1583-98.

Bonifacino, J. S. and Rojas, R. 2006. Retrograde transport from endosomes to the trans-Golgi network. *Nature Reviews Molecular Cell Biology* 7(8), p. 568-79.

Brahemi, G., Kona, F. R., Fiasella, A., Buac, D., Soukupová, J., Brancale, A., Burger, A. M. and Westwell, A. D. 2010. Exploring the structural requirements for inhibition of the ubiquitin E3 ligase breast cancer associated protein 2 (BCA2) as a treatment for breast cancer. *Journal of Medicinal Chemistry* 53(7), p. 2757-65.

Buac, D., Kona, F. R., Seth, A. K. and Dou, Q. P. 2013. Regulation of Metformin Response by Breast Cancer Associated Gene 2. *Neoplasia* 15(12), p. 1379-IN1312.

Buchwalow, I., Samoilova, V., Boecker, W. and Tiemann, M. 2011. Non-specific binding of antibodies in immunohistochemistry: fallacies and facts. *Scientific Reports* 1, p.28

Burger, A. M., Gao, Y., Amemiya, Y., Kahn, H. J., Kitching, R., Yang, Y., Sun, P., Narod, S. A., Hanna, W. M. and Seth, A. K. 2005. A novel RING-type ubiquitin ligase breast cancer-associated gene 2

correlates with outcome in invasive breast cancer. *Cancer Research* 65(22), p. 10401.

Burger, A. M. and Westwell, A. 2011. Anti-cancer therapeutic agents. Google Patents.

Cooper, S. 2004. Is whole-culture synchronization biology's 'perpetual-motion machine'? *TRENDS in Biotechnology* 22(6), pp. 266-269.

Cuervo, A. M. and Dice, J. F. 1996. A receptor for the selective uptake and degradation of proteins by lysosomes. *Science* 273(5274), pp. 501-3.

Decker, S. J. 1988. Epidermal growth factor induces internalization but not degradation of the epidermal growth factor receptor in a human breast cancer cell line. *Journal of Receptors and Signal Transduction* 8(6), p. 853-70.

Eskelinen, E.-L. 2006. Roles of LAMP-1 and LAMP-2 in lysosome biogenesis and autophagy. *Molecular Aspects of Medicine* 27(5), p. 495-502.

Eskelinen, E.-L., Illert, A. L., Tanaka, Y., Schwarzmann, G., Blanz, J., von Figura, K. and Saftig, P. 2002. Role of LAMP-2 in lysosome biogenesis and autophagy. *Molecular Biology of the Cell* 13(9), p. 3355-68.

Hendriks, B.S., Wiley, H.S. and Lauffenburger, D. 2003. HER2-mediated effects on EGFR endosomal sorting: analysis of biophysical mechanisms. *Biophysical Journal* 85(4), p. 2732-45.

Hotulainen, P. and Lappalainen, P. 2006. Stress fibers are generated by two distinct actin assembly mechanisms in motile cells. *The Journal of CellBbiology* 173(3), pp. 383-94.

Huang, Z., Haugland, R. P., You, W. and Haugland, R. P. 1992. Phallotoxin and actin binding assay by fluorescence enhancement. *Analytical biochemistry* 200(1), p. 199-204.

Jamur, M. C. and Oliver, C. 2010a. Cell fixatives for immunostaining.*Immunocytochemical Methods and Protocols*. Springer, p. 55-61.

Jamur, M. C. and Oliver, C. 2010b. Permeabilization of cell membranes.*Immunocytochemical Methods and Protocols*. Springer, p. 63-66.

Jin, J., Pastrello, D., Penning, N. A. and Jones, A. T. 2008. Clustering of endocytic organelles in parental and drug-resistant myeloid leukaemia cell lines lacking centrosomally organised microtubule arrays. *The International Journal of Biochemistry & Cell Biology* 40(10), p. 2240-52.

Jäger, S., Bucci, C., Tanida, I., Ueno, T., Kominami, E., Saftig, P. and Eskelinen, E. L. 2004. Role for Rab7 in maturation of late autophagic vacuoles. *Journal of Cell Science* 117(20), p. 4837.

Kona, F. R., Stark, K., Bisoski, L., Buac, D., Cui, Q. and Dou, Q. P. 2012. Transcriptional activation of breast cancer-associated gene 2 by estrogen receptor. *Breast Cancer Research and Treatment*, p. 1-9.

Korolchuk, V. I., Saiki, S., Lichtenberg, M., Siddiqi, F. H., Roberts, E. A., Imarisio, S., Jahreiss, L., Sarkar, S., Futter, M. and Menzies, F. M. 2011. Lysosomal positioning coordinates cellular nutrient responses. *Nature Cell Biology* 13(4), p. 453-60.

Kreis, T. E. and Birchmeier, W. 1980. Stress fiber sarcomeres of fibroblasts are contractile. *Cell* 22(2), p. 555-61.

Liu, A. P., Aguet, F., Danuser, G. and Schmid, S. L. 2010. Local clustering of transferrin receptors promotes clathrin-coated pit initiation. *The Journal of Cell Biology* 191(7), p. 1381-93.

Longva, K. E., Blystad, F. D., Stang, E., Larsen, A. M., Johannessen, L. E. and Madshus, I. H. 2002. Ubiquitination and proteasomal activity is required for transport of the EGF receptor to inner membranes of multivesicular bodies. *The Journal of Cell Biology* 156(5), p. 843-54.

Matteoni, R. and Kreis, T. E. 1987. Translocation and clustering of endosomes and lysosomes depends on microtubules. *The Journal of Cell Biology* 105(3), p. 1253-65.

Maxfield, F. R. and McGraw, T. E. 2004. Endocytic recycling. *Nature reviews Molecular Cell Biology* 5(2), p. 121-132.

Merrifield, C. J., Feldman, M. E., Wan, L. and Almers, W. 2002. Imaging actin and dynamin recruitment during invagination of single clathrin-coated pits. *Nature Cell Biology* 4(9), p. 691-98.

Merrifield, C. J., Perrais, D. and Zenisek, D. 2005. Coupling between clathrin-coated-pit invagination, cortactin recruitment, and membrane scission observed in live cells. *Cell* 121(4), p. 593-606.

Miyakawa, K., Ryo, A., Murakami, T., Ohba, K., Yamaoka, S., Fukuda, M., Guatelli, J. and Yamamoto, N. 2009. BCA2/Rabring7 promotes tetherin-dependent HIV-1 restriction. *PLoS Pathogens* 5(12), p. e1000700.

Mizuno, K., Kitamura, A. and Sasaki, T. 2003. Rabring7, a novel Rab7 target protein with a RING finger motif. *Molecular Biology of the Cell* 14(9), p. 3741-52.

Mizushima, N., Yoshimori, T. and Levine, B. 2010. Methods in mammalian autophagy research. *Cell* 140(3), p. 313-26.

Mu, F.-T., Callaghan, J. M., Steele-Mortimer, O., Stenmark, H., Parton, R. G., Campbell, P. L., McCluskey, J., Yeo, J.-P., Tock, E. P. and Toh, B.-H. 1995. EEA1, an early endosome-associated protein. EEA1 is a conserved α-helical peripheral membrane protein flanked by cysteine "fingers" and contains a calmodulin-binding IQ motif. *Journal of Biological Chemistry* 270(22), p. 13503-11.

Nishimura, Y., Sameni, M. and Sloane, B. F. 1998. Malignant transformation alters intracellular trafficking of lysosomal cathepsin D in human breast epithelial cells. *Pathology & Oncology Research* 4(4), p. 283-96.

Nityanandam, R. and Serra-Moreno, R. 2014. BCA2/Rabring7 Targets HIV-1 Gag for Lysosomal Degradation in a Tetherin-Independent Manner. *PLoS Pathogens* 10(5), p. e1004151.

Pirkmajer, S. and Chibalin, A.V. 2011. Serum starvation: caveat emptor. *American Journal of Cell Physiology* 301(2), p.202-9.

Press, B., Feng, Y., Hoflack, B. and Wandinger-Ness, A. 1998. Mutant Rab7 causes the accumulation of cathepsin D and cation-independent mannose 6–phosphate receptor in an early endocytic compartment. *The Journal of Cell Biology* 140(5), pp. 1075-89.

Reaves, B. J., Bright, N. A., Mullock, B. M. and Luzio, J. P. 1996. The effect of wortmannin on the localisation of lysosomal type I integral membrane glycoproteins suggests a role for phosphoinositide 3-kinase activity in regulating membrane traffic late in the endocytic pathway. *Journal of Cell Science* 109(4), p. 749-62.

Roepstorff, K., Grandal, M. V., Henriksen, L., Knudsen, S. L. J., Lerdrup, M., Grøvdal, L., Willumsen, B. M. and Van Deurs, B. 2009. Differential effects of EGFR ligands on endocytic sorting of the receptor. *Traffic* 10(8), p. 1115-27.

Rojas, R., van Vlijmen, T., Mardones, G. A., Prabhu, Y., Rojas, A. L., Mohammed, S., Heck, A. J., Raposo, G., van Der Sluijs, P. and Bonifacino, J. S. 2008. Regulation of retromer recruitment to endosomes by sequential action of Rab5 and Rab7. *The Journal of Cell Biology* 183(3), p. 513-26.

Sakane, A., Hatakeyama, S. and Sasaki, T. 2007. Involvement of Rabring7 in EGF receptor degradation as an E3 ligase. *Biochemical and Biophysical Research Bommunications* 357(4), p. 1058-64.

Sangale, Z., Prass, C., Carlson, A., Tikishvili, E., DeGrado, J., Lanchbury, J. and Stone, S. 2011. A robust immunohistochemical assay for detecting PTEN expression in human tumors. *Applied Immunohistochemistry & Molecular Morphology* 19(2), p. 173-83.

Schindler, M., Grabski, S., Hoff, E. and Simon, S. M. 1996. Defective pH regulation of acidic compartments in human breast cancer cells (MCF-7) is normalized in adriamycin-resistant cells (MCF-7adr). *Biochemistry* 35(9), p. 2811-17.

Schnell, U., Dijk, F., Sjollema, K. A. and Giepmans, B. N. 2012. Immunolabeling artifacts and the need for live-cell imaging. *Nature Methods* 9(2), p. 152-58.

Sigismund, S., Argenzio, E., Tosoni, D., Cavallaro, E., Polo, S. and Di Fiore, P. P. 2008. Clathrin-mediated internalization is essential for sustained EGFR signaling but dispensable for degradation. *Developmental Cell* 15(2), p. 209-19.

Simonsen, A., Lippe, R., Christoforidis, S., Gaullier, J.-M., Brech, A., Callaghan, J., Toh, B.-H., Murphy, C., Zerial, M. and Stenmark, H. 1998. EEA1 links PI (3) K function to Rab5 regulation of endosome fusion. *Nature* 394(6692), p. 494-98.

Simpson, J. C., Griffiths, G., Wessling-Resnick, M., Fransen, J. A., Bennett, H. and Jones, A. T. 2004. A role for the small GTPase Rab21 in the early endocytic pathway. *Journal of Cell Science* 117(26), p. 6297-311.

Smith, C. J., Berry, D. M. and McGlade, C. J. 2013. The E3 ubiquitin ligases RNF126 and Rabring7 regulate endosomal sorting of the epidermal growth factor receptor. *Journal of Cell Science* 126(6), p. 1366-80.

Sun, Y., Hedman, A. C., Tan, X., Schill, N. J. and Anderson, R. A. 2013. Endosomal type Iγ PIP 5-kinase controls EGF receptor lysosomal sorting. *Developmental Cell* 25(2), p. 144-55.

Toshima, J. Y., Toshima, J., Kaksonen, M., Martin, A. C., King, D. S. and Drubin, D. G. 2006. Spatial dynamics of receptor-mediated endocytic trafficking in budding yeast revealed by using fluorescent α-factor derivatives. *Proceedings of the National Academy of Sciences* 103(15), p. 5793-98.

Tsai, P.-C., Hsieh, C.-Y., Chiu, C.-C., Wang, C.-K., Chang, L.-S. and Lin, S.-R. 2012. Cardiotoxin III suppresses MDA-MB-231 cell metastasis through the inhibition of EGF/EGFR-mediated signaling pathway. *Toxicon* 60(5), p. 734-43.

Vallenius, T. 2013. Actin stress fibre subtypes in mesenchymal-migrating cells. *Open Biology* 3(6), p. 130001.

van Dam, E. M., ten Broeke, T., Jansen, K., Spijkers, P. and Stoorvogel, W. 2002. Endocytosed transferrin receptors recycle via distinct dynamin and phosphatidylinositol 3-kinase-dependent pathways. *Journal of Biological Chemistry* 277(50), p. 48876-83.

Wang, Z., Nie, Z., Chen, W., Zhou, Z., Kong, Q., Seth, A. K., Liu, R. and Chen, C. 2013. RNF115/BCA2 E3 ubiquitin ligase promotes breast cancer cell proliferation through targeting p21Waf1/Cip1 for ubiquitin-mediated degradation. *Neoplasia* 15(9), p. 1028.

Webber, J. P., Spary, L. K., Sanders, A. J., Chowdhury, R., Jiang, W., Steadman, R., Wymant, J., Jones, A. T., Kynaston, H. and Mason, M. D. 2015. Differentiation of tumour-promoting stromal myofibroblasts by cancer exosomes. *Oncogene*. 34(3):290-302.

Wheatley, S. and Wang, Y. 1998. *Methods in Cell Biology: Animal Cell Culture Methods*. Academic Press (Harcourt Brace & Co.).

Wiggins, H.L., Wymant, J.M., Solfa, F., Hiscox, S.E., Taylor, K.M., Westwell, A.D. and Jones, A.T. 2015. Disulfiram-induced cytotoxicity and endo-lysosomal sequestration of zinc in breast cancer cells. *Biochemical Pharmacology* 93(3), p. 332-42.

Wilcke, M., Johannes, L., Galli, T., Mayau, V., Goud, B. and Salamero, J. 2000. Rab11 regulates the compartmentalization of early endosomes required for efficient transport from early endosomes to the trans-Golgi network. *The Journal of Cell Biology* 151(6), p. 1207-20.

Chapter 5: Generating a stable HA-BCA2 expressing cell line

Transient transfection experiments can be used to generate meaningful data regarding protein function and localisation; however the approach is not without its limitations. One of the potential disadvantages of transient transfection is intercellular heterogeneity of protein expression, as exemplified by HA-BCA2 in Figure 4-18. Heterogeneity in protein expression levels and/or localisation makes biological effect patterns more difficult to identify and can impinge on experimental reproducibility. Another limitation of the approach is that the high levels of overexpression that can be achieved in transiently transfected cells can be many orders of magnitude greater than levels that would occur physiologically (Menke *et al*. 1998). This could lead to misinterpretation of transient overexpression data and potentially undermine the biological relevance of results.

Other drawbacks of transient protein overexpression are limited and/or variable transfection efficiencies which can, respectively, reduce the effect-sizes of results and increase inter-assay variability (Mosser *et al*. 1997). The reagents used in transient transfection have documented side-effects on cell viability and gene expression which in turn could have confounding effects on results and their interpretation (Calvin *et al*. 2006). Technical disadvantages of transient transfection include increased experimental complexity and time/labour intensiveness and the inability to study longer term effects of overexpression.

An experimental approach that can avoid some of the discussed problems with transient transfection is the use of stable cell lines. Stable cells are produced by co-expressing a gene of interest (GOI) with a selectable marker gene for antibiotic resistance. Cells are then cultured under the selection pressure of antibiotic-containing medium. Non-transfected cells succumb to antibiotic toxicity allowing resistant cells to be isolated and propagated. The drug-resistant clones produced by this approach will have all integrated the GOI at random, possibly multiple, genomic loci. Expression levels between clones may therefore vary but should be equal within a clonal population. One potential limitation of the stable cell line approach however arises due the gradual loss of cell differentiation that occurs with increasing passage number (O'Driscoll *et al*. 2006). Parental cells and stable clones overexpressing wild-type or mutant genes may all be affected differently by the passaging process (Arden *et al*. 2007).

In order to overcome some of the main problems observed here with transient HA-BCA2 overexpression, in particular the issue of intercellular heterogeneity, it was decided that a stable cell line would be produced. Cell lines stably overexpressing mutant BCA2 proteins were to be generated alongside the wild-type-overexpressing cells to allow functional comparison of protein domains. If successfully produced the stable cell lines would be a future resource for functional studies complementary to siRNA and transient transfection. Complementary transient and stable transfection experiments in HeLa cells would help to identify possible artefacts intrinsically generated by the separate

approaches. Flp-In™ HeLa S3 parental cells were generously donated by Prof. Michael Clague and Prof. Sylvie Urbé and this enabled the stable cell line development to proceed. The theory and process of stable cell line generation using a Flp-In system is discussed in more detail in section 5.1 which follows.

5.1 Overview of the theory and process of Flp-In stable cell line generation

Flp-FRT recombination strategies offer a further refinement to stable cell line development. The approach allows a GOI to be incorporated into a single genomic integration site which, theoretically, produces clonal, isogenic cell lines (O'Gorman *et al.* 1991). Overexpression with a Flp-In approach is therefore usually more moderate than in transient transfection so results may be more biologically relevant.

Flp-FRT recombination systems require two key components for site-specific recombination to occur (Turan and Bode 2011):

- Flp recombinase - an enzyme with nuclease and ligase activity that mediates homologous recombination of genes between two flippase recognition target (FRT) sites.
- FRT sites: Flp recombinase recognises and binds to two inverted repeat sequences of 13 bp that flank an 8 bp core region of the FRT site. Cleavage occurs upstream of the core (highlighted in red below). The FRT sequence is as follows:

  5'GAAGTTCCTATTC*c*GAAGTTCCTATTC*tctagaaa*G*t*ATAGGAACTTC3'

Flp-FRT mediated recombination allows genes to be introduced at specific sites and its use in stable cell line generation is illustrated later, in Figure 5-1.

The background summary in the paragraph that follows was synthesised from the Life Technologies product information for Flp-In systems along with indicated reference sources. To avoid repetition, the manufacturer's information will not be referenced every time but it should be noted that specific methodological details (vector names, promoters, cell lines etc.) were all based on the Flp-In system product information.

An overview of stable cell generation is shown in Figure 5-1. Flp-In HeLa cells have an Flp Recognition Target (FRT) site inserted downstream of an SV40 promoter and an ATG start codon for a Zeocin resistance gene. The pEF5/FRT/V5-D-TOPO vector contains a hygromycin resistance gene lacking an ATG start codon and promoter sequence. The plasmid also contains a TOPO site into which a GOI can be inserted. The GOI is then under the control of an hEF-1α promoter and an FRT site. The pOG44 plasmid codes for Flp recombinase (Flp). Once the pOG44 and pEF5/FRT/V5-D-TOPO plasmids have been co-transfected into the host Flp-in HeLa cells, Flp recombinase is expressed and mediates homologous recombination between the FRT sites in the genomic DNA and pEF5/FRT/V5-D-TOPO plasmid (O'Gorman *et al.* 1991). The result of this recombination event is that the Hygromycin B resistance gene is inserted into the genomic DNA in frame with the ATG start codon and SV40 promoter. The GOI is also

inserted into the genomic DNA along with its hEF-1α promoter and the Zeocin resistance gene is inactivated. The result of a successful stable transfection is an Hygromycin B resistant, Zeocin-sensitive HeLa cell that expresses the GOI. The process is summarised in Figure 5-1.

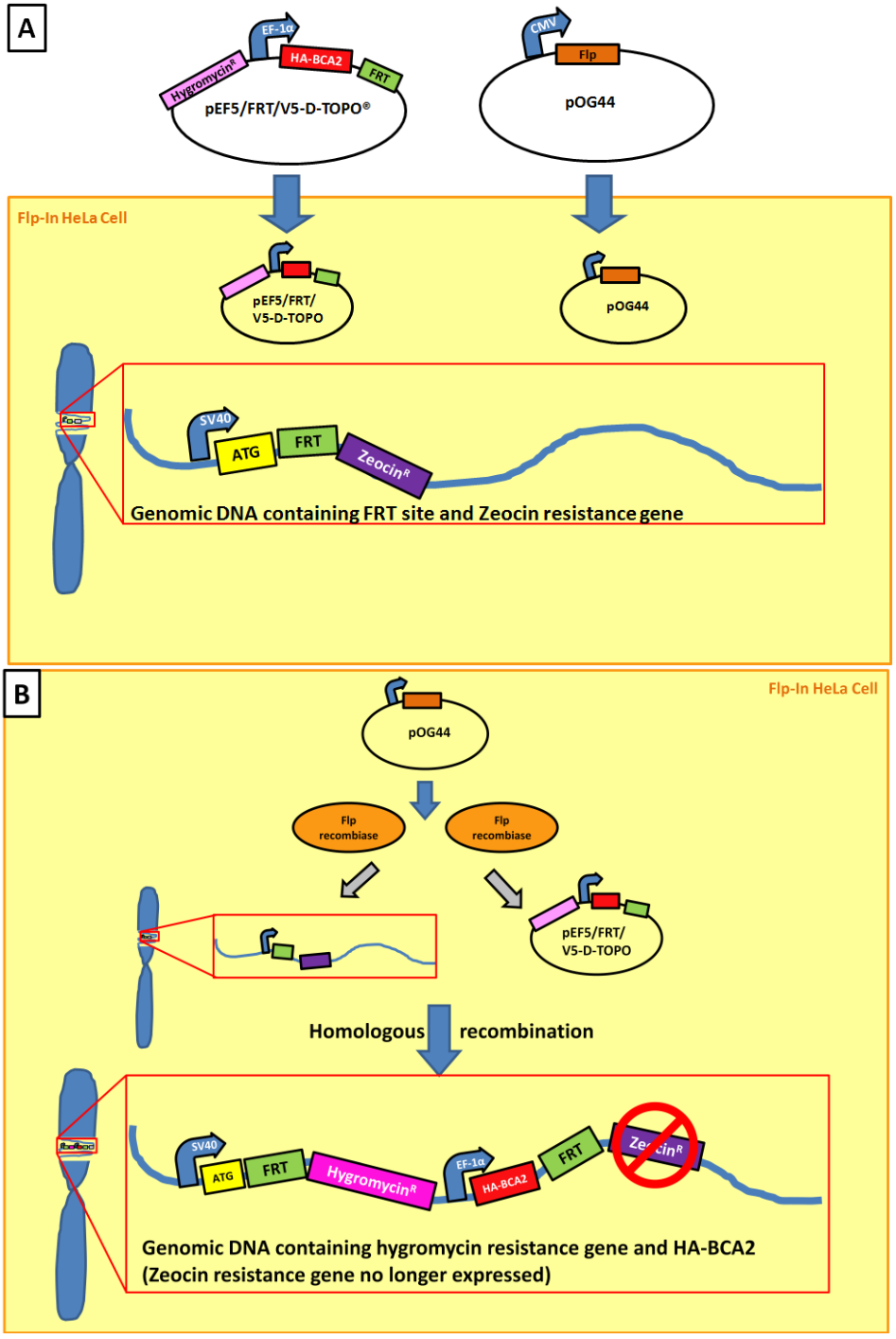

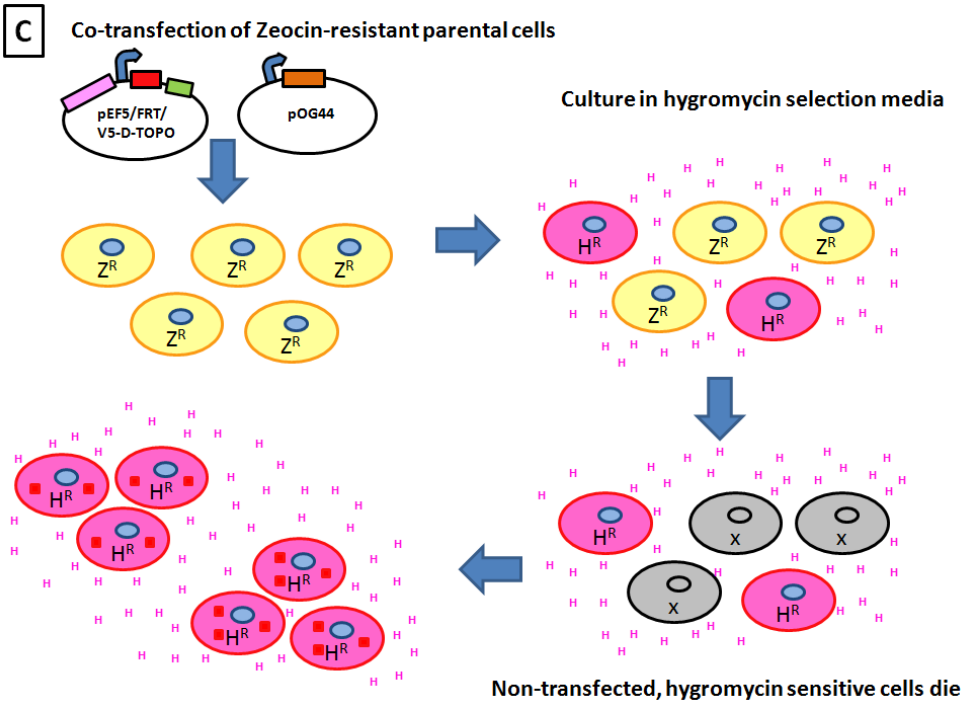

Figure 5-1: Schematic diagrams outlining the principle and process of stable cell generation. A) Demonstrates the FRT site and key adjacent sequence domains in HeLa S3 parental cells. B) Depicts homologous recombination in parental cells following co-transfection with Flp recombinase and GOI construct vectors. C) Summarizes key steps of the selection process following GOI integration.

Prior to stable cell line generation, truncation mutants were designed for BCA2 based on the location domains predicted by HHPred online (http://toolkit.tuebingen.mpg.de/hhpred). pEF5/FRT constructs were produced by designing PCR primers that would to allow wild-type HA-BCA2 ("WT-BCA2"), the zinc finger truncation mutant ("-Zn-BCA2") and RING-H2 mutant ("-RING-BCA2") to be amplified from the parent plasmid. These primers were then used to amplify the wild-type HA-BCA2 and the truncation mutants by PCR. The PCR products were TOPO cloned into the destination pEF5/FRT/V5-D-TOPO vector. The plasmid constructs were then used to transform TOP10 competent cells for amplification and purification. PCR analysis and restriction analysis were performed in order to verify that cloning was successful and that the inserts were correctly orientated in the vector.

5.2 Generating stable cell lines with wild-type HA-BCA2

Due to time constraints only the wild-type HA-BCA2 construct was utilised in the stable cell line development in this project.

Flp-In S3 HeLa cells were transfected with pOG44 (the plasmid coding for Flp recombinase) and wild-type HA-BCA2 plasmid construct (WT-BCA2). After a media change and a total of 24 hours post-transfection incubation, the cells in each well were split 1/6 and replated onto 10 cm dishes. 1/6 splits were also made from a well of untransfected cells to act as negative (i.e. hygromycin sensitive) controls.

5.2.1 Growth and maintenance of cells

Cells were maintained in the hygromycin selection media, which was changed every 3 days till day 18 of the experiment. During media changes the cells were monitored and their progress was documented with low resolution microscopy images, examples of which are shown in Figure 5-2.

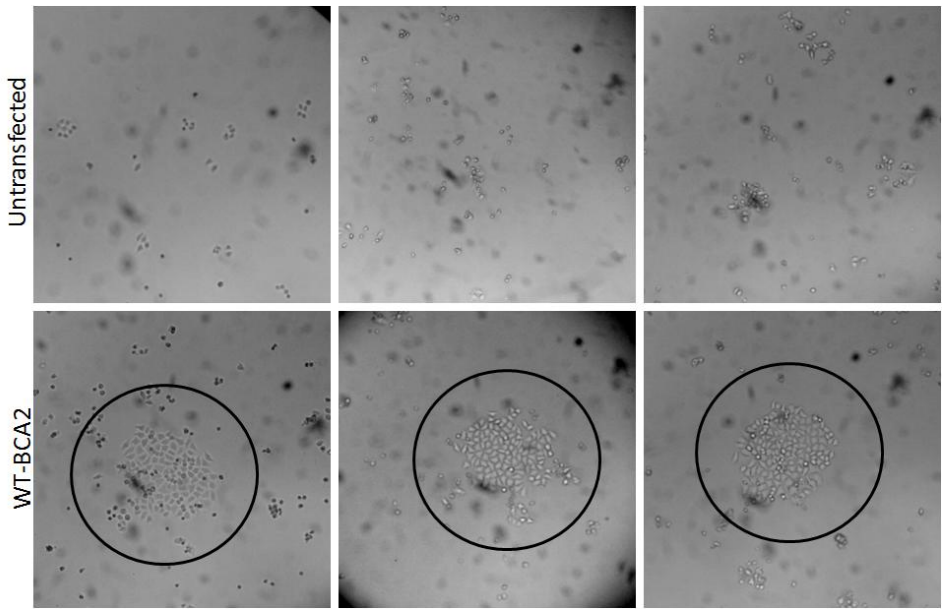

Figure 5-2: Light microscopy images of WT-BCA2 and untransfected/negative control cells taken 9 days after commencing hygromycin selection. Small colonies of hygromycin-resistant clones were only seen in the WT-BCA2 transfected cells and are indicated by circles.

The untransfected control cells showed increasing cytotoxicity and ultimately total cell death between 9 and 12 days of hygromycin treatment. Following a period of extensive cell death in the WT-BCA2 transfected cells, small colonies began forming after ~9-days.

Nineteen days after plating, large colonies had grown in all the transfected dishes and these colonies were then transferred into individual wells for amplification of the cell clones.

5.2.2 Colony picking

Candidate colonies for propagation were identified; those with the largest colony-size and with the greatest separation from neighbouring colonies were selected. Example images of marked colonies and their microscopic appearance are shown in Figure 5-3

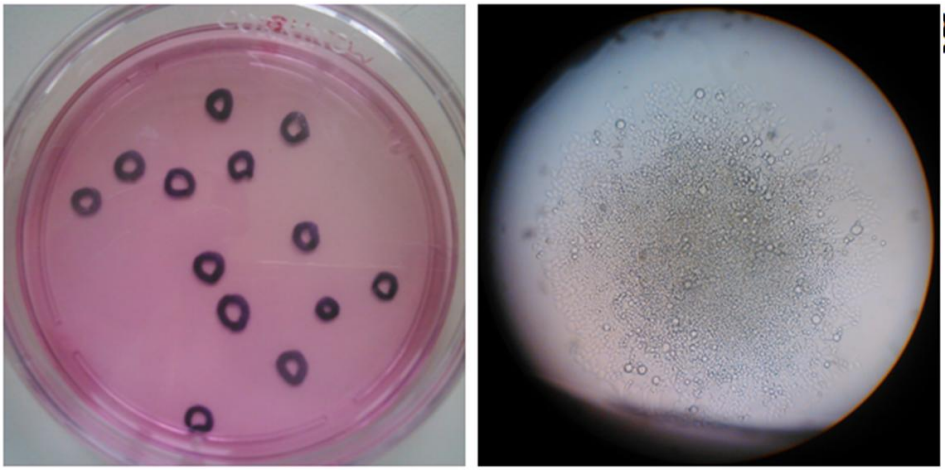

Figure 5-3: Colony picking of stable WT-BCA2 clones. 10 cm dishes with marked colonies are shown on the left and the microscopic appearance of example colonies are shown on the right.

5.2.3 Growth and maintenance of clones

The cells were left to grow in 24 well plates for a week and the media was changed every 2-3 days. After 7 days all the cells that had reached >60% confluency were replated into two wells of 12-well plates. When these cells then became ~70% confluent lysates were collected from one of the wells for expression testing by Western blotting. To maintain the cell population the second of each of the two clone wells was divided into two wells of separate 6-well plates. One of the 6-well plates was then used for creating frozen stocks and one was used for Zeocin sensitivity testing.

5.2.4 Zeocin sensitivity testing

Zeocin sensitivity testing was performed by seeding at low density into 6-well plates. Untransfected HeLa Flp-In S3 cells and normal HeLa cells were also seeded and used as negative control and positive controls for Zeocin sensitivity respectively.

The cells were grown in Zeocin media for one week and the media was changed twice. Zeocin's mechanism of killing is different from hygromycin, the cells do not round-up, rather they exhibit morphological and growth rate changes induced by the drug cleaving DNA. Highly sensitive cells will die after long term exposure.

Clones were classified according to changes in growth rate and morphology. Example images of cells exhibiting hallmarks of each sensitivity classification are shown in Figure 5-4.

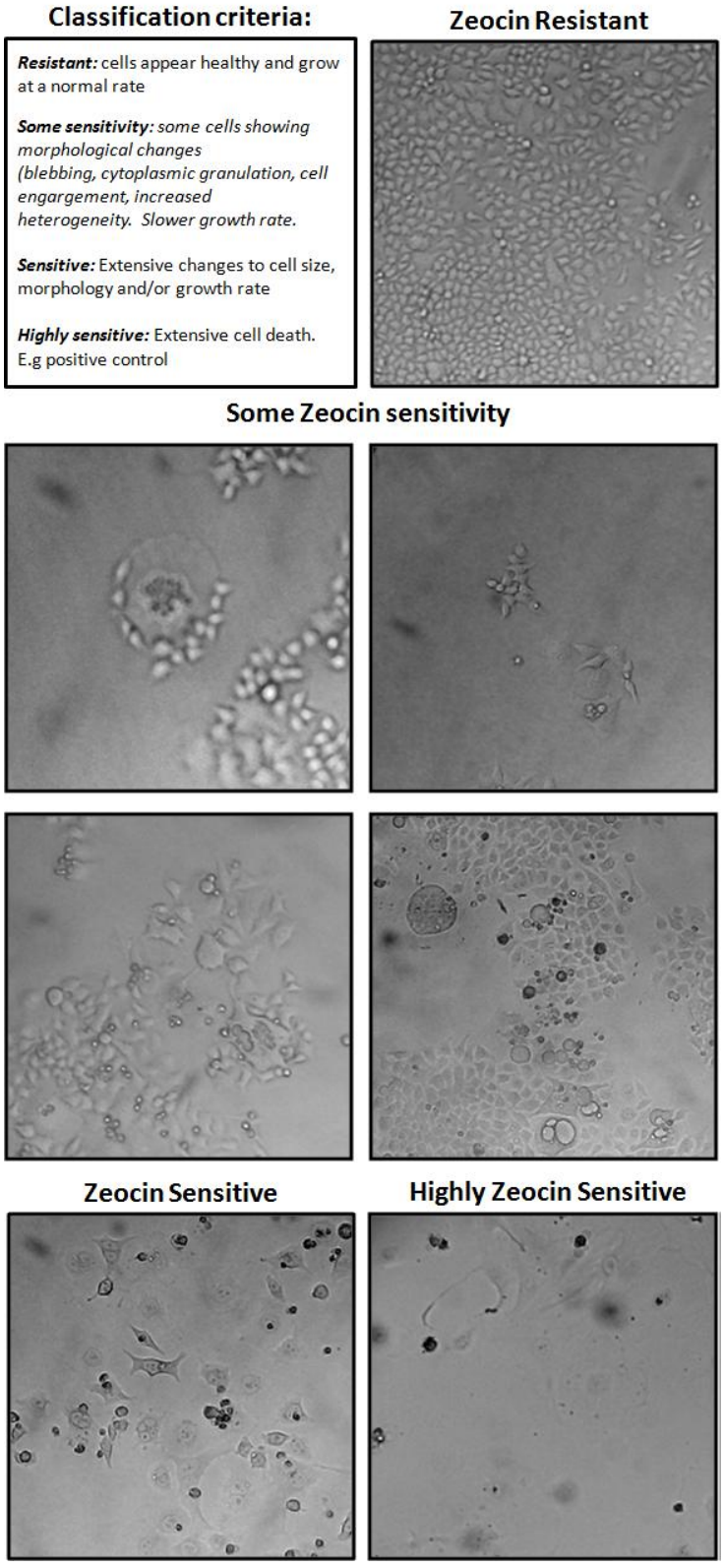

Figure 5-4: Classification criteria and examples of Zeocin sensitivity testing. Example images of WT-BCA2 clones from each classification are shown (except for the "highly sensitive" category which is positive control HeLa cells).

Varying degrees of Zeocin sensitivity were exhibited by the different WT-BCA2 clones. Each of the 78 clones was classified into one of the

Zeocin sensitivity categories and a tally for each of the sensitivity classes was taken. The results are summarized in Figure 5-5.

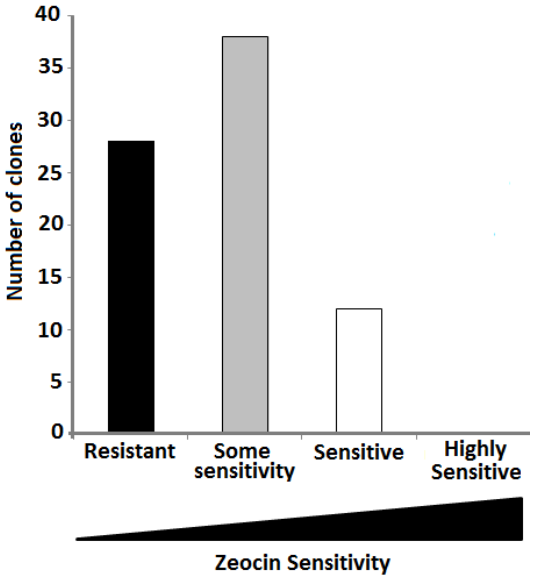

Figure 5-5: Number of clones falling into the different Zeocin sesntivity classes.

The finding that many of the clones were resistant to Zeocin was surprising. The Flp-In system documentation provided by Life Technologies however suggests that this is not uncommon. One possible explanation is a phenomenon called "transcriptional read-through". Transcriptional read through leading to doubly-resistant clones, has been reported previously in FLP-In CHO cells supplied by Life Technologies. In the CHO cells the FRT site is highly transcriptionally active and even after successful integration of an FRT construct the cells can retain Zeocin resistance. In CHO cells Life Technologies confirm that Zeocin sensitivity testing is not sufficiently indicative of successful Flp-In. Since some of the clones did demonstrate Zeocin sensitivity and not all the clones could be maintained, the Zeocin resistant cells were discarded at this stage.

5.3 WT-BCA2 expression analysis by Western blotting

All the Zeocin sensitive clones and a selection of those exhibiting some Zeocin sensitivity were then subjected to Western blotting analysis for WT-BCA2 expression. Lysates of untransfected parental cells and transient HA-BCA2 overexpressing HeLa cells served as negative and positive controls. Immunoblotting for HA was performed according to the protocol described in Section 1.15.3.2. In order to detect the lower protein overexpression levels in stable cells compared with transient transfects, Femto High sensitivity ECL reagent was applied to the immunoblotting membrane. Very low level but positive HA-BCA2 signals were detected in 10 of the clones after 10 min exposure on the Chemidoc imaging system (Fig. 5-6). This was significantly longer than the ~20 s that is usually required for detection in transiently transfected cells, despite ~2.5 x the amount of protein being loaded (50 µg).

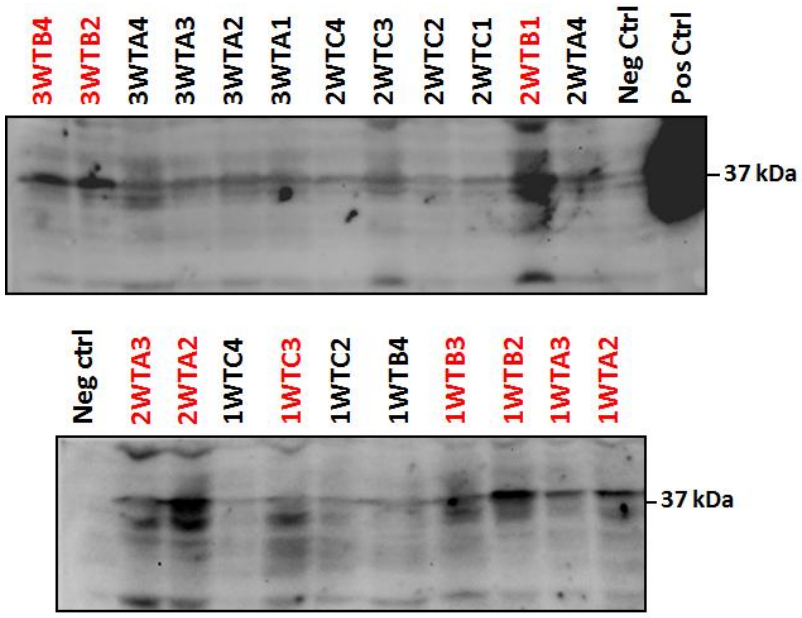

Figure 5-6: Immnuoblotting of WT-BCA2 clones for detection of stably expressed HA-BCA2. Clone nomenclature e.g. 1WTA1 relates to well and plate reference numbers and was simply means of distinguishing between individual clones. Red font indicates clones that were subject to further testing.

Following resurrection from frozen storage the ten clones that indicated positive (though still very low) HA-BCA2 expression were tested to determine whether expression was maintained over time. Lysates were collected after three passages post-resurrection. As previously Western blotting was used to determine HA expression.

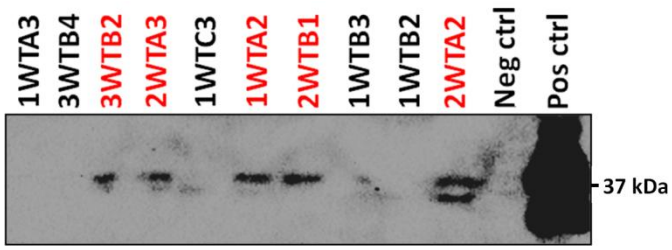

Figure 5-7: Immunoblotting of ten HA-BCA2 positive clones to determine whether HA-BCA2 expression was maintained over time.

Expression appeared to have been lost from five of the clones but was maintained in five others. Further lysates of the clones still expressing HA-BCA2 were taken after another two passages to test for HA-BCA2 expression. EGFR levels were also examined to see if any major differences in expression were apparent in the stable cells (as has been demonstrated with transient transfection in Chapter 5). However, due to the large amount of protein being loaded on the gel the EGFR immunoblotting signal was oversaturated, even with 1 s exposures and so could not be used for reliable quantitative comparison.

The immunoblotting results are shown in Figure 5-8.

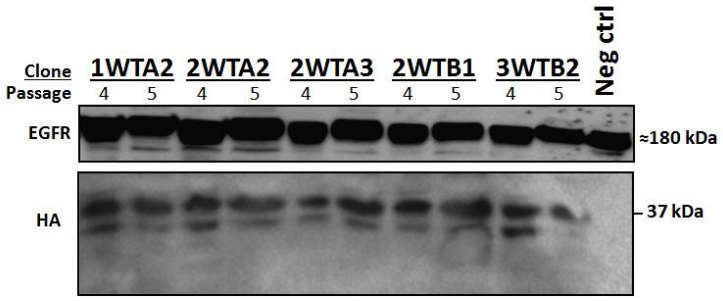

Figure 5-8: Immunoblotting of five HA-BCA2 positive clones at later passages to determine whether HA-BCA2 expression was lost or maintained with time.

HA-BCA2 expression appeared to be maintained in the remaining clones but was still at very low level. Experiments were conducted to try and elucidate and reverse the mechanism responsible for the minimal expression. Prior to this optimisation experiments needed to be carried out such that endogenous BCA2 protein levels could be examined.

5.4 Anti-BCA2 testing for Western blotting

A series of experiments were performed to find the best primary antibody and Western blotting protocol such that BCA2 protein expression could be examined in the clones. BCA2 is a poorly-studied protein so widely-used and/or validated commercial antibodies were not available for use in this project. Three antibodies were tried in the first instance: two polyclonal antibodies, raised in rabbit and in goat (also tested for IF in Chapter 4) and one monoclonal antibody raised in mouse. To test the antibodies, lysates were collected from a selection of cell lines. Included in the small panel of cells tested were cell lines that had been shown to express different levels of BCA2 at the protein level (Brahemi *et al*. 2010; Buac *et al*. 2013; Wang *et al*. 2013) and at the mRNA level (Fig 3-4).

A standard Western blotting protocol was adopted: lysates were separated by SDS-PAGE and transferred to PVDF membranes. The membranes were blocked in 5% milk in PBST for an hour at room temperature then incubated overnight at 4^{o}C with primary antibody diluted 1:250 in 2% milk in PBST. The following day the membranes were washed 3x 5 min in PBST then incubated with HRP-conjugated, species specific secondary antibodies diluted 1:2,000 in 2% milk in PBST for an hour. The membranes were washed thrice in PBST and the protein expression signal was detected by ECL. Figure 1 shows that the three antibodies produced highly varied results in detection of BCA2, a protein with a predicted molecular weight of 34 kDa. The mouse anti-BCA2 antibody failed to detect a signal (Fig. 5-9 A). The rabbit anti-BCA2 antibody (Fig. 5-9 B) did detect a faint band at approximately the right molecular weight (~36 kDa) but the immunoblot was dominated by a strong signal at ~48 kDa. This prominent signal is likely to be non-specific as it showed no variation between cell lines and was not the correct molecular weight. The immunoblot with the goat anti-BCA2 antibody was the most promising (Fig. 5-9 C). Despite high background it was possible to see bands/a large band at around 37 kDa that varied between the cell lines and was strongest in MCF-7s; reported to be high BCA2 expressers (Brahemi *et al*. 2010; Wang *et al*. 2013).

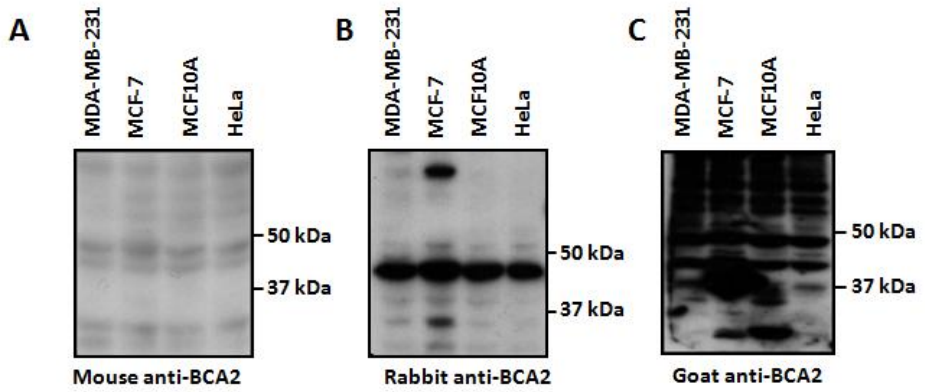

Figure 5-9: Anti-BCA2 primary antibody selection for Western blotting. Lysates of cells thought to express differing levels of BCA2 were separated by SDS-PAGE, transferred to PVDF and immunoblotted for BCA2 using different primary antibodies: A) Mouse anti-BCA2, B) Rabbit anti-BCA2 and C) Goat anti-BCA2.

The goat anti-BCA2 antibody was subjected to further optimisation experiments. Different blocking and antibody diluent solutions were tested: 5% milk and 2% milk were tested as antibody diluents and in one experiment BSA was substituted for milk. In all experiments a lower concentration of primary and secondary antibody was used (1:500 and 1:5,000 respectively). Given the uncertainty surrounding endogenous BCA2 levels, for these experiments some lysates were taken from MCF-7 and HeLa cells that were transiently transfected with HA-BCA2 to ensure different expression levels of the protein between lanes.

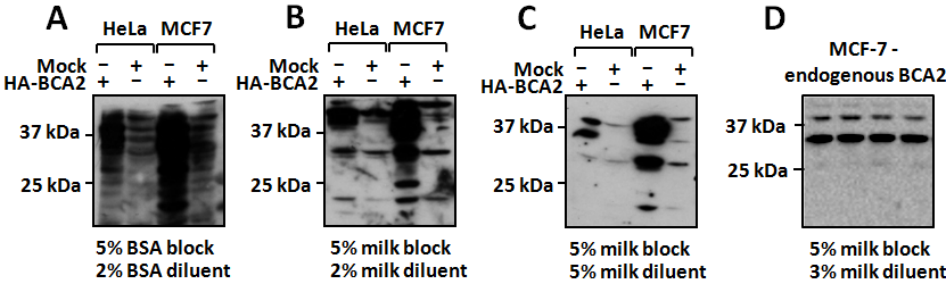

Figure 5-10: Optimisation of the goat anti-BCA2 primary antibody for Western blotting. HeLa and MCF-7 cells were transiently transfected with HA-BCA2 or an empty control vector (Mock). Western blotting for BCA2 was performed using different protocols. A) BSA was used in place of milk in blocking and antibody diluent buffers B) 5% milk blocking solution was used with 2% milk antibody diluent. C) 5% milk was used for both blocking solution and diluent. D) Optimised protocol for MCF-7 endogenous levels (n=4): 5% milk blocking buffer and 3% milk antibody diluent.

The protocol using 5% milk gave the best immunoblotting result for overexpressed BCA2 (Fig. 5-10 C) but a stronger signal was desirable for studying endogenous expression. A protocol was therefore tested wherein the percentage of milk in the antibody diluent was decreased to 3% in order to reduce antigen masking (Fig. 5-10 D). This method gave two strong, defined bands for BCA2 in MCF-7 cells and was therefore adopted for further experiments studying endogenous protein levels.

5.5 Investigating multiple BCA2 immunoblotting bands

Immunoblots of BCA2 demonstrate that both endogenous and overexpressed BCA2 form multiple bands following separation by SDS-PAGE, most frequently the protein appears as a doublet. This has been seen multiple times in the literature (Miyakawa *et al.* 2009; Bacopulos *et al.* 2012; Smith *et al*. 2013) but the phenomenon has not been fully explained.

Splice variants were ruled out as a source of the multiple BCA2 bands since they are present in both endogenous cells and those transiently overexpressing BCA2 (Fig. 5-10). It is also worth noting that in HA-BCA2 overexpressing cells multiple bands can also be detected with an anti-HA antibody (Fig. 5-6).

Reviewer's comments and the authors' responses to the 2012 paper by Bacopulos *et al.* are available to view online and in them the multiple BCA2 bands are discussed (http://www.biomedcentral.com/1471-2407/12/63/prepub). The authors attributed the two BCA2 bands seen by Western blotting to incomplete denaturation of the strong secondary

and tertiary structures of the protein's RING-H2 domain. Supporting this hypothesis was evidence that in immunoblots of cell lysates transfected with RING-H2 mutant (that could not form secondary structures) BCA2 only appeared as a single band (Bacopulos *et al*. 2012).

Experiments were conducted in order to determine whether the multiple BCA2 bands were the result of a failure of the RING-H2 domain to fully denature. Lysates of MCF-7 cells were collected, prepared and electrophoretically separated on a 12% acrylamide gel. A variety of gel and sample conditions were tested: reducing and non-reducing, denaturing and native. Table 5-1 summarises the experimental adjustments necessary to create the different Western blotting conditions:

Table 5-1: SDS and DTT requirements for buffers and gels to produce different Western blotting conditions

Conditions	SDS	DTT
Reducing, denaturing	✓	✓
Reducing, native	×	✓
Non-reducing, denaturing	✓	×
Non-reducing, native	×	×

Following separation, the proteins were transferred to PDVF membranes and immunoblotted for BCA2 (Fig. 5-11).

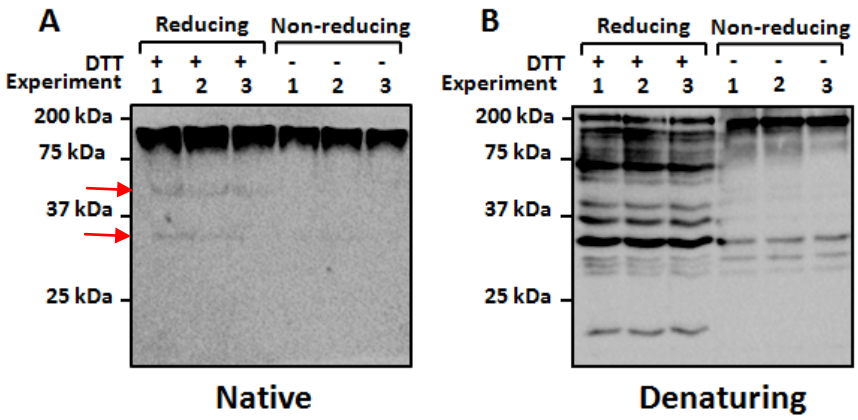

Figure 5-11: Immunoblots of endogenous BCA2 expression in MCF-7 cells under different Western blotting conditions. Cell lysates were prepared in reducing and non-reducing sample buffer and separated by electrophoresis on A) a native acrylamide gel and B) a denaturing acrylamide gel. After transfer to PVDF membrane separated proteins were subject to BCA2 immunoblotting. *Red arrows indicate faint bands.*

The immunoblots for BCA2 on lysates separated under native PAGE conditions (Fig. 5-11 A) feature a strong band at the top of the gel ~180 kDa. This suggests that in native conditions, BCA2 may be unable to move into the acrylamide gel. In the reducing conditions a faint band was visible at ~34 kDa and another at ~42 kDa. Under denaturing, reducing conditions (Fig. 5-11 B) the BCA2 immunoblotting signal appeared as multiple bands. On a 12% gel the doublet at 37 and 34 kDa was resolved into a triplet at 37, 39 and 34 kDa. Other heavier and rather smeared bands were also apparent at ~75, ~180 and ~200 kDa in these Western blotting conditions. The heavier bands were indicative of ubiquitinated BCA2 and have been previously reported in the literature (Burger *et al*. 2005). Under denaturing, non-reducing conditions, multiple BCA2 bands were again apparent in the immunoblot; the strongest signals in these conditions appearing at 34 and ~200 kDa.

For the purposes of further studies, both bands of the BCA2 doublet at ~37 and ~34 kDa were used to evaluate protein expression. This was in

light of data showing that both bands appeared in the immunoblots of cells transiently transfected with HA-BCA2 (Fig. 5-10 C). In some experiments the bands did not separate into doublet and in these instances the large unresolved band was shown for BCA2.

Once the BCA2 immunoblotting protocol had been developed, the endogenous BCA2 in the stable cell lines could be examined to provide more information about the low protein expression in the stable HA-BCA2 clones. Experiments were therefore conducted to attempt to enhance/restore BCA2 levels with pharmacological manipulation.

5.6 Investigating low BCA2 expression in the stable HA-BCA2 expressing clones

Transcriptional repression is known to be a potential pitfall in stable cell line generation (communication: S. Urbé, Liverpool University) and is referred to in the Life Technologies guide to mammalian expression systems. Epigenetic modifications that impair access of the transcription machinery to target DNA sequences are natural biological mechanisms for modulating gene transcription. Promoter methylation and histone acetylation are two such epigenetic modifications that are important in transcriptional control (Grassi *et al*. 2003). Methylation of cytosine nucleotides in promoter CpG islands (adjacent cyotsine and guanine bases) represses transcription of downstream genes (Robertson 2001). Acetylation of lysine residues in histone proteins reduces their affinity for DNA. This chromatin remodelling exposes more DNA to the transcription machinery and consequently enhances transcription. Histone deacetylases catalyse the removal of acetyl groups from histone

proteins and the resulting changes to chromatin structure reduce gene transcription (Marks *et al.* 2001). Silencing of the CMV promoter following exogenous introduction to mammalian cells, including HeLa, has been widely reported (Guo *et al*. 1996; Löser *et al*. 1998; Grassi *et al.* 2003). The Flp-In system utilises an EF-1A promoter for GOI expression and an SV40 promoter for expression of the hygromycin resistance gene (Fig. 5-1B). It is therefore possible that through specific epigenetic modification of the EF-1A promoter, stable clones could retain drug-resistance while reducing expression of the GOI. The EF-1A promoter has more CpG islands than the CMV promoter (Alméciga-Díaz *et al.* 2009) and therefore has more potential methylation sites. The EF-1A promoter has also been shown to be susceptible to silencing in cultured cells (Norrman *et al*. 2010). Promoter silencing can be prevented/minimised by compounds that inhibit DNA methylation, such as 5-azacytidine, and by inhibitors of histone decetylation such as butyric acid (Boffa *et al*. 1978; Escher *et al*. 2005).

BCA2 has been shown to regulate its own protein levels through autoubiquination (Amemiya *et al.* 2008). Another possible reason for low expression levels was therefore proteasomal degradation. To elucidate whether promoter silencing or proteasomal degradation were responsible for the low BCA2 expression levels, a number of inhibitor investigations were performed. One of the stable WT-BCA2 clones was selected for experimentation which was performed in 5-well plates. Cells were treated with 5-azacytidine or butyric acid for 48 hr or with the proteasome inhibitor MG132 for 8 hr. Prior to lysate collection the cells

were imaged by phase contrast microscopy on a Leica wide-field system. Western blotting for HA and for BCA2 was then performed and the results of the experiments are shown in Figure 5-12.

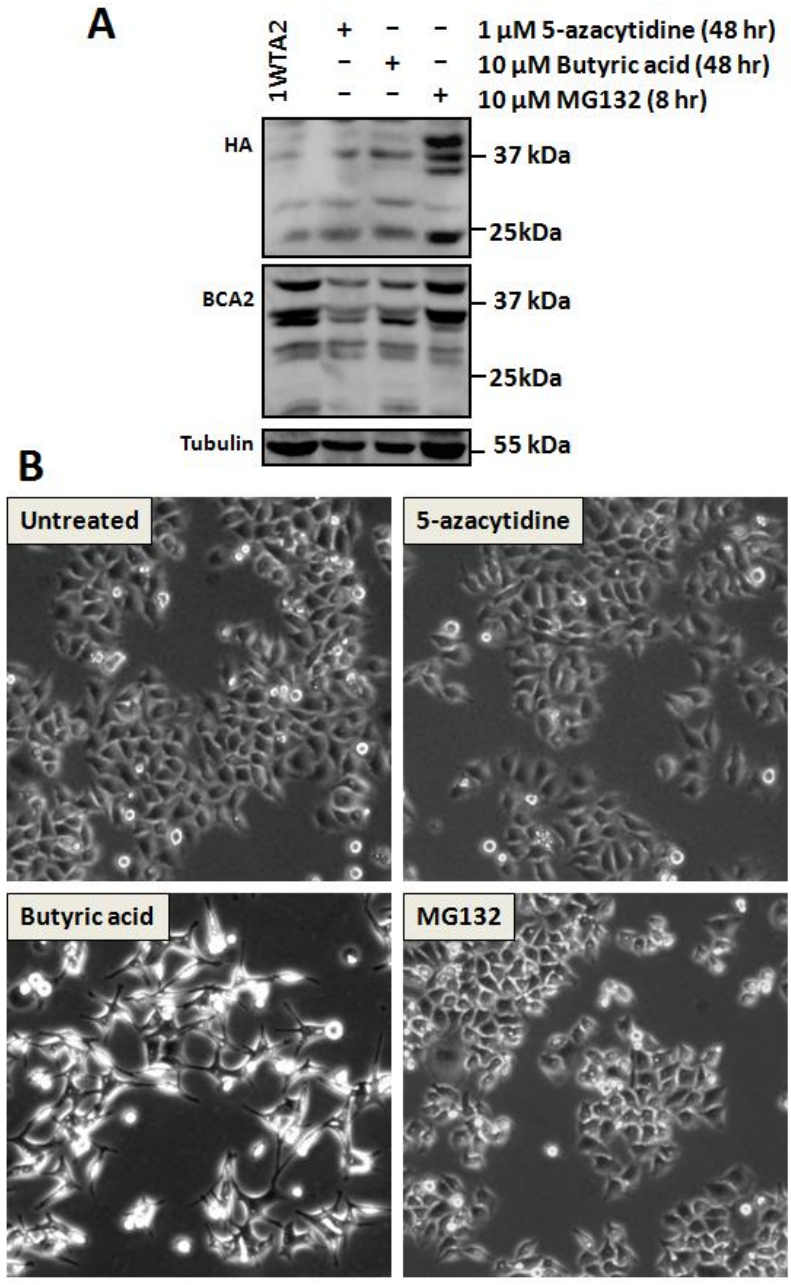

Figure 5-12: Immunoblotting and DIC microscopy images of stable WT-BCA2 cells treated with DNA-methylation, histone deacetylase and proteasome inhibitors. Cells were treated for 48 hours with either 5-azacytidine or butyric acid or for 8 hours with MG132. A) HA-BCA2 expression was measured by Western blotting after cells were imaged by DIC microscopy (B).

The HA-immunoblot confirmed low BCA2 expression in the stable clone 1WTA2 (Fig. 5-12 A). BCA2 was strongly detected but this is due to the

necessarily heavy sample loading (to detect HA) rather than due to high levels of BCA2 expression. Figure 5-12 A also shows that treatment of the WT-BCA2 clone with 5-azacytidine or butyric acid did not appear to significantly increase HA-BCA2 expression. This suggested that promoter repression was either not responsible for the low HA-BCA2 levels or that promoter silencing could not be adequately reversed by these treatments. The unusual, spiculated morphology of the cells following butyric acid treatment (Fig. 5-12 B) has been previously reported for other cell lines (Prasad and Sinha 1976). The morphological changes are thought to be due to the incorporation of the butyric acid into the lipid component of the plasma membrane altering its configuration and thereby changing cell morphology. These morphological changes seen with butyric acid were not therefore attributable to a BCA2-mediated effect. MG132 treatment increased the level of HA-BCA2 but had no effect on total BCA2 levels.

5.7 Discussion

The attempt to generate a stable BCA2 overexpressing cell line was both a failure and a success. Stable clones expressing BCA2 were indeed generated but were of limited value for further work due to the extremely low level at which BCA2 was expressed (Fig. 5-6). Large amounts of protein (50 µg) were required for positive detection by Western blotting and needed to be coupled with high-sensitivity ECL reagent with and long exposure times for signal detection. Because of these procedural requirements, the immunoblots that were produced had low signal to

noise ratios which made experiments difficult to perform and results difficult to analyse.

Exploring the reasons for the low expression levels in light of other data presented in previous chapters and in the context of BCA2 literature does provide some insights into BCA2 regulation. The significance of different experimental approaches in BCA2 also becomes more apparent.

Difficulties in stable cell line generation have been reported for proteins, such as transcription factors, where overexpression has cytotoxic effects. In the case of some transcription factors, overexpression leads to aberrant and ultimately fatal expression of their regulated genes (Wu and Chiang 1996). If BCA2 overexpression impinges on cell viability, which is suggested by IF in the cell context of MDA-MB-231 cells (Fig. 4-18), this may help to explain the failure of the clones to express high BCA2 levels. Perhaps HA-BCA2 stable cells represent a self-limiting system with higher expressing clones dying due to growth inhibition and thus only the lowest expressing cells surviving long enough to be tested. For potentially cytotoxic proteins, inducible expression approaches, such as the tetracycline controlled transcriptional activation (Tet-On/Tet-Off) systems, can be used. Such an approach may be useful for future BCA2 studies.

Typically for an E3 ligase, BCA2 is thought to regulate its own stability via autoubiquitination. One study has shown that an intact RING-H2 domain and ubiquitin binding sites are required for overexpressed BCA2 to accumulate upon proteasome inhibition (Amemiya *et al.* 2008). A cyclohexamide time course experiment in which endogenous BCA2

levels were monitored in MCF-7 cells suggested a protein half-life of between 6 and 12 hours (Kona *et al.* 2012). In an experiment where overexpressed, GST-BCA2 was examined in HEK293 cells however the half life appears to be much shorter (Bacopulos *et al.* 2012). Data presented in this paper show the relative level of GST-BCA2 falls from 1 to 0.39 in 6 hours. These numbers can be used to estimate BCA2 half-life using the following equation: $T1/2 = t * \ln(2)/\ln(P1/P2)$. Where P1 is the starting amount of protein (1), P2 is the final amount of protein (0.39) and t is the time interval (6). This gives an estimate half life of 1.62 hours ~ 96 minutes.

The apparent disparity in half life between endogenous and overexpressed BCA2 (Bacopulos *et al*. 2012; Kona *et al*. 2012) may relate to differences in proteasome function between the cell lines in which the experiments were conducted. However the variation in turnover rate may reflect differences in the way that epitope tagged and/or overexpressed BCA2 behaves within the cell, compared with the endogenous protein.

The average half-life of a protein is 46 hours (Schwanhäusser *et al*. 2011) so whether endogenous or overexpressed half-lives are considered, BCA2 has a high protein turnover rate. Rapid protein turnover may explain why such low levels of HA-BCA2 expression were achieved in the stable cell line (Fig. 5-6) and why proteasome inhibition was able to increase the expression (Fig. 5-12 A). The fact that total BCA2 protein levels (endogenous plus HA-BCA2) were not increased by proteasome inhibition suggests that BCA2 levels are tightly regulated.

It has been shown that proteins that have an increased tendency to aggregate have faster degradation rates (De Baets *et al.* 2011). It may be that BCA2 has a high propensity to aggregate and this is what necessitates strict control of protein levels. This is supported by confocal microscopy images showing large accumulations HA-BCA2 in transiently transfected cells (Fig. 4-17 and 4-18) and by various publications that demonstrate similar patterns of intracellular localisation upon overexpression (Mizuno *et al*. 2003; Miyakawa *et al*. 2009; Nityanandam and Serra-Moreno 2014).

So called "sticky" proteins tend to form aggregates when expressed in recombinant form and can give rise to false identification of interaction partners (Feller and Lewitzky 2012). BCA2 has been linked to a large number of proteins with very disparate functions and localisations: from Rab7 sorting at the late endosomes to c-myc in the nucleus to tetherin in plasma membrane microdomains (Miyakawa *et al*. 2009; Bacopulos *et al.* 2012; Narita *et al*. 2012). The majority of these interactions have been identified through fusion protein overexpression methods, predominantly yeast-two-hybrid and co-immunoprecipitation. Many proteins do have diverse functions and localisations but the large number and diversity of purported BCA2 binding partners may be indicative of artefacts generated by "stickiness".

In light of the findings presented in this chapter, it appears that stable overexpression systems may not be the most appropriate method for gathering meaningful data about BCA2 function. However, BCA2 stability has been shown to be regulated by other proteins. HR23a, for

example, has been shown to inhibit UbcH5 mediated poly-ubiquitination of BCA2 which prevents its proteasomal degradation (Bacopulos *et al.* 2012). It may be that to generate a stable overexpressing cell line one or more BCA2 regulator proteins/binding partners may need to be co-expressed to ensure the protein's stability.

Transient depletion with siRNA has been used in published BCA2 experiments and represents a useful tool for interrogating BCA2 function (Burger *et al*. 2005; Smith *et al*. 2013). However, as long-term effects of depletion have not been explored, stable loss-of-function approaches (such as shRNA) would provide valuable data. An alternative novel approach to understanding BCA2 function could be the use of transcription activator-like effector nucleases (TALENs) for targeted gene disruption. TALEN technology uses synthetically engineered restriction enzymes to cleave DNA at a specific sequence in the promoter of a GOI. The resulting frame-shift mutation prevents downstream transcription leading to complete and permanent silencing of the gene (Boch 2011). A TALEN-based approach would have the advantages of allowing loss of function phenotypes to be studied over long term culture and would facilitate experimentation in live cells.

Although stable HA-BCA2 expressing clones were generated, the protein levels were insufficient and so the cell models were ultimately not meaningful alternatives to transient transfection. In light of this, transient BCA2 overexpression was used in further investigations alongside transient siRNA studies.

5.8 References

Alméciga-Díaz, C. J., Rueda-Paramo, M. A., Espejo, A. J., Echeverri, O. Y., Montaño, A., Tomatsu, S. and Barrera, L. A. 2009. Effect of elongation factor 1α promoter and SUMF1 over in vitro expression of N-acetylgalactosamine-6-sulfate sulfatase. *Molecular Biology Reports* 36(7), p. 1863-70.

Amemiya, Y., Azmi, P. and Seth, A. 2008. Autoubiquitination of BCA2 RING E3 ligase regulates its own stability and affects cell migration. *Molecular Cancer Research* 6(9), p. 1385.

Arden, C., Trainer, A., de la Iglesia, N., Scougall, K. T., Gloyn, A. L., Lange, A. J., Shaw, J. A., Matschinsky, F. M. and Agius, L. 2007. Cell Biology Assessment of Glucokinase Mutations V62M and G72R in Pancreatic β-Cells Evidence for Cellular Instability of Catalytic Activity. *Diabetes* 56(7), p. 1773-82.

Bacopulos, S., Amemiya, Y., Yang, W., Zubovits, J., Burger, A., Yaffe, M. and Seth, A. K. 2012. Effects of partner proteins on BCA2 RING ligase activity. *BMC Cancer* 12(1), p. 63.

Boch, J. 2011. TALEs of genome targeting. *Nature Biotechnology* 29(2), p. 135.

Boffa, L. C., Vidali, G., Mann, R. and Allfrey, V. 1978. Suppression of histone deacetylation in vivo and in vitro by sodium butyrate. *Journal of Biological Chemistry* 253(10), p. 3364-66.

Burger, A. M., Gao, Y., Amemiya, Y., Kahn, H. J., Kitching, R., Yang, Y., Sun, P., Narod, S. A., Hanna, W. M. and Seth, A. K. 2005. A novel RING-type ubiquitin ligase breast cancer-associated gene 2 correlates with outcome in invasive breast cancer. *Cancer Research* 65(22), p. 10401.

Calvin, S., Calvin, J. E., Wang, J., Jacobsen, L. and Pitz, S. 2006. FuGENEÂ® HD Transfection Reagent: Choice of a Transfection Reagent with Minimal Off-Target Effect as Analyzed by Microarray Transcriptional Profiling. *Nature Methods Application Notes*.

De Baets, G., Reumers, J., Blanco, J. D., Dopazo, J., Schymkowitz, J. and Rousseau, F. 2011. An evolutionary trade-off between protein turnover rate and protein aggregation favors a higher aggregation

propensity in fast degrading proteins. *PLoS Computational Biology* 7(6), p. e1002090.

Escher, G., Hoang, A., Georges, S., Tchoua, U., El-Osta, A., Krozowski, Z. and Sviridov, D. 2005. Demethylation using the epigenetic modifier, 5-azacytidine, increases the efficiency of transient transfection of macrophages. *Journal of Lipid Research* 46(2), p. 356-65.

Feller, S. M. and Lewitzky, M. 2012. Very'sticky'proteins-not too sticky after all. *Cell Communnications and Signalling* 10, p. 15.

Grassi, G., Maccaroni, P., Meyer, R., Kaiser, H., D'ambrosio, E., Pascale, E., Grassi, M., Kuhn, A., Di Nardo, P. and Kandolf, R. 2003. Inhibitors of DNA methylation and histone deacetylation activate cytomegalovirus promoter-controlled reporter gene expression in human glioblastoma cell line U87. *Carcinogenesis* 24(10), p. 1625-35.

Guo, Z., Wang, L., Eisensmith, R. and Woo, S. 1996. Evaluation of promoter strength for hepatic gene expression in vivo following adenovirus-mediated gene transfer. *Gene Therapy* 3(9), p. 802-810.

Kona, F. R., Stark, K., Bisoski, L., Buac, D., Cui, Q. and Dou, Q. P. 2012. Transcriptional activation of breast cancer-associated gene 2 by estrogen receptor. *Breast Cancer Research and Treatment*, p. 1-9.

Löser, P., Jennings, G. S., Strauss, M. and Sandig, V. 1998. Reactivation of the previously silenced cytomegalovirus major immediate-early promoter in the mouse liver: involvement of NFκB. *Journal of Virology* 72(1), p. 180-90.

Marks, P. A., Rifkind, R. A., Richon, V. M., Breslow, R., Miller, T. and Kelly, W. K. 2001. Histone deacetylases and cancer: causes and therapies. *Nature Reviews Cancer* 1(3), p. 194-202.

Menke, A., McInnes, L., Hastie, N. D. and Schedl, A. 1998. The Wilms' tumor suppressor WT1: approaches to gene function. *Kidney International* 53(6), p. 1512-18.

Miyakawa, K., Ryo, A., Murakami, T., Ohba, K., Yamaoka, S., Fukuda, M., Guatelli, J. and Yamamoto, N. 2009. BCA2/Rabring7

promotes tetherin-dependent HIV-1 restriction. *PLoS Pathogens* 5(12), p. e1000700.

Mizuno, K., Kitamura, A. and Sasaki, T. 2003. Rabring7, a novel Rab7 target protein with a RING finger motif. *Molecular Biology of the Cell* 14(9), p. 3741-52.

Mosser, D., Caron, A., Bourget, L., Jolicoeur, P. and Massie, B. 1997. Use of a dicistronic expression cassette encoding the green fluorescent protein for the screening and selection of cells expressing inducible gene products. *Biotechniques* 22(1), p. 150-61.

Narita, R., Kitaura, H., Torii, A., Tashiro, E., Miyazawa, M., Ariga, H. and Iguchi-Ariga, S. M. M. 2012. Rabring7 Degrades c-Myc through Complex Formation with MM-1. *PloS One* 7(7), p. e41891.

Nityanandam, R., Serra-Moreno, R. 2014. BCA2/Rabring7 Targets HIV-1 Gag for Lysosomal Degradation in a Tetherin-Independent Manner. *PLoS Pathogens* 10(5), p. e1004151.

Norrman, K., Fischer, Y., Bonnamy, B., Sand, F. W., Ravassard, P. and Semb, H. 2010. Quantitative comparison of constitutive promoters in human ES cells. *PloS One* 5(8), p. e12413.

O'Gorman, S., Fox, D. T. and Wahl, G. M. 1991. Recombinase-mediated gene activation and site-specific integration in mammalian cells. *Science* 251(4999), p. 1351-55.

O'Driscoll, L., Gammell, P., McKiernan, E., Ryan, E., Jeppesen, P. B., Rani, S. and Clynes, M. 2006. Phenotypic and global gene expression profile changes between low passage and high passage MIN-6 cells. *Journal of Endocrinology* 191(3), p. 665-76.

Prasad, K. N. and Sinha, P. K. 1976. Effect of sodium butyrate on mammalian cells in culture: a review. *In Vitro-Plant* 12(2), p. 125-32.

Robertson, K. D. 2001. DNA methylation, methyltransferases, and cancer. *Oncogene* 20(24), p. 3139-55.

Schwanhäusser, B., Busse, D., Li, N., Dittmar, G., Schuchhardt, J., Wolf, J., Chen, W. and Selbach, M. 2011. Global quantification of mammalian gene expression control. *Nature* 473(7347), p. 337-42.

Smith, C. J., Berry, D. M., McGlade, C. J. 2013. The E3 ubiquitin ligases RNF126 and Rabring7 regulate endosomal sorting of the epidermal growth factor receptor. *Journal of Cell Science* 126(6), p. 1366-80.

Turan, S. and Bode, J. 2011. Site-specific recombinases: from tag-and-target-to tag-and-exchange-based genomic modifications. *The FASEB Journal* 25(12), p. 4088-107.

Wu, S.Y. and Chiang, C.M. 1996. Establishment of stable cell lines expressing potentially toxic proteins by tetracycline-regulated and epitope-tagging methods. *Biotechniques* 21(4), p. 718-22

Chapter 6: The Effects of BCA2 on EGFR Expression and Trafficking

A role for BCA2 in EGFR trafficking has been reported but is incompletely described in the literature (Mizuno *et al*. 2003; Sakane *et al.* 2007; Smith *et al.* 2013). To address some of the gaps and apparent discord in published BCA2 data, experiments were conducted to better characterise the effects and function of BCA2 in EGFR trafficking.

6.1 siRNA depletion of BCA2

In order to carry out loss-of-function studies and to help validate immunoblotting techniques, siRNA depletion of BCA2 needed to be optimised and used. Initial attempts to deplete BCA2 were carried out using an siRNA sequence as previously described (Burger *et al*. 2005). This sequence was dubbed BCA2-K. MCF-7 cells were incubated at 37ºC, 5% CO_2 in SFM with transfection reagent:siRNA complex. The complex was comprised of Oligofectamine and either BCA2-K siRNA or non-targeting GFP control siRNA at final concentrations of 50 nM. For the siRNA sequences see section 2.13.2.1. After four hours incubation 30% serum media was added to the cells to complete the media and the cells were returned to the incubator for 44 hours. Lysates were collected after 48 hrs total siRNA depletion time and Western blotting for BCA2 was performed. The immunoblots in Figure 6-1 A demonstrate that the initial attempt at BCA2 depletion was unsuccessful. In parallel with this experiment a positive control for the siRNA depletion protocol was

performed. An siRNA sequence for Flotillin-1A (Flot1A) was used as the siRNA had been previously validated in the laboratory (Al Soraj *et al*. 2012). Figure 6-1 B shows immunoblots for flotillin-1 and indicates significant depletion of the target protein. This suggested that the failure to deplete BCA2 shown in Fig. 6-1 A was less likely to be due to methodological error or problems with transfection efficiency.

Having failed to successfully deplete BCA2, a second siRNA sequence was obtained from a pre-designed but unvalidated selection at Eurofins MWG Operon. The MWG siRNA (herein called BCA2-1) was then tested alongside the BCA2-K sequence using the same protocol described above. Figure 6-1 C indicates that neither siRNA sequence was able to significantly reduce the BCA2 levels in MCF-7 cells, though saturation of the BCA2 signal band meant that a subtle reduction in BCA2 levels may have been masked. For the subsequent experiments a slightly reduced exposure time and longer SDS-PAGE separation time were used.

A SMARTpool cocktail of four BCA2 siRNA sequences were then purchased from Dharmacon (via Fisher Scientific). For depletion of BCA2 using the SMARTpool siRNAs: MCF-7 cells were incubated in complete media for 48 hr with a Dharmafect 1 transfection reagent-siRNA complex. The final concentration of the BCA2 siRNA cocktail (BCA2-SP) was 25 nM. Alongside the SMARTpool BCA2 depletion, and using the same method, cells were also incubated with non-targeting GFP control siRNA and the BCA2-1 siRNA. The data in Figure 6-1 D indicates that the BCA2-SP siRNA was able to deplete BCA2 in MCF-7 cells as indicated by the reduction in both bands of the BCA2 doublet.

This further confirms that both bands observed with this antibody represent BCA2. Quantification of the extent of BCA2 depletion in multiple experiments is provided in Figure 6-2.

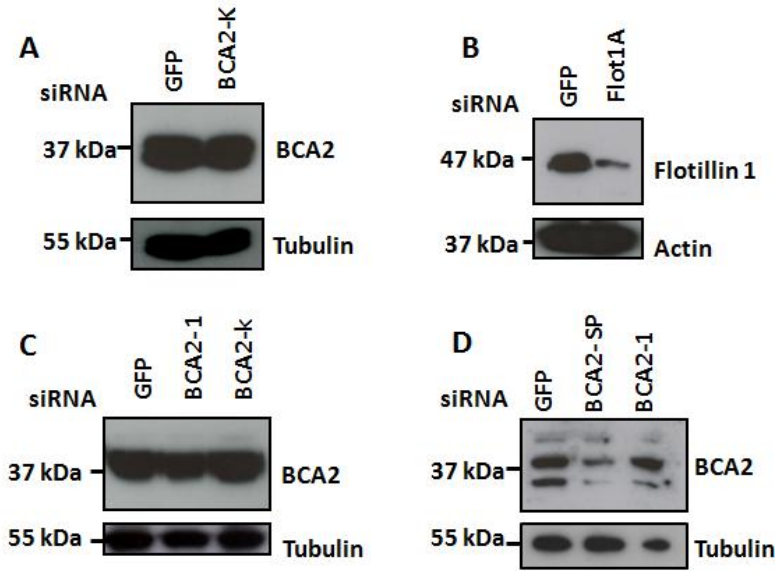

Figure 6-1: Optimisation of BCA2 siRNA depletion in MCF-7 cells. Cells were treated with siRNAs against BCA2 (A, C and D) and against Flotillin 1 (B). Lysates of siRNA treated cells subject to Western blotting for BCA2. A and C) unsuccessful attempts to deplete BCA2 siRNA with the BCA2-K and BCA2-1 siRNA sequences. B) Positive control for the protocol used in A and C showing successful siRNA depletion of Flotillin 1 D) Successful depletion of BCA2 by a SMARTpool siRNA cocktail and associated protocol.

The successful siRNA and Western blotting method demonstrated with Flot1A formed the basis of a small collaboration with a visiting scientist that has lead to a manuscript currently under review (Pereira *et al.* 2015, *accepted*).

6.2 BCA2 depletion and EGFR expression in MCF-7 cells

BCA2 depletion with the SMARTpool protocol and siRNAs was tested further in three-independent experiments, performed in MCF-7 cells as previously described. Lysates of the siRNA treated cells were subjected to Western blotting for BCA2. Immunoblotting for EGFR and transferrin receptor (TfR) were also performed to investigate whether changes in

BCA2 levels might also affect receptor protein expression levels. BCA2 has been shown to alter EGFR trafficking (Mizuno *et al*. 2003; Smith *et al*. 2013) but effects on levels of EGFR have not been explored. TfR has no known association with BCA2 and served as an indicator of the specificity of BCA2's possible effects on receptor levels.

As expected EGFR and TfR immunoblotting produced bands at ~180 and ~95 kDa respectively (Fig. 6-2A). Relative changes in BCA2, EGFR and TfR levels were quantified using ImageJ software. The results were statistically analysed with two-tailed, students independent T-tests. The results in Figure 6-2 show that BCA2 expression was reduced by ~80% in the BCA2 siRNA treated cells and this reduction was statistically significant ($p=0.012$; Fig. 6-2 B). In line with MCF-7 literature (Davidson *et al*. 1987) EGFR levels in the non-targeting control lysates were very low: Femto™ Maximum Sensitivity ECL substrate was required to detect a signal. EGFR protein levels were significantly elevated by 2.5 fold ($p=0.040$) in the BCA2 depleted cells (Fig. 6-2 C) while levels of TfR were unaffected ($p=0.451$; Fig. 6-2 D).

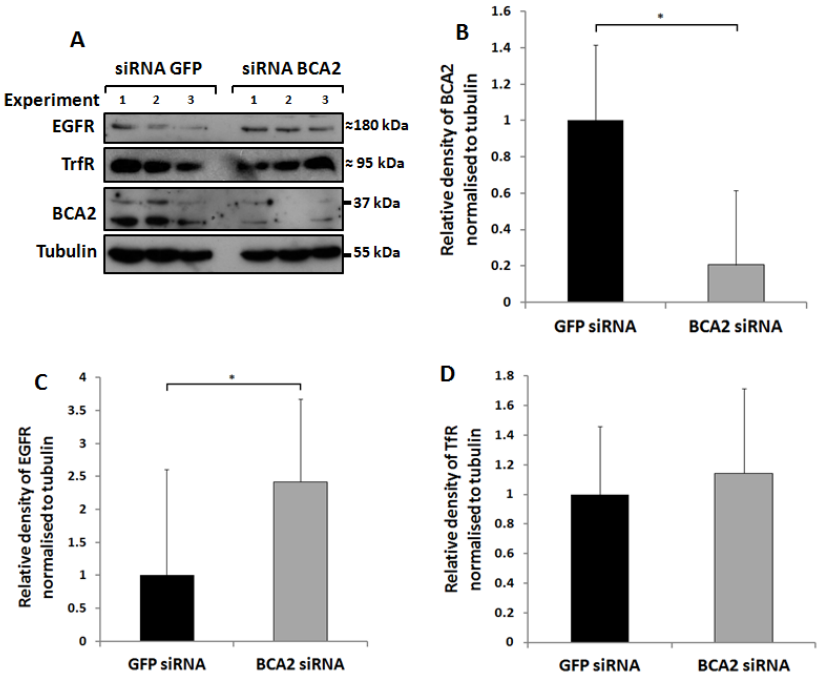

Figure 6-2: Relative levels of BCA2, EGFR and TfR in MCF-7 cells treated with BCA2 or non-targeting siRNA. A) Immunoblots for BCA2 and selected recptors in cells treated with BCA2 SMARTpool siRNA or GFP non-targeting control siRNA. B, C and D) Relative protein expression was quantified with ImageJ software and normalised to tubulin loading control. *Results from three independent, single experiments are shown. Error bars represent 95% confidence intervals. * statistical significance $p \leq 0.05$.*

6.3 BCA2 overexpression and EGFR expression in MCF-7 cells

To further investigate the effect of BCA2 on EGFR levels, MCF-7 cells were transiently transfected with HA-BCA2 (or mock transfected with an empty control vector). Cell lysates were collected in duplicate from three independent experiments and subject to immunoblotting for HA and for EGFR (Fig 6-3 A). EGFR expression was quantified using ImageJ software and a student's independent T-test was performed to determine the statistical significance of differences in receptor levels (Fig. 6-3 B).

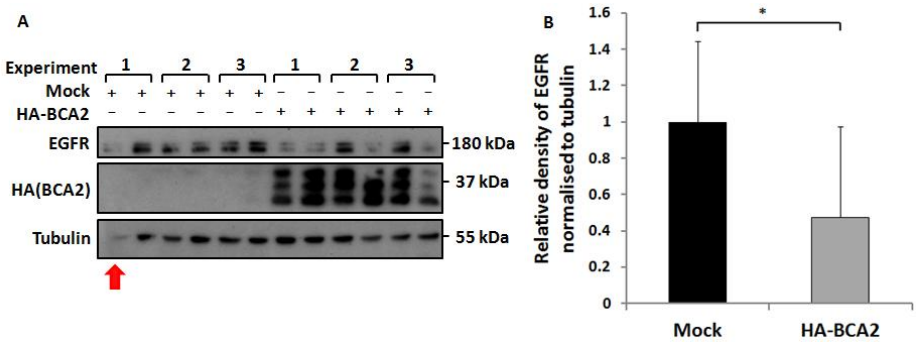

Figure 6-3: Relative EGFR levels in mock transfected and HA-BCA2 overexpressing MCF-7 cells. A) Immunoblots for HA and EGFR in cells transiently transfected with HA-BCA2 or mock transfected with an empty control vector. B) Relative protein expression was quantified with ImageJ software and normalised to tubulin loading control. *Results from three independent, duplicate experiments are shown. Red arrow indicates underloaded lane. Error bars represent 95% confidence intervals. * statistical significance $p \leq 0.05$*

There was a problem with incorrect loading in the first lane of the gel (the first mock transfected replicate of the first experiment). However, since EGFR band densities were quantified relative to the tubulin loading control this difference in loading was accounted for in the data analysis. There was some intra-experimental variation but overall the data show that HA-BCA2 overexpression significantly decreases EGFR levels in MCF-7 cells (p=0.028).

6.4 BCA2 expression in a panel of cell lines

The relative expression levels of BCA2 and EGFR in selected cell lines were measured by Western Blotting. Band intensities were quantified using ImageJ software, normalised to tubulin and calculated relative to MCF-10A levels (Fig. 6-4). Endogenous BCA2 expression varied across the panel of cell lines that included: immortalised breast epithelial cells (MCF-10A), luminal A, ER^+ breast cancer cells (MCF-7 and T47D), triple negative breast cancer (MDA-MB-231) and luminal B, $HER2^+$ breast cancer (BT474). This panel of cell lines also included the HeLa

cervical carcinoma line as EGFR trafficking in these cells is well characterised.

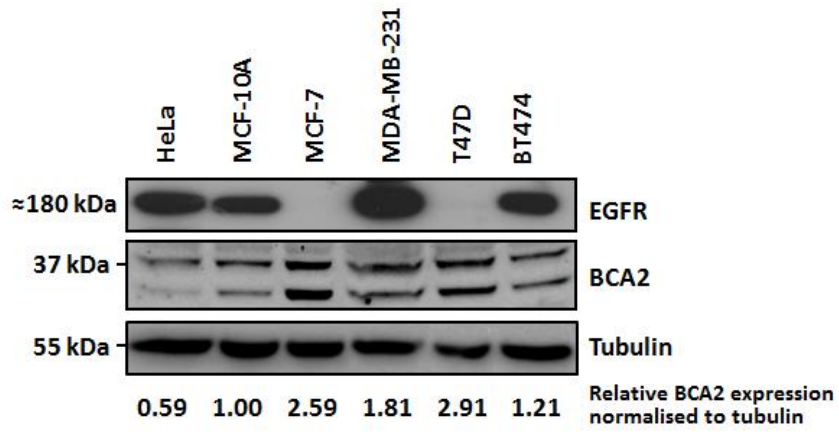

Figure 6-4: Immunoblots of endogenous BCA2 and EGFR levels in a panel of cell lines. BCA2 protein levels quantified with ImageJ software, normalised to the tubulin loading control and their expression levels were calculated relative to MCF-10A cells.

Figure 6-4 suggests a possible inverse relationship between BCA2 and EGFR expression, though the panel of cell lines tested was not sufficiently large to perform meaningful correlation analyses. T47D and MCF-7 cells expressed the highest levels of BCA2 while HeLa expressed the lowest. MDA-MB-231 cells were also found to express relatively high levels of BCA2, contrary to some published work on the protein (Brahemi *et al*. 2010) but in line with others (Buac *et al*. 2013).

6.5 BCA2 overexpression and EGFR levels in HeLa cells.

HeLa cells naturally express low quantities of BCA2 (Fig. 6-4) and EGFR trafficking in these cells has been extensively studied. This made the HeLa cell line a useful model for studying the effects of BCA2 overexpression on EGFR in cancer cells. Research involving further BCA2 depletion in HeLa has been previously published and was shown to impair ligand induced degradation of both EGFR and c-Met (Smith *et*

al. 2013). Having already demonstrated that altering BCA2 levels influenced total EGFR levels in MCF-7 cells (Fig. 6-2 and 6-3) it was hypothesised that HA-BCA2 overexpression in HeLa may produce similar effects. BCA2 induced changes in total EGFR and c-Met levels were investigated by Western blotting of HeLa cell lysates that had been transfected with HA-tagged BCA2 or mock transfected with an empty control vector. Three independent, duplicate experiments were performed and showed a significant decrease in total EGFR ($p=0.001$) and c-Met ($p=0.003$) levels in the HA-BCA2 overexpressing cells (Fig. 6-5 A-C). Levels of (non-tyrosine kinase) TfR were also analysed to determine whether other cell surface receptors internalised by CME were affected by BCA2 overexpression. TrfR expression was not found to be significantly altered by BCA2 overexpression ($p=0.365$. Figures 6-5 A and D).

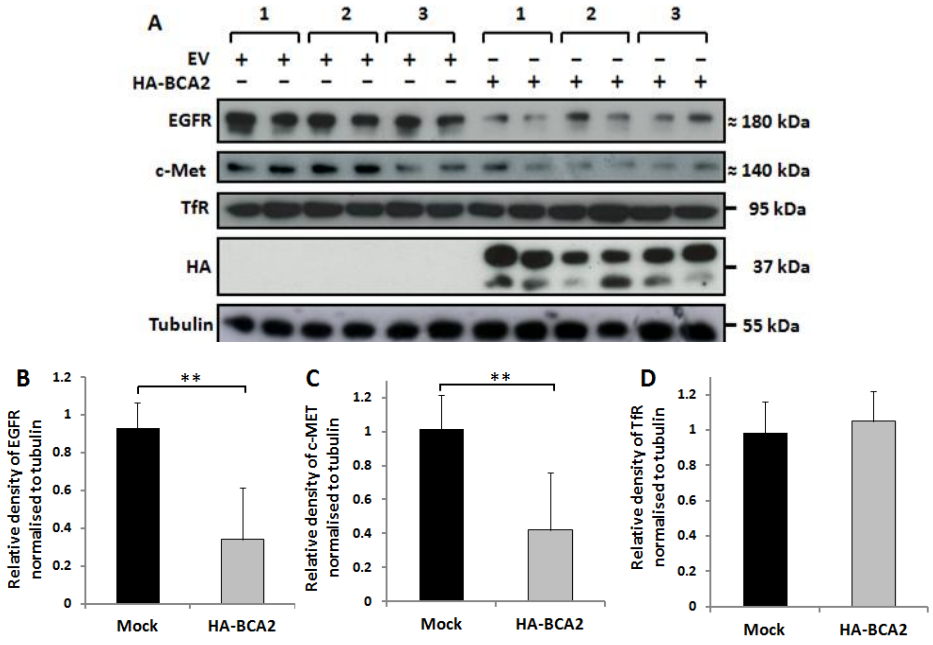

Figure 6-5: Relative levels of EGFR, c-Met and TfR in mock transfected control and HA-BCA2 overexpressing HeLa cells. A) Immunoblots for selected receptors in cells transfected with HA-BCA2 or mock transfected with an empty control vector. B) Protein expression was quantified with ImageJ software. *Results from three independent, duplicate experiments are shown. Error bars represent 95% confidence intervals. ** statistical significance $p \leq 0.01$. *** statistical significance $p \leq 0.001$*

In order to see if the changes in EGFR levels could be visualised in individual cells, two different immunofluorescence microscopy (IF) experiments were performed: one in which cells were treated with 20 ng/ml unlabelled EGF to induce EGFR accumulation in early endosomes and one in which cells were incubated with fluorescently labelled EGF on ice. Incubating cells with ligand at 4ºC for a sufficient time period allows the ligand to bind to surface receptors without inducing internalisation. In the case of EGF, 30 min has been shown to be sufficient to allow maximal surface binding (Roepstorff *et al*. 2009). Performing a 4ºC incubation with fluorescently labelled EGF has been used in the literature to demonstrate reduced EGFR levels (Wang *et al*. 2011).

Figure 6-6 A shows the results of double-labelling IF for HA and for EGFR. HA-BCA2 transfected HeLa cells were first stimulated with EGF for 15 min in order to uniformly localise the receptor into easily detectable vesicles throughout the cells. When immunofluorescence for HA and EGFR was then carried out, BCA2 overexpressing cells showed a marked reduction in EGFR labelling. Figure 6-6 B is a confocal microscopy image of HA-BCA2 over-expressing HeLa that were serum starved for 60 min prior to incubation with EGF Alexa 488 on ice. After 30 min incubation with EGF-488 the cells were fixed and IF for HA was performed. Confocal microscopy revealed some heterogeneity in labelling of the non-transfected cells, implying that the number of receptors on the membrane varies within the normal HeLa cell population. Despite this heterogeneity it was possible to observe a trend of reduced EGF-488 binding to the HA-BCA2 overexpressing cells, indicative of reduced receptor numbers on the cell surface.

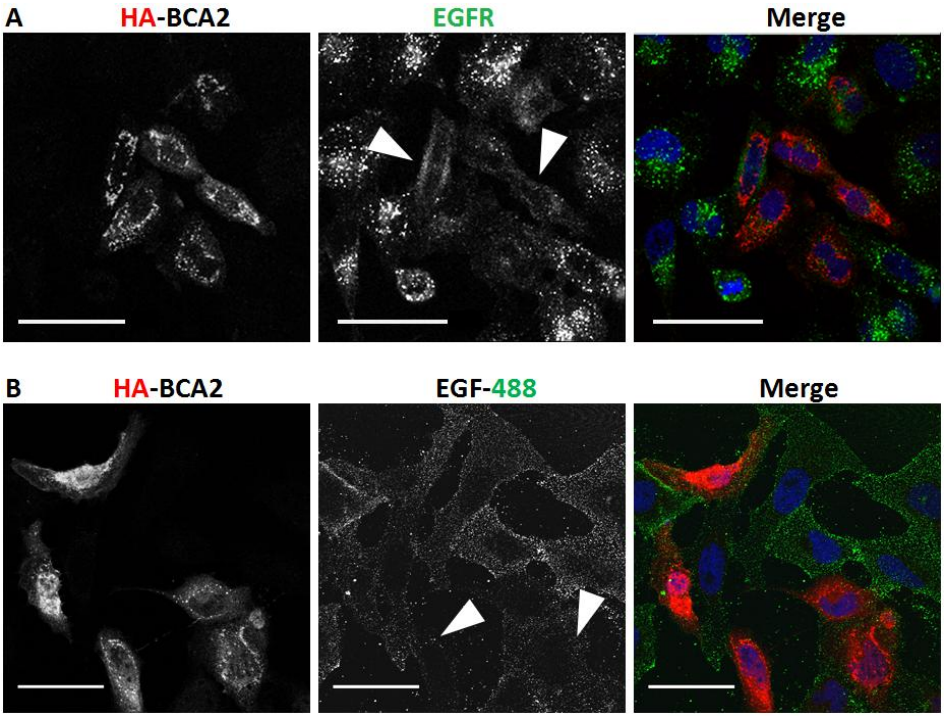

Figure 6-6: Confocal microscopy images of EGFR in HA-BCA2 overexpressing HeLa cells. HA-BCA2 transfected cells were serum starved for 60 min then either A) stimulated with 20 ng/mL EGF for 15 min or B) incubated with EGF Alexa 488 for 30 min on ice. Cells were then fixed and immunolabelled for HA-BCA2 (red) and for EGFR (green) in the cells stimulated with unlabelled EGF. Nuclei were stained blue with Hoechst. *Representative images from two independent, duplicate experiments are shown. Scale bars = 50 µm. Arrowheads indicate examples of HA-BCA2 transfected cells.*

Both Western blotting and IF experiments showed that there was a significant decrease ($p \leq 0.05$) in EGFR expression in the HA-BCA2 transfected cells after 24 hrs. From these initial findings it was not possible to determine whether increased degradation or reduced synthesis was responsible for the lower levels of EGFR in the HA-BCA2 overexpressing cells.

6.6 BCA2 overexpression delays EGFR degradation in HeLa cells

The binding of EGF to EGFR stimulates internalisation and trafficking of the receptor-ligand complex, primarily to the lysosomes for degradation (Roepstorff *et al*. 2009). BCA2 has been reported to alter ligand induced degradation of EGFR though there is some debate as to whether the

protein promotes or inhibits degradation of the receptor (Mizuno *et al*. 2003; Sakane *et al*. 2007; Smith *et al.* 2013). Having shown that total EGFR levels are influenced by changes in BCA2 expression we investigated the effect of BCA2 overexpression on EGF stimulated trafficking of EGFR (Fig. 6-7 to 6-10).

HA-BCA2 and mock transfected HeLa cells were serum starved for 60 min then either serum starved for a further 60 min or stimulated with 20 ng/mL EGF for the same time period. Cell lysates were collected in three independent, triplicate experiments. Western blotting was performed for EGFR, HA and tubulin (Fig. 6-7 A) and intensities were quantified using ImageJ software (Fig. 6-7 B).

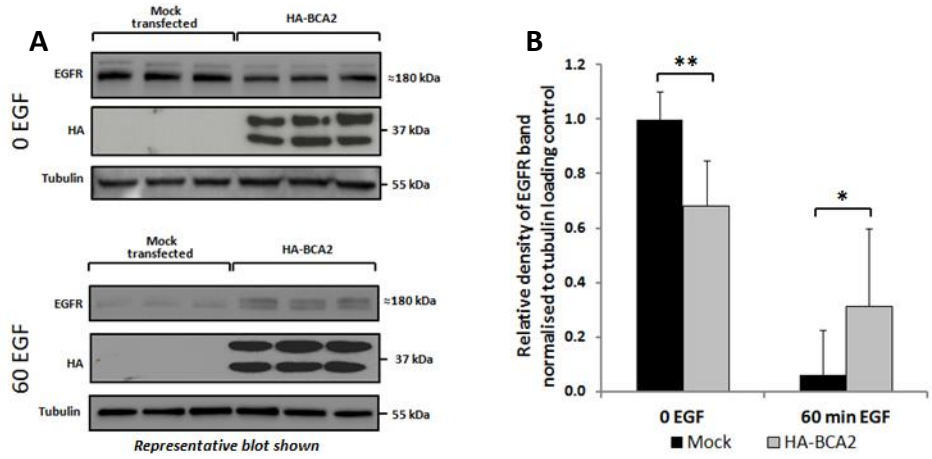

Figure 6-7: Immunoblots showing ligand induced EGFR degradation in mock transfected control and HA-BCA2 overexpressing HeLa cells. A) HA-BCA2 and mock transfected HeLa cells were serum starved for 60 min then stimulated with 20 ng/ml EGF for 0 or 60 min. Cell lysates were collected in three independent, triplicate experiments. Western blotting was performed for EGFR and HA. B) Band intensities were quantified using ImageJ software. *Error bars represent 95% confidence intervals. * statistical significance* $p \leq 0.05$. *** statistical significance* $p \leq 0.01$. *Representative blot of a single experiment is shown*

Student's independent two-tailed t-test of immunoblotting data showed that in unstimulated cells (0 EGF) there was a significant reduction in EGFR expression in HA-BCA2 overexpressing cells relative to mock

transfected controls (p=0.002). Conversely, after 60 min significantly more EGFR remained in the HA-BCA2 overexpressing cells (p=0.030) indicating that EGFR degradation was delayed by BCA2 overexpression.

Visualising the changes in EGFR degradation was achieved by IF of HA-BCA2 overexpressing HeLa cells stimulated with EGF. HA-BCA2 transfected HeLa were serum starved for 60 min then incubated with 20 ng/ml EGF for 15, 60 or 120 min as indicated. The cells were then fixed and sequentially immunolabelled for HA and for EGFR before imaging with confocal microscopy. The fluorescence microscopy images in Figure 6-8 show that EGF uptake is initially reduced in HA-BCA2 transfected cells at 15 min versus non-transfected cells. However, after 60 and 120 min incubation the EGF persists in the BCA2 overexpressers, indicating reduced degradation. At 15 min all non-transfected cells displayed fairly uniform EGFR internalisation and prominent fluorescent vesicles were observed throughout the cytoplasm. EGFR labelling in the HA-BCA2 overexpressing cells was markedly reduced by comparison, in line with the reduction in EGFR levels previously seen by Western blotting (Figs. 6-5 and 6-7). At the 60 min time point the EGFR in non-transfected cells was localised to perinuclear vesicles and the fluorescence signal had reduced in intensity, suggesting lysosomal degradation. In the BCA2 overexpressing cells however the EGFR signal remained visible and the receptor was localised to smaller, diffuse cytoplasmic vesicles. The data supported the Western blotting findings shown in Figure 6-7. By 120 min the EGFR signal had mostly

disappeared from the non-transfected cells however in the HA-BCA2 overexpressers the EGFR persisted.

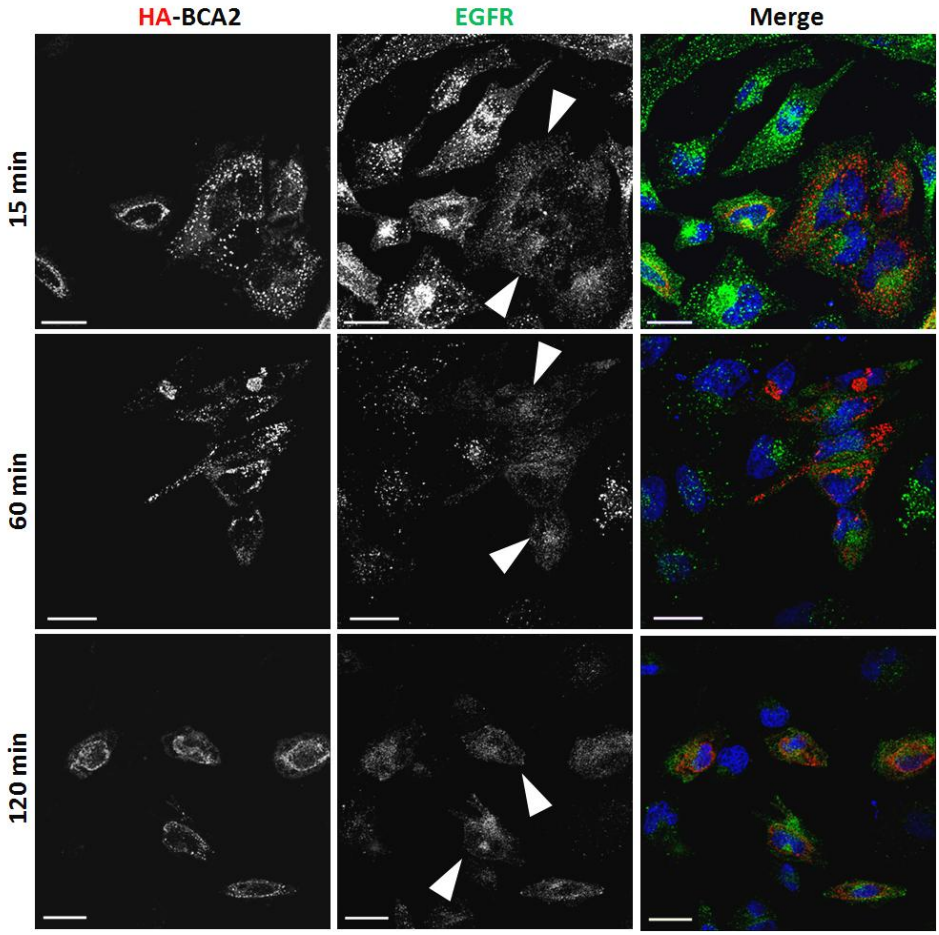

Figure 6-8: Confocal microscopy images of EGFR trafficking in HA-BCA2 overexpressing HeLa cells stimulated with 20 ng/ml EGF. 20 ng/mL EGF was applied to serum starved, HA-BCA2 transfected cells. After 15, 60 & 120 min the cells were fixed and immunolabelled for HA-BCA2 and EGFR. *Scale bar = 25 µm. Arrowheads indicate examples of HA-BCA2 transfected cells.*

The time-course experiment was also repeated with lower concentrations of EGF (1 ng/mL) as it has been suggested that EGFR is internalised via different mechanisms depending on ligand concentration. Sigismund *et al.* in (2005; 2008; 2013) published data showing that low concentrations of EGF (< 3 ng/mL) lead to EGFR internalisation solely by CME. However, higher EGF concentrations (> 20 ng/mL) stimulated EGFR internalisation by another endocytic pathway (caveolin mediated

endocytosis). In order to see whether ligand concentration altered the pattern of EGFR degradation in BCA2 overexpressing cells, the EGFR trafficking experiment was repeated as previously described but with a lower stimulating EGF concentration (1 ng/ml). Figure 6-9 shows the results of this experiment. After 15 min incubation with EGF, all non-transfected HeLa cells had begun to internalise EGFR and the EGFR had begun to accumulate in relatively large vesicles throughout the cytoplasm. EGFR labelling in the HA-BCA2 overexpressing cells was markedly less intense than in non-transfected cells. At the 1 hr time point the EGFR in non-transfected cells had moved to perinuclear vesicles and the fluorescence had diminished in intensity (compared with starting levels in these cells). However, in the BCA2 overexpressing cells the EGFR signal persisted. By 2 hrs the EGFR signal had almost entirely disappeared from the non-transfected cells through lysosomal degradation. In the HA-BCA2 overexpressing cells however the EGFR signal remained.

The results trend produced by stimulation with 20 ng/mL EGF (Fig. 6-8) and 1 ng/mL EGF (Fig. 6-9) were similar: HA-BCA2 overexpressing cells had less EGFR but the EGFR was degraded more slowly in response to EGF stimulation.

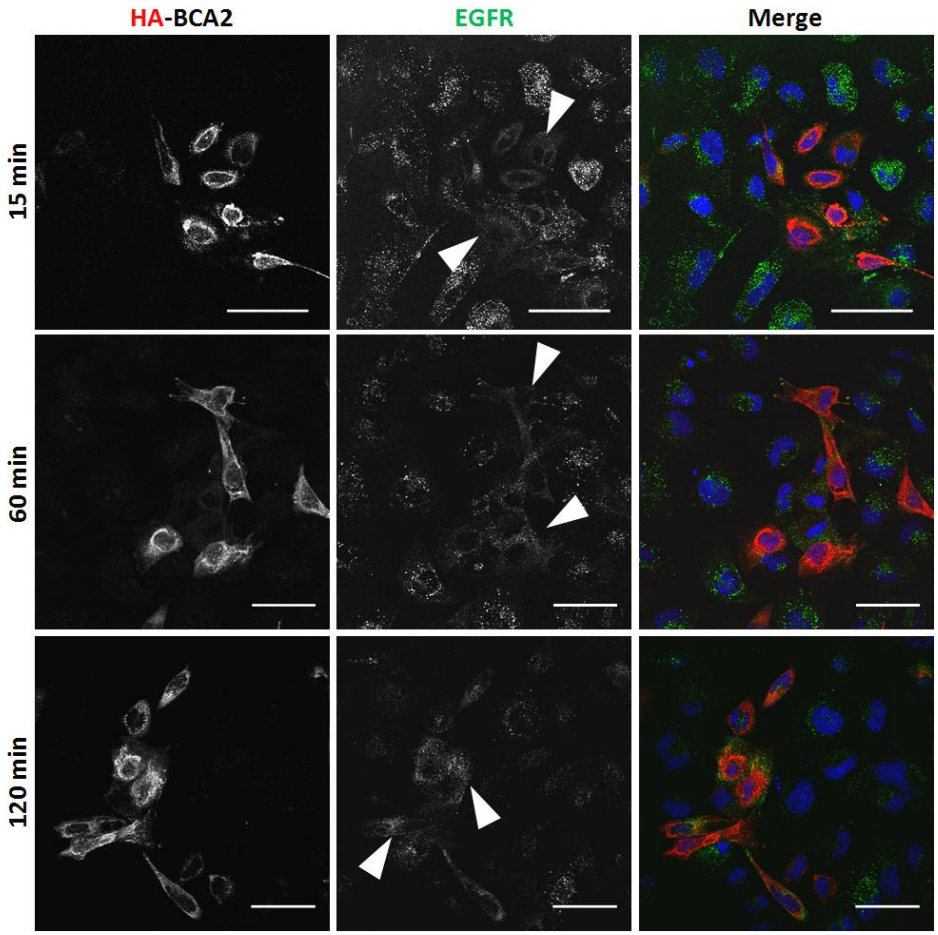

Figure 6-9: Confocal microscopy images of EGFR trafficking in HA-BCA2 overexpressing HeLa cells stimulated with 1 ng/ml EGF. 1 ng/mL EGF was applied to serum starved HA-BCA2 transfected cells. After 15, 60 & 120 min the cells were fixed and immunolabelled for HA-BCA2 and EGFR. *Scale bars = 50 µm. Arrowheads indicate examples of HA-BCA2 transfected cells*

6.7 BCA2 overexpression specifically alters EGF trafficking

Experiments were conducted to determine whether all receptor-ligand trafficking by CME was altered by BCA2 overexpression or if the effect was specific to EGFR. Trafficking of fluorescently labelled EGF was compared with that of transferrin (Tf) in HA-BCA2 overexpressing HeLa. Transfected cells were incubated for 15, 60 or 120 min with either 0.5 µg/mL Alexa-488 EGF or 100 nM Alexa-488 Tf. After incubation with the fluorescent ligands the cells were fixed and immunolabelled for HA-BCA2 (Fig. 6-10).

Tf internalisation was somewhat varied in terms of the quantity and intracellular distribution of ligand: even in the non-tranfected population there was heterogeneity between cells in the intensity of fluorescence and the degree of Tf enrichment in a perinuclear recycling compartment. There was little discernible difference between HA-BCA2 overexpressing cells and non-transfected controls. EGF internalisation on the other hand was delayed in the BCA2 overexpressing HeLa cells as indicated by the low EGF signal at the earlier time point. At the later time points (60 and 120 min) the EGF appeared to accumulate in the BCA2 overexpressing HeLa cells but appeared to be degraded in the non-transfected cells. This mirrors results seen for EGFR by Western blotting (Fig. 6-7) and immunofluorescence (Fig. 6-8).

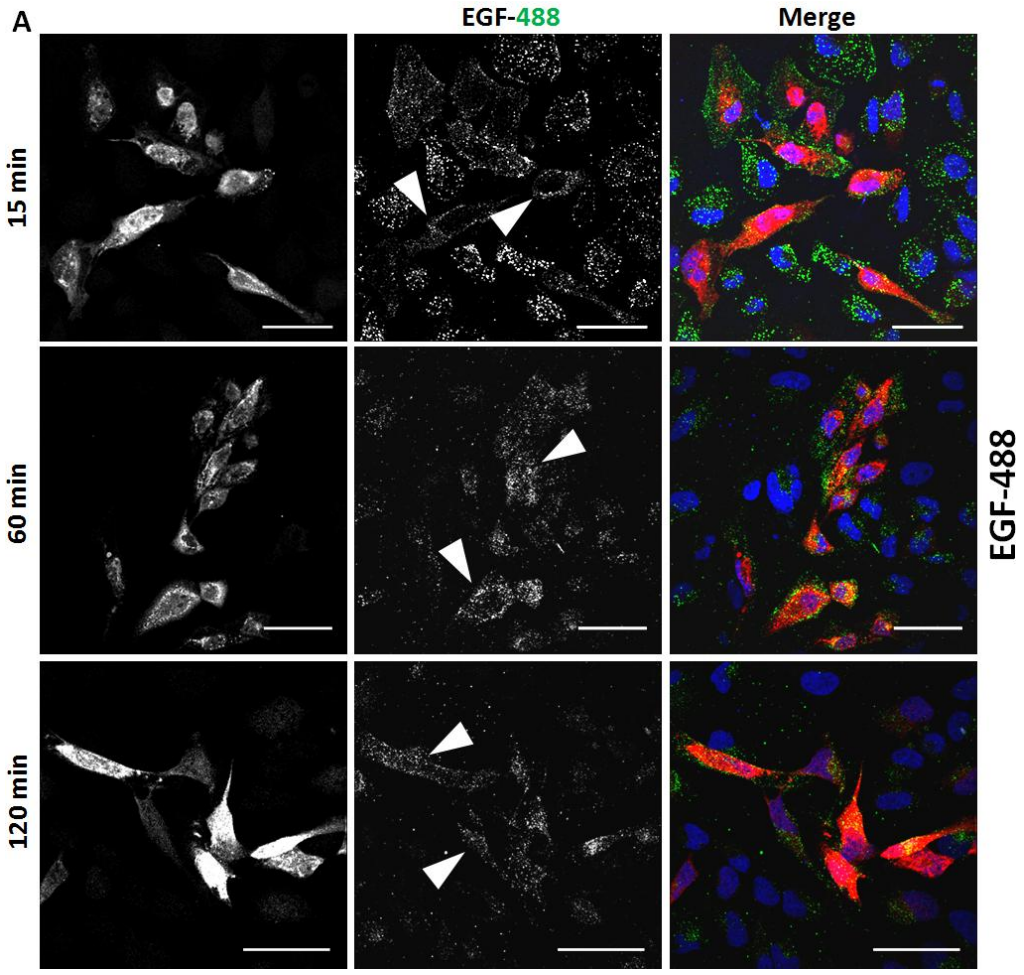

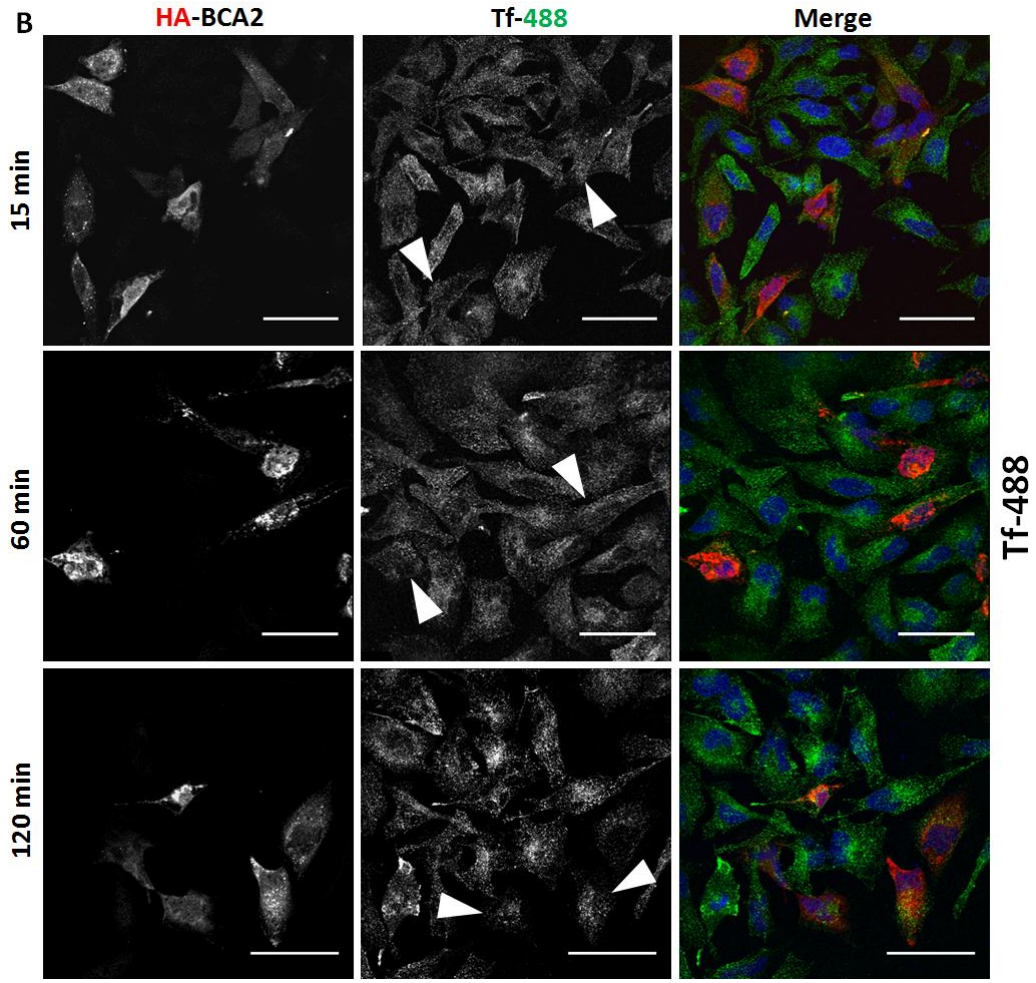

Figure 6-10: Confocal microscopy images of Fluorescent EGF and Tf trafficking in HA-BCA2 overexpressing HeLa cells. HA-BCA2 transfected cells were incubated with 0.5 µg/mL Alexa-488 EGF (A) or 100 nM Alexa-488 Tf (B) for 15, 60 or 120 min before being fixed and immunolabelled for HA (red). Nuclei were stained blue with Hoechst. *Scale bar = 50 µm. Arrowheads indicate examples of HA-BCA2 transfected cells. The red channel for the 120 min time point in the EGF time course was overexposed to show all transfected cells.*

The EGF trafficking experiment was also performed in HA-BCA2 overexpressing MDA-MB-231 cells. MDA-MB-231 cells express very high levels of EGFR so in this cell line trafficking of the EGF-rhodamine (EGF-rhd), a less-sensitive fluorescent EGF probe, was examined (Fig. 6-11).

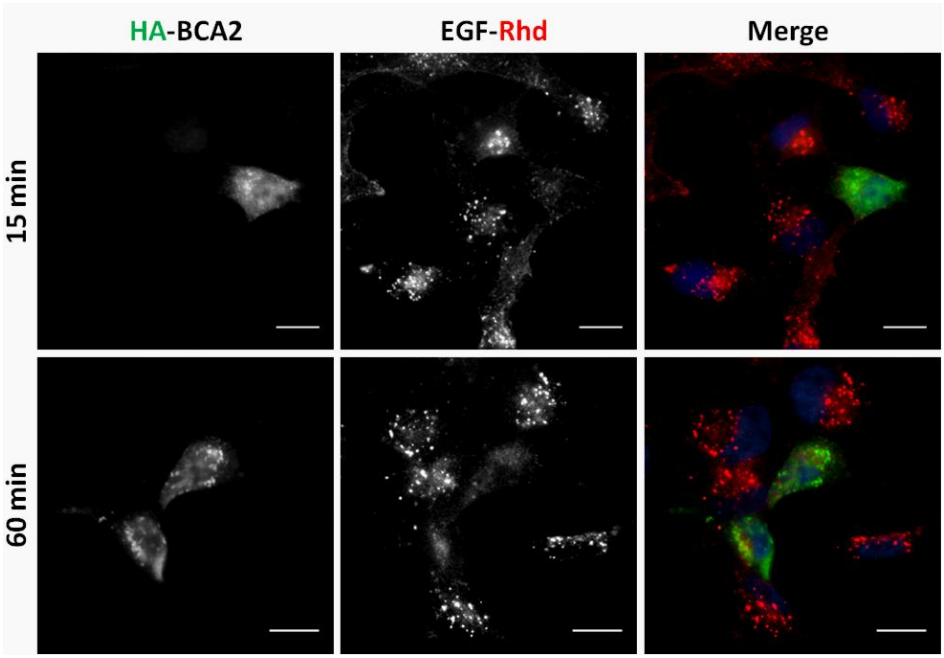

Figure 6-11: Epifluorescence microscopy images of EGF-Rhd trafficking in HA-BCA2 overexpressing MDA-MB-231 cells. Cells were transfected with HA-BCA2 and after 24 hrs were serum starved and incubatated with 0.5 µg/mL of EGF-Rhd. *Scale bar = 15 µm.*

Figure 6-11 demonstrates that in untransfected MDA-MB-231 cells, EGF-Rhd was not degraded after 60 min. The failure of MDA-MB-231 cells to degrade EGF/EGFR has been previously reported but not thoroughly explored or explained (Decker 1988).

As had been previously observed (Fig. 4-17 and 4-18) the transfection efficiency with HA-BCA2 in the MDA-MB-231 cells was very low (< 5%) and many of the overexpressing cells had morphological indications of poor viability. The HA-BCA2 overexpressing cells appeared to be unable to internalise EGF-Rhd after 15 or 60 min. However, there were very few transfected cells to examine and most HA-BCA2 overexpressing cells appeared to be in very poor health. It was therefore very difficult to make reliable inferences regarding a direct

effect on EGF trafficking and it was decided that no further experiments would be conducted with the MDA-MB-231 cell line.

EGF trafficking experiments were also tested in MCF-7 cells. However, even with very high EGF levels (2 µg/mL) and attempts at pre-binding EGF to the membrane on ice, no EGF-488 was detected in the cells or on the plasma membrane (data not shown) so this experimental approach was not pursued.

6.8 Subcellular localisation of EGF during delayed internalisation in HA-BCA2 overexpressing HeLa cells

Having established that EGF degradation was delayed/impaired by HA-BCA2 overexpression we then wanted to determine which endocytic compartment/s the EGF accumulated in. Following 60 min of serum starvation, HA-BCA2 overexpressing HeLa cells were incubated with EGF-488 for 15 and 60 min. After fixation, double-immunofluorescence labelling for HA and either EEA1 or LAMP1 was performed. Figure 6-12 A shows that at the 15 min time point there was some colocalisation between EGF and EEA1. This indicates that 15 min after internalisation a moderate proportion of the EGF-488 was localised to early endosomes in untransfected cells. At this time point the EGF was excluded from the late endosomes and lysosomes as no colocalisation was seen between the EGF containing vesicles and the LAMP1 positive compartments (LAMP1 merge channel insert). As previously seen (Fig. 6-10) very little EGF was internalised by HA-BCA2 overexpressing cells at 15 min, making colocalisation experiments difficult to perform. After 60 min EGF incubation (Fig. 6-12 B) EGF-488 accumulated in the early

endosomes of HA-BCA2 overexpressing cells but did not appear to have reached the late endolysosomal compartments (merge channel inserts). In the untransfected cells the EGF-488 signal had largely been lost, indicative of degradation.

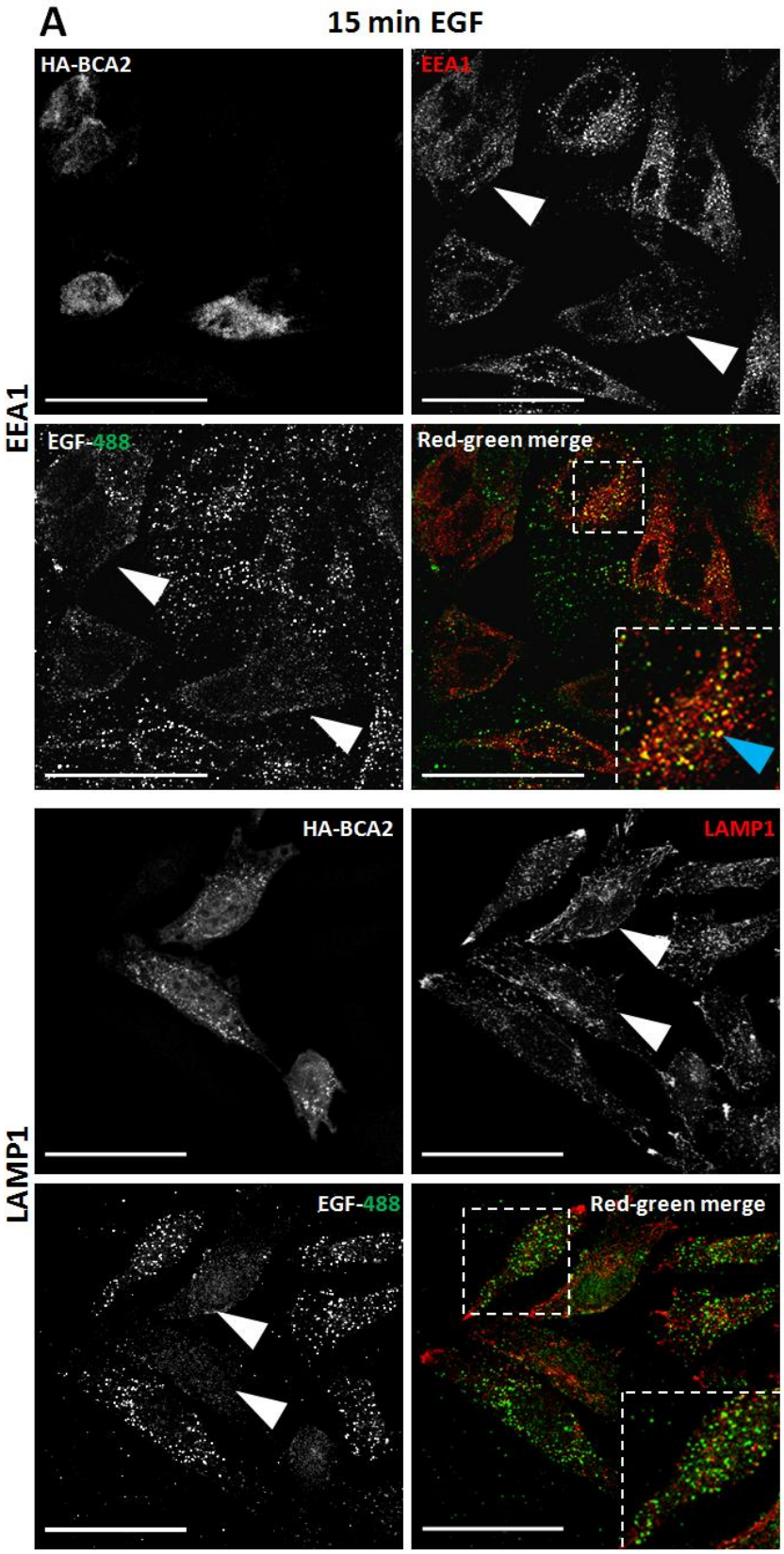
A
15 min EGF
EEA1
LAMP1
HA-BCA2
EEA1
EGF-488
Red-green merge
HA-BCA2
LAMP1
EGF-488
Red-green merge

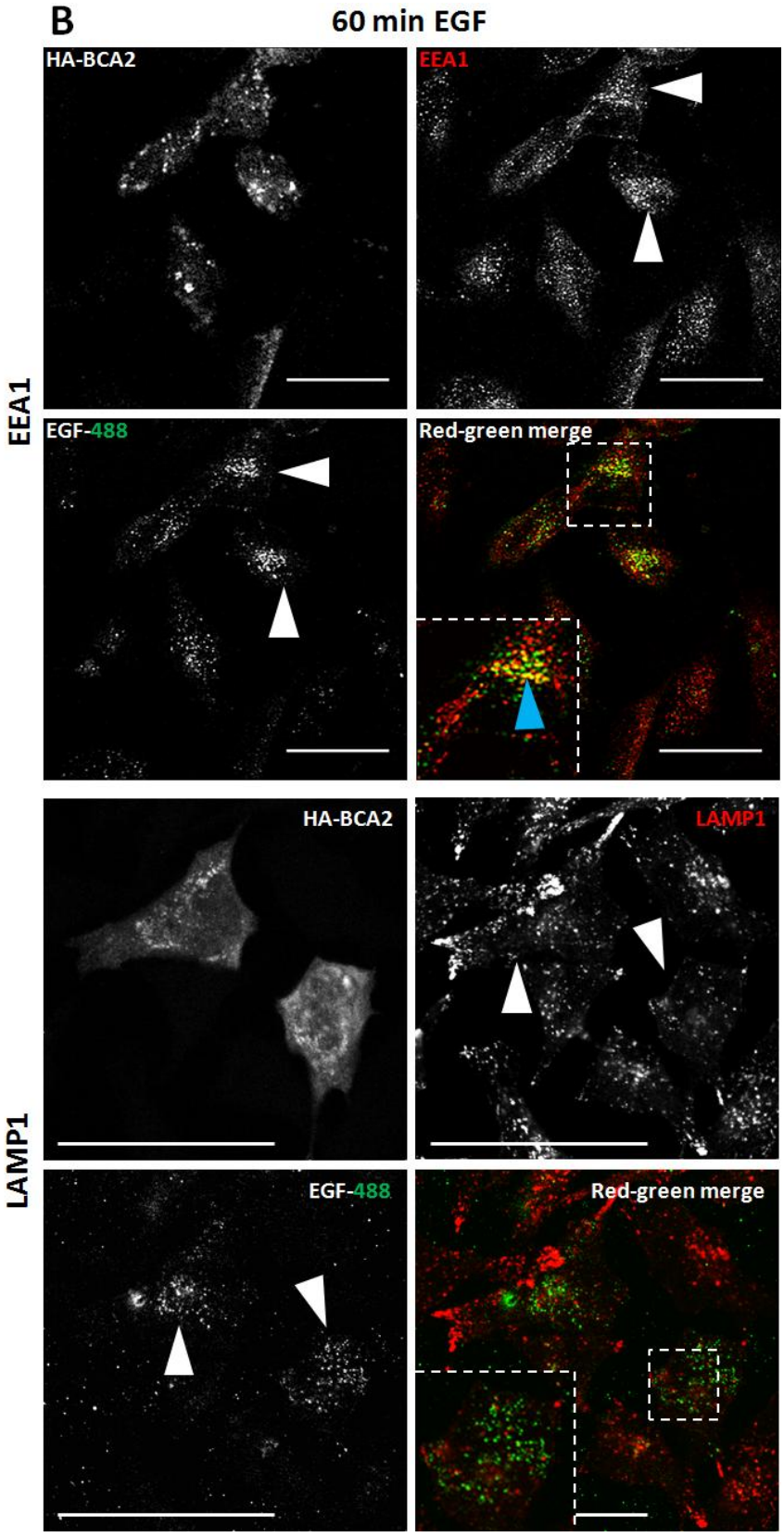

Figure 6-12: Confocal microscopy images showing the endocytic localisation of EGF Alexa-488 during trafficking in HA-BCA2 overexpressing HeLa cells. HA-BCA2 transfected cells were incubated with 0.5 ug/mL Alexa-488 EGF (green) for 15 min (A), or 60 min (B) before being fixed and immunolabelled for HA (far red) and either EEA1 or LAMP1 (red). *Scale bar = 50 µm. White arrowheads indicate examples of HA-BCA2 transfected cells. Blue arrowheads indicate colocalisation.*

6.9 The effect of BCA2 overexpression on downstream EGFR signalling in HeLa cells

Upon EGF binding and receptor dimerisation, the intracellular domain of EGFR becomes phosphorylated. Activation of EGFR initiates downstream activation of oncogenic signalling, predominantly via the MAPK and PI3K/Akt pathways. EGFR is internalised following activation and there is a strong body of evidence to indicate that EGFR continues actively signalling during endocytosis. It has been shown that disrupting EGFR endocytosis, via mutation of the endocytic protein dynamin, inhibits ligand-induced activation of PI3K and ERK1/2 (Vieira *et al*. 1996). This finding suggested that internalisation of EGFR was required for some components of downstream signalling. In another study, signalling proteins were shown to be recruited to endosomes and to induce activation of Akt and ERK1/2 in response to EGFR signals generated from early endosomes, post-receptor internalisation. Cells were stimulated with EGF in the presence of inhibitors that prevented EGFR activation and recycling but allowed internalisation. When the inhibitors were then withdrawn after ligand stimulation, endosome signalling of EGFR was initiated and lead to downstream stimulation of pro-survival signalling pathways (Wang *et al*. 2002).

Since EGFR is capable of signalling following internalisation, it was hypothesised that BCA2 induced changes in receptor trafficking and degradation rate might give rise to differences in downstream signalling pathways. Three independent experiments were performed to test this hypothesis. HA-BCA2 or mock transfected HeLa cells were serum starved then stimulated with 20 ng/mL of EGF for 5 or 60 min before

lysates were collected on ice. No baseline phosphorylation of EGFR was observed in unstimulated cells (data not shown) so a 5 min pulse of EGF was selected as the starting point. 5 min EGF stimulation was sufficient to provide a measure of the initial EGFR activation and signalling response with no/minimal endocytic downregulation effects on receptor levels. The cell lysates were subjected to Western blotting for HA and a panel of signalling proteins: phosphorylated EGFR (pEGFR) and total EGFR, phosphorylated and total Akt and phosphorylated and total ERK1/2. The complete panel of immunoblots shown in Figure 6-13 A was achieved by stripping and re-probing of PVDF membranes cut into low and high molecular weight strips. Band intensities were quantified using ImageJ software and protein activation was determined by the ratio of phosphoprotein to total protein (Fig. 6-13 B, D and E). Activation of EGFR was also examined in terms of the ratio of pEGFR to total Akt. In this instance total Akt acted as a loading control and enabled further information to be obtained about the relative proportion of active EGFR while taking into account changes in total protein levels (Fig. 6-13 C).

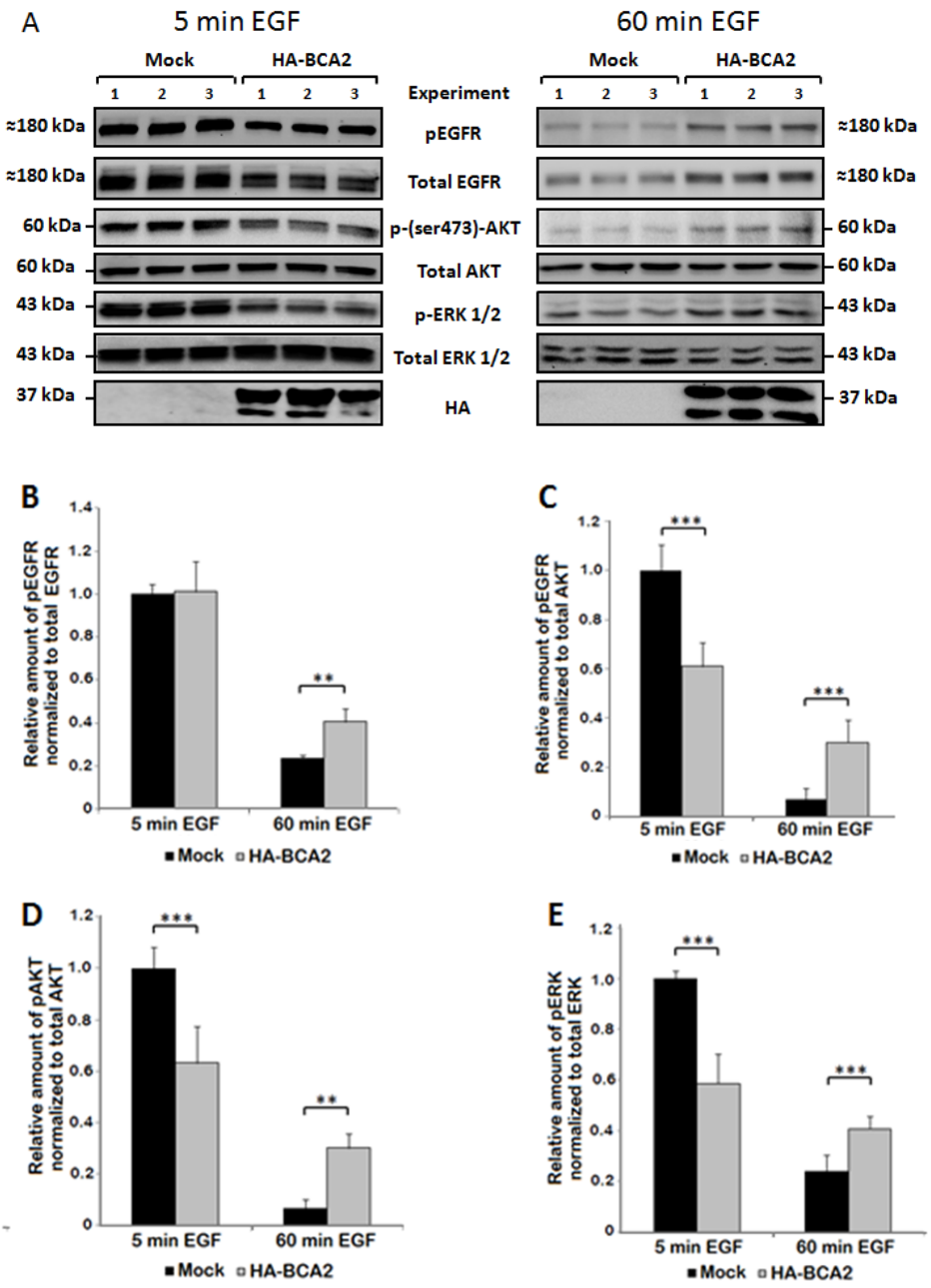

Figure 6-13: Immunoblots of EGFR activation and signalling in HA-BCA2 overexpressing HeLa cells following EGF stimulation. HA-BCA2 and mock transfected cells were serum starved for 60 min then stimulated with 20 ng/mL EGF for 5 or 60 min. Cell lysates were collected in three independent experiments. A) Western blotting was performed for EGFR, pEGFR, AKT, pAKT, ERK, pERK and HA. B) Band intensities were quantified using ImageJ software. *Error bars represent 95% confidence intervals. ** statistical significance* $p \leq 0.01$. **** statistical significance* $p \leq 0.001$.

Quantification and student's independent two-tailed t-test of the immunoblotting data in Figure 6-13 A revealed that after 5 min EGF stimulation there was a significant reduction in total EGFR, pEGFR, p

Akt and pERK in BCA2 overexpressing HeLa cells compared with mock transfected controls (6-13 C, D and E). Conversely, although there was a fall in both transfected and untransfected cells, after 60 min EGF stimulation, significantly more EGFR, Akt and ERK remained active in those overexpressing BCA2 (Fig. 6-13 B, D and E). The changes in EGFR activation at the early time point were proportional to the reduction in total receptor level. However, after an hour of EGF stimulation, the increase in pEGFR activation in HA-BCA2 overexpressing cells relative to controls was greater than the increase in total EGFR i.e. in HA-BCA2 overexpressing cells at 60 min post-EGF stimulation, a greater proportion of the remaining EGFR was active.

6.10 The effect of BCA2 overexpression on HeLa cell viability

The results from the signalling experiment indicated that BCA2 overexpression permits a downstream EGFR signalling response of reduced magnitude (at 5 min) but prolonged duration (at 60 min) in EGF stimulated HeLa cells. Cell viability studies were conducted to see whether these changes in signalling translated to changes in cell behaviour. To this end: 24 hr post-transfection HA-BCA2 or Mock transfected HeLa cells were serum starved in SFM for 1 hr. Cells were then either grown in reduced serum media (0.5% FBS) or in media supplemented with 10% FBS or 20 ng/ml EGF for 48 hr. Cell Viabilities were analysed by CellTitre-Blue assay. Three-independent, triplicate experiments were conducted and data was processed by converting mean fluorescence intensity values to “cell viability” as a percentage of mock-transfected controls grown in complete media (10% serum). The data in

Fig. 6-14 demonstrate that the viability of HA-BCA2 overexpressing cells was significantly less than controls in all tested conditions. For cells grown in complete media (10% serum): viability of the HA-BCA2 transfected population was ~20% lower than the mock transfected controls (viability = 82% and 100% respectively). Both BCA2 and mock transfected cells grown in reduced serum media showed diminished viability compared with those grown in 10% serum: viabilities were 46% and 53% respectively. The HA-BCA2 overexpressing cells therefore demonstrated a ~15% reduction in viability compared with mock transfected cells under the same conditions. Mock transfected cells grown in media supplemented with 20 ng/mL EGF showed approximately equal cell viability with those grown in complete media (viability = 96%). The viability of BCA2 overexpressing cells was 70% of the complete media control which equated to a 27% reduction in viability compared to the mock transfected cells grown with EGF.

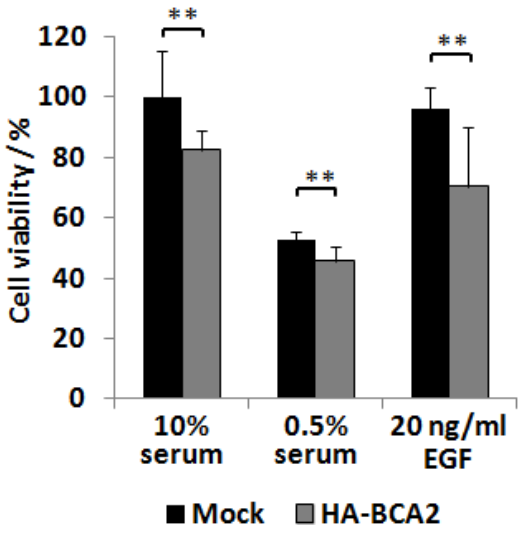

Figure 6-14: The effect of BCA2 overexpression on the viability of transiently transfected HeLa cells. HA-BCA2 or Mock transfected cells were either serum-starved or grown in the presence of 10% FBS or 20 ng/ml EGF for 48 hr. Cell Viabilities were analysed by CellTitre- Blue™ assay. Results from three independent, triplicate experiments were normalised relative to mock transfected control cells grown in FBS. *Error bars represent 95% confidence intervals. ** statistical significance $p \leq 0.001$.*

Mitochondria are key regulators of cell viability: they are the source of cellular energy and have a critical role in apoptosis via cytochrome c release and activation of caspases. Caspases are cysteine proteases that are responsible for the degradation of intracellular proteins in apoptosis (Gottlieb 2000). Mitochondria make use of oxidisable substrates generated by glycolysis to maintain a proton gradient across their inner membrane. It has been shown that the concentration of external growth factors can influence the delivery of oxidisable substrates to the mitochondria. Reduction in interleukin-3 (IL-3) availability leads to a loss of mitochrondrial membrane potential and sustained withdrawal induces apoptosis. (Vander Heiden *et al.* 2001). Changes in mitochondrial morphology associated with a loss in cell viability have been associated with growth factor withdrawal. Reduced IL-3 concentration causes mitochondria to condense due to reconfiguration of the mitochondrial matrix in response to lost membrane potential (Gottlieb *et al*. 2003).

To see whether the mitochondria of HeLa cells were affected by BCA2 overexpression, confocal microscopy was performed on HA-BCA2 transfected cells incubated with the fluorescent mitochondrial probe Mitotracker Red and immunolabelled for HA. Figure 6-15 indicates that HA-BCA2 overexpressing cells were associated with a slightly more condensed mitochondrial phenotype with some loss of the filamentous morphology typically seen in the control cells. There was no apparent decrease in Mitotracker fluorescence intensity that would correspond to a loss of membrane potential. There was however a suggestion that in

some transfected cells HA-BCA2 co-localised with the condensed mitochondria; this is demonstrated by areas of yellow fluorescence in the merge image indicated by arrowheads. HA-BCA2 colocalisation with mitochondria and alteration in mitochondrial structure were not previously observed in equivalent experiments performed in MCF-7 cells (Fig. 4-21 E).

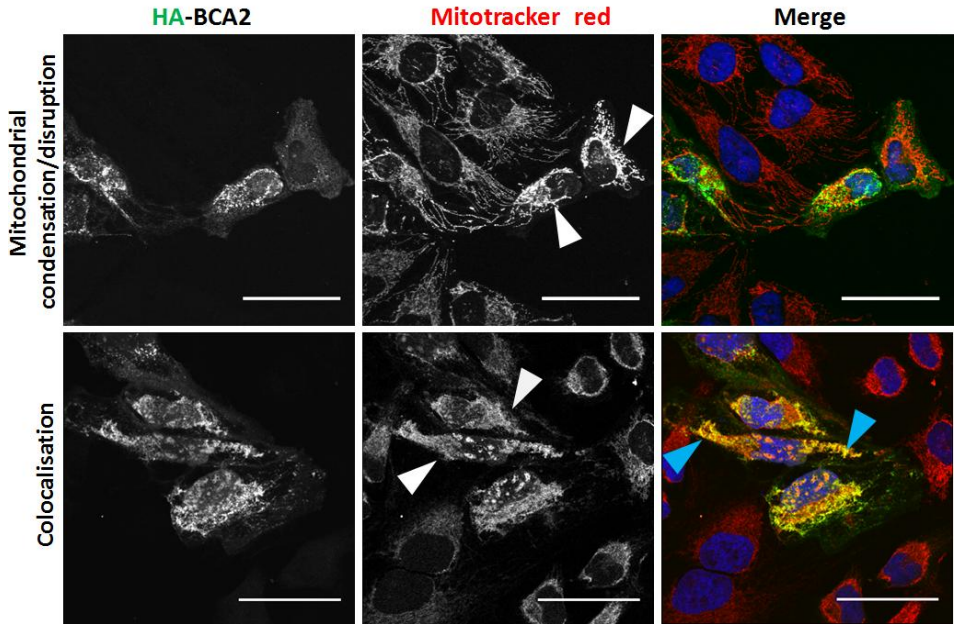

Figure 6-15: Confocal microscopy image showing mitochondrial morphology and colocalisation with HA-BCA2 in transfected HeLa cells. HA-BCA2 overexpressing cells were incubated with Mitotracker red for 30 min prior to fixation. Immunofluoresnce labelling for HA (green) was then performed and nuclei were stained blue with Hoechst. *White arrowheads indicate transfected cells, blue arrowheads indicate colocalisation. Scale bars = 50 µm.*

6.11 The relationship between BCA2 and Rab7 in HeLa cells.

BCA2 and Rab7 (also called Rab7a) have been shown to interact and in agreement with this colocalisation was found between EGFP-Rab7 and HA-BCA2 in dual-transfected MCF-7 cells (Fig. 4-26 A). HeLa were simultaneously transfected with HA-BCA2 and either EGFP-tagged Rab7a, Rab7b, Rab5 or Rab21. Rab7b was chosen since this protein has

been shown to 50% identity and 65% similarity with Rab7 (Yang *et al*. 2004).

IF for HA was performed and cells were imaged by confocal microscopy. The images in Figure 6-16 provide evidence of HA-BCA2 colocalisation with all the tested EGFP-Rab proteins.

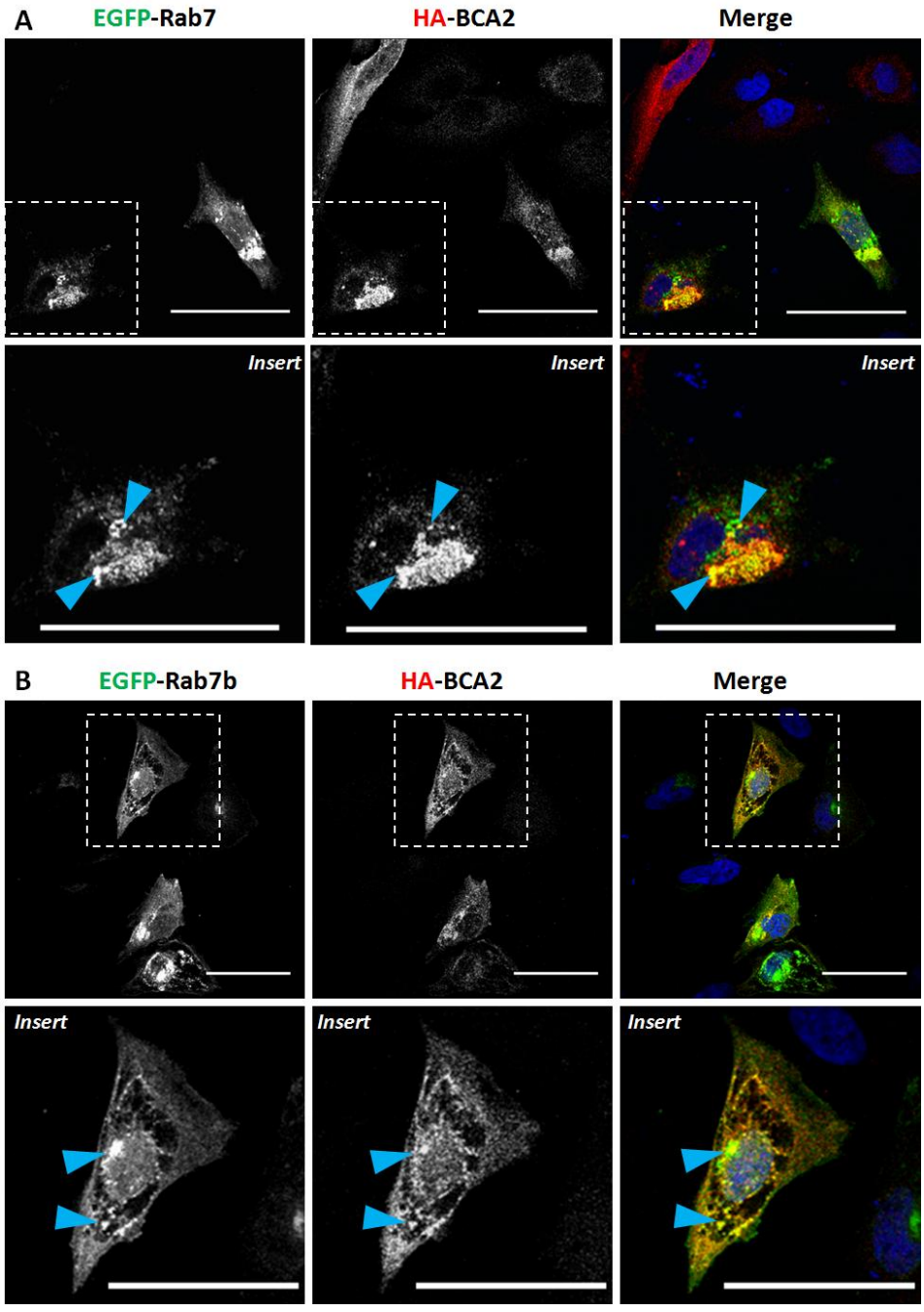

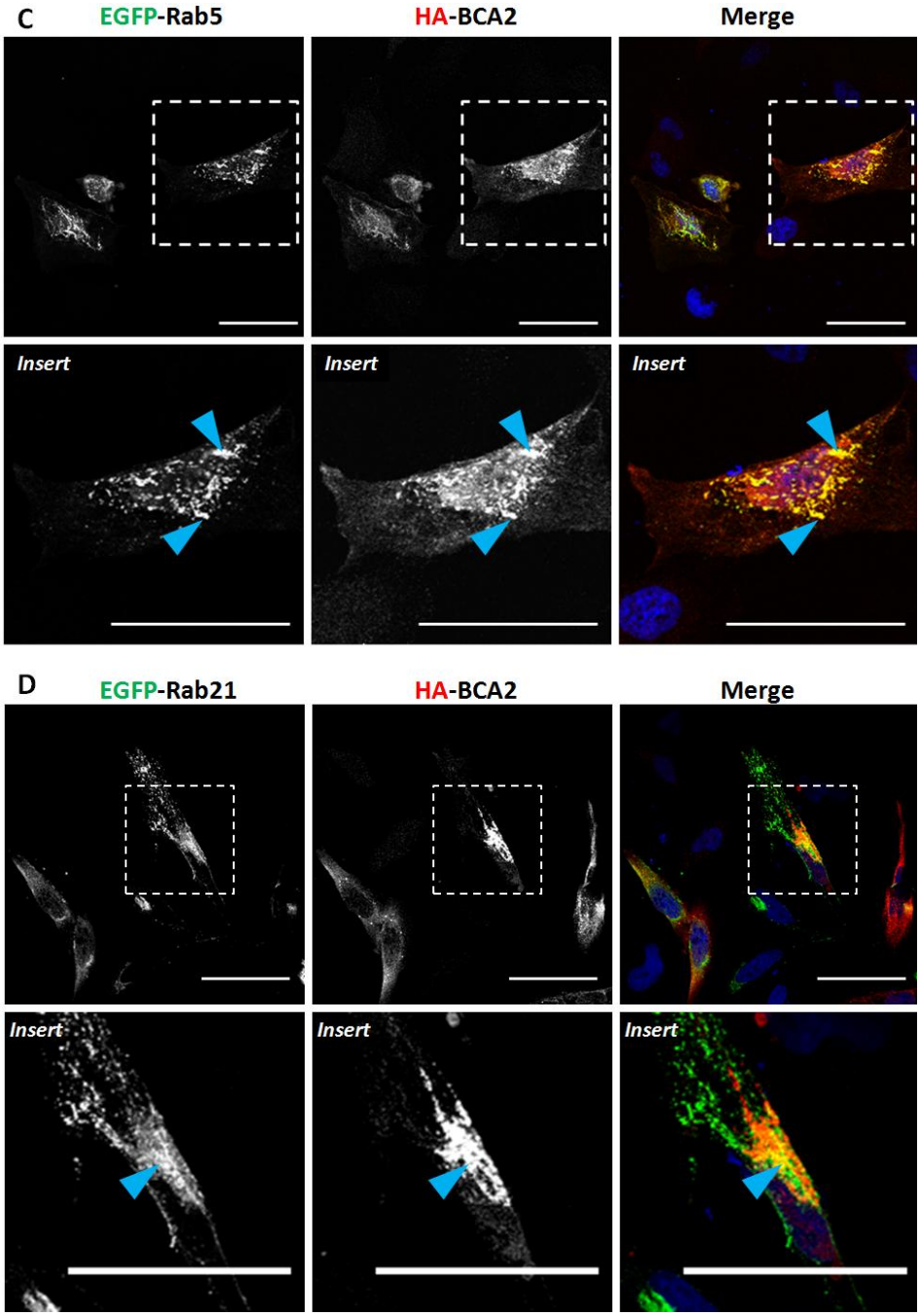

Figure 6-16: Confocal microscopy images of HeLa cells cotransfected with HA-BCA2 and selected EGFP-tagged Rab proteins. Cells were transiently transfected with HA-BCA2 and A) EGFP-Rab7, B) EGFP-Rab7b, C) EGFP-Rab5 and D) EGFP-Rab21. IF was performed for HA (red) and nuclei were stained blue with Hoechst. *Blue arrowheads indicate colocalisation. Scale bars = 50 µm.*

BCA2 had only previously been shown to co-localise with Rab7 and this was deemed specific since BCA2 did not colocalise with Rab4 or Rab8 (Mizuno *et al*. 2003). Since we had not been able to demonstrate specificity of HA-BCA2 colocalisation with EGFP-Rab7 we decided to

examine the effects of HA-BCA2 overexpression on endogenous Rab7. In order to achieve this an IF protocol needed to be developed and optimised to detect endogenous Rab7. The optimised IF protocol deviated from the standard IF method and mirrored the protocol for anti-LC3B labelling (Fig. 4-24). For Rab7 IF: 0.3% Triton-X was in the blocking buffer and antibody diluent (which were made with 5% and 3% BSA respectively). The primary antibody incubation step was performed overnight in a 12-well plate enclosed in a humidified chamber. An example of the Rab7 immunofluorescence produced in HeLa is shown in Figure 6-17. Clusters of Rab7 positive vesicles were apparent in the perinuclear region of cells, typical of the morphology and subcellular localisation of late endolysosomal structures (Korolchuk *et al*. 2011).

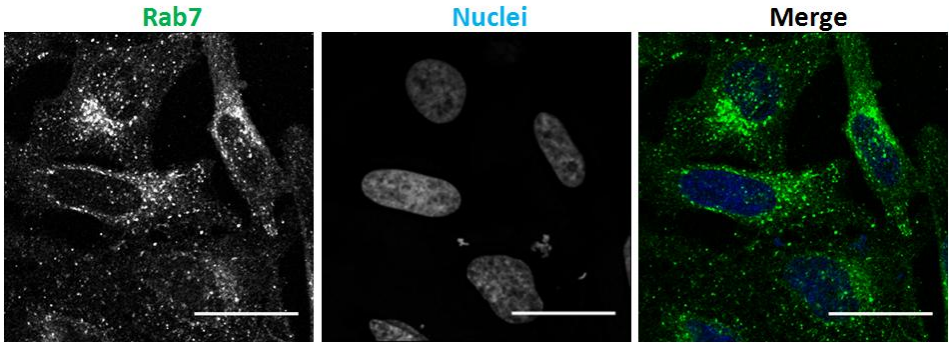

Figure 6-17: Confocal microscopy images of optimised Rab7 immunofluorescence in HeLa cells. Cells were PFA fixed then permeabilised and blocked before being immunolabelled overnight at 4ºC with anti-Rab7 antibody (1:100) in diluent buffer. Secondary antibody incubation was performed the following day and was preceded and followed by PBS washes. Nuclei were stained blue with Hoechst. *Scale bars = 25 µm.*

Using the optimised Rab7 IF method, HeLa cells that had been transiently transfected with HA-BCA2 were sequentially labelled first for Rab7 then for HA. The Rab7 protocol was followed up to the final wash steps then the standard immunofluorescence protocol was followed for HA, starting with the blocking step in 2% BSA, 2% FBS. The doubly-

labelled cells were eventually imaged by confocal microscopy. As seen previously in Fig. 6-17, the untransfected cells featured perinuclear clusters of Rab7 positive vesicles. In the HA-BCA2 overexpressing cells there was a marked reduction Rab7 fluorescence and in the number of the Rab7 positive vesicles (Fig. 6-18). Contrary to expected findings, based on the literature (Mizuno *et al.* 2003) and our EGFP-Rab7 data in HeLa (Fig. 6-16A) and in MCF-7 cells (Fig 4-26), there was no evidence of colocalisation between HA-BCA2 and Rab7.

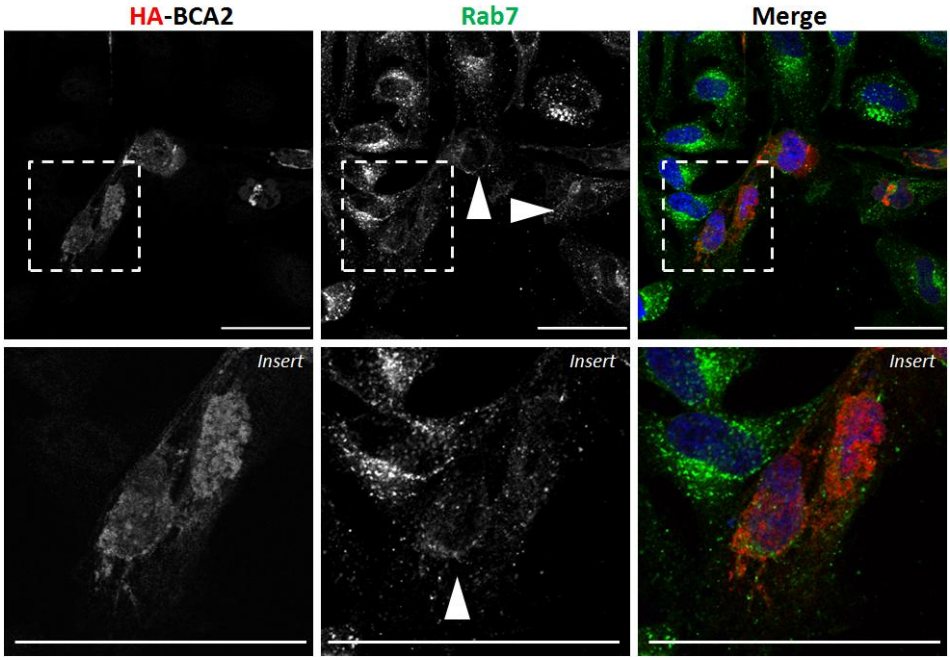

Figure 6-18: Confocal microscopy images of Rab7 in HA-BCA2 overexpressing HeLa cells. HA-BCA2 overexpressing cells were subject to sequential IF for Rab7 (green) then HA (Red). Nuclei were stained blue with Hoechst. *Arrowheads indicate examples of HA-BCA2 transfected cells. Scale bars = 50 µm.*

Rab proteins are able to associate with intracellular membranes through geranylgeranyl lipid groups which are attached to the Rab carboxy terminus by Rab geranylgeranyl transferase (RGGT). This post-translational modification is known as prenylation and is critical for Rab membrane targeting and association. Unprenylated Rabs remain

cytosolic and are unable to carry out their roles in vesicle docking and fusion (Pfeffer and Aivazian 2004).

The reduction in vesicular Rab7 labelling seen in Figure 6-18 could have been the result of the protein remaining cytosolic or be due to a decrease in Rab7 protein levels in the transfected cells. Therefore, to help interpret the IF data, Western blotting for Rab7 was performed. Rab7 protein levels were examined in HA-BCA2 overexpressing and mock transfected HeLa after 5 and 60 min EGF incubation. Residual lysates from the signalling experiment in Figure 6-13 were repurposed for this experiment. The data in Figure 6-19 demonstrates that Rab7 levels were unchanged by HA-BCA2 overexpression at either time point with EGF. This suggests that the loss of vesicular Rab7 seen by IF was the result of altered localisation rather than a reduction in protein level.

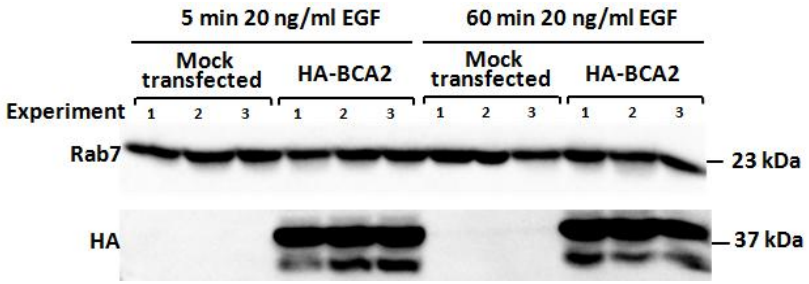

Figure 6-19: Immunoblot showing Rab7 levels in mock transfected and HA-BCA2 overexpressing HeLa following EGF stimulation. HA-BCA2 and mock transfected cells were serum starved for 60 min then stimulated with 20 ng/mL EGF for 5 or 60 min. Cell lysates were collected in three independent experiments. Western blotting was performed for HA and Rab7.

6.12 The effect of HA-BCA2 overexpression on early and late endosomal organelles

No significant HA-BCA2 induced effects on endolysosomal structure or localisation were observed in the EGF trafficking and EEA1/LAMP1 colocalisation experiment presented in Figure 6-12. However, given the

effect of BCA2 overexpression on Rab7 localisation (Fig. 6-18), early and late endosomes/lysosomes were re-examined in unstimulated cells. To investigate the effect of BCA2 on these endocytic organelles double-labelling of HA with EEA1 and with LAMP1 was performed in HA-BCA2 transfected HeLa. Results are presented in Figure 6-20.

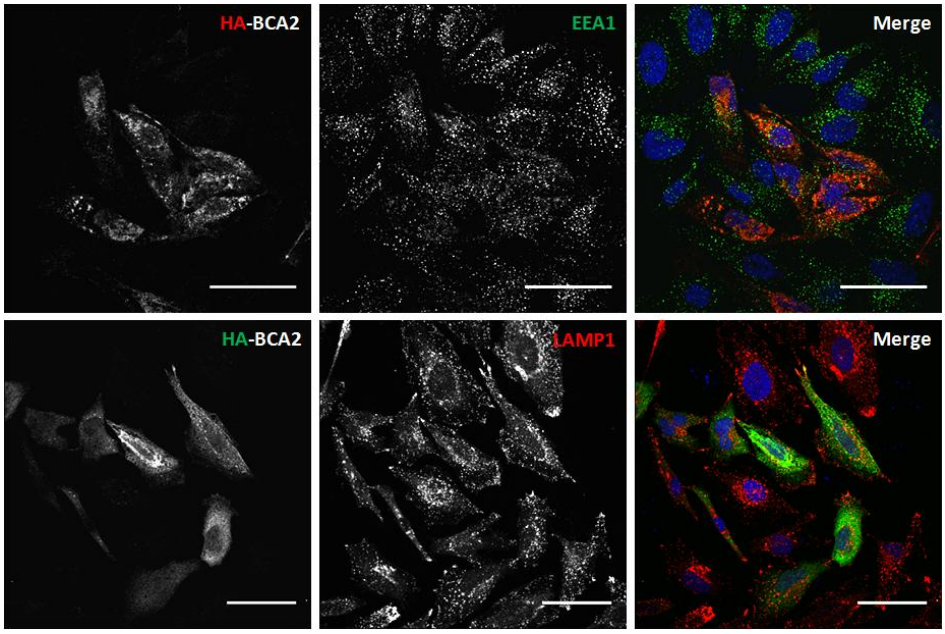

Figure 6-20: Confocal microscopy images showing the effects of HA-BCA2 overexpression on early and late endocytic organelles in HeLa cells. Cells were fixed and IF for HA-BCA2 and EEA1 or LAMP1 was performed. Nuclei were counterstained blue with Hoechst. *Scale bars = 50 µM.*

Mirroring observations made in EGF stimulated cells (Fig 6-12) no significant changes in early endosomes or late endolysosomes were detected in the HA-BCA2 overexpressing HeLa cells.

6.13 Discussion

The accumulated data for this thesis suggest that BCA2 has an important role in breast cancer with both positive and negative contributions and can have a regulatory function in the trafficking and expression of EGFR impacting on signalling and viability of cancer cells.

Correlation between BCA2 and ER expression has been described in the literature (Burger *et al*. 2005), and Chapter 3 here, and transcriptional regulation of BCA2 by the ER has been demonstrated (Kona *et al*. 2012). To some extent the correlation between expression of the two proteins is reflected in the findings presented in Figure 6-4. The highest, luminal A ER^+ cell lines MCF-7 and T47D showed the highest BCA2 expression, however the ER^- cell line MDA-MB-231 also had relatively high levels. The results suggest that while the ER may have a role in BCA2 regulation it is not obligate for expression. After HeLa, the MCF-10A breast epithelial cell line had the next lowest levels of BCA2. This is in keeping with the *in silico* findings that BCA2 expression increases with increasing malignant transformation of breast epithelial cells (Fig. 3-6) and also the lack of ER in this cell line. The $HER2^+$ BT474 cell line also showed relatively low BCA2 expression which is in line with *in silico* findings that BCA2 expression is reduced by HER2 expression (Fig. 3-11**)**. BCA2 expression at the protein level in the breast cell lines correlated with mRNA levels examined in Figure 3-4. The exception was the T47D cell line which appeared to express higher BCA2 levels than MCF-7s at the protein level but not the mRNA level. This might reflect a difference in BCA2 regulation between the two cell lines that may be specific for BCA2 or relate to global differences in proteasomal degradation of ubiquitinated proteins.

The data demonstrating that BCA2 overexpression reduces total levels of EGFR (Fig. 6-3 and 6-5) while inhibiting the receptors degradation (Fig.

6-7 to 6-13) initially appears to be contradictory. However, there are a number of possible theories that could reconcile this apparent paradox.

Others have shown that BCA2 interacts with Rab7 and supporting this we find co-localisation between EGFP-Rab7 and HA-BCA2 when they are co-expressed in MCF-7 (Fig. 4-26 A) and in HeLa (Fig. 6-16 A). Contrary to this however we do not see colocalisation between HA-BCA2 and endogenous Rab7; rather HA-BCA2 overexpression appears to induce a failure of Rab7 membrane association (Fig. 6-18 and 6-19). BCA2's interaction with Rab7 may help to explain these seemingly disparate findings with regards to EGFR levels and trafficking. The interaction between the GTP-bound (active) form of Rab7 and BCA2 has previously been shown to inhibit EGFR degradation (Mizuno *et al.* 2003). In other studies, siRNA depletion of Rab7 has been shown to inhibit lysosomal degradation of EGFR (Vanlandingham and Ceresa 2009). The strongest hypothesis to explain the data presented in this thesis is that overexpressed BCA2 sequesters Rab7 and prevents the GTPase from carrying out its endosomal function. In this manner BCA2 overexpression produces an effect analogous to Rab7 depletion i.e. it induces a *functional* Rab7 depletion. Such an effect is not uncommon with transient overexpression approaches: in a systematic study of overexpression systems ~23% of the phenotypes produced by overexpression were attributed to disruption of a stoichometric balance between interacting proteins (Sopko *et al*. 2006; Prelich 2012). Disruption of a stoichometric balance between BCA2 and its interactors may include effects on BCA2 regulation by deubiqutinating enzymes

(DUBs). As their name suggests, DUBs are responsible for the cleavage of ubiquitin moieties from Ub-tagged proteins. A BCA2 specific DUB has not been identified but it is likely that BCA2 has a partner DUB since they are known to associate with E3 ligases (Wilkinson 2009).

Other literature supporting the "functional Rab7 depletion" hypothesis are the findings from a study which showed that cellular transfection with Rab7 siRNA led to a concomitant decrease in total EGFR levels and an inhibition of EGFR degradation. In this study it was shown that Rab7 depletion rendered EGFR (and HER2) more susceptible to proteasome mediated degradation (Wang *et al.* 2011). Applying this to the "functional Rab7 depletion" hypothesis: overexpressed BCA2 may competitively inhibit Rab7's function at the late endosome thereby inhibiting *lysosomal* degradation of EGFR while potentially enhancing its *proteasomal* degradation. Counter to the Rab7 hypothesis is the data in Figure 6-20 showing that late endolysosomes are not significantly altered by HA-BCA2 overexpression. Rab7 depletion with siRNA has been associated with the enlargement of late endosomes (Vanlandingham and Ceresa 2009). However, no late endosomal enlargement was demonstrated in Figure 6-20 so further studies are required to confirm or refute the Rab7 hypothesis. One possibly informative experiment would be to conduct an autophagy induction experiment with serum starvation in HA-BCA2 overexpressing cells. If Rab7 function is impaired then autophagosome maturation will be inhibited and this would manifest as a reduction in the number of LC3B positive structures (Jäger *et al.* 2004). Also informative would be to

examine the effects of BCA2 on EGFR biosynthesis by carrying out RT-PCR experiments with/without BCA2 depletion and HA-BCA2 overexpression to determine whether EGFR mRNA levels were altered in addition to the protein level changes (Fig. 6-2, 6-3 and 6-5). Investigations of EGFR protein levels following HA-BCA2 expression in the presence of the proteasome inhibitor MG132 would also provide information regarding BCA2's influence on regulation of the receptor.

An alternative theory is that the inhibition of EGFR degradation arises *because* of the reduced EGFR levels (which may be reduced as result of enhanced proteasomal degradation or an alternative mechanism). Having fewer receptors on the cell surface reduces the chance of ligand binding and receptor dimerisation. This would in turn delay the internalisation and degradation of EGFR. It has been shown that reducing EGFR levels by RNA*i* leads to reduced dimerisation, ligand binding and activation (Chung *et al*. 2010). The effects of reduced EGFR levels on receptor endocytosis and endosomal signalling however have not been directly examined. One study demonstrated that decreased EGFR phosphorylation, prevents c-Cbl from associating with the receptor which in turn leads to reduced EGFR polyubiquitination and internalisation (Schmidt *et al*. 2003). The data in Figure 6-13 however show that the reduction in EGFR activity in HA-BCA2 overexpressing cells is proportional to the reduction in total receptor levels. The findings reported by Schmitt *et al.* were based on scenarios where EGFR phosphorylation was reduced by chemical inhibition or due to mutations in the intracellular domain i.e. total receptor levels were conserved but

the *proportion* of active receptors was reduced. It cannot therefore be inferred from these findings that the reduction in EGFR activity demonstrated in Fig. 6-13 could account for changes in EGFR degradation rate.

Another possible theory to explain the data presented in this chapter is that BCA2 overexpression leads to reduced degradation of EGFR and that intracellular accumulation of the receptor triggers apoptosis. In 2012 (Rush *et al.*) demonstrated that accumulation of EGFR in the early endosome, after blockade of late endocytic transport, gave rise to EGF induced apoptosis in HeLa cells. Apoptotic activation of caspase-3 has been shown to lead to direct enzymatic cleavage of EGFR which could then account for the reduced receptor levels (He *et al*. 2006). Potentially supporting this theory are the observations that: a) transfection of BCA2 into the EGFR overexpressing cell line MDA-MB-231 appears to be cytotoxic (Figs. 4-17 and 4-18). B) Overexpression of BCA2 in HeLa leads to decreased cell viability and disruption of the mitochondria (Figs. 6-14 and 6-15). C) Overexpression of BCA2 in (caspase-3-deficient) MCF-7 cells does not appear to affect the mitochondria of the cells (Fig. 4-21 E) and unlike in MDA-MB-231 cells, HA-BCA2 transfected MCF-7 cells appear to retain morphological integrity (Fig. 4-17 and 4-18).

BCA2 may also be triggering apoptosis by an unknown mechanism as caspase 3-mediated cleavage of EGFR during apoptosis has also been shown to be associated with a reduced rate of receptor degradation (He *et al*. 2005).

BCA2 has many putative interaction partners and it is not uncommon for proteins that have a variety of partners to have multiple, antagonistic functions. An example of such a protein is the E3 ligase Mdm2. Mdm2 downregulates the so called "guardian of the genome" p53 and its role as an oncogene is well documented. There is however increasing evidence that through its other binding partners Mdm2 may have a separate role as a tumour suppressor (Manfredi 2010). There may be a threshold expression level for BCA2 and either positive or negative deviations from this cause disruptions in functional pathways that produce similar global cellular effects. For example, Figure 6-14 demonstrates that BCA2 overexpression decreases cell viability while others have shown that viability is reduced by BCA2 depletion (Wang *et al*. 2013). Such findings are not paradoxical when viewed in the context of BCA2 having multiple cellular functions and/or interaction partners and in light of the collective evidence of context dependent BCA2 effects.

The findings that BCA2 overexpression inhibits EGFR trafficking (Figs. 6-7 to 6-13) are directly supported by some literature (Mizuno *et al*. 2003) but appear to be contrary to others (Smith *et al.* 2013).

In research published by (Sakane *et al*.) in 2007, BCA2 overexpression was suggested to accelerate ligand induced EGFR degradation. Interestingly, analysis of the Western blotting data from this study reveals that in the unstimulated cells the total amount of EGFR was lower in the BCA2 overexpressing cells. Quantification and statistical analysis were not performed/presented in the paper but using ImageJ software it was possible to roughly quantify the changes in EGFR.

Quantification suggested that BCA2 overexpression was associated with a reduction in total EGFR levels of ~25%, an observation not described in the publication but in keeping with the findings presented in Figures 6-3 and 6-5. Overexpression of BCA2 in the Sakane study appeared to enhance the degradation of EGFR by ~30%.

The HEK293 cell line used in the Sakane study did not appear to readily degrade EGFR in response to EGF stimulation: after three hours the receptor levels had still only been reduced to 80% in the mock transfected control cells. When compared with the large and rapid decrease in EGFR levels in HeLa cells shown in Figure 6-7 it is apparent that the two cell lines have very different receptor trafficking kinetics. HEK293 cells do not naturally express detectable levels of EGFR so in order to conduct the degradation experiment, EGFR and ubiquitin had to be transfected into the cells along with BCA2. This is a potentially important methodological difference between the investigations conducted in this thesis and those performed by Sakane *et al*.

Cells that do not express or have very low levels of a receptor may also lack other proteins that are needed for its regulation and function. In another experiment from the Sakane study, HEK293 cells were transfected with c-Cbl in addition to EGFR, ubiquitin and BCA2 or a vector control. A RING domain mutant of BCA2 was also examined as part of these experiments. c-Cbl expression greatly accelerated EGFR degradation in the control cells compared with the earlier experiment performed in its absence. After 1 hr EGF stimulation, receptor levels in the c-Cbl co-transfected cells were reduced to 18% of their starting

amount, significantly different from the drop to 80% that occurred without c-Cbl. Overexpression of BCA2 or the RING mutant in the presence of c-Cbl delayed receptor degradation compared with the control but the effect was more pronounced with the RING mutant.

In the experimental conditions that more closely mimic those of normal EGFR endocytosis i.e. in the presence of c-Cbl, EGFR degradation was shown to be inhibited by BCA2 overexpression, as here. The fact that the RING mutant produced a greater inhibitory effect than wild-type BCA2 is interesting and can potentially be explained by its interaction with Rab7. GTP-bound Rab7 interacts with the N-terminus of BCA2, a region of the protein that would potentially remain functionally intact in a RING mutant. Truncation mutants of BCA2 have been shown to retain their affinity for Rab7 *in vitro* (Mizuno *et al.* 2003). What the RING mutant lacks is the ability to autoubiquinate (Amemiya *et al*. 2008) so intracellular levels of this protein could be much higher than the wild-type protein would reach. If the Rab7 interacting domain was still present and functional this could explain Sakane *et al.*'s findings that RING mutant BCA2 has a more potent inhibitory effect on EGFR degradation than the wild-type protein.

As with many EGFR degradation experiments, the cells in the Sakane study were serum starved for a long duration (24 hr) prior to EGF stimulation. Extended serum starvation times are often used in research as a method for cell synchronisation. However despite its wide usage there is relatively little supporting evidence for serum starvation being an effective means of synchronising cells (Cooper 2003). Serum starvation

has also been shown to induce irregular and inconsistent signalling responses in different cell lines and experimental conditions (Pirkmajer and Chibalin 2011). For our experiments, serum starvation time was restricted to one hour in order to limit possible confounding experimental effects. For similar reasons we also refrained from using cyclohexamide (CHX) in our experiments. Although it is common to use CHX to inhibit protein synthesis when performing receptor degradation assays, the drug has been shown to induce EGFR internalisation in a ligand independent manner (Oksvold *et al*. 2012). To minimise the potential for added complexity and error CHX was omitted from our experiments.

The data in Fig. 6-16 raise some potentially important methodological questions about the validity of performing BCA2 and EGFP-Rab protein co-transfection. There was no apparent specificity of BCA2 for Rab7 compared with the other three EGFP-Rab proteins that were tested. Although Rab7a and Rab7b share a high level of sequence identity (Yang *et al*. 2004) the interaction properties of the two proteins have been shown to be very different (Stein *et al*. 2012). This study also demonstrated that Rab5 and Rab21 are dissimilar from each other and from Rab7a and -b in terms of their electrostatic charge. These findings would appear to reduce the likelihood that the Rab proteins share a common interaction partner in BCA2. Direct protein binding however is not obligate for co-localisation. For example, a study has demonstrated endosomal colocalisation of Rab5 and Rab7 in compartments thought to denote intermediary stages of early to late endosomal transport (Vonderheit and Helenius 2005)

Based on the findings in Figure 6-16, dual overexpression of BCA2 and EGFP-Rab proteins may not be an appropriate experimental approach for interrogating BCA2 function. However, Mizuno *et al.* showed colocalisation between BCA2 and EGFP-Rab7 but not with EGFP-Rabs 4 and 8 so some specificity has been previously demonstrated. Further experimental work to investigate the suitability of the co-transfection approach should therefore include EGFP-Rab4 and –Rab8 as putative negative controls.

The BCA2 research that invites the closest comparison and is potentially the most directly applicable to the work presented in this chapter is that conducted by (Smith *et al*.) in 2013. These studies also examined the relationship between BCA2 and EGFR trafficking using a HeLa cell model. Using a BCA2 depletion approach the group were able to demonstrate that reduction in BCA2 levels delays the degradation of EGFR. This was the first study to then examine EGFR activation and signalling and it was shown that BCA2 depletion lead to increased EGFR phosphorylation between 30 and 45 min following EGF stimulation. This was mirrored by an increased association between EGFR and the signalling protein SHC1 at these time points. We extend this work by showing novel downstream signalling effects, induced in a BCA2 overexpression system (Fig. 6-13). Our findings indicate that BCA2 overexpression leads to an initially smaller but ultimately more prolonged signalling response in MAPK (ERK1/2) and Akt pathways. The consequences of such a signalling pattern are not fully resolved, though it may well be the cause of the reduced cell viability seen in

Figure 6-14. There is very little in the literature about how signal magnitude and duration interact to control cell behaviour. Proliferation of fibroblasts is associated with sustained ERK1/2 activation ***or*** with weak activation, and fibroblast differentiation is associated with transient ***or*** strong ERK1/2 activity (Ebisuya *et al.* 2005). It might be a reasonable hypothesis to suggest that since weaker or more prolonged ERK1/2 activity are both associated with proliferation that enhanced growth would be the ultimate consequence of the combined signalling properties but this does not have a strong evidence base and would need to be tested. Fundamentally this is the basis of a computational question. Is a signal of half the size but twice the duration the same in the cellular context? We can consider this question in the context of two very simplified signalling scenarios. Figure 6-21 A shows a scenario with a signal of large size but short duration and Figure 6-21 B shows the result of a signal of half the strength and twice the duration. It can be seen that in terms of overall signalling output that there no difference between these two cases: the net result is that 4 signals are generated in each instance. This model quickly becomes much more complicated when you consider the multitude of signalling proteins and cell context. Further complexity is added if the spatial component of signalling is taken into consideration. As EGFR moves through the cell via endocytosis its active cytoplasmic tail remains exposed to the cytoplasm and so is exposed to a different pallet of substrates which coordinate different downstream effects (Burke *et al*. 2001). The subcellular localisation of EGFR has been shown to differentially regulate the

growth and survival of MDA-MB-468 breast cancer cells which overexpress the receptor (Hyatt and Ceresa 2008).

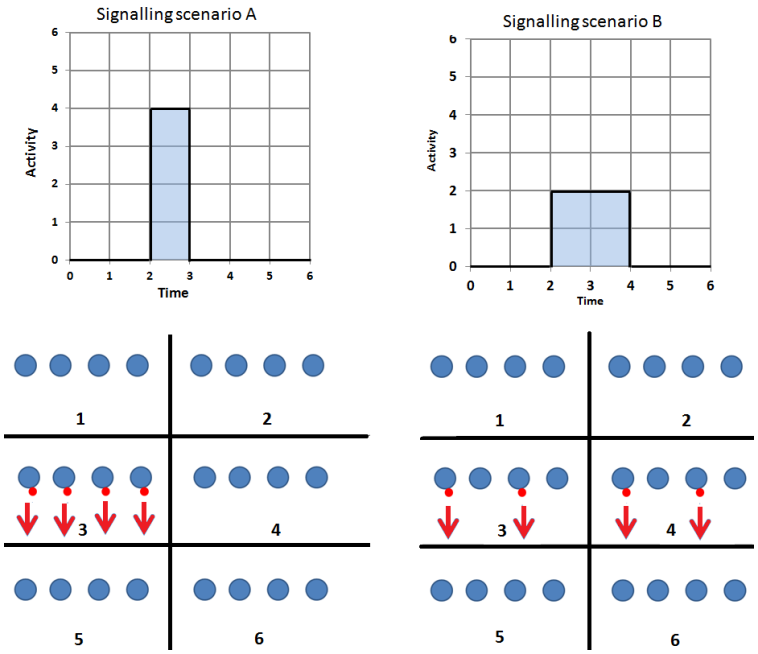

Figure 6-21: Simplified computational signalling illustration. A) Scenario with a signal of twice the size but half the duration. B) Scenario with a signal of half the size and twice the duration

Trying to interpret the possible cellular consequence of a signal of smaller size and altered duration is clearly not a simple matter but it presents an opportunity for future collaborations with systems biologists. Results of experiments run with some computational models of EGFR trafficking have been published and potentially have implications for this project, for example (Pérez-Jiménez and Romero-Campero 2006). Changes in EGF concentration in this model were shown to alter EGFR phosphorylation but had relatively little impact on downstream MEK activation. This is actually not surprising given that the lowest concentration of EGF tested in the model was 100 nM which is still equates to a large excess of ligand compared to receptor number. Unlike EGF concentration, alterations in receptor numbers profoundly impacted

on MEK phosphorylation. This supports our findings that in the EGFR reduced HA-BCA2 overexpressing cells downstream signalling is reduced (Fig. 6-13). It also highlights a limitation of the model that does not take into account changes in duration or receptor localisation.

Given the interaction between BCA2 and Rab7 we hypothesise an inter-related role for these two proteins in EGFR regulation and trafficking. The findings present an interesting insight into BCA2-mediated EGFR regulation through altered endocytosis.

6.14 References

Al Soraj, M. , He, L. , Peynshaert, K. , Cousaert, J. , Vercauteren, D. , Braeckmans, K. , De Smedt, S. and Jones, A. T. 2012. siRNA and pharmacological inhibition of endocytic pathways to characterize the differential role of macropinocytosis and the actin cytoskeleton on cellular uptake of dextran and cationic cell penetrating peptides octaarginine (R8) and HIV-Tat. *Journal of Controlled Release* 161(1), p. 132-41.

Amemiya, Y. , Azmi, P. and Seth, A. 2008. Autoubiquitination of BCA2 RING E3 ligase regulates its own stability and affects cell migration. *Molecular Cancer Research* 6(9), p. 1385.

Brahemi, G. , Kona, F. R. , Fiasella, A. , Buac, D. , Soukupová, J. , Brancale, A. , Burger, A. M. and Westwell, A. D. 2010. Exploring the structural requirements for inhibition of the ubiquitin E3 ligase breast cancer associated protein 2 (BCA2) as a treatment for breast cancer. *Journal of Medicinal Chemistry* 53(7), p. 2757-65.

Buac, D. , Kona, F. R. , Seth, A. K. and Dou, Q. P. 2013. Regulation of Metformin Response by Breast Cancer Associated Gene 2. *Neoplasia* 15(12), p. 1379-IN1312.

Burger, A. M. , Gao, Y. , Amemiya, Y. , Kahn, H. J. , Kitching, R. , Yang, Y. , Sun, P. , Narod, S. A. , Hanna, W. M. and Seth, A. K. 2005. A novel RING-type ubiquitin ligase breast cancer-associated gene 2 correlates with outcome in invasive breast cancer. *Cancer research* 65(22), p. 10401.

Burke, P., Schooler, K. and Wiley, H.S. 2001. Regulation of epidermal growth factor receptor signaling by endocytosis and intracellular trafficking. *Molecular Biology of the Cell* 12, p. 1897-1910.

Chung, I. , Akita, R. , V, len, R. , Toomre, D. , Schlessinger, J. and Mellman, I. 2010. Spatial control of EGF receptor activation by reversible dimerization on living cells. *Nature* 464(7289), p. 783-87.

Cooper, S. 2003. Rethinking synchronization of mammalian cells for cell cycle analysis. *Cellular and Molecular Life Sciences CMLS* 60(6), p. 1099-1106.

Davidson, N. E. , Gelmann, E. P. , Lippman, M. E. and Dickson, R. B. 1987. Epidermal growth factor receptor gene expression in estrogen receptor-positive and negative human breast cancer cell lines. *Molecular Endocrinology* 1(3), p. 216-23.

Decker, S. J. 1988. Epidermal growth factor induces internalization but not degradation of the epidermal growth factor receptor in a human breast cancer cell line. *Journal of Receptors and Signal Transduction* 8(6), pp. 853-870.

Ebisuya, M., Kondoh, K. and Nishida, E. 2005. The duration, magnitude and compartmentalization of ERK MAP kinase activity: mechanisms for providing signaling specificity. *Journal of Cell Science* 118(Pt 14), p. 2997-3002.

Gottlieb, E. , Armour, S. , Harris, M. and Thompson, C. 2003. Mitochondrial membrane potential regulates matrix configuration and cytochrome c release during apoptosis. *Cell Death & Differentiation* 10(6), p. 709-17.

Gottlieb, R. A. 2000. Mitochondria: execution central. *FEBS letters* 482(1), p. 6-12.

He, Y. , Huang, J. and Chignell, C. 2005. Cleavage of epidermal growth factor receptor by caspase during apoptosis is independent of its internalization. *Oncogene* 25(10), p. 1521-31.

Hyatt, D. C. and Ceresa, B. P. 2008. Cellular localization of the activated EGFR determines its effect on cell growth in MDA-MB-468 cells. *Experimental Cell Research* 314(18), p. 3415-25.

Jäger, S. , Bucci, C. , Tanida, I. , Ueno, T. , Kominami, E. , Saftig, P. and Eskelinen, E. L. 2004. Role for Rab7 in maturation of late autophagic vacuoles. *Journal of Cell Science* 117(20), p. 4837.

Kona, F. R. , Stark, K. , Bisoski, L. , Buac, D. , Cui, Q. and Dou, Q. P. 2012. Transcriptional activation of breast cancer-associated gene 2 by estrogen receptor. *Breast Cancer Research and Treatment*, p. 1-9.

Korolchuk, V. I. , Saiki, S. , Lichtenberg, M. , Siddiqi, F. H. , Roberts, E. A. , Imarisio, S. , Jahreiss, L. , Sarkar, S. , Futter, M. and Menzies, F. M. 2011. Lysosomal positioning coordinates cellular nutrient responses. *Nature Cell Biology* 13(4), p. 453-60.

Manfredi, J. J. 2010. The Mdm2–p53 relationship evolves: Mdm2 swings both ways as an oncogene and a tumor suppressor. *Genes & Development* 24(15), p. 1580-89.

Miyakawa, K. , Ryo, A. , Murakami, T. , Ohba, K. , Yamaoka, S. , Fukuda, M. , Guatelli, J. and Yamamoto, N. 2009. BCA2/Rabring7 promotes tetherin-dependent HIV-1 restriction. *PLoS Pathogens* 5(12), p. e1000700.

Mizuno, K. , Kitamura, A. and Sasaki, T. 2003. Rabring7, a novel Rab7 target protein with a RING finger motif. *Molecular Biology of the Cell* 14(9), p. 3741-52.

Oksvold, M. P. , Pedersen, N. M. , Forfang, L. and Smeland, E. B. 2012. Effect of cycloheximide on epidermal growth factor receptor trafficking and signaling. *FEBS letters* 586(20), p. 3575-581.

Pereira, P., Pedrosa, S. S., Wymant, J., Sayers, E., Correia, A., Vilanova, M., Jones, A. T., and Gama, F. M. 2015, *accepted.* siRNA inhibition of endocytic pathways to characterise the cellular uptake mechanisms of folic acid functionalised glycol chitosan nanogels. *Molecular Pharmaceutics*.

Pfeffer, S. and Aivazian, D. 2004. Targeting Rab GTPases to distinct membrane compartments. *Nature Reviews Molecular Cell Biology* 5(11), pp. 886-896.

Pirkmajer, S. and Chibalin, A. V. 2011. Serum starvation: caveat emptor. *American Journal of Physiology-Cell Physiology* 301(2), p. C272-C279.

Prelich, G. 2012. Gene overexpression: uses, mechanisms, and interpretation. *Genetics* 190(3), p. 841-54.

Pérez-Jiménez, M. J. and Romero-Campero, F. J. 2006. P systems, a new computational modelling tool for systems biology.*Transactions on Computational Systems Biology VI*. Springer, p. 176-97.

Roepstorff, K. , Gr, al, M. V. , Henriksen, L. , Knudsen, S. L. J. , Lerdrup, M. , Grøvdal, L. , Willumsen, B. M. and Van Deurs, B. 2009. Differential effects of EGFR ligands on endocytic sorting of the receptor. *Traffic* 10(8), p. 1115-27.

Rush, J. S. , Quinalty, L. M. , Engelman, L. , Sherry, D. M. and Ceresa, B. P. 2012. Endosomal accumulation of the activated epidermal growth factor receptor (EGFR) induces apoptosis. *Journal of Biological Chemistry* 287(1), p. 712-22.

Sakane, A. , Hatakeyama, S. and Sasaki, T. 2007. Involvement of Rabring7 in EGF receptor degradation as an E3 ligase. *Biochemical and Biophysical Research Communications* 357(4), p. 1058-64.

Schmidt, M. H. , Furnari, F. B. , Cavenee, W. K. and Bögler, O. 2003. Epidermal growth factor receptor signaling intensity determines intracellular protein interactions, ubiquitination, and internalization. *Proceedings of the National Academy of Sciences* 100(11), p. 6505-10.

Sigismund, S. , Algisi, V. , Nappo, G. , Conte, A. , Pascolutti, R. , Cuomo, A. , Bonaldi, T. , Argenzio, E. , Verhoef, L. G. and Maspero, E. 2013. Threshold-controlled ubiquitination of the EGFR directs receptor fate. *The EMBO journal* 32(15), p. 2140-57.

Sigismund, S. , Argenzio, E. , Tosoni, D. , Cavallaro, E. , Polo, S. and Di Fiore, P. P. 2008. Clathrin-mediated internalization is essential for sustained EGFR signaling but dispensable for degradation. *Developmental Cell* 15(2), p. 209-19.

Sigismund, S. , Woelk, T. , Puri, C. , Maspero, E. , Tacchetti, C. , Transidico, P. , Di Fiore, P. P. and Polo, S. 2005. Clathrin-independent endocytosis of ubiquitinated cargos. *Proceedings of the National Academy of Sciences of the United States of America* 102(8), p. 2760-65.

Smith, C. J. , Berry, D. M. and McGlade, C. J. 2013. The E3 ubiquitin ligases RNF126 and Rabring7 regulate endosomal sorting of the epidermal growth factor receptor. *Journal of Cell Science* 126(6), p. 1366-80.

Sopko, R. , Huang, D. , Preston, N. , Chua, G. , Papp, B. , Kafadar, K. , Snyder, M. , Oliver, S. G. , Cyert, M. and Hughes, T. R. 2006. Mapping pathways and phenotypes by systematic gene overexpression. *Molecular Cell* 21(3), p. 319-30.

Stein, M. , Pilli, M. , Bernauer, S. , Habermann, B. H. , Zerial, M. and Wade, R. C. 2012. The interaction properties of the human Rab GTPase family–a comparative analysis reveals determinants of molecular binding selectivity. *PloS One* 7(4), p. e34870.

Vander Heiden, M. G. , Plas, D. R. , Rathmell, J. C. , Fox, C. J. , Harris, M. H. and Thompson, C. B. 2001. Growth factors can influence cell growth and survival through effects on glucose metabolism. *Molecular and Cellular Biology* 21(17), p. 5899-912.

Vanlandingham, P. A. and Ceresa, B. P. 2009. Rab7 regulates late endocytic trafficking downstream of multivesicular body biogenesis and cargo sequestration. *Journal of Biological Chemistry* 284(18), p. 12110-24.

Vieira, A. V. , Lamaze, C. and Schmid, S. L. 1996. Control of EGF receptor signaling by clathrin-mediated endocytosis. *Science* 274(5295), p. 2086-9.

Vonderheit, A. and Helenius, A. 2005. Rab7 associates with early endosomes to mediate sorting and transport of Semliki forest virus to late endosomes. *PLoS Biology* 3(7), p. e233.

Wang, T. , Zhang, M. , Ma, Z. , Guo, K. , Tergaonkar, V. , Zeng, Q. and Hong, W. 2011. A role of Rab7 in stabilizing EGFR-Her2 and in sustaining Akt survival signal. *Journal of Cellular Physiology* 227(6), p. 2788-97.

Wang, Y. , Pennock, S. , Chen, X. and Wang, Z. 2002. Endosomal signaling of epidermal growth factor receptor stimulates signal transduction pathways leading to cell survival. *Molecular and Cellular Biology* 22(20), pp. 7279-90.

Wang, Z. , Nie, Z. , Chen, W. , Zhou, Z. , Kong, Q. , Seth, A. K. , Liu, R. and Chen, C. 2013. RNF115/BCA2 E3 ubiquitin ligase promotes breast cancer cell proliferation through targeting p21Waf1/Cip1 for ubiquitin-mediated degradation. *Neoplasia (New York, NY)* 15(9), p. 1028.

Wilkinson, K.D. 2009. DUBs at a glance. Journal of Cell Science 122(Pt 14), p.2325-9.

Yang, M. , Chen, T. , Han, C. , Li, N. , Wan, T. and Cao, X. 2004. Rab7b, a novel lysosome-associated small GTPase, is involved in monocytic differentiation of human acute promyelocytic leukemia cells. *Biochemical and Biophysical Research Communications* 318(3), p. 792-9.

Chapter 7: General Discussion

Since BCA2 was first discovered in 2003, interest in the protein (originally named Rabring7) has been steadily increasing. As the pool of BCA2 research has expanded so too has the apparent conflict in the literature surrounding the protein's role in receptor trafficking and breast cancer. In addition to gaining more functional information on BCA2 and thus extending the research field, this project aimed to address and explain some of the disparities in the existing BCA2 literature. In these respects the project has been fairly successful.

Meeting the aim of describing BCA2's subcellular localisation was impinged by the limited availability of reliable commercial antibody resources. Extensive preliminary optimisation and validation work for BCA2 and endosome markers (including Rab7) needed to be carried out before basic experiments could be performed. However, the development of reliable methods of determining the subcellular distribution of endocytic proteins such as EEA1 and LAMP2 in addition to robust siRNA and Western blotting methods led to two small collaborations. The collaborations resulted in one publication (Webber *et al.* 2015) and a manuscript that is currently under review (Pereira *et al.* 2015, *accepted*).

Ultimately it was through the use of a transient overexpression system and confocal microscopy techniques that the most detailed images of BCA2 localisation were produced. In line with published findings (Mizuno *et al.* 2003) evidence of colocalisation between overexpressed BCA2 and Rab7 was obtained via co-transfection of epitope tagged

proteins. However, diverging/extending from previous reports, BCA2:Rab colocalisation was not found to be unique to Rab7. Co-transfection results also demonstrated BCA2 colocalisation with EGFP tagged Rab5, Rab21 and Rab7b. Further experiments would need to be conducted to ascertain whether the colocalisation was a universal phenomenon for all EGFP-Rab proteins and therefore, potentially, an artefact of the method. Ideally further experiments would include Rab4 and Rab8 which were originally shown not to colocalise with BCA2 (Mizuno *et al.* 2003). A Rab protein that has not been shown to associate with endocytic pathways such as Rab1 could also be incorporated into co-transfection studies to serve as a negative control for BCA2 colocalisation.

It had been previously reported that BCA2 was recruited to late endosomes and lysosomes by Rab7 (Mizuno *et al.* 2003). However, in dual IF experiments conducted as part of this project, no colocalisation was observed between BCA2 and the late endolysosomal markers LAMP1 or (endogenous) Rab7. Furthermore, it was observed that endogenous Rab7 failed to localise to late endosomes and lysosomes in HA-BCA2 overexpressing cells. This novel demonstration of a BCA2-mediated effect on the endolysosomal recruitment of Rab7 provides a possible mechanistic explanation for the protein's effects on receptor trafficking. This data therefore helped to meet the second aim of the project: to further characterise the role of BCA2 in receptor endocytosis.

The role of BCA2 in receptor endocytosis was predominately examined in Chapter 6 wherein the data extended the existing body of knowledge

(and fulfilled the second project aim) with a few key findings. BCA2 overexpression was shown to reduce total EGFR levels and to delay internalisation and degradation of the receptor and EGF ligand. These effects were shown to have a degree of specificity as TfR levels and Tf trafficking were not significantly altered by BCA2 overexpression. The reduction in total EGFR levels and delay in ligand induced degradation was shown to be associated with a downstream signalling response that was tempered in size but prolonged in duration. It was demonstrated that protein levels of Rab7 were unaltered by HA-BCA2 overexpression and as previously described in this thesis the overexpression led to a failure of Rab7 membrane association.

The effects of BCA2 overexpression on cell viability were novel findings and as discussed in Chapter 6, have potential impact as either a cause or consequence of BCA2's role in EGFR trafficking. A network of the possible mechanisms linking BCA2 overexpression with cell viability and receptor trafficking is presented in Figure 7-1 which summaries different hypotheses discussed in Chapter 6.

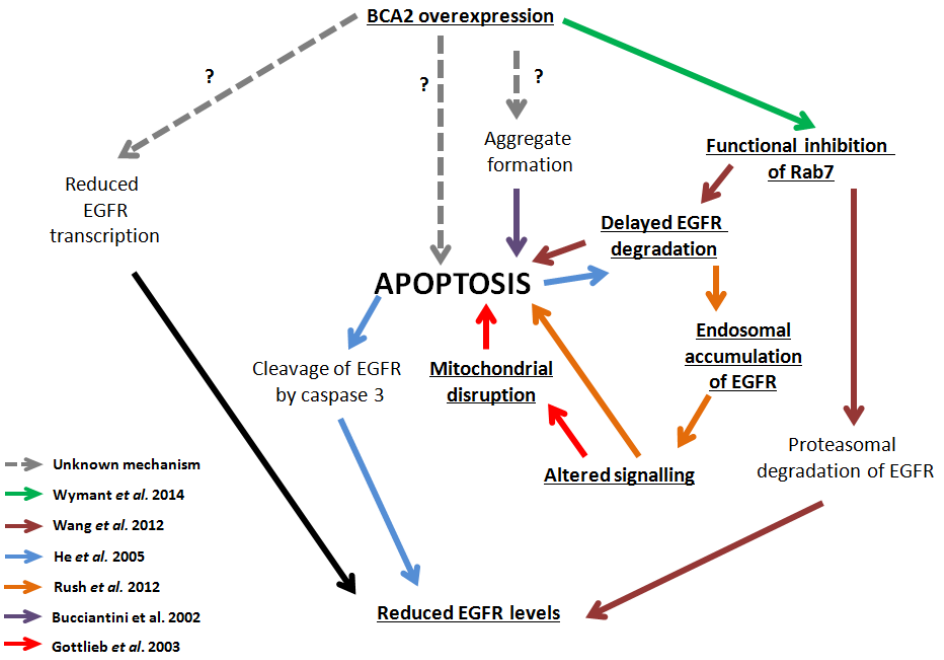

Figure 7-1: Summary of the possible mechanisms to explain BCA2 mediated effects on cell survival and on total receptor levels and trafficking. *Novel or confirmatory BCA2 findings from this thesis are underlined and in bold.*

The investigations into the endocytic function of BCA2 formed the basis of an abstract that was presented as a poster at the 23rd European Cancer Research Association Congress (Wymant *et al.* 2014). During the conference there was particular interest in the downstream signalling data and the concept of magnitude versus duration of signalling. There is potential for further work to explore this principle more generically i.e. to investigate how receptor number affects trafficking and downstream responses. Novel and potentially impactful investigations could be made into the cellular responses induced by different ratios of signalling magnitude and duration. Collaboration with systems biologists would greatly enrich such studies.

Novel findings from the *in silico* MEM and DAVID analyses demonstrated that BCA2 expression was significantly correlated with a

number of membrane trafficking proteins. Notable coexpressed genes included VPS37A (a component of the ESCRT-1 complex), VAMP7 a regulator of late endolysosomal fusion and AP2B1 a critical adaptor subunit for CME. The list of ontologically related and co-expressed genes warrants further investigation in terms of possible BCA2 binding partners and effectors. The possibility of a BCA2-mediated impact on Golgi trafficking should also be explored in light of the protein's association with Rab7 and the number of co-expressed proteins with known or putative functions at the Golgi apparatus (Rojas *et al.* 2008).

The first aim of the project was to investigate the role of BCA2 in breast cancer development, progression and prognosis; in these respects the project was moderately successful. A limitation to meeting this aim more fully was that *in vitro* work primarily focused on receptor trafficking using the (well-characterised) HeLa cell line as a model for EGFR endocytosis. Once a clearer mechanism for BCA2's effects on EGFR trafficking has been elucidated by further work, breast cancer cell line models should then be examined. In doing so it may then be determined if/how the BCA2-mediated effects on receptor trafficking apply in breast cancer. Overexpression of BCA2 in a cellular model of normal breast epithelium, such as the MCF-10A cell line, would enable exploration of a potential role for BCA2 in breast cancer development. The possible involvement of BCA2 in mammary carcinogenesis was suggested by *in silco* data showing BCA2 upregulation in a putative stem cell population of breast epithelial cells and progressive BCA2 upregulation in an increasingly transformed breast epithelial cell line.

Other promising findings to emerge from the *in silico* work that present opportunities for *in vitro* study were results showing that overexpression of HER2 and EGFR/oncogenic signalling reduced BCA2 levels. In light of the effects of BCA2 on EGFR trafficking, it may be the case that BCA2 and HER2 and EGFR/Ras are involved in a mutually regulatory interaction/network. Further studies would ideally extend to examining the BCA2's effects on the total levels of HER2 in addition to receptor internalisation, trafficking and downstream signalling. Methods to determine expression of this oncoprotein have now been developed in the laboratory.

The most successful component of the *in silico* work in terms of meeting the first project aim, was the survival analysis. Increased BCA2 was shown to be associated with better relapse free survival across all breast cancers and in ER+, high grade and lymph node positive disease. This data may reflect a tumour suppressive function of BCA2 and is in keeping with the observed effects on cell viability and on EGFR and c-Met levels presented in Chapter 6. How these findings fit in with some of the pro-proliferation and invasion effects that BCA2 has previously exhibited remains to be discovered (Burger *et al.* 2005; Amemiya *et al.* 2008). How these results link with *in silico* findings that BCA2 levels appear to be enriched in stem cells and to increase with increasing transformation is also unknown. Understanding this apparent conflict will be essential for determining whether BCA2 is a potential therapeutic target in breast cancer and is something that should be prioritised in future BCA2 studies.

Context-dependency of BCA2 on survival was highlighted by the evidence that high BCA2 levels were associated with poorer prognosis in HER2+ breast cancers. Interpretation of survival analyses in luminal B breast cancer was complicated as KMPlotter and GOBO data presented slightly differing relationships between BCA2 expression and relapse free survival. In KMPlotter the data showed clearly that high BCA2 expression adversely impinged on luminal B patient survival. However, GOBO data suggested a more complex picture whereby moderate BCA2 expression was associated with better chance of survival but low and high expressing breast cancers had poorer prognosis. This may relate to the complexity of the luminal B disease as a single classification for potentially quite different types of breast cancer, particularly in terms of HER2 expression. Evidence of context dependency of BCA2 extended to *in vitro* studies where overexpression of the protein induced differing cellular effects, particularly striking were effects (or lack thereof) in mitochondria between MCF-7 and HeLa and differences in viability between MCF-7 and MDA-MB-231 cells.

An important aspect of this project has been in highlighting some potentially significant issues involving and affecting BCA2 research methods. The first problem is that of the intracellular heterogeneity that arises from BCA2 overexpression**.** Transient transfection with HA-BCA2 did not produce uniform patterns of protein expression and localisation in all transfected cells. It may be that BCA2s localisation is naturally heterogeneous and depends on factors such as cell confluency and stage of cell cycle. However, the issue of heterogeneity does raise

some questions about the validity of this approach for interrogating BCA2 localisation and/or function.

One possible limitation of the work in this thesis is that the effects of nuclear versus cytoplasmic BCA2 were not examined. Localisation in the nucleus was not observed for endogenous or overexpressed BCA2 but how and why this is the case is not clear. How the data therefore relate to publications in which nuclear BCA2 has been examined is also not certain. Further studies are required to determine whether nuclear BCA2 localisation (or lack thereof) has a real physiological/pathological basis, or if the presence (or absence) of nuclear detection is an artefact of the method by which BCA2 localisation is interrogated.

Another possible factor that needs further consideration and investigation is that of BCA2 aggregate formation. Despite heterogeneity, the most commonly seen patterns of BCA2 localisation were: large perinuclear accumulations and cytoplasmic inclusions that resembled large vesicles. Whether the structures were true vesicles, i.e. membrane-bound, was not determined so they are intentionally not defined as such. The localisation patterns seen with BCA2 may indicate a natural tendency for the protein to cluster and/or aggregate but they may also be an artefact of overexpression. Protein aggregation is known to cause cytotoxicity (Bucciantini *et al.* 2002) and is a known limitation of transient transfection as research technique (Feller and Lewitzky 2012). Misfolding and aggregation of ubiqutinated proteins is a hallmark of a number of neurodegenerative diseases and is thought to potentially be of importance in cancer (Bence *et al.* 2001; Rodriguez-Gonzalez *et al.*

2008). Aggresomes are cytoplasmic inclusions into which aggregates of ubiquinated, often misfolded, proteins are deposited. Aggresomes are believed to be form when the production rate of aggregation-prone proteins exceeds proteasome capacity (Johnston *et al.* 1998). Overexpression of BCA2 may lead to aggresome formation for a number of reasons: a natural propensity of the native protein to aggregate or insufficient chaperone availability for the high levels of protein expression, leading to BCA2 misfolding and aggregation. Aggregation may be a side-effect of the HA epitope tag and/or possibly the result of the H70L mutation in the HA-BCA2 sequence. It is of critical importance to determine whether a) protein aggregation definitely occurs and b) whether it the aggregation is a physiological phenomenon, an artefact of BCA2 overexpression generally or a specific issue for the HA-BCA2 sequence used in this project and by (Miyakawa *et al.* 2009).

Further work will be carried out using three different plasmids: one containing a sequence corrected HA-BCA2 insert (L70H) and one (sequence corrected) plasmid in which the HA-tag sequence has been removed. Experiments will also be conducted using the EGFP-BCA2 plasmid that was synthesised as part of this project. The EGFP-BCA2 plasmid has also been sequence corrected and the protein has now been brought into frame with the tag. Initial research will focus on protein half-life and localisation and will then extend to cover effects on receptor trafficking, signalling and cell survival.

The demonstration of endogenously occurring, BCA2 positive accumulations in a small subpopulation of MCF-7 cells was a novel

finding of this project. The similarity in labelling compared with HA-BCA2 provides confidence that the localisation produced by BCA2 overexpression has a biological basis but does not however rule out aggresome formation. Further experiments to try and characterise the subpopulation of MCF-7 cells and their intracellular BCA2 positive structures would potentially yield novel and informative data for BCA2 function. Initial work would involve MG132 treatment to try and enhance BCA2 levels and increase the number of visible structures. Colocalisation experiments with endocytic marker proteins would also be performed and finally other breast cancer cell lines would be examined to determine whether or not the subpopulation was unique to MCF-7 cells.

Although many questions remain to be answered, this project has achieved a critical exploration of BCA2 research methodology. This thesis provides an interesting insight into the role of BCA2 in receptor endocytosis and breast cancer, including the likely importance of cellular context in understanding the impact of this interesting protein.

7.1 References

Amemiya, Y., Azmi, P. and Seth, A. 2008. Autoubiquitination of BCA2 RING E3 ligase regulates its own stability and affects cell migration. *Molecular Cancer Research* 6(9), p. 1385.

Bence, N. F., Sampat, R. M. and Kopito, R. R. 2001. Impairment of the ubiquitin-proteasome system by protein aggregation. *Science* 292(5521), p. 1552-55.

Bucciantini, M., Giannoni, E., Chiti, F., Baroni, F., Formigli, L., Zurdo, J., Taddei, N., Ramponi, G., Dobson, C. M. and Stefani, M. 2002. Inherent toxicity of aggregates implies a common mechanism for protein misfolding diseases. *Nature* 416(6880), p. 507-11.

Burger, A. M., Gao, Y., Amemiya, Y., Kahn, H. J., Kitching, R., Yang, Y., Sun, P., Narod, S. A., Hanna, W. M. and Seth, A. K. 2005. A novel RING-type ubiquitin ligase breast cancer-associated gene 2 correlates with outcome in invasive breast cancer. *Cancer Research* 65(22), p. 10401.

Feller, S. M. and Lewitzky, M. 2012. Very'sticky'proteins-not too sticky after all. *Cell Communication and Signalling* 10, p. 15.

Johnston, J. A., Ward, C. L. and Kopito, R. R. 1998. Aggresomes: a cellular response to misfolded proteins. *The Journal of Cell Biology* 143(7), p. 1883-98.

Miyakawa, K., Ryo, A., Murakami, T., Ohba, K., Yamaoka, S., Fukuda, M., Guatelli, J. and Yamamoto, N. 2009. BCA2/Rabring7 promotes tetherin-dependent HIV-1 restriction. *PLoS Pathogens* 5(12), p. e1000700.

Mizuno, K., Kitamura, A. and Sasaki, T. 2003. Rabring7, a novel Rab7 target protein with a RING finger motif. *Molecular Biology of the Cell* 14(9), p. 3741-52.

Pereira, P., Pedrosa, S. S., Wymant, J., Sayers, E., Correia, A., Vilanova, M., Jones, A. T. and Gama, F. M. 2015 *accepted*. siRNA inhibition of endocytic pathways to characterise the cellular uptake mechanisms of folic acid functionalised glycol chitosan nanogels. *Molecular Pharmaceutics*.

Rodriguez-Gonzalez, A., Lin, T., Ikeda, A. K., Simms-Waldrip, T., Fu, C. and Sakamoto, K. M. 2008. Role of the aggresome pathway in cancer: Targeting histone deacetylase 6–dependent protein degradation. *Cancer Research* 68(8), p. 2557-60.

Rojas, R., van Vlijmen, T., Mardones, G. A., Prabhu, Y., Rojas, A. L., Mohammed, S., Heck, A. J., Raposo, G., van Der Sluijs, P. and Bonifacino, J. S. 2008. Regulation of retromer recruitment to endosomes by sequential action of Rab5 and Rab7. *The Journal of Cell Biology* 183(3), p. 513-26.

Webber, J.P., Spary, L.K., Sanders, A.J., Chowdhury, R., Jiang, W.G., Steadman, R., Wymant, J., Jones, A.T., Kynaston, H., Mason, M.D., Tabi, Z. and Clayton, A. 2015. Differentiation of tumour-

promoting stromal myofibroblasts by cancer exosomes**.** *Oncogene* 34: 290-302.

Wymant, J., Hiscox, S., Westwell, A., Urbé, S., Clague, M. and Jones, A. 2014. 479: The role of Breast Cancer Associated gene 2 in EGFR endocytosis, downregulation and breast cancer survival. *European Journal of Cancer* 50(Supplement 5).

Appendix A: Products and suppliers

Biorad (Hemel Hempstead, UK):
- Precision plus protein dual colour standards (#161-0374)
- Clarity, Western ECL substrate (#170-5060)
- Agarose (#161-3100)
- SDS (#161-0301)

Cambridge Biosciences (Cambridge, UK):
- PrecisionShuttle vector pCMV6-AC-HA (#PS100008)

DAKO (Ely, UK):
- Fluorescence mounting medium "Dako oil" / (#S3023)

Fisher Scientific (Loughborough, UK):
- Coverslips No. 1 circle 16mm diameter (#12313138)
- 40% acrylamide/Bis (#10376643)
- PVDF membrane (#10344661)
- SuperSignal West Femto Chemiluminescent Substrate (#34094)
- SMARTpool: ON-TARGETplus RNF115 siRNA (#L-006974-00-0005)
- Dharmafect 1 transfection reagent (#11866654)

Life Technologies (Paisley, UK):
- DMEM (#21885)
- RPMI 1640 (#21875)
- DMEM/F12 (#11330)
- FBS (#16000-044)
- Horse serum (#16050)
- 0.05% Trypsin EDTA (#25300062)
- Hoechst 33342 (#H3570)
- Rhodamine Phalloidin (#R415)
- Alexa 488-EGF (#E-13345)
- EGF-Rhd (#E-3481)
- Transferrin Alexa 488 (#T-13342)
- Transferrin Alexa 647 (#T-23366)
- DH5α competent E.coli and SOC medium (#18263-012)
- BigDye Direct cycle sequencing kit (#4458687)
- Dynabeads Sequencing Clean-Up Kit (#66101)
- Lipofectamine 2000 transfection reagent (#11668027)
- Oligofectamine transfection reagent (#12252-011)
- pEF5/FRT/V5 Directional TOPO® Expression Kit (#K6035-01)
- Zeocin (#R25001)

Mast Group Ltd, (Merseyside, UK):
- Cryobank ceramic bead bacterial storage system (#CRYO/M)

Merck Millipore (Feltham, UK):
- GeneJuice transfection reagent (#70967-3)

New England Biolabs (Hitchin, UK):

- EcoRI (#R0101)
- PspOMI (#R0653)
- NotI (#R0189)
- BstEII (#R0162)
- Antarctic Phosphatase (#M0289S)
- 1 kb DNA Ladder (#N3232)
- T4 ligase (#M0102S)

Promega (Loughborough, UK)

- Fugene 6 transfection reagent (#E2691)
- CellTitre Blue viability assay (#G8080)

Qiagen (Manchester, UK)

- Miniprep kit (#27014)
- Maxiprep kit (#12262)
- HotStar HiFidelity Polymerase Kit (#202602)
- QIAquick gel extraction kit (#28704)

Roche Diagnostics (Burgess Hill, UK):

- cOmplete Protease Inhibitor Cocktail Tablets (#11836153001)
- PhosStop Phosphatase inhibitor cocktail (#4906837001)
- Hygromycin (#10843555001)

Sigma Aldrich (Poole, UK):

- EGF (#E9644)
- Hydrocortisone (#H0888)
- Cholera toxin (#S8052)
- Insulin (#I9278)
- Triton X-100 (#X100)
- BSA (#A7906)
- Saponin (#47036)
- Bicinchoninic Acid solution (#B9643)
- Copper (II) Sulphate solution (#C2284)
- TEMED (#T9281)
- Ponceau S solution (#P7170)
- Tween 20 (#P1379)
- **LB AGAR (#A5306)**
- LB Broth (#L3022)
- Ampicillin (#A1593)
- Kanamycin (#K1377)
- Ethidium bromide (#E1510)
- MG132 (#C2211)
- Butyric acid (#B103500)
- 5-azacytidine (#A2385)

Appendix B: Coexpressed gene list from MEM analysis

#Gene name	Gene locus	#Score	#probeset id
RNF115	1q21.1	#QUERY	212742_AT
POLR3C	1q21.1	4.52E-44	209382_at
RNF14	5q31.3	1.37E-36	201823_s_at
SBDS	7q11.21	7.21E-36	1554089_s_at
ANXA7	10q22.2	3.69E-35	209860_s_at
CALM1	14q32.11	6.24E-35	211985_s_at
VDAC2	10q22	6.88E-35	211662_s_at
C3ORF38	3p11.1	7.95E-35	226524_at
VAMP7	Xq28 / yq12	8.88E-35	202829_s_at
TIMM17A	1q32.1	1.97E-34	201821_s_at
PTPLAD1	15q22.2	2.06E-34	222404_x_at
YME1L1	10p14	2.21E-34	201351_s_at
BCAP29	7q22.3	4.91E-34	205084_at
RAB18	10p12.1	7.64E-34	224787_s_at
YWHAQ	2p25.1	1.55E-33	200693_at
AZIN1	8q22.3	1.83E-33	201772_at
TM9SF3	10q24.1	3.51E-33	222399_s_at
PTPLAD1	15q22.2	4.57E-33	234000_s_at
TNPO1	5q13.2	5.63E-33	209226_s_at
AP2B1	17q11.2-q12	6.26E-33	200615_s_at
TMCO1	1q22-q25	7.59E-33	208716_s_at
ATF7	12q13	8.87E-33	228829_at
ANKIB1	7q21.2	1.09E-32	224687_at
ABI1	10p11.2	1.09E-32	209027_s_at
DLD	7q31-q32	1.19E-32	209095_at
NAA35	9q21.33	1.45E-32	220925_at
METTL2B	7q32.1	1.88E-32	225253_s_at
SLC25A32	8q22.3	1.89E-32	221020_s_at
SERINC3	20q13.12	2.23E-32	211769_x_at
CSRNP2	12q13.11-.12	2.60E-32	221260_s_at
TRAM1	8q13.3	3.32E-32	201399_s_at
PSMA3	14q23	4.19E-32	201532_at
RNASEH1	2p25	5.45E-32	218497_s_at
TMEM189	20q13.2	1.03E-31	201001_s_at
ARL1	12q23.2	1.21E-31	201659_s_at
PSMD12	17q24.2	2.06E-31	202352_s_at
VIMP	15q26.3	2.08E-31	223209_s_at
COPB1	11p15.2	2.32E-31	201359_at
UBE2Q1	1q21.3	2.34E-31	217978_s_at
TROVE2	1q31	2.43E-31	210438_x_at
BUB3	10q26	2.52E-31	201457_x_at
SPPL2A	15q21.2	2.60E-31	226353_at
VPS37A	8p22	2.71E-31	225378_at
RHEBP2	10q11.22	3.39E-31	1555780_a_at
INTS12	4q24	3.82E-31	218616_at
PPP2CB	8p12	3.97E-31	201375_s_at
HAX1	1q21.3	4.11E-31	201145_at
RC3H2	9q34	4.27E-31	220202_s_at

Appendix C: Functional annotation clustering analysis for the genes co-expressed with RNF115 (BCA2)

Category	Term	Count	%	Genes	P -value	Benjamini
SP_PIR_KEYWORDS	protein transport	9	19	BCAP29, RAB18, AP2B1, COPB1, TIMM17A, TRAM1, TNPO1, VPS37A, VAMP7	1.50E-05	9.40E-04
GOTERM_BP_FAT	protein transport	11	23	BCAP29, RAB18, AP2B1, COPB1, VIMP, TIMM17A, TRAM1, TNPO1, YWHAQ, VPS37A, VAMP7	3.40E-05	1.70E-02
GOTERM_BP_FAT	establishment of protein localization	11	23	BCAP29, RAB18, AP2B1, COPB1, VIMP, TIMM17A, TRAM1, TNPO1, YWHAQ, VPS37A, VAMP7	3.70E-05	9.00E-03
GOTERM_BP_FAT	intracellular transport	10	21	ARL1, BCAP29, AP2B1, COPB1, VIMP, TIMM17A, TRAM1, TNPO1, YWHAQ, VAMP7	6.50E-05	1.10E-02
GOTERM_BP_FAT	intracellular protein transport	8	17	BCAP29, AP2B1, COPB1, VIMP, TIMM17A, TRAM1, TNPO1, YWHAQ	7.00E-05	8.70E-03
GOTERM_BP_FAT	protein localization	11	23	BCAP29, RAB18, AP2B1, COPB1, VIMP, TIMM17A, TRAM1, TNPO1, YWHAQ, VPS37A, VAMP7	1.20E-04	1.10E-02
GOTERM_BP_FAT	cellular protein localization	8	17	BCAP29, AP2B1, COPB1, VIMP, TIMM17A, TRAM1, TNPO1, YWHAQ	1.30E-04	1.00E-02
GOTERM_BP_FAT	cellular macromolecule localization	8	17	BCAP29, AP2B1, COPB1, VIMP, TIMM17A, TRAM1, TNPO1, YWHAQ	1.30E-04	9.40E-03
GOTERM_CC_FAT	endomembrane system	9	19	HAX1, AP2B1, ANXA7, COPB1, RC3H2, VIMP, TRAM1, TNPO1, VAMP7	1.20E-03	1.70E-01
SP_PIR_KEYWORDS	Transport	11	23	BCAP29, RAB18, AP2B1, COPB1, SLC25A32, TIMM17A, TRAM1, TNPO1, VPS37A, VAMP7, *VDAC2**	4.50E-03	1.80E-01
GOTERM_CC_FAT	organelle membrane	9	19	HAX1, AP2B1, COPB1, VIMP, SLC25A32, TIMM17A, TRAM1, TNPO1, VAMP7, *VDAC2**	9.90E-03	5.20E-01
GOTERM_MF_FAT	protein transporter activity	3	6	AP2B1, TIMM17A, TNPO1	2.00E-02	7.40E-01
GOTERM_BP_FAT	vesicle-mediated transport	6	13	ARL1, BCAP29, RAB18, AP2B1, COPB1, VAMP7	2.20E-02	3.80E-01
GOTERM_BP_FAT	protein targeting	4	8	TIMM17A, TRAM1, TNPO1, YWHAQ	2.20E-02	3.60E-01
INTERPRO	Armadillo-like helical	3	6	AP2B1, COPB1, TNPO1	4.30E-02	9.30E-01

**pseudogene*

Appendix D: Vector map for pCMV-HA-N produced by vector into which BCA2 insert was cloned by Miyakawa *et al*. (2009)

Vector Map

Clontech

Catalog No(s).
631604, 635690

pCMV-HA-N Vector Information

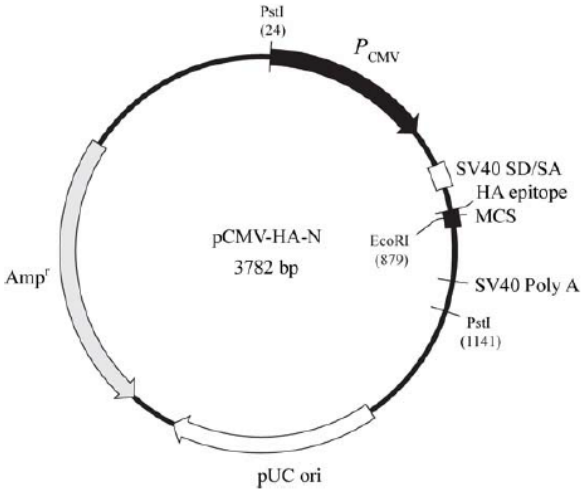

Location of Features

- P_{CMV} (human cytomegalovirus promoter): 27–526
- SV40 SD/SA (SV40 donor/acceptor splice sites): 672–768
- MCS (multiple cloning site): 864–917
- HA epitope: 829–858
- SV40 polyA (SV40 polyA signal): 1044–1063
- pUC ori (pUC origin of replication): 1536–2179
- Amp^r (ampicillin resistance gene): 2327–3187 (complementary)

pCMV-HA-N vector map and multiple cloning site.

Hemagglutinin (HA) epitope — SfiI

```
829  ATG TAC CCA TAC GAT GTT CCA GAT TAC GCT CTT ATG GCC ATG GAG
     TAC ATG GGT ATG CTA CAA GGT CTA ATG CGA GAA TAC CGG TAC CTC
```

SfiI — XhoI — NotI

EcoRI — SalI — BglII — KpnI

```
874  GCC CGA ATT CGG TCG ACC GAG ATC TCT CGA GGT ACC GCG GCC GC
     CGG GCT TAA GCC AGC TGG CTC TAG AGA GCT CCA TGG CGC CGG CG
```

Appendix E: Vector maps for pEGFP-C1 and pEGFP-N1

pEGFP-C1 Vector Information PT3028-5

GenBank Accession #: U55763 Catalog #6084-1

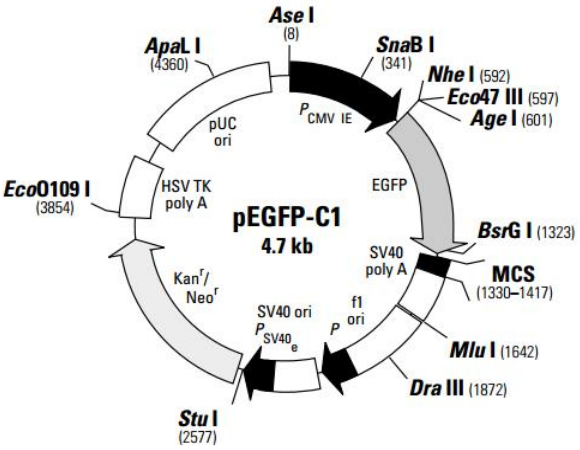

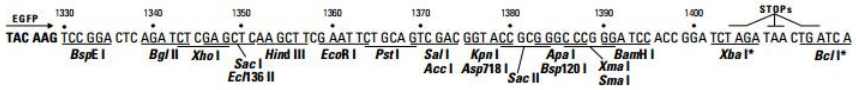

Restriction Map and Multiple Cloning Site (MCS) of pEGFP-C1. (Unique restriction sites are in bold). The *Xba* I and *Bcl* I sites (*) are methylated in the DNA provided by CLONTECH. If you wish to digest the vector with these enzymes, you will need to transform the vector into a *dam*- host and make fresh DNA.

pEGFP-N1 Vector Information PT3027-5

GenBank Accession #U55762 Catalog #6085-1

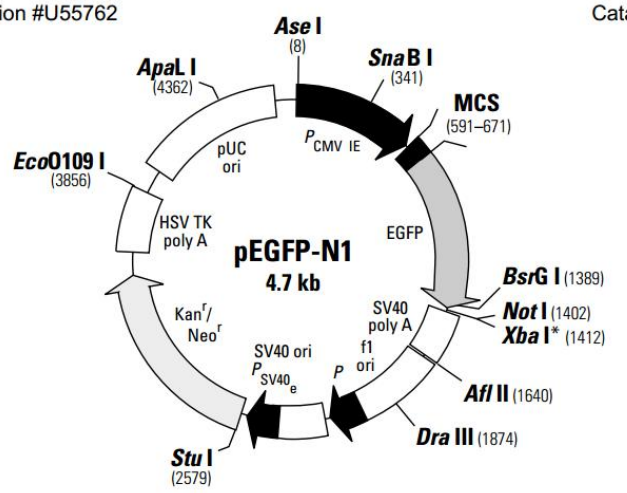

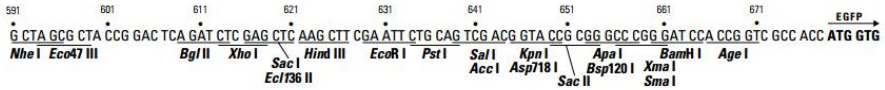

Restriction Map and Multiple Cloning Site (MCS) of pEGFP-N1 Vector. All restriction sites shown are unique. The *Not* I site follows the EGFP stop codon. The *Xba* I site (*) is methylated in the DNA provided by BD Biosciences Clontech. If you wish to digest the vector with this enzyme, you will need to transform the vector into a *dam*- and make fresh DNA.

Appendix F: Electropherograms for forward and reverse HA-BCA2 sequencing

HA-BCA2 forward sequencing electropherogram

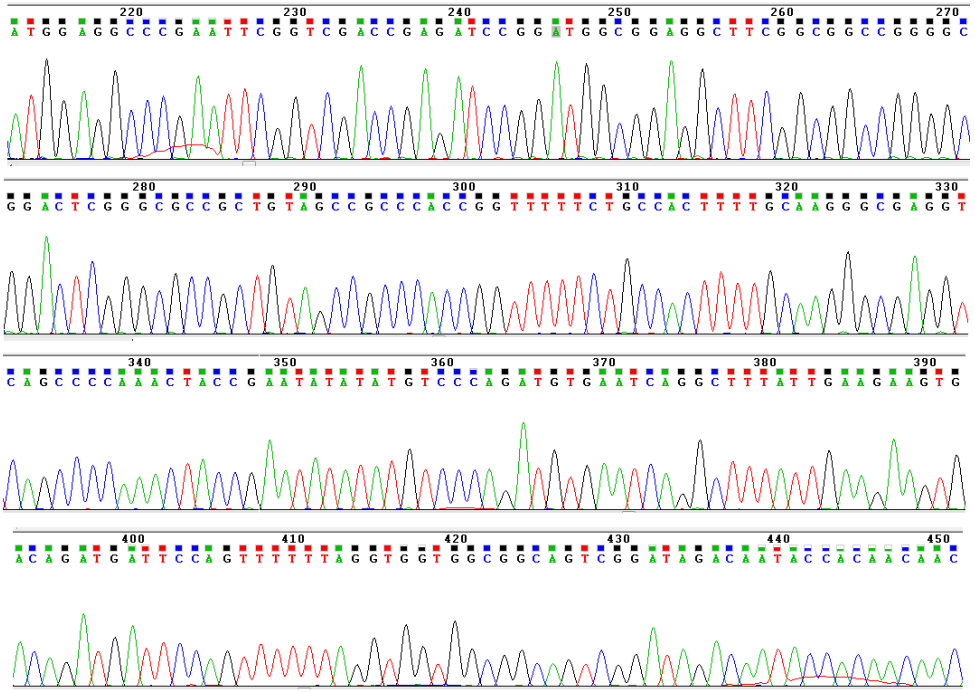

HA-BCA2 reverse sequencing electropherogram

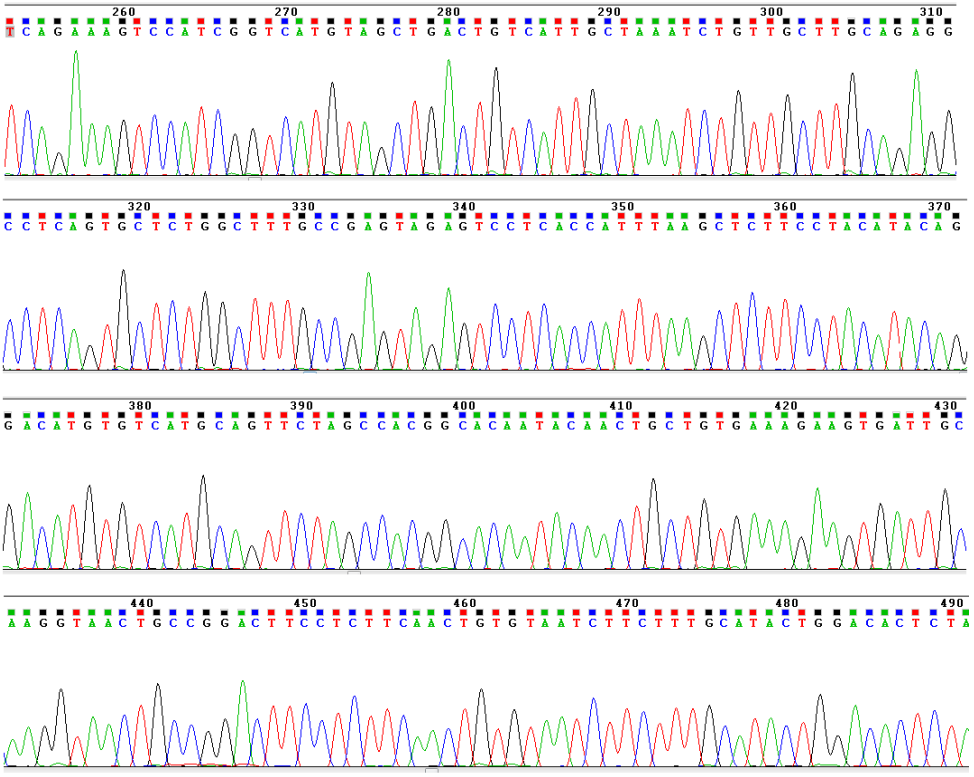

Appendix G: Vector map for pEF5-FRT/D-TOPO for stable cell generation

pEF5/FRT/V5-D-TOPO® Map

The figure below shows the features of pEF5/FRT/V5-D-TOPO® vector. The complete sequence of pEF5/FRT/V5-D-TOPO® is available for downloading from our Web site (www.invitrogen.com) or by contacting Technical Service (page 32).

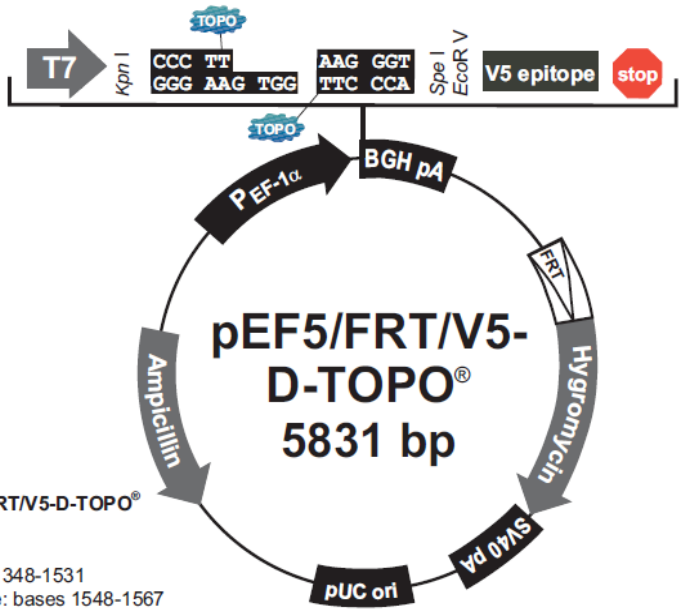

Comments for pEF5/FRT/V5-D-TOPO®
5831 nucleotides

EF-1α promoter: bases 348-1531
T7 promoter/priming site: bases 1548-1567
TOPO® recognition site 1: bases 1612-1616
Overhang: bases 1617-1620
TOPO® recognition site 2: bases 1621-1625
V5 epitope: bases 1705-1746
BGH reverse priming site: bases 1784-1801
BGH polyadenylation signal: bases 1790-2014
FRT site: bases 2297-2344
Hygromycin resistance gene (no ATG): bases 2352-3372
SV40 early polyadenylation signal: bases 3504-3634
pUC origin: bases 4017-4690
bla promoter: bases 5696-5794 (complementary strand)
Ampicillin (*bla*) resistance gene: bases 4835-5695 (complementary strand)

Appendix H: Site directed mutagenesis strategies for sequence correction and tag removal using HA-BCA2 construct and combined sequence correction and frame shift in EGFP-BCA2 construct

Sequence correction: L70H mutation back to native sequence

Mutation	Original sequence	Mutated sequence	Position within gene (bp #)	**Mutation frame***
Substitution	ACAACACTTTTTGCA	ACAACACaTTTTGCA	281 - T	1 bp

Epitope tag deletion (plus L70H sequence correction)

Mutation	Original sequence	Mutated sequence	Position within gene (bp #)	**Mutation frame***
Substitution	ACAACACTTTTTGCA	ACAACACaTTTTGCA	281 - T	1 bp
Deletion	CACC --- ATGG	CACCATGG	**Deletion region within gene** 72 bp deletion between 0C and 73A	

Frame correction to bring BCA2 into frame with EGFP (plus L70H correction)

Mutation	Original sequence	Mutated sequence	Position within gene (bp #)	**Mutation frame***
Substitution	ACAACACTTTTTGCA	ACAACACaTTTTGCA	209 - T	1 bp
Deletion	AATTCGGTCGACC	AATTCGTCGACC	-16 G *upstream*	1 bp

Appendix I: Homology detection and structure prediction by HMM-HMM comparison

Key BCA2 structural domains predicted by the HHPred online bioinformatics software: http://toolkit.tuebingen.mpg.de/hhpred

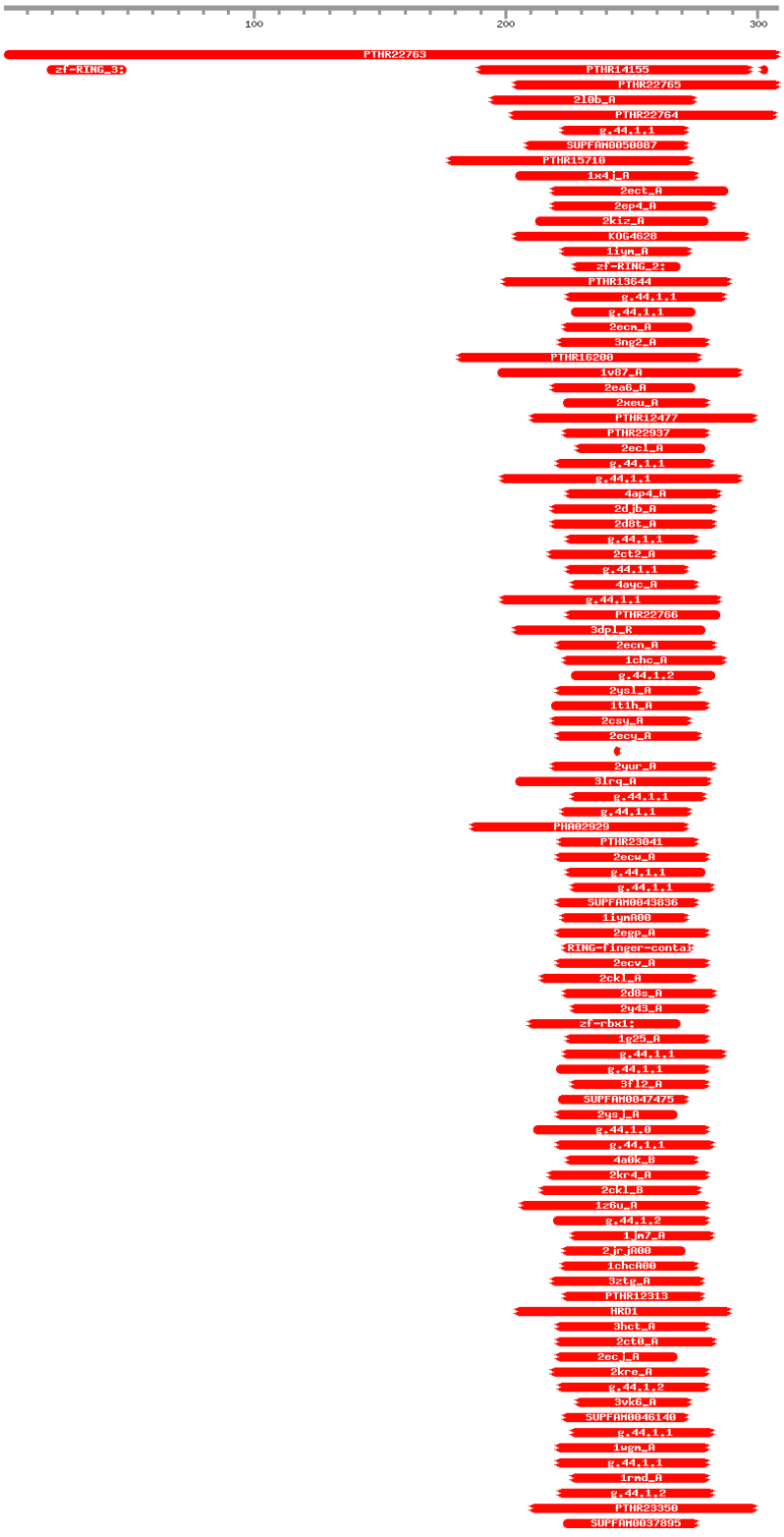

Appendix J: KM Plotter and GOBO patient numbers

KM Plotter

Stratification	Number of patients
None (all tumours)	3458
ER Positive	2000
ER Negative	806
Grade 1	306
Grade 2	716
Grade 3	792
LN Positive	1178
LN Negative	1973
Luminal A	2069
Luminal B	1165
Basal-like	669
HER2	239

GOBO

Stratification	Number of patients
None (all tumours)	914
ER Positive	738
ER Negative	166
Grade 1	190
Grade 2	411
Grade 3	257
LN Positive	229
LN Negative	662
Luminal A	268
Luminal B	204
Basal-like	114
HER2	122
Normal-like	160